frontiers | Research Topics

Chagas disease novel drug targets and treatments

Edited by
Vilma G. Duschak, Gustavo Benaim
and Alberto Enrique Paniz Mondolfi

Published in
Frontiers in Cellular and Infection Microbiology

ISSN 1664-8714
ISBN 978-2-8325-2674-3
DOI 10.3389/978-2-8325-2674-3

About Frontiers

Frontiers is more than just an open access publisher of scholarly articles: it is a pioneering approach to the world of academia, radically improving the way scholarly research is managed. The grand vision of Frontiers is a world where all people have an equal opportunity to seek, share and generate knowledge. Frontiers provides immediate and permanent online open access to all its publications, but this alone is not enough to realize our grand goals.

Frontiers journal series

The Frontiers journal series is a multi-tier and interdisciplinary set of open-access, online journals, promising a paradigm shift from the current review, selection and dissemination processes in academic publishing. All Frontiers journals are driven by researchers for researchers; therefore, they constitute a service to the scholarly community. At the same time, the *Frontiers journal series* operates on a revolutionary invention, the tiered publishing system, initially addressing specific communities of scholars, and gradually climbing up to broader public understanding, thus serving the interests of the lay society, too.

Dedication to quality

Each Frontiers article is a landmark of the highest quality, thanks to genuinely collaborative interactions between authors and review editors, who include some of the world's best academicians. Research must be certified by peers before entering a stream of knowledge that may eventually reach the public - and shape society; therefore, Frontiers only applies the most rigorous and unbiased reviews. Frontiers revolutionizes research publishing by freely delivering the most outstanding research, evaluated with no bias from both the academic and social point of view. By applying the most advanced information technologies, Frontiers is catapulting scholarly publishing into a new generation.

What are Frontiers Research Topics?

Frontiers Research Topics are very popular trademarks of the *Frontiers journals series*: they are collections of at least ten articles, all centered on a particular subject. With their unique mix of varied contributions from Original Research to Review Articles, Frontiers Research Topics unify the most influential researchers, the latest key findings and historical advances in a hot research area.

Find out more on how to host your own Frontiers Research Topic or contribute to one as an author by contacting the Frontiers editorial office: frontiersin.org/about/contact

Chagas disease novel drug targets and treatments

Topic editors

Vilma G. Duschak — National Scientific and Technical Research Council (CONICET), Argentina

Gustavo Benaim — Fundación Instituto de Estudios Avanzados (IDEA), Venezuela

Alberto Enrique Paniz Mondolfi — Icahn School of Medicine at Mount Sinai, United States

Citation

Duschak, V. G., Benaim, G., Mondolfi, A. E. P., eds. (2023). *Chagas disease novel drug targets and treatments*. Lausanne: Frontiers Media SA.

doi: 10.3389/978-2-8325-2674-3

Table of contents

05 Editorial: Chagas disease novel drug targets and treatments
Vilma G. Duschak, Alberto E. Paniz Mondolfi and Gustavo Benaim

10 Fenofibrate Increases the Population of Non-Classical Monocytes in Asymptomatic Chagas Disease Patients and Modulates Inflammatory Cytokines in PBMC
Azul V. Pieralisi, Ágata C. Cevey, Federico N. Penas, Nilda Prado, Ana Mori, Mónica Gili, Gerardo A. Mirkin, Juan Gagliardi and Nora B. Goren

25 The Impact of the CTHRSSVVC Peptide Upon Experimental Models of *Trypanosoma cruzi* Infection
Gabriela Rodrigues Leite, Denise da Gama Jaén Batista, Ana Lia Mazzeti, Rosemeire Aparecida Silva, Ademar Benévolo Lugão and Maria de Nazaré Correia Soeiro

33 Role of the Complement System in the Modulation of T-Cell Responses in Chronic Chagas Disease
María Belén Caputo, Josefina Elias, Gonzalo Cesar, María Gabriela Alvarez, Susana Adriana Laucella and María Cecilia Albareda

39 Miltefosine and Benznidazole Combination Improve Anti-*Trypanosoma cruzi In Vitro* and *In Vivo* Efficacy
Julián Ernesto Nicolás Gulin, Margarita María Catalina Bisio, Daniela Rocco, Jaime Altcheh, María Elisa Solana and Facundo García-Bournissen

51 Structural New Data for Mitochondrial Peroxiredoxin From *Trypanosoma cruzi* Show High Similarity With Human Peroxiredoxin 3: Repositioning Thiostrepton as Antichagasic Drug
Lucio Rivera-Santiago, Ignacio Martínez, Ruben Arroyo-Olarte, Paulina Díaz-Garrido, Roberto I. Cuevas-Hernandez and Bertha Espinoza

63 The Role of the Na^+/Ca^{2+} Exchanger in Aberrant Intracellular $Ca2^+$ in Cardiomyocytes of Chagas-Infected Rodents
Jose R. Lopez, Nancy Linares, Jose A. Adams and Alfredo Mijares

72 The Use of AlphaFold for *In Silico* Exploration of Drug Targets in the Parasite *Trypanosoma cruzi*
Albert Ros-Lucas, Nieves Martinez-Peinado, Jaume Bastida, Joaquim Gascón and Julio Alonso-Padilla

85 Broadening the spectrum of ivermectin: Its effect on *Trypanosoma cruzi* and related trypanosomatids
Laura Fraccaroli, María Daniela Ruiz, Virginia Gabriela Perdomo, Agustina Nicole Clausi, Darío Emmanuel Balcazar, Luciana Larocca and Carolina Carrillo

95 The repositioned drugs disulfiram/diethyldithiocarbamate combined to benznidazole: Searching for Chagas disease selective therapy, preventing toxicity and drug resistance
Juliana Almeida-Silva, Diego Silva Menezes, Juan Mateus Pereira Fernandes, Márcio Cerqueira Almeida, Deyvison Rhuan Vasco-dos-Santos, Roberto Magalhães Saraiva, Alessandra Lifsitch Viçosa, Sandra Aurora Chavez Perez, Sônia Gumes Andrade, Ana Márcia Suarez-Fontes and Marcos André Vannier-Santos

115 In Chagas disease, transforming growth factor beta neutralization reduces *Trypanosoma cruzi* infection and improves cardiac performance
Roberto Rodrigues Ferreira, Elen Mello de Souza, Glaucia Vilar-Pereira, Wim M. S. Degrave, Rayane da Silva Abreu, Marcelo Meuser-Batista, Nilma Valéria Caldeira Ferreira, Steve Ledbeter, Robert H. Barker, Sabine Bailly, Jean-Jacques Feige, Joseli Lannes-Vieira, Tania C. de Araújo-Jorge and Mariana Caldas Waghabi

frontiers | Frontiers in Cellular and Infection Microbiology

TYPE Editorial
PUBLISHED 26 May 2023
DOI 10.3389/fcimb.2023.1199715

OPEN ACCESS

EDITED AND REVIEWED BY
Nahed Ismail,
University of Illinois Chicago, United States

*CORRESPONDENCE
Vilma G. Duschak
vduschak@conicet.gov.ar

RECEIVED 03 April 2023
ACCEPTED 02 May 2023
PUBLISHED 26 May 2023

CITATION
Duschak VG, Paniz Mondolfi AE and Benaim G (2023) Editorial: Chagas disease novel drug targets and treatments. *Front. Cell. Infect. Microbiol.* 13:1199715. doi: 10.3389/fcimb.2023.1199715

Editorial: Chagas disease novel drug targets and treatments

Vilma G. Duschak[1]*, Alberto E. Paniz Mondolfi[2,3] and Gustavo Benaim[4,5]

[1]National Council of Scientific and Technical Research (CONICET) and National Institute of Parasitology (INP), "Dr.Mario Fatala Chaben", Administración Nacional de Laboratorios de Institutos de Salud (ANLIS)-Malbrán, National Health Department, Ciudad Autónoma de Buenos Aires (CABA), Buenos Aires, Argentina, [2]Molecular Microbiology Laboratory, Department of Pathology, Molecular and Cell-Based Medicine, Icahn School of Medicine at Mount Sinai, New York, NY, United States, [3]Incubadora Venezolana de la Ciencia (IVC), Centro de Investigaciones Biomédicas IDB, Barquisimeto, Venezuela, [4]Unidad de Señalización Celular y Bioquímica de Parásitos, Instituto de Estudios Avanzados (IDEA), Caracas, Venezuela, [5]Instituto de Biología Experimental, Facultad de Ciencias, Universidad Central de Venezuela, Caracas, Venezuela

KEYWORDS

Chagas disease, drug targets, treatment strategies, drug repurposing, neglected diseases

Editorial on the Research Topic
Chagas disease novel drug targets and treatments

Chagas disease (ChD), also known as American Trypanosomiasis, is a parasitic disease caused by the hemoflagellate protozoan *Trypanosoma cruzi*. The disease is endemic to Latin America with an estimated 6-7 million people infected. Today, ChD is considered and emerging global health concern due to imported cases through traveling and migration, as well as to its broadening geographic endemism, like in the case of the United States (Paniz Mondolfi et al., 2020). Despite this, treatment options for ChD remain limited and exhibit significant adverse effects. Current treatment options are based on two nitroderivative and nitrofuran compounds, Benznidazole (Bz) and Nifurtimox (Nx), which were introduced in clinical medicine over 50 years ago and despite being the only two drugs approved for the treatment of ChD, present several limitations for their use.

First, both drugs Bz and Nx exhibit significant side effects, ranging from mild to severe systemic signs and symptoms, including skin rashes, nausea, vomiting, anorexia, anemia, leukopenia and peripheral neuropathy, that usually lead to discontinuation of treatment. Second, the efficacy of these drugs varies depending on the developmental phase of the parasite, stage of the disease (acute or chronic) and the geographical location of the patient, with cure rates ranging from 60 to 80%. This is important, because geographic location is intimately related to the genomic variability of the parasite and its respective Discrete Typing Units (DTUs) which are known to exhibit differential trends in response to treatment (Higuera et al., 2013). Thirdly, the duration of therapy is prolonged, ranging from 60 to 120 days, requiring close monitoring due to potential adverse effects. Lastly, the emergence of drug-resistant strains of *T. cruzi* has represented a major obstacle to the successful treatment of ChD. Hence, there is an urgent need to identify new drugs and drug targets to improve the efficacy and safety profile of ChD therapy.

As a result, significant efforts are being made in search for novel chemotherapeutic approaches for this invariably inveterate infection, particularly at its chronic phase, the most insidious and frequent clinical expression of the disease. Therefore, breaking ground in

Chagas disease treatment, this topic is unveiling novel drug targets and drug repurposing strategies. The increase in the understanding of the biology and biochemistry of the parasite have allowed the identification of new therapeutic targets to identify new trypanocidal agents, in addition to rational drug design and screening of natural products. Existing drugs are active in treating congenital infection by *T. cruzi*, acute ChD, and children up to 12 years, without any evidence for its effectiveness of treatment in adults at the chronical (and more frequent) phase of the infection. Therefore, novel active trypanocidal compounds, with low toxicities and increased efficacies during the chronic phase as stated above are immediately required and reviewed in detail (Duschak, 2011; Duschak, 2016; Duschak, 2017). In the last years, different types of parasite targets have been classified in three main groups based in those that most researchers are working on (Duschak, 2019). One of the main approaches on the search for new drugs consists in exploiting biological differences between the parasite and the mammalian host-cells. For example, since the early recognition that these parasites possess ergosterol at their membranes as a final products of sterol synthesis (sharing this property with fungi), instead of cholesterol (which is characteristic of mammalian cells), ergosterol synthesis have shown to be potentially candidates for a rational therapeutic approach (Urbina et al., 1998).

Another interesting approach would base itself in drug repurposing and combination therapy, which represent potentially cost-effective strategies. In these lines, Miltefosine (Milt), a synthetic alkyllysophospholipid initially developed for treatment of breast cancer and successfully repurposed for oral treatment of leishmaniasis (Croft et al., 1996), has been proposed as a promising candidate against *T. cruzi* infection (Rodriguez-Duran et al., 2019; Benaim et al., 2020).

Interestingly, its mechanism of action on trypanosomatids has been recently elucidated (Pinto-Martinez et al., 2018; Rodriguez-Duran et al., 2019). In fact, one of the papers included in this collection, *"Miltefosine and Benznidazole combination improves anti-T. cruzi in vitro and in vivo efficacy'*, precisely touches on the efficacy of Milt monotherapy as well as in combination with Bz, both in *in vitro* and *in vivo* models of *T. cruzi* infection. It is worth noting that the results described here support the efficacy of Milt's activity in clinically relevant stages of *T. cruzi* infection and lend further support for evaluating combined schemes using Milt and other synthetic alkyllysophospholipids as likely drug candidates (Gulin et al.).

Along the lines of drug-repurposing candidates are the benzofuran derivatives, specifically amiodarone and dronedarone. Amiodarone, a commonly prescribed antiarrhythmic in Chagas cardiomyopathy as an antiarrhythmic, has shown promising effects against *T. cruzi* and other trypanosomatids (Benaim et al., 2021) either as monotherapy or in combination with sterol biosynthesis inhibitors, such as posaconazole and itraconazole, acting in a synergistic mode (Benaim et al., 2006). The combination of amiodarone and itraconazole (a triazole from which posaconazole derived) has proved successful in treating naturally infected dogs, resulting in the parasitological cure of all animals tested in what is considered the largest investigational drug trial for ChD performed in dogs to date (Madigan et al., 2019).

The work presented by Almeida-Silva et al. conducted a study using the repurposed drug disulfiram (DSF) and its derivative diethyldithiocarbamate (DETC) in combination with Bz to treat *T. cruzi* both *in vitro* and *in vivo*. Their findings demonstrated that the DETC-Bz combination exhibited a synergistic effect, reducing epimastigotes proliferation and increasing selective indexes over a 10-fold. Further evidence revealed through electron microscopy imaging revealed membrane discontinuities, cell body volume reduction, and significant enlargement of endoplasmic reticulum cisternae. Additionally, dilated mitochondria with decreased electron density and disorganized kinetoplast DNA were observed substantiating the effects of this combination. According to the authors, the combination of DSF and DETC has the potential to reduce the toxicity of other drugs as well as the emergence of drug resistance phenotypes, making it a safe and effective option for ChD treatment.

The studies presented in this collection also provide important insights on other emerging therapeutic strategies. As an example, novel structural data on mitochondrial *T. cruzi* peroxiredoxin (PRXs), expressed in all stages of the parasite, central for the survival and replication of the parasite, have been proposed as virulence factors which detoxify oxidizing agents, central for the survival and replication of the parasite have been considered as possible therapeutic targets but there is still no specific drug against them. Structural data for mitochondrial *T. cruzi* peroxiredoxin as novel target were compared with several PRXs showing high similarity with human peroxiredoxin 3, paves the way for exploiting similar targets with enhanced efficacy. Additionally, the antibiotic Thiostrepton has also been considered as a promising potential inhibitor molecule as trypanocidal drug within the frame of drug repurposing. The results have also demonstrated a synergic effect of Thriostepton and Bz (Rivera Santiago et al.).

Here, the role of ivermectin as a potential trypanocidal drug against *T. cruzi* and other trypanosomatids was also investigated. Ivermectin, was found to affect the proliferation of different *T. cruzi* developmental stages (epimastigotes, amastigotes, and trypomastigotes) in a dose-dependent manner. At 50 µM, the drug had a trypanostatic effect on the epimastigote stage, while at 100 µM, it exhibited trypanocidal effects. Moreover, combination treatment of ivermectin with Bz or Nx demonstrated important synergistic effects (Fraccaroli et al.).This pan-stage targeted coverage of ivermectin against *T. cruzi* is without doubt a promising finding that would allow the potential to treat ChD all across its clinical spectrum, which are governed by different life cycle stages of the parasite.

A related paper to this topic explored the role of Na^+/Ca^{2+} exchange (NCX) in C57BL/6 *T. cruzi* Y strain infected mice. Two NCX blockers, KB-R7943 and YM-244769, were found to reduce diastolic Ca^{2+} concentration ($[Ca^{2+}]_d$) in cardiomyocytes during the early acute, acute, and chronic phases, and prevented the increase in ($[Ca^{2+}]_d$) associated with exposure to a Na^+-free solution. These findings suggest that Ca^{2+}entry through NCX in reverse mode plays a significant role in the observed disrupted [Ca2+]d homeostasis in infected cardiomyocytes. Furthermore, NCX inhibitors may be a viable therapeutic approach for treating patients with ChD cardiomyopathy, thus improving therapeutic options for the disease (Lopez et al.).

Another important aspect of ChD pathogenesis relates to immunity against the parasite. The immune response to *T. cruzi* is complex and involves action of both, the innate and adaptive immune components. However, within the promising approaches currently being developed for ChD therapy, immunomodulatory drugs and compounds play an important role, and some have already shown to enhance the immune response to *T. cruzi* and promoting parasite clearance. Along these lines, this collection also includes several pieces dealing with important aspects not only on the innate and adaptive immune responses responsible for controlling infection and preventing disease progression, but also on the potential immunomodulatory effects of several compounds such as PepA and fenofibrate.

For example, the synthetic peptide, PepA, containing the CTHRSSVVC sequence, is a mimicker of the CD163 and TNF-α tripeptide "RSS" motif, which binds to atheromatous plaques in carotid biopsies of human patients, spleen tissues, as well as low-density lipoprotein receptor knockout (LDLr−/−) mouse model of atherosclerosis. Here, the potential theranostic role of PepA was investigated by studying its effect on experimental models of *T. cruzi* infection both *in vitro* and *in vivo*. Findings of this study demonstrated that PepA and PepB, a peptide with a random sequence, reduced the intracellular parasitism of peritoneal mouse macrophages but were inactive during cardiac cell infection. However, PepA and PepB did not display trypanocidal effects on bloodstream trypomastigotes and did not exhibit *in vivo* efficacy when administered after parasite inoculation. The *in vitro* activity of PepA and PepB on the infection of peritoneal mouse macrophages by *T. cruzi* was reported, as possibly triggering the microbicidal arsenal of host professional phagocytic cells, capable of controlling parasitic invasion and proliferation (Leite et al.).

On the other hand, fenofibrate was shown to increase the population of non-classical monocytes in asymptomatic ChD patients, and to modulate inflammatory cytokines in PBMCs. Chronic ChD cardiomyopathy is the most relevant clinical manifestation of ChD infection. In previous studies, fenofibrate, a PPARα agonist, has shown to control inflammation, prevent fibrosis, and improve cardiac function in a murine infection model. In the current study, the authors investigated the spontaneous release of inflammatory cytokines and chemokines, changes in the frequencies of monocyte subsets, and the effects of fenofibrate on PBMCs of seropositive patients amongst different clinical stages of ChD. Their findings suggest a potential therapeutic role for fenofibrate as a modulator of monocyte subpopulations towards an anti-inflammatory profile in different stages of chronic ChD (Pieralisi et al.). Also, regarding the role of the complement system in the modulation of T-cell responses in chronic Chagas disease a minireview has been presented in this Topic (Albareda et al.).

Drug discovery, remains an important component in the quest for ChD therapy. An example of a most recent breakthrough was the discovery of the orally active benzoxaborole prodrugs which have proved effective not only against the parasite but against the various *T. cruzi* lineages (DTUs) described to date (Kingwell, 2022; Padilla et al., 2022). In this collection, an interesting *in silico* work by Ros-Lucas et al., used the AlphaFold Protein Structure Database, which homes 19,036 protein models from *T. cruzi*, to demonstrate not only key functions on describing new therapeutic approaches, but also to shed light on molecular mechanisms of action for known compounds. In what they call "proof-of-concept study", they screened the AlphaFold *T. cruzi* set of predicted protein models to find prospective targets for a pre-selected list of compounds with known anti-trypanosomal activity using docking-based inverse virtual screening. The results obtained in this work provide insight into the mechanisms of action of the compounds and their targets, and points to new strategies to finding novel compounds or optimize already existing ones.

Understanding the physio-pathological substrates of disease is of extreme importance to understand how components of the innate immune and adaptive immune system intervene and modulate disease progression. Here, Caputo et al. explore the intricacies of the interaction between the complement system and the T cell response and discuss on the potential role that anaphylatoxins (C3a and C5a) might play in T cell responses during chronic human *T. cruzi* infection. Also herein, Rodrigues Ferreira et al. also discuss on the role that transforming growth factor beta (TGF-β) signaling pathway on *T. cruzi*-infection and its biological implications. The authors found that addition of the 1D11 monoclonal antibody to cardiac cells greatly reduced *T. cruzi* cardiomyocyte invasion. In addition, the authors also demonstrated most importantly that treatment with 1D11 reduced cardiac fibrosis and reversed electrical abnormalities improving cardiac performance. The latter finding is of utmost importance, because it validates a two-target approach in treating the disease, not only by directly reducing parasitemia but also by modulating host component promoting tissue repair. This "killing two birds with one stone" strategy is also the mainstay for Amiodarone's' broad mechanism of action in treating Chagas cardiomyopathy (Benaim and Paniz Mondolfi, 2012).

Amiodarone acts through a dual mechanism of action, not only aiding in the recovery of cardiac function but also by exerting specific anti-*T. cruzi* effects, based on the drugs ability to disrupt the parasite's Ca^{2+} homeostasis, claimed to be an important target of drug action in these parasites (Benaim et al., 2020) and by blocking *de novo* ergosterol biosynthesis in its membrane (Benaim et al., 2006). Additionally, amiodarone promotes cardiac cell recovery by inducing reassembling of cytoskeleton elements and re-establishing essential gap protein communication such as connexin 43 between myocardiocytes, which are essential to re-establish cardiac contractility and control arrythmogenic events (Adesse et al., 2008; Adesse et al., 2011). This is why Amiodarone remains as the archetype examples of drug repurposing in ChD given its dual role, not only as an antiarrhythmic drug, but also as an antiparasitic agent (Benaim and Paniz Mondolfi, 2012).

Chagas disease (ChD) remains a major public health concern in Latin America, where it is endemic, and its prevalence is expanding globally, including the United States. The limited treatment options for ChD, based on the old nitroimidazole and nitrofuran derivatives Benznidazole (Bz) and Nifurtimox (Nx), have significant limitations in terms of efficacy, side effects, and duration of the treatment. There is an urgent need for novel drugs and therapeutic strategies to improve the efficacy and safety profile of ChD therapy. The

collection of studies presented here highlights several promising approaches, including drug repurposing and combination therapy, targeting ergosterol synthesis inhibitors, benzofuran derivatives, mitochondrial *T. cruzi* peroxiredoxin and the use of macrocyclic lactones (ivermectin) and the alkylphosphocholine drug Miltefosine as potential therapeutic agents. We also emphasize on the role of key innate and adaptive immune components, as well as the immunomodulatory effects of Fenofibrate and potential for monoclonal antibody therapy. These approaches, along with others presented here, offer hope to those affected by this neglected infectious disease.

Author contributions

VG has contributed editing 8 articles. AM edited 3 articles. GB has contributed to the edition of 2 articles. The contribution among co-editors has been interactive during the whole process. All authors contributed to the article and approved the submitted version.

Acknowledgments

We acknowledge to CONICET and INP, "Dr.Mario Fatala Chaben",ANLIS-Malbrán, National Health Department, Argentina; to Molecular Microbiology Laboratory, Department of Pathology, Molecular and Cell-Based Medicine, Icahn School of Medicine at Mount Sinai. from New York, USA. to IIVC/IDB, Unidad de Señalización Celular y Bioquímica de Parásitos, Instituto de Estudios Avanzados e Instituto de Biología Experimental. Facultad de Ciencias. Universidad Central de Venezuela, and to FONACIT, Fondo Nacional de Ciencia, Tecnología e Innovación, Venezuela.

Conflict of interest

The authors declare that the research was conducted in the absence of any commercial or financial relationships that could be construed as a potential conflict of interest.

Publisher's note

References

Adesse, D., Azzam, E. M., Meirelles Mde, N., Urbina, J. A., and Garzoni, L. R. (2011). Amiodarone inhibits *Trypanosoma cruzi* infection and promotes cardiac cell recovery with gap junction and cytoskeleton reassembly *in vitro*. *Antimicrob. Agents Chemother.* 55 (1), 203–210. doi: 10.1128/AAC.01129-10

Adesse, D., Garzoni, L. R., Huang, H., Tanowitz, H. B., de Nazareth Meirelles, M., and Spray, D. C. (2008). *Trypanosoma cruzi* induces changes in cardiac connexin43 expression. *Microbes Infect.* 10 (1), 21–28. doi: 10.1016/j.micinf.2007.09.017

Adesse, D., Azzam, E. M., Meirelles Mde, N., Urbina, J. A., and Garzoni, L. R. (2011). Amiodarone inhibits Trypanosoma cruzi infection and promotes cardiac cell recovery with gap junction and cytoskeleton reassembly in vitro. *Antimicrob Agents Chemother.* 55 (1), 203-10. doi: 10.1128/AAC.01129-10

Almeida-Silva, J., Silva Menezes, D., Pereira Fernandes, J. M., Cerqueira Almeida, M., Vasco-Dos-Santos, D. R., Magalhães Saraiva, R., et al. (2022). The repositioned drug disulfiram combined to benznidazole for chagas disease therapy: search for selectivity, precluding toxicity and drug resistance. *Front. Cell Infect. Microbiol.* 12. doi: 10.3389/fcimb.2022.926699

Benaim, G., and Paniz Mondolfi, A. E. (2012). The emerging role of amiodarone and dronedarone in chagas disease. *Nat. Rev. Cardiol.* 9 (10), 605–609. doi: 10.1038/nrcardio.2012.108

Benaim, G., Paniz-Mondolfi, A. E., and Sordillo, E. M. (2021). Rationale for use of amiodarone and its derivatives for treatment of chagas' disease and leishmaniasis. *Curr. Pharmac. Design.* 27, 1825–1833. doi: 10.2174/1381612826666200928161403

Benaim, G., Paniz-Mondolfi, A. E., Sordillo, E. M., and Martinez-Sotillo, N. (2020). Disruption of intracellular calcium homeostasis as a therapeutic target against *Trypanosoma cruzi*. *Front. Cell. Infect. Microbiol.* 10. doi: 10.3389/fcimb.2020.00046

Benaim, G., Sanders, J. M., Garcia-Marchán, Y., Colina, C., Lira, R., Caldera, A. R., et al. (2006). Amiodarone has intrinsic anti-trypanosoma cruzi activity and acts synergistically with posaconazole. *J. Med. Chem.* 49 (3), 892–899. doi: 10.1021/jm050691f

Croft, S. L., Snowdon, D., and Yardley, V. (1996). The activities of four anticancer alkyllysophospholipids against leishmania donovani, *Trypanosoma cruzi* and *Trypanosoma brucei*. *J. Antimicrob. Chemother.* 38, 1041–1047. doi: 10.1093/jac/38.6.1041

Duschak, V. G. (2011). A decade of targets and patented drugs for chemotherapy of chagas disease. *Recent Pat. Antiinfect Drug Discov.* 6, 216–259. doi: 10.2174/157489111796887864

Duschak, V. G. (2016). Targets and patented drugs for chemotherapy of chagas disease in the last 15 years-period. *Recent patents anti-infective Drug Discov.* 11 (2), 74–173. doi: 10.2174/1574891X11666161024165304

Duschak, V. G. (2017). Advances in the neglected chagas disease: drug targets and trypanocide compounds. *Curr. Trends Biomed. Eng. Biosci.* 6, 5556–5560. doi: 10.2174/1574891X11666161024165304

Duschak, V. G. (2019). Major kinds of drug targets in chagas disease or American trypanosomiasis. *Curr. Drug Targets* 20 (11), 1203–1216. doi: 10.2174/1389450120666190423160804

Higuera, S. L., Guhl, F., and Ramírez, J. D. (2013). Identification of trypanosoma cruzi discrete typing units (DTUs) through the implementation of a high-resolution melting (HRM) genotyping assay. *Parasit Vectors* 6, 112. doi: 10.1186/1756-3305-6-112

Kingwell, K. (2022). New therapeutic candidate for chagas disease. *Nat. Rev. Drug Discov.* 21 (11), 796. doi: 10.1038/d41573-022-00168-1

Madigan, R., Majoy, S., Ritter, K., Luis Concepción, J., Márquez, M. E., Silva, S. C., et al. (2019). Investigation of a combination of amiodarone and itraconazole for treatment of American trypanosomiasis (Chagas disease) in dogs. *J. Am. Vet. Med. Assoc.* 255 (3), 317–329. doi: 10.2460/javma.255.3.317

Padilla, A. M., Wang, W., Akama, T., Carter, D. S., Easom, E., Freund, Y., et al. (2022). Discovery of an orally active benzoxaborole prodrug effective in the treatment of chagas disease in non-human primates. *Nat. Microbiol.* 7 (10), 1536–1546. doi: 10.1038/s41564-022-01211-y

Paniz Mondolfi, A. E., Madigan, R., Perez-Garcia, L., and Sordillo, E. M. (2020). Chagas disease endemism in the united states. *Clin. Infect. Dis.* 70 (4), 717–718. doi: 10.1093/cid/ciz465

Pinto-Martinez, A., Rodriguez-Durán, J., Serrano-Martin, X., Hernandez-Rodriguez, V., and Benaim, G. (2018). Mechanism of action of miltefosine on *Leishmania donovani* involves the impairment of acidocalcisome function and the activation of the sphingosine-dependent plasma membrane Ca^{2+} channel. *Antimicrob. Agents Chemother.* 62, 1–10.

Rodriguez-Duran, J., Pinto-Martinez, A., Castillo, C., and Benaim, G. (2019). Identification and electrophysiological properties of a sphingosine-dependent plasma membrane Ca2+ channel in *Trypanosoma cruzi*. *FEBS J.* 286, 3909–3925. doi: 10.1111/febs.14947

Urbina, J. A., Payares, G., Contreras, L. M., Liendo, A., Sanoja, C., Molina, J., et al. (1998). Antiproliferative effects and mechanism of actionof SCH 56592 against *Trypanosoma (Schizotrypanum) cruzi: in vitro* and *in vivo* studies. *Antimicrob. Agents Chemother.* 42, 1771–1777. doi: 10.1128/AAC.42.7.1771

frontiers in Cellular and Infection Microbiology

ORIGINAL RESEARCH
published: 11 March 2022
doi: 10.3389/fcimb.2021.785166

Fenofibrate Increases the Population of Non-Classical Monocytes in Asymptomatic Chagas Disease Patients and Modulates Inflammatory Cytokines in PBMC

Azul V. Pieralisi[1,2], Ágata C. Cevey[1,2†], Federico N. Penas[1,2†], Nilda Prado[3], Ana Mori[3], Mónica Gili[4], Gerardo A. Mirkin[1,5], Juan Gagliardi[3] and Nora B. Goren[1,2]*

[1] Universidad de Buenos Aires. Facultad de Medicina. Departamento de Microbiología, Parasitología e Inmunología, Buenos Aires, Argentina, [2] CONICET Universidad de Buenos Aires. Instituto de Investigaciones Biomédicas en Retrovirus y SIDA (INBIRS), Buenos Aires, Argentina, [3] Division of Cardiology, Hospital del Gobierno de la Ciudad de Buenos Aires "Dr. Cosme Argerich", Buenos Aires, Argentina, [4] Hospital Municipal de Rehabilitación Respiratoria María Ferrer, Buenos Aires, Argentina, [5] CONICET Universidad de Buenos Aires. Instituto de Investigaciones en Microbiología y Parasitología Médica (IMPaM), Buenos Aires, Argentina

OPEN ACCESS

Edited by:
Vilma G Duschak,
Consejo Nacional de Investigaciones Científicas y Técnicas (CONICET), Argentina

Reviewed by:
Santiago Partida Sanchez,
Nationwide Children's Hospital, United States
Chiranjib Pal,
West Bengal State University, India

***Correspondence:**
Nora B. Goren
ngoren@fmed.uba.ar

[†]These authors have contributed equally to this work

Specialty section:
This article was submitted to Parasite and Host, a section of the journal Frontiers in Cellular and Infection Microbiology

Received: 28 September 2021
Accepted: 10 December 2021
Published: 11 March 2022

Citation:
Pieralisi AV, Cevey ÁC, Penas FN, Prado N, Mori A, Gili M, Mirkin GA, Gagliardi J and Goren NB (2022) Fenofibrate Increases the Population of Non-Classical Monocytes in Asymptomatic Chagas Disease Patients and Modulates Inflammatory Cytokines in PBMC. Front. Cell. Infect. Microbiol. 11:785166. doi: 10.3389/fcimb.2021.785166

Chronic Chagas disease cardiomyopathy (CCC) is the most important clinical manifestation of infection with *Trypanosma cruzi* (*T. cruzi*) due to its frequency and effects on morbidity and mortality. Peripheral blood mononuclear cells (PBMC) infiltrate the tissue and differentiate into inflammatory macrophages. Advances in pathophysiology show that myeloid cell subpopulations contribute to cardiac homeostasis, emerging as possible therapeutic targets. We previously demonstrated that fenofibrate, PPARα agonist, controls inflammation, prevents fibrosis and improves cardiac function in a murine infection model. In this work we investigated the spontaneous release of inflammatory cytokines and chemokines, changes in the frequencies of monocyte subsets, and fenofibrate effects on PBMC of seropositive patients with different clinical stages of Chagas disease. The results show that PBMC from Chagas disease patients display higher levels of IL-12, TGF-β, IL-6, MCP1, and CCR2 than cells from uninfected individuals (HI), irrespectively of the clinical stage, asymptomatic (Asy) or with Chagas heart disease (CHD). Fenofibrate reduces the levels of pro-inflammatory mediators and CCR2 in both Asy and CHD patients. We found that CHD patients display a significantly higher percentage of classical monocytes in comparison with Asy patients and HI. Besides, Asy patients have a significantly higher percentage of non-classical monocytes than CHD patients or HI. However, no difference in the intermediate monocyte subpopulation was found between groups. Moreover, monocytes from Asy or CHD patients exhibit different responses upon stimulation *in vitro* with *T. cruzi* lysates and fenofibrate treatment. Stimulation with *T. cruzi* significantly increases the percentage of classical monocytes in the Asy group whereas the percentage of intermediate monocytes decreases. Besides, there are no changes in their frequencies in CHD or HI. Notably, stimulation with *T. cruzi* did not modify the frequency of the non-classical monocytes

subpopulation in any of the groups studied. Moreover, fenofibrate treatment of *T. cruzi*-stimulated cells, increased the frequency of the non-classical subpopulation in Asy patients. Interestingly, fenofibrate restores CCR2 levels but does not modify HLA-DR expression in any groups. In conclusion, our results emphasize a potential role for fenofibrate as a modulator of monocyte subpopulations towards an anti-inflammatory and healing profile in different stages of chronic Chagas disease.

Keywords: fenofibrate, chronic Chagas disease, inflammation, monocyte subsets, cytokine

INTRODUCTION

The acute phase of *Trypanosoma cruzi* (*T. cruzi*) infection is characterized by the presence of parasites in the host bloodstream that disseminate to the heart and other organs. This promotes a severe inflammatory response with recruitment of mononuclear cells, activation of resident macrophages, and release of pro-inflammatory mediators. This response is associated with parasite persistence in the heart and other tissues, due to the fact that the immune response is not efficient to wipe out the infection, leading to lifelong infection (Trachtenberg and Hare, 2017). Therefore, it goes forward to a chronic stage with a wide spectrum of manifestations, ranging from minor myocardial involvement to chronic Chagas disease cardiomyopathy (CCC) in which the tropism of the parasite for cardiac tissue constitutes one of the factors that lead to cardiac pathology (Tanowitz et al., 2015). Moreover, inflammatory processes also promote heart muscle fibrosis. Consequently, infected individuals may undergo heart chamber remodeling, congestive heart failure, and eventually death. Likewise, the persistence of activated macrophages in the tissues may create an inflammatory microenvironment that, in turn, contributes to developing tissue damage during the course of these pathological processes (Rőszer et al., 2013).

It has been described that, in response to infection with *T. cruzi*, cardiomyocytes and macrophages release nitric oxide (NO), cytokines and chemokines that are important to control parasite proliferation (Petray et al., 1994). However, the excess of these mediators generates harmful effects, contributing to the pathogenesis of chronic CCC (Machado et al., 2000; Gutierrez et al., 2009; Hovsepian et al., 2011; Penas et al., 2013).

Monocytes are heterogeneous, multifunctional cells that participate in cellular processes, namely, tissue repair and regeneration during heart diseases (Apostolakis et al., 2010). Advances in pathophysiology demonstrate that some subpopulations of myeloid cells contribute to cardiac homeostasis (Bajpai et al., 2018). Monocytes may differentiate into tissue-resident macrophages in specific microenvironmental conditions (Guilliams and Scott, 2017). Currently, the circulating human monocytic cells can be divided into subpopulations based on the surface expression of CD14 (a cell co-receptor for LPS) and CD16 (the low-affinity IgG receptor). They are further divided into three major subsets: a high percentage of monocytes, named classical monocytes, are $CD14^{++}$ $CD16^{-}$ but, to a lesser extent we find two other subpopulations, such as $CD14^{++}$ $CD16^{+}$, intermediate monocytes, and $CD14^{+}$ $CD16^{++}$, which are non-classical monocytes (Wong et al., 2011). Human peripheral blood monocytes are also defined by the expression of the cell surface markers CD64 (Fcγ RI) and the chemokine receptor CD192 (also known as CCR2, a key mediator of monocyte migration) whose most prominent role is the mobilization of monocytes under physiologic and also inflammatory conditions. Besides, monocyte subpopulations can be characterized according to different levels of human leukocyte antigen D related (HLA-DR) (Shi, 2014).

CCR2 was first identified on monocytes, which constitutively express the receptor, and is dowregulated after differentiation into macrophages (Fantuzzi et al., 1999). Particularly, CCR2 plays important roles in tissue recruitment and transmigration of monocytes through the endothelial layer under inflammatory conditions. After myocardial injury, $CCR2^{-}$ macrophages promote the regeneration of cardiac tissue and functional recovery of the heart, through expansion of the coronary vasculature and physiological proliferation of cardiomyocytes (Lavine et al., 2014; Leid et al., 2016). The resident macrophage population was shown to expand in response to cardiac injury by participating in the immune surveillance of this tissue, which raises important questions about the fate and function of macrophages during the development of heart failure (Epelman et al., 2014; Heidt et al., 2014). On the other hand, the recruitment of monocytes, their differentiation into macrophages and their activation have a causal role in ventricular dysfunction (Hulsmans et al., 2018) and fibrosis (Sica et al., 2014; Satoh et al., 2017).

Like in many other situations, monocytes/macrophages as innate immune cells recognize *T. cruzi* pathogen-associated molecular patterns (PAMPs) and activate lymphocytes and the adaptive immune response during Chagas disease (Teixeira et al., 2011; Andrade and Gollob KJ, 2014). It has been shown that individuals infected with *T. cruzi*, with severe heart disease, display a profile of subsets of monocytes that suggests a more pronounced inflammatory environment compared with patients with heart failure unrelated to *T. cruzi* infection (Pérez-Mazliah et al., 2018). Besides, it was reported that the intermediate monocyte subpopulation is associated with CCC (Gómez-Olarte et al., 2019). On the other hand, it has been proposed that monocytes play a role as immunoregulators in asymptomatic Chagas disease patients by activating lymphocytes and, thus, the adaptive immunity through the expression of the co-stimulatory molecules CD80 and CD86.

Indeed, the expression of the latter was associated with a higher frequency of Treg cells in asymptomatic individuals (Pinto et al., 2018).

Peroxisome proliferator-activated receptors (PPARs), members of the steroid hormone receptor superfamily, are ligand-dependent nuclear transcription factors. Fenofibrate, a PPAR-α ligand, is a third-generation fibric acid derivative currently used clinically as a hypolipidemic agent to lessen the risk of atherosclerosis (Ling and Luoma, 2013). More than two decades ago, it was shown that PPARs and their ligands can repress inflammatory genes in activated monocytes and macrophages (Ricote et al., 1998; Tontonoz et al., 1998). However, the role of the PPARα receptors and their ligands on cardiac remodeling, repair and functionality exerted by monocytes/macrophages in the context of infection with *T. cruzi* has not been extensively studied. The efficacy of PPARα agonists, including fenofibrate, as regulators of inflammation and remodeling of the extracellular matrix of the heart has been reported (Lockyer et al., 2010). Fenofibrate has been shown to be able to prevent cardiac inflammation and fibrosis in diabetic mice (Zhang et al., 2016). Furthermore, it has been shown to exert cardioprotective effects against various cardiac disorders, namely, *in vivo* models of cardiac hypertrophy produced by pressure overload (Zou et al., 2013) or experimental autoimmune myocarditis in rats (Cheng et al., 2016) and also in patients with systolic dysfunction (Yin et al., 2013) or experimental myocardial infarction (Garg et al., 2016). Due to its ability to prevent interstitial and perivascular fibrosis in kidney, liver, lung and heart in different experimental models, fenofibrate has recently been proposed as a potential antifibrotic agent (McVicker and Bennett, 2017).

In previous studies, our group developed an experimental model of Chagas disease, in which mice were sequentially infected with two *T. cruzi* strains, which differ in genetic background and lethality, leading to clear signs of left ventricular dysfunction. In this model, we show that fenofibrate controls inflammation, prevents fibrosis, and improves heart function (Cevey et al., 2017). Furthermore, PPAR agonists contribute to neovascularization and redirect pro-inflammatory to healing macrophages in experimental trypanosomiasis (Penas et al., 2013; Penas et al., 2015; Cevey et al., 2016; Garg et al., 2016; Penas et al., 2016; Cevey et al., 2017; McVicker and Bennett, 2017; Penas et al., 2017; Rada et al., 2020).

Consequently, the aim of this work was to characterize the monocyte populations of patients in different phases of CCC and to study the effect of fenofibrate on these cells in culture. This would allow identifying possible therapeutic targets promoting fenofibrate as a coadjuvant to anti-parasitic treatment.

MATERIALS AND METHODS

Ethics Statement

Informed consent was signed by each subject. The study protocol is in line with the ethical guidelines of the Declaration of Helsinki and was approved by the Ethics Committee of the "Hospital General de Agudos Dr. Cosme Argerich" and of the "Hospital Municipal de Rehabilitación Respiratoria María Ferrer", Buenos Aires, Argentina.

Study Cohort

Subjects were recruited at the Cardiology Department of both Hospital General de Agudos Dr. Cosme Argerich and Hospital Municipal de Rehabilitación Respiratoria MaríaFerrer (Ciudad Autónoma de Buenos Aires, Argentina).

Inclusion Criteria

Men and women between 18 and 60 years, with positive serology for Chagas disease were included. Each seropositive participant underwent a clinical and cardiological evaluation to determine the clinical stage of the disease. The classification of patients was carried out according to the Chagas Consensus (Healthy or Chagas Stage 0, I, II, and III) in accordance with the criteria of the Argentine Society of Cardiology (Mitelman, 2011). In this work and consistent with this classification, we named the different groups according to the absence of symptoms (Asy) or the presence of any cardiac damage (CHD). Control group included healthy individuals (HI), men and women between 18 and 60 years, with negative serology for Chagas disease. None of the subjects should have co-morbidities at the time of sample collection, nor have received previous treatment for Chagas disease nor with lipid-lowering agents from the group of fibrates or statins.

Peripheral Blood Mononuclear Cells (PBMC) Isolation

Whole blood (10 to 15 ml) was collected from participants by venipuncture into heparinized tubes (Vacutainer, BD Biosciences). Plasma was obtained by centrifugation and stored at −80°C. Peripheral blood mononuclear cells (PBMC) were isolated by Ficoll–Paque™ PLUS density gradient centrifugation (GE Healthcare, Amersham, Sweden). PBMC were washed twice and suspended in complete culture medium: RPMI 1640 (Invitrogen Life Technologies, Grand Island, NY, USA) supplemented with fetal bovine serum (FBS) 10% (Internegocios S.A., Argentina) and antibiotics (50 μg/ml of PenStrep®). All experiments were performed using freshly isolated PBMC.

T. cruzi Culture and Lysate

Vero cells were cultured in cell culture flasks of 175 cm^2 with RPMI supplemented with 10% fetal bovine serum (FBS), 100 IU/ml Penicillin, 0.1 mg/ml Streptomycin and 2 mM L-glutamine. When culture reached an approximate 50% confluence, it was infected with parasites of the RA strain of *T. cruzi*. After 6 h, the cells were washed with fresh culture medium to remove non-infective parasites and incubated at 37°C for 48 h.

On day 5 post-infection (dpi), trypomastigotes were harvested from the supernatant. The culture medium was collected, two washes were performed with cold PBS and then it was centrifuged at 18,000×*g* at 4°C for 5 min. The parasite pellet was stored at −80°C. After one month of collection, all sediments were pooled and lysed to obtain trypomastigote proteins. Briefly, sediments were resuspended in lysis buffer (PBS, 10 μM E-64 and 3 μg/ml protease inhibitor) and subjected to 3 freeze/thaw cycles (−80°C/room temperature) of

30 min each. Then, it was incubated overnight at −80°C and centrifuged at 17,000×*g* at 4°C for 10 min. Supernatant was collected, and the protein concentration was quantified by the Bradford method using a commercial protein assay (Bio-Rad, USA) and bovine serum albumin (BSA) (Sigma-Aldrich Co, USA) as a standard (Kruger, 1994) as described previously by our group (Cevey et al., 2019; Penas et al., 2020; Rada et al., 2020).

In Vitro Treatments

According to the experiment, cells were pre-treated for 15 min with 100 μM Fenofibrate® (Daunlip®, Montpellier S.A, Argentina. PubChem Compound Database CID = 3339, Fen) resuspended in PBS (Cevey et al., 2017). Then, cells were stimulated or not with *T. cruzi* lysate (10 μg/ml) for 20 h.

Flow Cytometry

This experiment included 17 healthy individuals, 7 asymptomatic patients with positive serology for Chagas disease and 9 with Chagas heart disease. Cells from all experimental groups were cultured for 16–20 h after treatment.

PBMC were stained with LIVE/DEAD™ fixable dye (Invitrogen) at room temperature for 15 min and labeled with the following antibodies at 4°C for 30 min: CD14 (#E-AB-F1209C, Elabscience), CD16 (#E-AB-F1005M, Elabscience), HLA-DR (#E-AB-F1111H, Elabscience), and CCR2 (#357209, Elabscience). Then, cells were washed, fixed and acquired using a FACS Canto (Becton Dickinson). Post-acquisition analysis was performed using FlowJo version 10 software (FlowJo LLC, Ashland, Oregon, USA). In all cases, isotype-matched mAb were used as controls.

Gating Strategies

Peripheral blood mononuclear cells (PBMC) were gated based on forward scatter (FSC) and side scatter (SSC) parameters. After excluding doublets and debris using FSC-Width *vs*. FSC-Area, the strategy used to differentiate the three subsets of monocytes was based on CD14 and CD16 expression: classical (CD14high/CD16neg), intermediate (CD14high/CD16pos) and non-classical (CD14low/CD16pos) monocytes. Then, in both total monocytes and subpopulations, the percentage (%) and mean fluorescence intensity (MFI) of the membrane markers CCR2 and HLA-DR was calculated. The MFI was calculated as the geometric mean of the expression.

RNA Purification

Total RNA was obtained from PBMC using Quick-zol reagent (Kalium Technologies, Argentina), treated with RQ1 RNase-Free DNase (PromegaCo., USA). Total RNA was reverse-transcribed using M-MLV Reverse Transcriptase (Promega Co., USA), according to manufacturer's instructions as described previously by our group (Cevey et al., 2019; Penas et al., 2020; Rada et al., 2020).

Quantitative Reverse Transcription Polymerase Chain Reaction (RT-qPCR)

mRNA expression was performed using 5× HOT FIREPOL EVAGREEN qPCR (SolisBioDyne, Estonia) in a StepOnePlus Real-Time PCR System. Parameters were: 52°C for 2 min, 95°C for 15 min, and 40 cycles at 95°C for 15 s, specific Tm °C for 30 s and 72°C for 1 min. Normalization was carried out using β-Actin mRNA. Quantification was performed using the comparative threshold cycle (Ct) method, as all the primer pairs (target gene/reference gene) were amplified using comparable efficiencies (relative quantity, $2^{-\Delta\Delta Ct}$) (Schmittgen and Livak, 2008; Bustin et al., 2009). To evaluate the expression of inflammatory mediators in the PBMC of both the asymptomatic (Asy) and cardiac (CHD) patient groups, the PBMC of healthy individuals (HI) were used as reference control (**Figure 1**). On the other hand, to study the effects of fenofibrate treatment *in vitro*, on the expression of inflammatory mediators in PBMC of Asy and CHD patients, PBMC samples from each patient not treated with fenofibrate were taken as reference controls (**Figure 2**). mRNA expression of IL-12, TGF-β, IL-6 and MCP-1 was measured in 20 healthy individuals, 13 asymptomatic patients and 28 cardiac patients. CCR2 mRNA expression was measured in 6 healthy individuals, 4 asymptomatic patients and 5 cardiac patients.

Primer Sequences

	Forward (5'-3')	Reverse (5'-3')
IL-12	CTCCTGGACCACCTCAGTTT	TGGTGAAGGCATGGGAACAT
TGF-β	ATGGAGAGAGGACTGCGGAT	TGGTCCCCTGTCCTATGA
IL-6	TATTAGAGTCTCAACCCCCAATAAA	ACCAGGCAAGTCTCCTCATT
MCP-1	CTCTCGCCTCCAGCATGAAA	CTTGAAGATCACAGCTTCTTTGG
CCR2	CATTAGTTGCCCTGTATCTC	ATGCGTCCTTGTTCAATCC
β-Actin	GTGGGGCGCCCCAGGCACCA	CGGTTGGCCTTGGGGTTCAGGGGG

Statistical Analysis

Different statistical tests were used for this work. To compare baseline cytokine mRNA expression between healthy donors, asymptomatic or Chagas heart disease patients, nonparametric Kruskal–Wallis test, and then the Dunn´s multiple comparisons test were performed. For the study of the effect of fenofibrate in mRNA expression, a non-parametric Wilcoxon test was used for paired samples. Mixed-effects model analysis was performed to analyze differences between experimental groups in flow cytometry assays. The Tukey *post-hoc* test was performed to compare every mean with every other mean. Differences were considered statistically significant when $P < 0.05$. All analyses were performed using the Prism 7.0 Software.

RESULTS

Cohort Characteristics of Chagas Disease Patients

Table 1 shows clinical and electrocardiographic findings in the cohort of Chagas disease patients under study. They were classified according to the absence of symptoms (Asy) or the

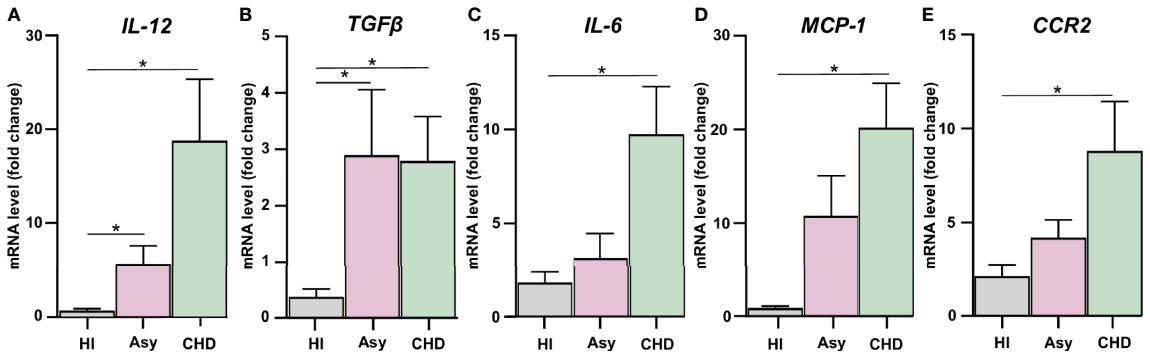

FIGURE 1 | Assessment of the expression of pro-inflammatory mediators and CCR2. Expression of IL-12 **(A)**, TGF-β **(B)**, IL-6 **(C)**, MCP-1 **(D)**, and CCR2 **(E)** were determined by RT-qPCR in PBMC of healthy individuals (HI), seropositive asymptomatic (Asy) or Chagas heart disease (CHD) after 48 h of culture. mRNA expression was analyzed and normalized against β-Actin. Results are expressed as the mean of 3 independent experiments. Differences between groups were analyzed by Kruskal–Wallis test (mean ± SEM) followed by Dunn's *post hoc* test. *P < 0.05. PBMC of Asy or CHD vs. PBMC of HI.

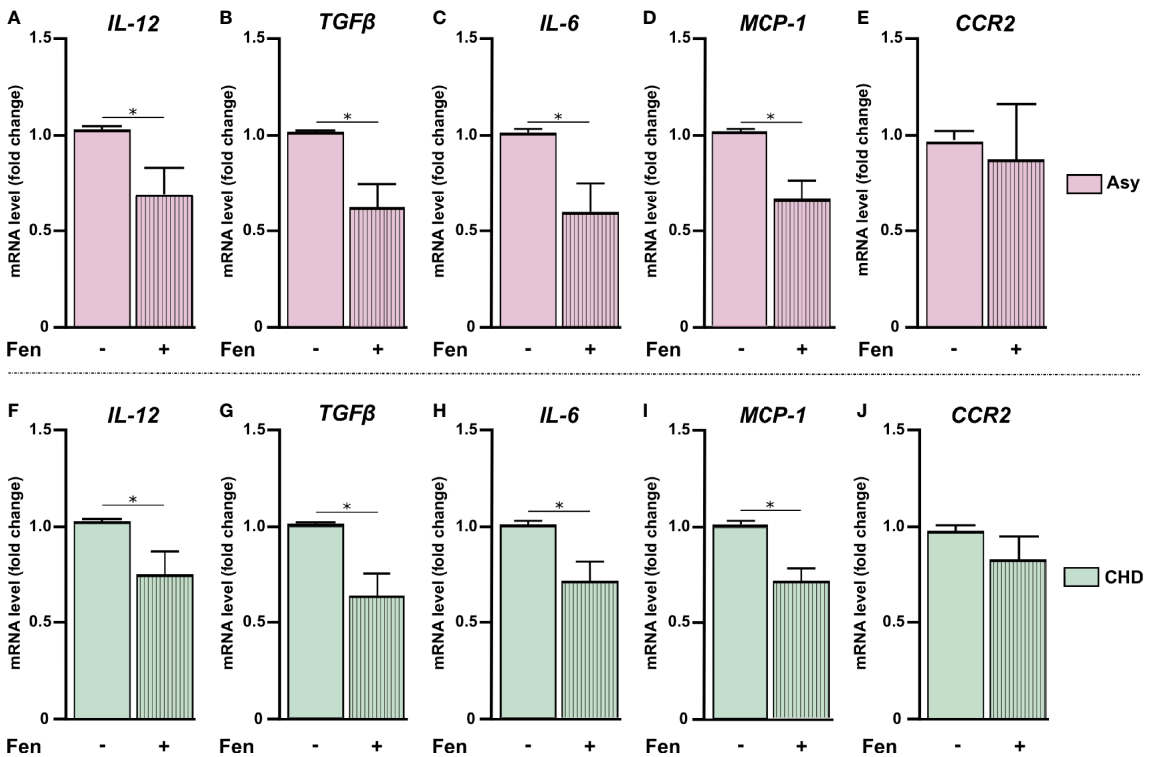

FIGURE 2 | Fenofibrate modulates pro-inflammatory mediators' expression. PBMC were treated *in vitro* or not with 100 μM of fenofibrate. After 48 h, IL-12, TGF-β, IL-6, MCP-1, and CCR2 mRNA was measured in asymptomatic (Asy) **(A-E)** and Chagas heart disease patients (CHD) **(F-J)**. mRNA levels were determined by RT-qPCR and normalized against β-Actin. Results are expressed as mean of 3 independent experiments. Differences between fenofibrate-treated PBMC were analyzed using the Wilcoxon test for paired samples and are shown as the mean of the experiments ± SEM. *P < 0.05. Fen-treated PBMC vs. untreated PBMC.

presence of any cardiac damage (CHD) in stage I, II, or III according to severity. Control group included healthy individuals (HI), men and women between 18 and 60 years, with negative serology for Chagas disease. Most patients were born in disease endemic areas with vectorial transmission.

Pro-Inflammatory Mediators' Expression in PBMC From Chagas Disease Patients

Groups of seropositive patients with different clinical forms for Chagas disease were included in this study, namely, with cardiomyopathy and without evidence of cardiac symptoms,

TABLE 1 | Clinical details of the study population.

Group[a]	No. of individuals	Age range (median), yr	Born in endemic areas	Clinical Finding(s)[b]	ECG finding(s)[c]
HI	23	40–81 (53)	NA	Normal	Normal/NA
Asy	19	33–75 (53)	18/19	Asymptomatic	Normal
CHD-Stage I	14	44–78 (66,5)	14/14	AV block, AF, PMK, isolated VE, DCM	LAFB, RBBB, PMK, AF
CHD-Stage II	8	31–78 (57)	8/8	NSVT with VEs, VEs, SVT, PPM with ICD, DCM	Repolarization/NA
CHD-Stage III	19	45–69 (58)	19/19	VT with ICD, AVS, AF, PMK, AV block, PPM with ICD, VEs, CHD	RBBB, PPM, LAFB, AF, AV block, LBBB, PMK

[a]*The patients were categorized as follows: healthy individuals (HI), patients with positive serology for Chagas disease but asymptomatic (Asy), and patients with chronic heart disease (CHD). The latter, separated into Stage I if there is an abnormal ECG but a normal chest X-ray, Stage II if the X-ray is also abnormal and Stage III, if there are more symptoms of heart failure.*
[b]*The main clinical findings were different arrhythmias: Atrioventricular block (AV block), atrial fibrillation (AF), pacemaker (PMK), ventricular extrasystoles (VE or VEs if frequent), dilated cardiomyopathy (DCM), no sustained ventricular tachycardia (NSVT), supraventricular tachycardia (SVT), permanent pacemaker (PPM), implantable cardioverter defibrillator (ICD), ventricular tachycardia (VT), acute vestibular syndrome (AVS) and coronary heart disease (CHD).*
[c]*ECG (electrocardiographic) findings: Left anterior fascicular block (LAFB), right bundle branch block (RBBB) and left bundle branch block (LBBB); data not available (NA).*
Endemic areas of patients: Argentinean provinces: Santiago del Estero, Chaco, Salta, Córdoba, Santa Fé, Jujuy, San Juan, Mendoza. Other countries: Bolivia and Paraguay.

and also healthy individuals. In order to evaluate whether spontaneous release of inflammatory cytokines and chemokines were differentially expressed, cultured PBMC from patients with Chagas disease were analyzed. mRNA levels of IL-12, IL-6, TGF-β, MCP-1, and CCR2 were determined by RT-qPCR, to assess the basal level production of pro-inflammatory mediators. We observed that PBMC from Chagas disease patients displayed a higher level of cytokines than cells from HI, irrespective of the clinical stage of the disease. The expression of IL-12 in PBMC of Asy patients with positive serology for Chagas but without heart disease was higher than HI. However, in patients with CHD its expression was even higher, as shown in **Figure 1A**. A similar result can be observed in the evaluation of TGF-β, since PBMC of both groups of patients show increased levels of this cytokine with respect to the values of healthy individuals (**Figure 1B**). However, when the expression of IL-6, MCP-1, and CCR2 was evaluated, we found that only PBMC from patients with heart disease displayed significantly increased levels of these cytokines in comparison with healthy individuals (**Figures 1C–E**).

Fenofibrate Reduces Inflammatory Mediator Levels in PBMC From Chagas Heart Disease Patients

We have previously reported that fenofibrate significantly reduces the extension of heart infiltrates and the expression of pro-inflammatory cytokines in a murine model of mixed-stains infection with bloodstream trypomastigotes (Cevey et al., 2017; Rada et al., 2020). In this work, we observed that pro-inflammatory mediators displayed higher levels of expression in cultured PBMC from Chagas disease patients in comparison with those of HI. In order to evaluate whether treatment with fenofibrate was able to promote a reduction of pro-inflammatory cytokines in isolated PBMC *in vitro*, we assessed the levels of mRNA expression of those mediators. We previously demonstrated, in a work by our group and in line with other studies, that 100 μM of fenofibrate is the optimal concentration at which inflammatory mediators are inhibited without affecting the viability of primary cardiomyocyte cultures (Penas et al., 2015; Nahrendorf, 2018). As shown in **Figure 2**, *in vitro* treatment of PBMC from Asy and CHD patients with 100 μM fenofibrate, reduces the levels of IL-12, TGF-β, IL-6, MCP1 in comparison with untreated cells (**Figures 2A–D, F–I**). However, CCR2 expression levels were not significantly modified in Asy or CHD patients (**Figures 2E, J**). Likewise, fenofibrate does not modify the expression of any of the studied cytokines in PBMC from healthy individuals (**Supplementary Figure S1A**).

Patients With Different Stages of Chagas Disease Display Changes in the Frequencies of Monocyte Subsets

Different subpopulations of monocytes are involved in the progression of Chagas disease cardiomyopathy. To determine whether certain monocyte subsets were particularly expressed in Chagas disease patients, according to the disease stage, the monocyte population in whole PBMC from HI, Asy and CHD patients was characterized by flow cytometry analysis (FACS), according to the expression of CD14 and CD16, as classical ($CD14^{high}$ $CD16^{neg}$), intermediate ($CD14^{high}$ $CD16^{pos}$) and non-classical ($CD14^{low}$ $CD16^{pos}$) (**Figure 3A**). **Figures 3B–D** show the effects of *T. cruzi* stimulation and treatment of PBMC with Fen, on the percentage of classical, intermediate, and non-classical monocytes from uninfected, asymptomatic and Chagas heart disease patients. The results depicted in **Figure 3B** in *T. cruzi* unstimulated and untreated cells, show a significantly higher level of classical monocytes in CHD patients in comparison with Asy. However, under the same conditions the subpopulation of intermediate monocytes, $CD14^{high}$ $CD16^{pos}$, does not show differences between CHD and Asy or HI (**Figure 3C**). Notably, *T. cruzi* unstimulated and untreated cells from Asy patients have a significantly higher percentage of non-classical monocytes than HI (**Figure 3D**).

In Vitro Stimulation With *T. cruzi* and Fenofibrate Treatment Changes the Prevalence of Monocyte Subsets According to the Stage of the Disease

We sought to determine whether monocytes from Asy or CHD patients exhibit different responses against the parasite. To this aim, purified PBMC were stimulated *in vitro* with *T. cruzi* lysates

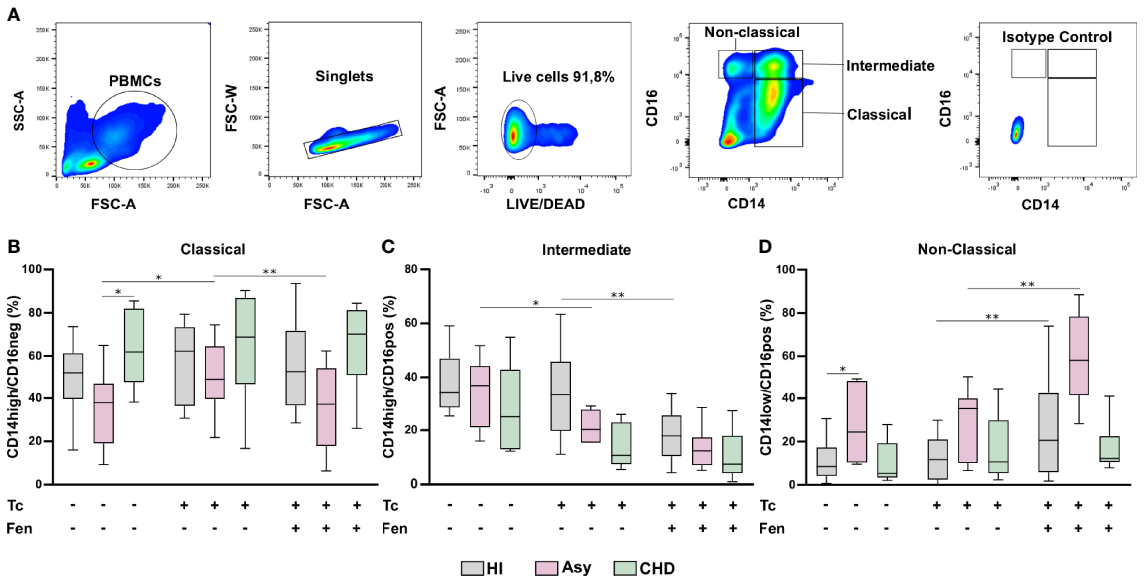

FIGURE 3 | Percentage of monocyte subpopulations in patients with Chagas heart disease (CHD), asymptomatic (Asy) and healthy individuals (HI) with/without *in vitro* treatment. A representative analysis of the gating strategy used in this study to differentiate the three monocyte subpopulations is shown **(A)**. PBMC were stimulated or not with *T. cruzi* lysate (Tc) and treated or not with fenofibrate (Tc + Fen). After 20 h according to CD14 and CD16 expression, they were classified as Classical (CD14high/CD16neg), Intermediate (CD14high/CD16pos) and Non-Classical (CD14low/CD16pos). Percentage of classical **(B)**, intermediate **(C)** and non-classical **(D)** monocytes for HI, Asy and CHD unstimulated, stimulated with Tc lysate and with Tc lysate + Fen treatment. These data were analyzed by fitting a mixed model with a Tukey *post-hoc* test and the results are expressed as the mean of the experiments ± SEM. *P < 0.05. CHD vs. Asy; Asy vs. HI. *P < 0.05. Tc vs. untreated; **P < 0.01. Tc + Fen vs. Tc.

(10 μg/ml) for 24 h. **Figure 3B** shows that stimulation with lysates significantly increases the percentage of $CD14^{high}$ $CD16^{neg}$, classical monocytes, of the Asy group, but does not change their frequencies in CHD or HI groups. On the other hand, stimulation with *T. cruzi* lysates decreases the percentage of $CD14^{high}$ $CD16^{pos}$, Intermediate monocytes, in Asy patients, and a trend to decreased frequencies is also observed in CHD patients (**Figure 3C**). However, no changes were observed in the percentage of this monocyte subset in HI (**Figure 3C**). Notably, the stimulation with *T. cruzi* did not modify the frequency of non-classical subpopulation, $CD14^{low}CD16^{pos}$, monocytes in any of the groups studied (**Figure 3D**).

Fenofibrate pre-treatment of *T. cruzi*-stimulated monocytes exerted a modulatory effect, decreasing the percentage of classic monocytes in the Asy population (**Figure 3B**). **Figure 3C** shows that fenofibrate decreases the frequency of $CD14^{high}CD16^{pos}$ cells in HI, but we only observed a trend to decrease this cell subset in Asy and CHD patients. Interestingly, fenofibrate significantly increased the percentage of non-classical cells in the HI and Asy groups but this was not modified in the CHD group (**Figure 3D**). Of note, fenofibrate alone does not modify any monocyte subpopulation in HI, Asy, and CHD (**Figure S1B**).

In Vitro T. cruzi Stimulation and Fenofibrate Treatment Modify CCR2 and HLA-DR Expression in Monocyte Subsets

The most prominent role of CCR2 is believed to be in the mobilization of monocytes under physiologic and also inflammatory conditions. With the purpose to establish the expression of CCR2 on total monocytes ($CD14^+$ cells), according to clinical status, PBMC from CHD, Asy, and HI groups were stained with CD14 and CCR2 and analyzed by FACS (**Figure 4A**). The results show high basal levels of CCR2 in $CD14^+CCR2^+$ monocytes of all groups (**Figures 4B-D**). When $CD14^+CCR2^+$ cells were stimulated with *T. cruzi* lysates, its percentage in Asy and CHD patients decreased significantly, and also in healthy controls (**Figures 4B–D**). Furthermore, especially in Asy, the pretreatment with fenofibrate of monocytes stimulated with *T. cruzi* induces a trend to restore the basal levels of $CD14^+CCR2^+$ cells (**Figure 4C**). Besides, that fenofibrate does not modify $CCR2^+$ levels in unstimulated $CD14^+$ cells (**Supplementary Figure S1C**).

When CCR2 expression was analyzed in the different monocyte subpopulations, we observed that the percentage of $CCR2^+$ cells in HI and CHD decreased in the classical monocyte subpopulation stimulated with *T. cruzi* lysates. Furthermore, fenofibrate treatment restored the baseline level only in monocytes from CHD patients and HI (**Figure 5A**). The intermediate monocyte subpopulation showed a decrease in its expression upon stimulation with *T. cruzi*, which was only significant in monocytes from HI. However, fenofibrate did not restore the decreased expression of CCR2 (**Figure 5B**). Regarding the subpopulation of non-classical monocytes, the stimulation with *T. cruzi* significantly decreased the percentage of cells expressing CCR2 in the CHD and HI groups, although only with a trend in Asy patients. Treatment with fenofibrate

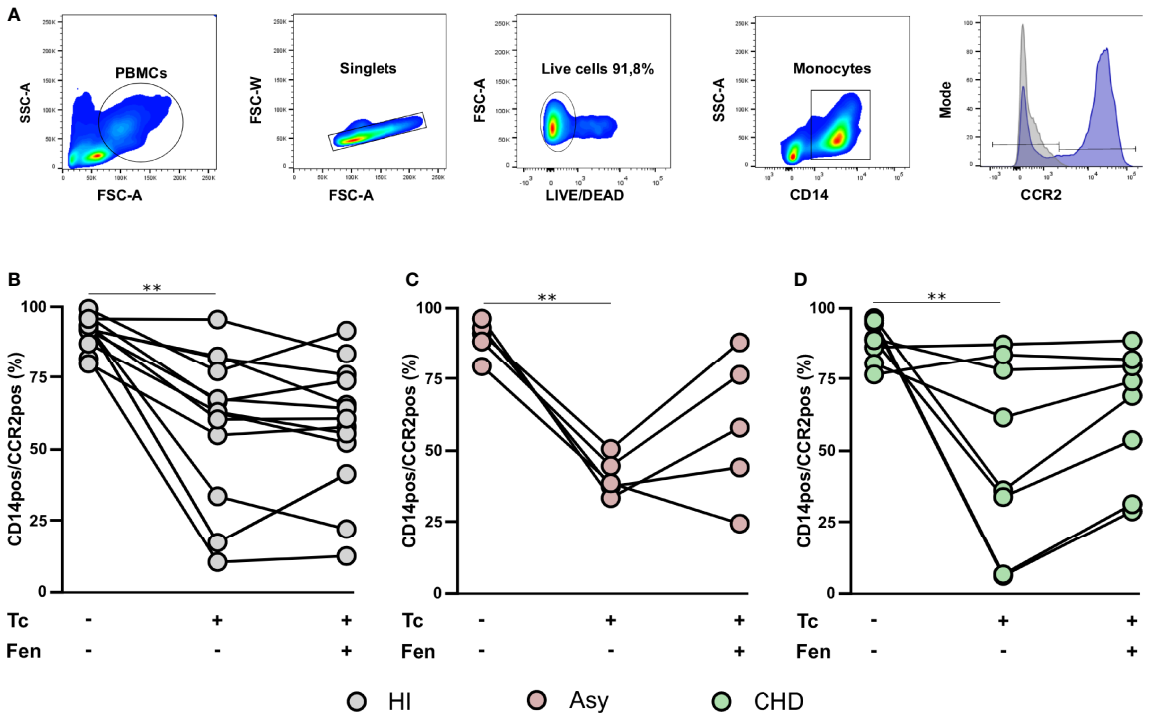

FIGURE 4 | *T. cruzi* stimulation and fenofibrate treatment modify CCR2 in CD14pos cells. Percentage of CCR2 was determined in basal CD14pos cells after 20 h of *T. cruzi* lysate (Tc) stimulation or fenofibrate (Tc + Fen) treatment. Monocytes were selected based on FSC and SSC. After excluding doublets and debris, live cells were selected, monocytes were classified by CD14 positive staining. Representative histograms show the number of events and expression level of CCR2 **(A)**. The percentages of CD14pos/CCR2pos monocytes are shown in healthy individuals (HI) **(B)**, asymptomatic (Asy) **(C)** and patients with Chagas heart disease (CHD) **(D)**, where each patient is represented by a circle. The results are shown as the mean of the experiments ± SEM. These data were analyzed by fitting a mixed model with a Tukey *post-hoc* test. **P < 0.01. Tc vs. untreated.

significantly increased the percentage of CCR2 in Asy and CHD as shown in **Figure 5C**. In order to determine the expression of HLA-DR in different disease stages, PBMC of the three experimental groups were stained with CD14 and HLA-DR (**Figure 6A**). **Figures 6B, C** show no significant differences between cells stimulated *in vitro* with *T. cruzi* lysates in comparison with unstimulated cells, in both Asy and HI. However, there is a trend to increased expression of HLA-DR with *T. cruzi* stimulation in CHD patients, according to its mean fluorescence intensity (MFI) (**Figure 6D**). As in the case of CCR2, fenofibrate alone did not modify the increased expression of HLA-DR in unstimulated and treated cells (**Supplementary Figure S1C**). This was also observed in cells from Asy and HI stimulated with *T. cruzi*. However, fenofibrate shows a clear tendency to inhibit the increased HLA-DR expression of PBMC from CHD upon stimulation with *T. cruzi* (**Figure 6D**).

When we studied HLA-DR expression in the classical monocyte subpopulation, we observed that stimulation with *T. cruzi* tends to raise the MFI of monocytes from CHD patients and treatment with fenofibrate displays a trend to restore it to basal levels (**Figure 7A**). We found that both stimulation with *T. cruzi* lysates and fenofibrate treatment did not modify HLA-DR expression in intermediate or non-classical monocyte subpopulations, as shown in **Figures 7B, C**. Besides, fenofibrate neither modifies $CCR2^{+}$ nor HLA-DR levels in unestimulated monocytes subsets of CHD, Asy or HI (**Supplementary Figure S2A**).

DISCUSSION

Monocytes are heterogeneous and multifunctional cells. As components of the innate immune response, they participate not only in inflammation and fibrosis, but also in tissue repair and regeneration during heart diseases (Apostolakis et al., 2010). Consequently, inflammatory cells, such as monocytes, are increasingly being considered as potential drug targets for the treatment of different heart conditions (Nahrendorf, 2018). Regarding Chagas disease, while the relevance of parasite persistence as a trigger of tissue damage is currently acknowledged in the development of CCC, the role of the different components of the inflammatory response remains unclear (Zhang and Tarleton, 1999; Lopez et al., 2018; Wesley et al., 2019).

In the present work, we first determined the spontaneous expression of pro-inflammatory mediators, such as MCP-1 and its receptor CCR2, and IL-12, TGF-β, IL-6 in cultured PBMC from seropositive patients with different clinical forms of Chagas disease.

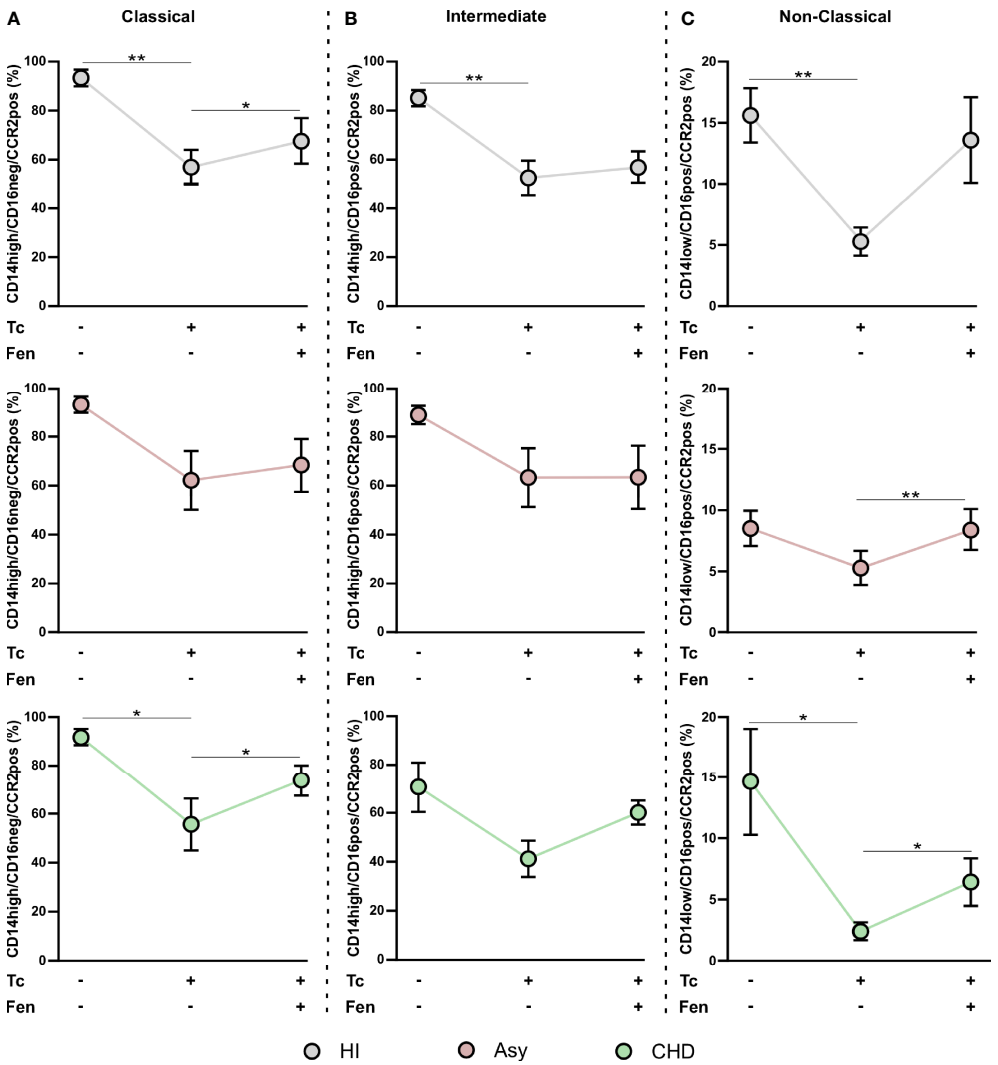

FIGURE 5 | *T. cruzi* stimulation and fenofibrate treatment modify CCR2 in monocyte subpopulations. Percentage of $CCR2^+$ cells was determined in PBMC stimulated or not with *T. cruzi* lysate (Tc) and treated or not with fenofibrate (Tc + Fen) after 20 h, according to CD14 and CD16 expression. It shows the percentage of classical (CD14high/CD16neg) **(A)**, intermediate (CD14high/CD16pos) **(B)** and non-classical (CD14low/CD16pos) **(C)** monocytes with $CCR2^+$ expression. The results are shown as the mean of the experiments ± SEM. These data were analyzed by fitting a mixed effect model with a Tukey *post-hoc* test. *P < 0.05; **P < 0.01.

The results show that PBMC from CHD patients displayed a significantly higher expression level of these mediators than cells from uninfected individuals. Moreover, in Asy patients we observed a significantly increased expression of IL-12 and TGF-β, and a trend to increase in the other cytokines evaluated (**Figure 1**). These results are in consonance with those found by other authors in neutrophils and monocytes for similar groups of patients (Souza et al., 2004; Campi-Azevedo et al., 2015; Medeiros et al., 2017; Pinto et al., 2018).

Recently, Dey et al. showed that mouse $CD11c^+$ classical dendritic cells, but not $CD11b^+$ $Ly6c^+$ inflammatory monocytes, are the source of IL-6 required for the expansion of protective Th17 cells against drug-resistant *Leishmania donovani* (Dey et al., 2020). Previous studies by Stäger et al. also reported that IL-6 deficiency was associated with the expansion of IL-10-producing Treg cells, while expansion was not observed in IL-12p40-deficient mice, stressing the role of IL-6 in the control of infection (Stäger et al., 2006). Regarding our results, it must be noted however, that the actual source of these, and also the other cytokines was not investigated. Independently of this fact, it is clear that both IL-12 and IL-6 are associated with a more severe outcome, since they were particularly elevated in symptomatic patients in comparison with asymptomatic ones or healthy controls. Since in the context of parasite persistence in the tissues, *T. cruzi* induces a substantial increase in pro-inflammatory mediators and reactive oxygen and nitrogen species (Cevey et al., 2017; Penas et al., 2017), this scenario would favor tissue damage and contributes to the clinical outcome observed in symptomatic patients with Chagas disease. For this reason, it is desirable to find an anti-

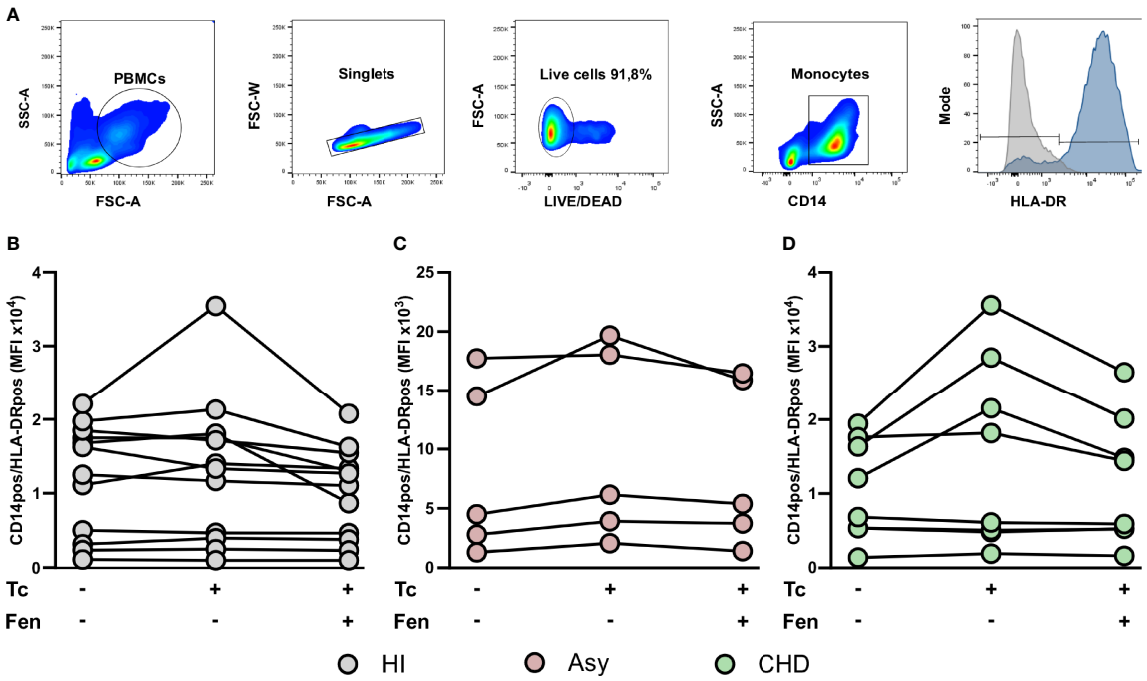

FIGURE 6 | HLA-DR expression in monocyte. The mean fluorescence intensity (MFI) of HLA-DR was determined in basal CD14pos cells after 20 h of *T. cruzi* lysate (Tc) stimulation or fenofibrate (Tc + Fen) treatment. Monocytes were selected based on FSC and SSC. After excluding doublets and debris, live cells were selected, monocytes were classified by CD14 positive staining. The mean fluorescence intensity (MFI) of HLA-DR was calculated both in total monocytes **(A)**. It shows the mean fluorescence intensity (MFI) of CD14pos/HLA-DRpos monocytes in healthy (HI) **(B)**, asymptomatic (Asy) **(C)** and chronic Chagas disease (CHD) patients **(D)**, where each patient is represented by a circle. The results are shown as the mean of the experiments ± SEM. These data were analyzed by fitting a mixed effect model with a Tukey *post-hoc* test.

inflammatory therapy that might be useful as a coadjuvant of the antiparasitic treatment to preclude the onset of heart damage during the course of infection.

Previous studies from our group showed that PPAR agonists, such as fenofibrate, a potent hypolipidemic drug, also bears anti-inflammatory properties in the context of experimental Chagas disease (Cevey et al., 2017; Rada et al., 2020). In this work we demonstrated that *in vitro* treatment with fenofibrate significantly reduces the expression of pro-inflammatory mediators, in PBMC (**Figure 2**). These findings are in line with those of Krysiak et al., in which fenofibrate decreased the release of TNFα, IL-1β, IL-6, and MCP-1 by human monocytes. Those effects were accompanied by a decrease in plasma C-reactive protein levels, which could be clinically relevant in the prevention of vascular complications (Krysiak et al., 2011). In this regard, we demonstrated that fenofibrate controls inflammation, prevents fibrosis, contributes to neovascularization and improves left ventricular function, in an experimental murine model of Chagas disease (Cevey et al., 2017). Moreover, in another work, we showed that this occurs through IL-10-dependent and -independent mechanisms (Rada et al., 2020). These anti-inflammatory and protective effects of fenofibrate have been also evaluated in models of autoimmune myocarditis (Cheng et al., 2016), skeletal muscle inflammation (Dai et al., 2016), and cardiac ischemia/reperfusion models (Sugga et al., 2012).

In this work, we studied the monocyte population of patients with different stages of Chagas disease. Our results show that patients with CHD have a significantly higher percentage of classical monocytes. Besides, we determined that there are no significant differences between HI, Asy, or with CHD individuals in the intermediate monocyte subpopulation. Interestingly, we found that Asy patients have a significantly higher percentage of non-classical monocyte subpopulation (**Figure 3**), suggesting they are in an alert and patrolling state. In this sense, the work of Cros et al. demonstrated that human non-classical monocytes exhibited endothelial crawling behavior after adoptive transfer to mice (Cros et al., 2010). Our results are in line with a work by Pérez-Mazliah et al. who showed increased levels of non-classical monocytes in *T. cruzi*-infected individuals with mild or no signs of cardiac disease, as well as in patients suffering from dilated cardiomyopathy unrelated to *T. cruzi* infection. In contrast, they also showed that the monocyte profile in *T. cruzi*-infected individuals with severe cardiomyopathy was slanted to the classical and intermediate subsets (Pérez-Mazliah et al., 2018). Consequently, *in vitro* experiments showed that $CD16^+$ monocytes have higher mobility than their $CD16^-$ counterparts (Randolph et al., 2002). This behavior suggests that non-classical monocytes are constantly inspecting the endothelium for signs of inflammation or damage and preparing to rapidly transmigrate (Wong et al., 2012). Another study attributed the differences in

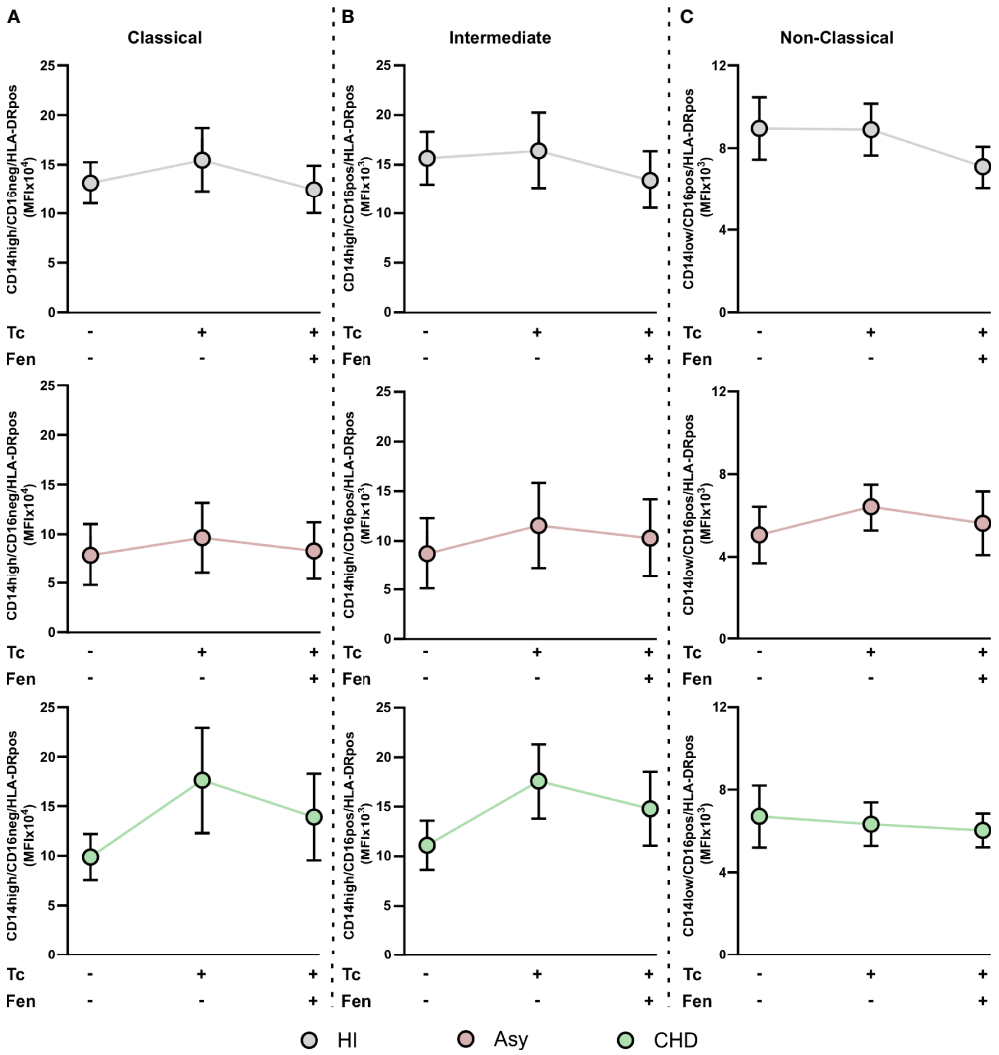

FIGURE 7 | HLA-DR expression in *T. cruzi* stimulated and fenofibrate treated monocyte subpopulations. The mean fluorescence intensity percentage of HLA-DR$^+$ cells was determined in PBMC stimulated or not with *T. cruzi* lysate (Tc) and treated or not with fenofibrate (Tc + Fen) after 20 h, according to CD14 and CD16 expression. It shows the mean fluorescence intensity (MFI) of classical (CD14high/CD16neg) **(A)**, intermediate (CD14high/CD16pos) **(B)** and non-classical (CD14low/CD16pos) **(C)** monocytes with HLA-DR$^+$ expression. The results are shown as the mean of the experiments ± SEM. These data were analyzed by fitting a mixed effect model with a Tukey *post-hoc* test.

the characterization of the monocyte subpopulations, partly due to the fact that individuals infected with parasites of different discrete typing units (DTU) triggers different immunological impact which could influence the progression of the disease (Passos et al., 2015).

In our work, we evaluated whether *in vitro* treatment with fenofibrate promotes changes in monocyte subpopulations. We determined that *T. cruzi* increased the percentage of classical monocytes of Asy patients, while fenofibrate treatment inhibited this effect. In contrast, there were no changes in the classical monocyte population from patients with CHD. On the other hand, *T. cruzi* produced a significant decrease in the intermediate population of Asy patients that was not modified by fenofibrate. Notably, fenofibrate significantly increased the percentage of non-classical monocytes in Asy patients, suggesting that this treatment promotes a repairing and patrolling behavior. Also, it should be noted that both *T. cruzi* and fenofibrate were not able to significantly modify the percentage of any of the monocyte subpopulations of patients with CHD (**Figure 3**).

CCR2 is a chemokine receptor involved in monocyte mobilization and plays a key role in extravasation and transmigration of monocytes under inflammatory conditions (Conductier et al., 2010; Chu et al., 2014). MCP-1, ligand of CCR2, is a potent monocyte activator that is abundantly expressed in various pathological conditions. It has been demonstrated that the loss of MCP-1 by targeted gene disruption is sufficient to impair monocyte trafficking in several inflammation models (Lu et al., 1998). Studies carried

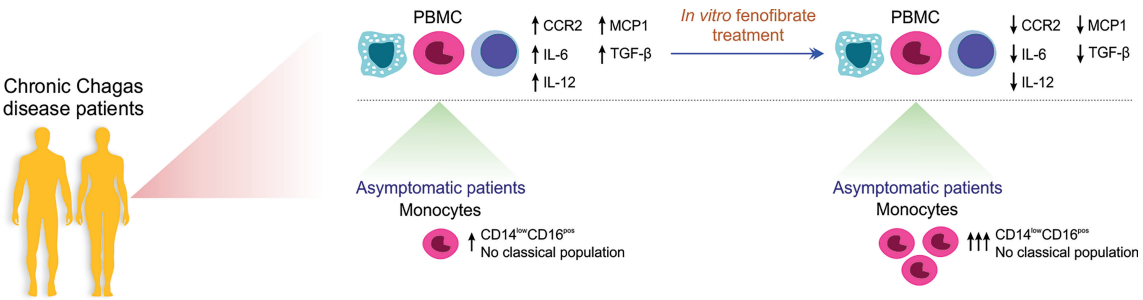

FIGURE 8 | Schematic representation of the *in vitro* effect of Fenofibrate in PBMC and monocytes from patients with chronic Chagas disease. PBMC from Chagas disease patients display higher levels of IL-12, TGF-β, IL-6, MCP1, and CCR2 than cells from uninfected individuals. *In vitro* fenofibrate treatment exerts modulatory effect, decreasing the expression of CCR2, IL-6, IL-12, TGF-β, and MCP-1. Asymptomatic patients have a high percentage of non-classical monocytes, which increases even more after fenofibrate treatment.

out with $CCR2^{-/-}$ mice clearly demonstrated that this receptor exhibits functions as a major mediator of macrophage recruitment and trafficking in host defense to bacterial and parasitic infections (Hardison et al., 2006). Our results clearly show that when monocytes are stimulated with *T. cruzi* lysates, the percentage of CCR2 decreases in all the groups (**Figure 4**). It has been postulated that this might occur due to the fact that during chemotaxis, $CCR2^{+}$ expressed on monocytes internalizes with the bound chemoattractant, but cycles rapidly back to the plasma membrane to maintain high responsiveness (Volpe et al., 2012; Zhao et al., 2019). Notably, fenofibrate tends to restore baseline levels of CCR2 in cells stimulated with *T. cruzi* (**Figure 4**). It has been described that $CCR2^{-}$ and $CCR2^{+}$ macrophages have distinct functions in the heart. $CCR2^{-}$ macrophages are involved in various forms of tissue remodeling such as coronary development, postnatal coronary growth, and cardiac regeneration (Lavine et al., 2014; Leid et al., 2016). Moreover, some studies revealed that after neonatal cardiomyocyte injury, $CCR2^{-}$ macrophages contribute to cardiac tissue regeneration and functional recovery of the heart, expanding the coronary vasculature, cardiomyocyte proliferation, and physiological cardiomyocyte hypertrophy. Particularly, in the pediatric mouse heart, the absence of $CCR2^{-}$ macrophages demonstrated poor regenerative capacity (Epelman et al., 2014; Lavine et al., 2014; Leid et al., 2016). However, analysis of heart transplant recipients in humans revealed that $CCR2^{-}$ macrophages are a tissue-resident population exclusively replenished through local proliferation, whereas $CCR2^{+}$ macrophages do it through monocyte recruitment and proliferation. In patients with heart failure, $CCR2^{+}$ macrophage abundance is associated with left ventricular remodeling and systolic function (Bajpai et al., 2018).

Although fenofibrate restored $CCR2^{+}$ in classical subpopulation of CHD patients, the significant increase in the non-classical subpopulation of Asy and CHD is of great interest due to its restorative characteristics (**Figure 5**). This could also explain, together with the inhibition of pro-inflammatory mediators in the heart, the improvement in cardiac function that we have demonstrated in the murine model of mixed infection by *T. cruzi* under treatment with fenofibrate (Cevey et al., 2017; Rada et al., 2020). Further case control studies, namely, cohorts of fenofibrate vs. placebo treated patients, are needed to test the hypothesis that fenofibrate restores the percentage of $CCR2^{+}$ non-classical monocytes leading to improvement of ventricular function in patients with Chagas disease.

In this work, the expression of HLA-DR in all the groups of patients was studied. We observed a trend to increase in HLA-DR expression in *T. cruzi* stimulated monocytes from CHD patients. Besides, fenofibrate tends to inhibit this effect (**Figure 6**). Furthermore, we have shown that HLA-DR tends to increase its expression in the classical monocyte subpopulation from CHD patients stimulated with *T. cruzi*. Fenofibrate treatment showed a tendency to restore HLA-DR expression to baseline levels (**Figure 7A**). However, another study shows that not only HLA-DR increased in the classical monocytes of cardiac patients but also in those of indeterminate. Likewise, in that work a lower expression of HLA-DR on intermediate monocytes of Asy patients was observed when compared to the CHD patients (Pinto et al., 2018). Deficiency in the expression of HLA-DR may reflect the severity of a disease. The low HLA-DR MFI constitutes an independent risk factor in predicting mortality, since decreased expression of HLA-DR on monocytes was associated with impaired antigen presentation and poor prognosis (Li et al., 2020). The fact that in our study fenofibrate treatment did not modify HLA-DR expression is encouraging, since it would mean that it does not inhibit antigen presentation capacity.

In conclusion, monocyte profiling through analysis of inflammatory markers may be of value to direct appropriate coadjuvant therapies, like the one envisioned in this work by means of fenofibrate treatment, with the aim to help reduce the extensive and noxious inflammatory and profibrotic response arising in chronic Chagas heart disease patients (**Figure 8**).

DATA AVAILABILITY STATEMENT

The original contributions presented in the study are included in the article/**Supplementary Material**. Further inquiries can be directed to the corresponding author.

ETHICS STATEMENT

The studies involving human participants were reviewed and approved by the Comité de Ética del Hospital General de Agudos Cosme Argerich, Ciudad Autónoma de Buenos Aires, Argentina. The patients/participants provided their written informed consent to participate in this study.

AUTHOR CONTRIBUTIONS

NG and AP designed experiments and analyzed data. NG, AP, GM, AC, and FP and contributed to the writing of the manuscript. AP, AC and FP did experiments. NP, AM, JG, and MG performed the clinical studies and the collection of blood samples. NG, GM, FP, AC, and AP contributed to final approval of the version to be published. All authors contributed to the article and approved the submitted version.

FUNDING

This work was supported by the Universidad de Buenos Aires [Grant number 20020170100562BA] and the Agencia Nacional de Promoción Científica y Tecnológica [Grant number PICT 2016-0629].

ACKNOWLEDGMENTS

We would also like to thank Mr. Sergio Mazzini for his assistance in English grammar and spelling corrections. The authors thank to Dr. Lourdes Arruvito for her contributions to the analysis of cytometry results and to Virginia Gonzalez Polo for her technical assistance in flow cytometry.

SUPPLEMENTARY MATERIAL

The Supplementary Material for this article can be found online at: https://www.frontiersin.org/articles/10.3389/fcimb.2021.785166/full#supplementary-material

Supplementary Figures 1 | PBMC were treated *in vitro* or not with 100 μM of fenofibrate (Fen). After 48 h, IL-12, TGF-β, IL-6, MCP-1 and CCR2 mRNAs were measured in healthy individuals (HI) **(A)**. PBMC were treated or not with 100 μM of Fen. After 20 h according to CD14 and CD16 expression, they were classified as Classical (CD14high/CD16neg), Intermediate (CD14high/CD16pos) and Non-Classical (CD14low/CD16pos). The percentages of Classical, Intermediate and Non-Classical and are shown for HI, asymptomatic (Asy) and patients with Chagas heart disease (CHD) **(B)**. PBMC were treated or not with 100 μM of Fen. After 16-20 h, PBMC were classified according to CD14 and CCR2 expression. The percentages of CD14pos/CCR2pos monocytes are shown in HI, Asy and CHD, where each patient is represented by a circle **(C)**. PBMC were treated or not with 100 μM of Fen. The mean fluorescence intensity (MFI) of HLA-DR was determined in basal CD14pos cells after 20 h of Fen treatment. It shows the MFI of CD14pos/HLA-DRpos monocytes in HI, Asy and CHD patients, where each patient is represented by a circle **(D)**. For **(A)**, mRNA levels were determined by RT-qPCR and normalized against β-Actin. Results are expressed as the mean of 3 independent experiments. Differences between fenofibrate-treated PBMC were analyzed using the Wilcoxon test for paired samples and are shown as the mean of the experiments ± SEM. For **(B-D),** the data were analyzed by fitting a mixed effect model with a Tukey *post-hoc* test and the results are expressed as the mean of the experiments ± SEM.

Supplementary Figures 2 | PBMC were treated or not with 100 μM of fenofibrate (Fen). After 20 h according to CD14 and CD16 expression, they were classified as Classical (CD14high/CD16neg), Intermediate (CD14high/CD16pos) and Non-Classical (CD14low/CD16pos) for healthy individuals (HI), asymptomatic (Asy) and patients with Chagas heart disease (CHD). It shows the percentage of classical, intermediate and non-classical monocytes with $CCR2^+$ expression **(A)** and the mean fluorescence intensity (MFI) of classical, intermediate and non-classical monocytes with $HLA\text{-}DR^+$ expression **(B).** For **(A, B)**, the results are shown as the mean of the experiments ± SEM. These data were analyzed by fitting a mixed effect model with a Tukey *post-hoc* test.

REFERENCES

Andrade, D. V., and Gollob KJ, D. W. (2014). Acute Chagas Disease: New Global Challenges for an Old Neglected Disease. *PloS Negl. Trop. Dis.* 8 (7), e3010:1–10. doi: 10.1371/journal.pntd.0003010

Apostolakis, S., Lip, G. Y. H., and Shantsila, E. (2010). Monocytes in Heart Failure: Relationship to a Deteriorating Immune Overreaction or a Desperate Attempt for Tissue Repair? *Cardiovasc. Res.* 85, 649–660. doi: 10.1093/cvr/cvp327

Bajpai, G., Schneider, C., Wong, N., Bredemeyer, A., Hulsmans, M., Nahrendorf, M., et al. (2018). The Human Heart Contains Distinct Macrophage Subsets With Divergent Origins and Functions. *Nat. Med.* 24, 1234–1245. doi: 10.1038/s41591-018-0059-x

Bustin, S. A., Benes, V., Garson, J. A., Hellemans, J., Huggett, J., Kubista, M., et al. (2009). The MIQE Guidelines: Minimum Information for Publication of Quantitative Real-Time PCR Experiments. *Clin. Chem.* 55, 611–622. doi: 10.1373/clinchem.2008.112797

Campi-Azevedo, A. C., Gomes, J. A. S., Teixeira-Carvalho, A., Silveira-Lemos, D., Vitelli-Avelar, D. M., Sathler-Avelar, R., et al. (2015). Etiological Treatment of Chagas Disease Patients With Benznidazole Lead to a Sustained Pro-Inflammatory Profile Counterbalanced by Modulatory Events. *Immunobiology* 220, 564–574. doi: 10.1016/j.imbio.2014.12.006

Cevey, Á. C., Mirkin, G. A., Donato, M., Rada, M. J., Penas, F. N., Gelpi, R. J., et al. (2017). Treatment With Fenofibrate Plus a Low Dose of Benznidazole Attenuates Cardiac Dysfunction in Experimental Chagas Disease. *Int. J. Parasitol. Drugs Drug Resist.* 7, 378–387. doi: 10.1016/j.ijpddr.2017.10.003

Cevey, Á. C., Mirkin, G. A., Penas, F. N., and Goren, N. B. (2016). Low-Dose Benznidazole Treatment Results in Parasite Clearance and Attenuates Heart Inflammatory Reaction in an Experimental Model of Infection With a Highly Virulent Trypanosoma Cruzi Strain. *Int. J. Parasitol. Drugs Drug Resist.* 6, 12–22. doi: 10.1016/j.ijpddr.2015.12.001

Cevey, Á. C., Penas, F. N., Alba Soto, C. D., Mirkin, G. A., and Goren, N. B. (2019). IL-10/STAT3/SOCS3 Axis Is Involved in the Anti-Inflammatory Effect of Benznidazole. *Front. Immunol.* 10, 1267. doi: 10.3389/fimmu.2019.01267

Cheng, H., Xi, Y., Chi, X., Wu, Y., and Liu, G. (2016). Fenofibrate Treatment of Rats With Experimental Autoimmune Myocarditis by Alleviating Treg/Th17 Disorder. *Cent. J. Immunol.* 41, 64–70. doi: 10.5114/ceji.2016.58817

Chu, H. X., Arumugam, T. V., Gelderblom, M., Magnus, T., Drummond, G. R., and Sobey, C. G. (2014). Role of CCR2 in Inflammatory Conditions of the Central Nervous System. *J. Cereb. Blood Flow Metab.* 34, 1425–1429. doi: 10.1038/jcbfm.2014.120

Conductier, G., Blondeau, N., Guyon, A., Nahon, J. L., and Rovère, C. (2010). The Role of Monocyte Chemoattractant Protein MCP1/CCL2 in Neuroinflammatory Diseases. *J. Neuroimmunol.* 224, 93–100. doi: 10.1016/j.jneuroim.2010.05.010

Cros, J., Cagnard, N., Woollard, K., Patey, N., Zhang, S. Y., Senechal, B., et al. (2010). Human CD14dim Monocytes Patrol and Sense Nucleic Acids and Viruses *via* TLR7 and TLR8 Receptors. *Immunity* 33, 375–386. doi: 10.1016/j.immuni.2010.08.012

Dai, F., Jiang, T., Bao, Y., Chen, G., Chen, L., Zhang, Q., et al. (2016). Fenofibrate Improves High-Fat Diet-Induced and Palmitate-Induced Endoplasmic

Reticulum Stress and Inflammation in Skeletal Muscle. *Life Sci.* 157, 158–167. doi: 10.1016/j.lfs.2016.06.008

Dey, S., Mukherjee, D., Sultana, S. S., Mallick, S., Dutta, A., Ghosh, J., et al. (2020). Combination of Mycobacterium Indicus Pranii and Heat-Induced Promastigotes Cures Drug-Resistant Leishmania Infection: Critical Role of Interleukin-6-Producing Classical Dendritic Cells. *Infect. Immun.* 88 (6), e00222–19. doi: 10.1128/IAI.00222-19

Epelman, S., Lavine, K. J., Beaudin, A. E., Sojka, D. K., Carrero, J. A., Calderon, B., et al. (2014). Embryonic and Adult-Derived Resident Cardiac Macrophages Are Maintained Through Distinct Mechanisms at Steady State and During Inflammation. *Immunity* 40, 91–104. doi: 10.1016/j.immuni.2013.11.019

Fantuzzi, L., Borghi, P., Ciolli, V., Pavlakis, G., Belardelli, F., and Gessani, S. (1999). Loss of CCR2 Expression and Functional Response to Monocyte Chemotactic Protein (MCP-1) During the Differentiation of Human Monocytes: Role of Secreted MCP-1 in the Regulation of the Chemotactic Response. *Blood* 94, 875–883. doi: 10.1182/blood.v94.3.875.415k28_875_883

Garg, M., Khanna, D., Kalra, S., and Balakumar, P. (2016). Chronic Oral Administration of Low-Dose Combination of Fenofibrate and Rosuvastatin Protects the Rat Heart Against Experimentally Induced Acute Myocardial Infarction. *Fundam. Clin. Pharmacol.* 30, 394–405. doi: 10.1111/fcp.12204

Gómez-Olarte, S., Bolaños, N. I., Echeverry, M., Rodríguez, A. N., Cuéllar, A., Puerta, C. J., et al. (2019). Intermediate Monocytes and Cytokine Production Associated With Severe Forms of Chagas Disease. *Front. Immunol.* 10, 1671. doi: 10.3389/fimmu.2019.01671

Guilliams, M., and Scott, C. L. (2017). Does Niche Competition Determine the Origin of Tissue-Resident Macrophages? *Nat. Rev. Immunol.* 17, 451–460. doi: 10.1038/nri.2017.42

Gutierrez, F. R. S., Guedes, P. M. M., Gazzinelli, R. T., and Silva, J. S. (2009). The Role of Parasite Persistence in Pathogenesis of Chagas Heart Disease. *Parasite Immunol.* 31, 673–685. doi: 10.1111/j.1365-3024.2009.01108.x

Hardison, J. L., Kuziel, W. A., Manning, J. E., and Lane, T. E. (2006). Chemokine CC Receptor 2 Is Important for Acute Control of Cardiac Parasitism But Does Not Contribute to Cardiac Inflammation After Infection With Trypanosoma Cruzi. *J. Infect. Dis.* 193, 1584–1588. doi: 10.1086/503812

Heidt, T., Courties, G., Dutta, P., Sager, H. B., Sebas, M., Iwamoto, Y., et al. (2014). Differential Contribution of Monocytes to Heart Macrophages in Steady-State and After Myocardial Infarction. *Circ. Res.* 115, 284–295. doi: 10.1161/CIRCRESAHA.115.303567

Hovsepian, E., Mirkin, G. A., Penas, F., Manzano, A., Bartrons, R., and Goren, N. B. (2011). Modulation of Inflammatory Response and Parasitism by 15-Deoxy-Δ(12,14) Prostaglandin J(2) in *Trypanosoma Cruzi*-Infected Cardiomyocytes. *Int. J. Parasitol.* 41, 553–562. doi: 10.1016/j.ijpara.2010.12.002

Hulsmans, M., Sager, H. B., Roh, J. D., Valero-Muñoz, M., Houstis, N. E., Iwamoto, Y., et al. (2018). Cardiac Macrophages Promote Diastolic Dysfunction. *J. Exp. Med.* 215 (2), 423–440. doi: 10.1084/jem.20171274

Kruger, N. J. (1994). The Bradford Method for Protein Quantitation. *Methods Mol. Biol.* 32, 9–15. doi: 10.1385/0-89603-268-X:9

Krysiak, R., Gdula-Dymek, A., and Okopien, B. (2011). Effect of Simvastatin and Fenofibrate on Cytokine Release and Systemic Inflammation in Type 2 Diabetes Mellitus With Mixed Dyslipidemia. *Am. J. Cardiol.* 107, 1010–1018.e1. doi: 10.1016/j.amjcard.2010.11.023

Lavine, K. J., Epelman, S., Uchida, K., Weber, K. J., Nichols, C. G., Schilling, J. D., et al. (2014). Distinct Macrophage Lineages Contribute to Disparate Patterns of Cardiac Recovery and Remodeling in the Neonatal and Adult Heart. *Proc. Natl. Acad. Sci. U. S. A.* 111, 16029–16034. doi: 10.1073/pnas.1406508111

Leid, J., Carrelha, J., Boukarabila, H., Epelman, S., Jacobsen, S. E. W., and Lavine, K. J. (2016). Primitive Embryonic Macrophages Are Required for Coronary Development and Maturation. *Circ. Res.* 118, 1498–1511. doi: 10.1161/CIRCRESAHA.115.308270

Ling, H., and Luoma, J. T. (2013). Hilleman D. A Review of Currently Available Fenofibrate and Fenofibric Acid Formulations. *Rev. Cardiol. Res.* 4, 47–55. doi: 10.4021/cr270w

Li, J., Tang, Z., Xie, M., Hang, C., Yu, Y., and Li, C. (2020). Association Between Elevation of Plasma Biomarkers and Monocyte Dysfunction and Their Combination in Predicting Sepsis: An Observational Single-Centre Cohort Study. *Innate Immun.* 26, 514–527. doi: 10.1177/1753425920926602

Lockyer, P., Schisler, J. C., Patterson, C., and Willis, M. S. (2010). Minireview: Won't Get Fooled Again: The Nonmetabolic Roles of Peroxisome Proliferator-Activated Receptors (PPARs) in the Heart. *Mol. Endocrinol.* 24, 1111–1119. doi: 10.1210/me.2009-0374

Lopez, M., Tanowitz, H. B., and Garg, N. J. (2018). Pathogenesis of Chronic Chagas Disease: Macrophages, Mitochondria, and Oxidative Stress. *Curr. Clin. Microbiol. Rep.* 5, 45–54. doi: 10.1007/s40588-018-0081-2

Lu, B., Rutledge, B. J., Gu, L., Fiorillo, J., Lukacs, N. W., Kunkel, S. L., et al. (1998). Abnormalities in Monocyte Recruitment and Cytokine Expression in Monocyte Chemoattractant Protein 1-Deficient Mice. *J. Exp. Med.* 187, 601–608. doi: 10.1084/jem.187.4.601

Machado, F. S., Martins, G. A., Aliberti, J. C., Mestriner, F. L., Cunha, F. Q., and Silva, J. S. (2000). *Trypanosoma Cruzi*-Infected Cardiomyocytes Produce Chemokines and Cytokines That Trigger Potent Nitric Oxide-Dependent Trypanocidal Activity. *Circulation* 102, 3003–3008. doi: 10.1161/01.CIR.102.24.3003

McVicker, B. L., and Bennett, R. G. (2017). Novel Anti-Fibrotic Therapies. *Front. Pharmacol.* 8, 318. doi: 10.3389/fphar.2017.00318

Medeiros, N. I., Fares, R. C. G., Franco, E. P., Sousa, G. R., Mattos, R. T., Chaves, A. T., et al. (2017). Differential Expression of Matrix Metalloproteinases 2, 9 and Cytokines by Neutrophils and Monocytes in the Clinical Forms of Chagas Disease. *PloS Negl. Trop. Dis.* 11, 1–16. doi: 10.1371/journal.pntd.0005284

Mitelman, J. (2011). Argentinian Society of Cardiology. Consensus Statement on Chagas-Mazza Disease. *Argentinian J. Cardiol.* 79, 544–564.

Nahrendorf, M. (2018). Myeloid Cell Contributions to Cardiovascular Health and Disease. *Nat. Med.* 24, 711–720. doi: 10.1038/s41591-018-0064-0Myeloid

Passos, S., Carvalho, L. P., Costa, R. S., Campos, T. M., Novais, F. O., Magalhães, A., et al. (2015). Intermediate Monocytes Contribute to Pathologic Immune Response in Leishmania Braziliensis Infections. *J. Infect. Dis.* 211, 274–282. doi: 10.1093/infdis/jiu439

Penas, F. N., Carta, D., Cevey, Á. C., Rada, M. J., Pieralisi, A. V., Ferlin, M. G., et al. (2020). Pyridinecarboxylic Acid Derivative Stimulates Pro-Angiogenic Mediators by PI3K/AKT/mTOR and Inhibits Reactive Nitrogen and Oxygen Species and NF-κb Activation Through a Pparγ-Dependent Pathway in *T. Cruzi*-Infected Macrophages. *Front. Immunol.* 10, 2955. doi: 10.3389/fimmu.2019.02955

Penas, F. N., Carta, D., Dmytrenko, G., Mirkin, G. A., Modenutti, C. P., Cevey, Á. C., et al. (2017). Treatment With a New Peroxisome Proliferator-Activated Receptor Gamma Agonist, Pyridinecarboxylic Acid Derivative, Increases Angiogenesis and Reduces Inflammatory Mediators in the Heart of Trypanosoma Cruzi-Infected Mice. *Front. Immunol.* 8, 1738. doi: 10.3389/fimmu.2017.01738

Penas, F. N., Cevey, Á. C., Siffo, S., Mirkin, G. A., and Goren, N. B. (2016). Hepatic Injury Associated With Trypanosoma Cruzi Infection Is Attenuated by Treatment With 15-Deoxy-Δ12,14prostaglandin J2. *Exp. Parasitol.* 170, 100–108. doi: 10.1016/j.exppara.2016.09.015

Penas, F., Mirkin, G. A., Hovsepian, E., Cevey, Á., Caccuri, R., Sales, M. E., et al. (2013). Pparγ Ligand Treatment Inhibits Cardiac Inflammatory Mediators Induced by Infection With Different Lethality Strains of Trypanosoma Cruzi. *Biochim. Biophys. Acta - Mol. Basis Dis.* 1832, 239–248. doi: 10.1016/j.bbadis.2012.08.007

Penas, F., Mirkin, G. A., Vera, M., Cevey, Á. C., González, C. D., Gómez, M. I., et al. (2015). Treatment *In Vitro* With Pparα and Pparγ Ligands Drives M1-To-M2 Polarization of Macrophages From *T. Cruzi*-Infected Mice. *Biochim. Biophys. Acta* 1852, 893–904. doi: 10.1016/j.bbadis.2014.12.019

Pérez-Mazliah, D. E., Castro Eiro, M. D., Álvarez, M. G., Lococo, B., Bertocchi, G., César, G., et al. (2018). Distinct Monocyte Subset Phenotypes in Patients With Different Clinical Forms of Chronic Chagas Disease and Seronegative Dilated Cardiomyopathy. *PloS Negl. Trop. Dis.* 12, e0006887. doi: 10.1371/journal.pntd.0006887

Petray, P. B., Rottenberg, M. E., Grinstein, S., and Örn, A. (1994). Release of Nitric Oxide During the Experimental Infection With *Trypanosoma Cruzi*. *Parasite Immunol.* 16, 193–199. doi: 10.1111/j.1365-3024.1994.tb00340.x

Pinto, B. F., Medeiros, N. I., Teixeira-Carvalho, A., Eloi-Santos, S. M., Fontes-Cal, T. C. M., Rocha, D. A., et al. (2018). CD86 Expression by Monocytes Influence an Immunomodulatory Profile in Asymptomatic Patients With Chronic Chagas Disease. *Front. Immunol.* 9, 454. doi: 10.3389/fimmu.2018.00454

Rőszer, T., Menéndez-Gutiérrez, M. P., Cedenilla, M., and Ricote, M. (2013). Retinoid X Receptors in Macrophage Biology. *Trends Endocrinol. Metab.* 24, 460–468. doi: 10.1016/j.tem.2013.04.004

Rada, J., Donato, M., Penas, F. N., Alba Soto, C., Cevey, Á. C., Pieralisi, A. V., et al. (2020). IL-10-Dependent and -Independent Mechanisms Are Involved in the Cardiac Pathology Modulation Mediated by Fenofibrate in an Experimental Model of Chagas Heart Disease. *Front. Immunol.* 11, 572178. doi: 10.3389/fimmu.2020.572178

Randolph, G. J., Sanchez-Schmitz, G., Liebman, R. M., and Schäkel, K. (2002). The CD16+ (Fcγriii+) Subset of Human Monocytes Preferentially Becomes Migratory Dendritic Cells in a Model Tissue Setting. *J. Exp. Med.* 196, 517–527. doi: 10.1084/jem.20011608

Ricote, M., Li, A. C., Willson, T. M., Kelly, C. J., and Glass, C. K. (1998). The Peroxisome Proliferator-Activated Receptor-Gamma Is a Negative Regulator of Macrophage Activation. *Nature* 391, 79–82. doi: 10.1038/34178

Satoh, T., Nakagawa, K., Sugihara, F., Kuwahara, R., Ashihara, M., Yamane, F., et al. (2017). Identification of an Atypical Monocyte and Committed Progenitor Involved in Fibrosis. *Nature* 541, 96–101. doi: 10.1038/nature20611

Schmittgen, T. D., and Livak, K. J. (2008). Analyzing Real-Time PCR Data by the Comparative CTmethod. *Nat. Protoc.* 3, 1101–1108. doi: 10.1038/nprot.2008.73

Shi, C. (2014). Monocyte Recruitment During Infection and Inflammation. *Nat. Rev. Immunol.* 11, 762–774. doi: 10.1038/nri3070

Sica, A., Invernizzi, P., and Mantovani, A. (2014). Macrophage Plasticity and Polarization in Liver Homeostasis and Pathology. *Hepatology* 59, 2034–2042. doi: 10.1002/hep.26754

Souza, P. E. A., Rocha, M. O. C., Rocha-Vieira, E., Menezes, C. A. S., Chaves, A. C. L., Gollob, K. J., et al. (2004). Monocytes From Patients With Indeterminate and Cardiac Forms of Chagas' Disease Display Distinct Phenotypic and Functional Characteristics Associated With Morbidity. *Infect. Immun.* 72, 5283–5291. doi: 10.1128/IAI.72.9.5283-5291.2004

Stäger, S., Maroof, A., Zubairi, S., Sanos, S. L., Kopf, M., and Kaye, P. M. (2006). Distinct Roles for IL-6 and IL-12p40 in Mediating Protection Against Leishmania Donovani and the Expansion of IL-10+ CD4+ T Cells. *Eur. J. Immunol.* 36, 1764–1771. doi: 10.1002/eji.200635937

Sugga, G. S., Khanam, R., Khan, M. U., and Khanam, R. (2012). Protective Role of Fibrates in Cardiac Ischemia/Reperfusion. *J. Adv. Pharm. Technol. Res.* 3, 188. doi: 10.4103/2231-4040.101016

Tanowitz, H. B., Machado, F. S., Spray, D. C., Friedman, J. M., Weiss, O. S., Lora, J. N., et al. (2015). Developments in the Management of Chagas Cardiomyopathy. *Expert Rev. Cardiovasc. Ther.* 9072, 1–17. doi: 10.1586/14779072.2015.1103648

Teixeira, A. R. L., Hecht, M. M., Guimaro, M. C., and Sousa AO, N. N. (2011). Pathogenesis of Chagas' Disease: Parasite Persistence and Autoimmunity. *Clin. Microbiol. Rev.* 24, 592–630. doi: 10.1128/CMR.00063-10

Tontonoz, P., Nagy, L., Alvarez, J. G., Thomazy, V. A., and Evans, R. M. (1998). Pparγ Promotes Monocyte/Macrophage Differentiation and Uptake of Oxidized LDL. *Cell* 93, 241–252. doi: 10.1016/S0092-8674(00)81575-5

Trachtenberg, B. H., and Hare, J. M. (2017). Inflammatory Cardiomyopathic Syndromes. *Circ. Res.* 121, 803–818. doi: 10.1161/CIRCRESAHA.117.310221

Volpe, S., Cameroni, E., Moepps, B., Thelen, S., Apuzzo, T., and Thelen, M. (2012). CCR2 Acts as Scavenger for CCL2 During Monocyte Chemotaxis. *PloS One* 7, 1–10. doi: 10.1371/journal.pone.0037208

Wesley, M., Moraes, A., Rosa A de, C., Lott Carvalho, J., Shiroma, T., Vital, T., et al. (2019). Correlation of Parasite Burden, kDNA Integration, Autoreactive Antibodies, and Cytokine Pattern in the Pathophysiology of Chagas Disease. *Front. Microbiol.* 10, 1856. doi: 10.3389/fmicb.2019.01856

Wong, K. L., Tai, J. J. Y., Wong, W. C., Han, H., Sem, X., Yeap, W. H., et al. (2011). Gene Expression Profiling Reveals the Defining Features of the Classical, Intermediate,and Nonclassical Human Monocyte Subsets. *Blood* 118(5), e16-31. doi: 10.1182/blood-2010-12-326355

Wong, K. L., Yeap, W. H., Tai, J. J. Y., Ong, S. M., Dang, T. M., and Wong, S. C. (2012). The Three Human Monocyte Subsets: Implications for Health and Disease. *Immunol. Res.* 53, 41–57. doi: 10.1007/s12026-012-8297-3

Yin, W.-H., Chen, J.-W., Chen, Y.-H., and Lin, S.-J. (2013). Fenofibrate Modulates HO-1 and Ameliorates Endothelial Expression of Cell Adhesion Molecules in Systolic Heart Failure. *Acta Cardiol. Sin.* 29 (3), 251–260.

Zhang, J., Cheng, Y., Gu, J., Wang, S., Zhou, S., Wang, Y., et al. (2016). Fenofibrate Increases Cardiac Autophagy *via* FGF21/SIRT1 and Prevents Fibrosis and Inflammation in the Hearts of Type 1 Diabetic Mice. *Clin. Sci.* 130 (8), 625–641. doi: 10.1042/CS20150623

Zhang, L., and Tarleton, R. L. (1999). Parasite Persistence Correlates With Disease Severity and Localization in Chronic Chagas' Disease. *J. Infect. Dis.* 180, 480–486. doi: 10.1086/314889

Zhao, B. N., Campbell, J. J., Salanga, C. L., Ertl, L. S., Wang, Y., Yau, S., et al. (2019). CCR2-Mediated Uptake of Constitutively Produced CCL2: A Mechanism for Regulating Chemokine Levels in the Blood. *J. Immunol.* 203, 3157–3165. doi: 10.4049/jimmunol.1900961

Zou, J., Le, K., Xu, S., Chen, J., Liu, Z., Chao, X., et al. (2013). Fenofibrate Ameliorates Cardiac Hypertrophy by Activation of Peroxisome Proliferator-Activated Receptor-α Partly via Preventing P65-Nfκb Binding to Nfatc4. *Mol. Cell Endocrinol.* 370 (1-2), 103–112. doi: 10.1016/j.mce.2013.03.006

Conflict of Interest: The authors declare that the research was conducted in the absence of any commercial or financial relationships that could be construed as a potential conflict of interest.

Publisher's Note: All claims expressed in this article are solely those of the authors and do not necessarily represent those of their affiliated organizations, or those of the publisher, the editors and the reviewers. Any product that may be evaluated in this article, or claim that may be made by its manufacturer, is not guaranteed or endorsed by the publisher.

frontiers | Frontiers in Cellular and Infection Microbiology

ORIGINAL RESEARCH
published: 06 May 2022
doi: 10.3389/fcimb.2022.882555

The Impact of the CTHRSSVVC Peptide Upon Experimental Models of *Trypanosoma cruzi* Infection

Gabriela Rodrigues Leite[1], *Denise da Gama Jaén Batista*[1], *Ana Lia Mazzeti*[1,2], *Rosemeire Aparecida Silva*[3], *Ademar Benévolo Lugão*[4] *and Maria de Nazaré Correia Soeiro*[1]*

[1] Laboratório de Biologia Celular, Instituto Oswaldo Cruz (FIOCRUZ), Fundação Oswaldo Cruz, Rio de Janeiro, Brazil, [2] Universidade do Estado de Minas Gerais (UEMG), Laboratório de Parasitologia Aplicada, Unidade Passos, Belo Horizonte, Brazil, [3] Hospital das Clínicas, Faculdade de Medicina, Universidade de São Paulo (HCFMUSP), São Paulo, Brazil, [4] Instituto de Pesquisas Nucleares e Energéticas (IPEN), CNEN, São Paulo, Brazil

OPEN ACCESS

Edited by:
Vilma G. Duschak,
Consejo Nacional de Investigaciones Científicas y Técnicas (CONICET), Argentina

Reviewed by:
María Paula Faral-Tello,
Institut Pasteur de Montevideo, Uruguay
Concepción J. Puerta,
Pontifical Javeriana University, Colombia
Greta Volpedo,
The Ohio State University, United States

***Correspondence:**
Maria de Nazaré Correia Soeiro
soeiro@ioc.fiocruz.br

Specialty section:
This article was submitted to Clinical Microbiology, a section of the journal Frontiers in Cellular and Infection Microbiology

Received: 23 February 2022
Accepted: 07 April 2022
Published: 06 May 2022

Citation:
Leite GR, Batista DGJ, Mazzeti AL, Silva RA, Lugão AB and Soeiro MdNC (2022) The Impact of the CTHRSSVVC Peptide Upon Experimental Models of Trypanosoma cruzi Infection. Front. Cell. Infect. Microbiol. 12:882555. doi: 10.3389/fcimb.2022.882555

Chagas disease (CD), caused by the hemoflagellate protozoan *Trypanosoma cruzi*, affects more than six million people worldwide and presents an unsatisfactory therapy, based on two nitroderivatives, introduced in clinical medicine for decades. The synthetic peptide, with CTHRSSVVC sequence (PepA), mimics the CD163 and TNF-α tripeptide "RSS" motif and binds to atheromatous plaques in carotid biopsies of human patients, spleen tissues, and a low-density lipoprotein receptor knockout (LDLr–/–) mouse model of atherosclerosis. CD163 receptor is present on monocytes, macrophages, and neutrophils, acting as a regulator of acute-phase processes and modulating aspects of the inflammatory response and the establishment of infections. Due to the potential theranostic role of PepA, our aim was to investigate its effect upon *T. cruzi* infection *in vitro* and *in vivo*. PepA and two other peptides with shuffled sequences were assayed upon different binomials of host cell/parasite, including professional [as peritoneal mouse macrophages (PMM)] and non-professional phagocytes [primary cultures of cardiac cells (CM)], under different protocols. Also, their impact was further addressed *in vivo* using a mouse model of acute experimental Chagas disease. Our *in-vitro* findings demonstrate that PepA and PepB (the peptide with random sequence retaining the "RS" sequence) reduced the intracellular parasitism of the PMM but were inactive during the infection of cardiac cells. Another set of *in-vitro* and *in-vivo* studies showed that they do not display a trypanocidal effect on bloodstream trypomastigotes nor exhibit *in-vivo* efficacy when administered after the parasite inoculation. Our data report the *in-vitro* activity of PepA and PepB upon the infection of PMM by *T. cruzi*, possibly triggering the microbicidal arsenal of the host professional phagocytes, capable of controlling parasitic invasion and proliferation.

Keywords: Chagas disease, *Trypanosoma cruzi*, experimental chemotherapy, CTHRSSVVC peptide, immunomodulation

INTRODUCTION

According to the World Health Organization (WHO), neglected tropical diseases (NTDs) are communicable diseases that lack attention, care, and investments in areas of research and development of vaccines and medicines, affecting very poor communities with impaired public health access to early diagnosis and treatment (WHO, 2022).

Among the list of 20 NTDs, Chagas disease (CD), also known as American trypanosomiasis, affects more than six million people worldwide and is responsible for about 10,000 deaths per year (Sales Junior et al., 2017).

The etiological agent of CD is the protozoan *Trypanosoma cruzi* that presents different forms in both vertebrate and invertebrate hosts and that can be transmitted by distinct pathways, including via a vector insect and the oral route (Chatelain, 2017; Lidani et al., 2019). CD has two phases, acute and chronic, and since its discovery in 1909 by Carlos Chagas, it poses as a serious public health problem (WHO, 2022). Vaccines are not available and then control and treatment are exclusively related to drug therapy based on two very old pharmacological entities—benznidazole (Bz) and nifurtimox (NF)—introduced in clinical use for more than five decades (Soeiro and de Castro, 2009; Soeiro and de Castro, 2011; Soeiro, 2022). Both nitroderivatives have serious drawbacks including their limited efficacy, especially in the later chronic phase, and severe side effects with discontinuation (about 20%) of treatment (Soeiro and de Castro, 2011; Vieira et al., 2019; de Araújo et al., 2020).

Different experimental therapeutic approaches have been pursued aiming to find new drug candidates to face this sad scenario. The search includes several strategies such as i) repositioning studies of drugs already available in the market for other illness conditions, ii) identification of new antiparasitic agents using diverse libraries (composed of natural and synthetic products), iii) design and synthesis of new chemical entities selectively directed to molecular targets as well as iv) combined therapy, and v) molecular hybridization (hybrid compounds) combining two molecules (or parts of them) in a single new chemical entity to act on multiple targets of interest (Scarim et al., 2018; Simões-Silva et al., 2019; Soeiro, 2022).

The knowledge regarding the mechanisms involved in the pathological manifestations of CD has still not been fully gained (Soeiro, 2022). This knowledge could bring relevant contributions to the identification of more selective and complementary therapy for CD. In fact, despite being able to control and reduce the parasitic load in the acute phase, the host immune response and triggered inflammation are not able to fully eliminate the infection, and a progressive unbalanced inflammatory response (triggered by residual parasitism) is associated with the deteriorated conditions and may represent an important target for CD therapy (Benvenuti et al., 2017; Soeiro, 2022).

An interesting study demonstrated the ability of a peptide sequence—CTHRSSVVC (PepA), which mimics the CD163 molecule tripeptide "RSS" motif (Etzerodt et al., 2014) to bind inflammatory foci present in atheroma plaques in carotid biopsies of human patients, spleen tissues, and a low-density lipoprotein receptor knockout (LDLr−/−) mouse model of atherosclerosis (Silva et al., 2016). CD163 is present on professional phagocytes such as monocytes, macrophages, and neutrophils; eliminates hemoglobin and haptoglobin complexes; and acts as an acute-phase controller. Moreover, it plays a role in modulating inflammatory responses and the establishment of infections (Fabriek et al., 2009). *In-vitro* studies showed that the tracer [18F]AlF-NODAMP-C6-CTHRSSVVC binds CD163 receptors allowing a clear visualization of cancer cells using positron emission tomography (PET), although it was not able to detect subtle differences in CD163 levels of tumors induced by different treatments (Fernandes et al., 2021). No selective binding of the sulfo-Cy5-CTHRSSVVC peptide into macrophages could be noticed *in vitro*, but this tracer accumulates in a 4T1 tumor-bearing BALB/c mice model (Kovacs et al., 2022). Besides CD163, the RSS motif is likewise present in TNF-α (Etzerodt et al., 2014; Riethmueller et al., 2016; Zunke and Rose-John, 2017), stimulating its analysis in additional theranostic approaches (Silva et al., 2016; Fernandes et al., 2021; Kovacs et al., 2022).

Thus, as these previous reports suggest the potential theranostic role of PepA, our aim was to investigate its effect upon *T. cruzi* infection *in vitro* and *in vivo*. PepA and PepB (the peptide with random sequence retaining the "RS" sequence) reduced the intracellular parasitism of peritoneal mouse macrophages but were inactive during the infection of cardiac cells. Additional *in-vitro* and *in-vivo* studies showed that they do not display a trypanocidal effect on bloodstream trypomastigotes nor exhibit *in-vivo* efficacy when administered in a mouse model of acute *T. cruzi* infection after the parasite inoculation. The bulk of our data demonstrates the *in-vitro* activity of PepA and PepB upon the infection of PMM by *T. cruzi*, possibly triggering the microbicidal arsenal of the host professional phagocytes, capable of controlling parasitic invasion and proliferation.

MATERIALS AND METHODS

Tested Compounds

Peptide sequences (**Figure 1**) were synthesized by the Chinese Peptides Company (Hangzhou, China) and fully characterized by nuclear magnetic resonance (NMR); carbon, hydrogen, and nitrogen (C, H, N) composition analyses; and MALDI/FAB mass spectrometry as reported (Silva et al., 2016). Stock solutions were prepared at 6 mM in sterile deionized water. The original sequence (CTHRSSVVC) which mimics the "RSS" motif of the CD163 molecule was named peptide A (PepA), the random sequence retaining the "RS" sequence of peptide A was called peptide B (CGRSKAMFC, PepB), and a scrambled sequence of peptide A was named peptide C (CHVSVRTSC, PepC). The reference compound for trypanocidal activity was the nitroderivative benznidazole [N-benzyl-2-(2-nitroimidazol-1-yl) acetamide2-nitroimidazole, Bz] (Laboratório Farmacêutico do Estado de Pernambuco, Brazil) (**Figure 1**), which was prepared in a stock concentration of 50 mM diluted in dimethylsulfoxide (100% DMSO), with the final in-test concentration never exceeding 0.6% for *in-vitro* experiments to avoid non-specific toxicity. For *in-vivo* assays, the peptides were diluted daily and prepared in sterile and deionized water. The reference drug was

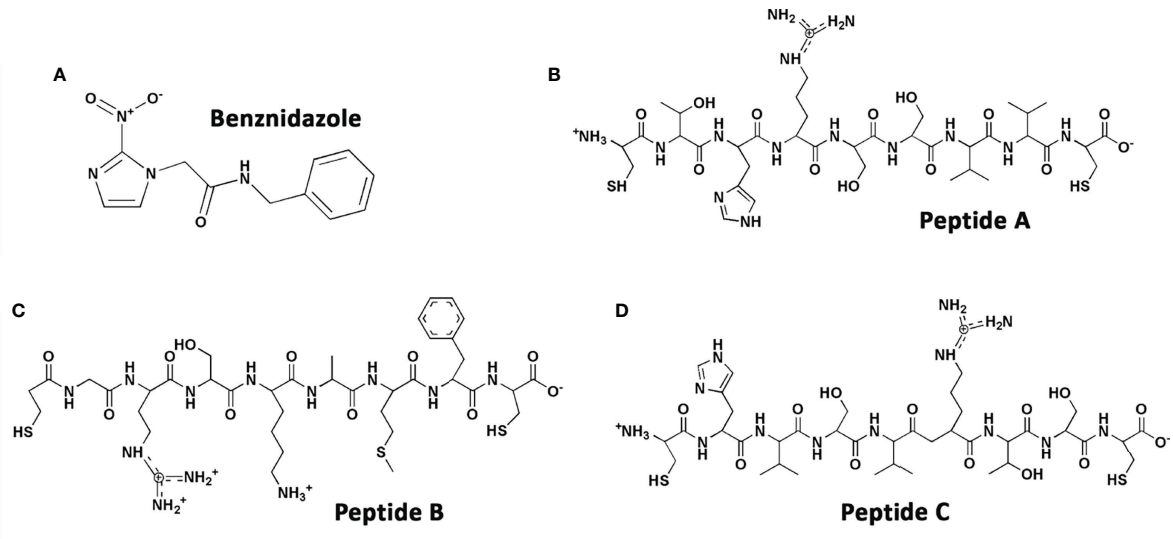

FIGURE 1 | Chemical structures of **(A)** benznidazole, **(B)** PepA, **(C)** PepB, and **(D)** PepC.

diluted in a solution composed of sterile and deionized water with 3% of Tween 80 (Guedes-da-Silva et al., 2016).

Parasites

Bloodstream trypomastigote forms of the Y strain of *T. cruzi* were obtained from male Swiss Webster mice at the peak of parasitemia by cardiac puncture (Meirelles et al., 1986; Batista et al., 2010).

Mammalian Host Cells

Primary cultures of mouse embryonic cardiac cells (CM) were obtained as described (Meirelles et al., 1986). CM were seeded into 24-well plates with 50×10^3 cells per well. Peritoneal mouse macrophages (PMM) were obtained by peritoneal lavage of male Swiss mice (Santos et al., 2020). PMM were plated into 96-well plates (50×10^3 cells per well) and 24-well plates (30×10^4 cells per well). All cultures were maintained at 37°C/5% CO_2.

Mammalian Toxicity

The toxicity of the peptides was investigated upon PMM using the alamarBlue test (Invitrogen, Waltham, MA, USA) according to the manufacturer's recommendations (Timm et al., 2014; Guedes-da-Silva et al., 2016). PMM were treated for 48 h with increasing concentrations of the tested peptides (up to 500 μM). Following the exposition period, the colorimetric test was performed with alamarBlue® (cell viability detection test) and absorbance was determined by a spectrophotometer (570 and 600 nm). All assays were performed in triplicate in at least two individual assays (Timm et al., 2014; Guedes-da-Silva et al., 2016).

The Activity of the Peptides on Intracellular Forms of the Y Strain Present in Primary Cell Cultures (PMM and CM)

The effect of the peptides on intracellular forms in PMM was performed under the following protocols: i) *pretreatment*: PMM were rinsed and incubated for 24 h with different concentrations of the tested peptides and with Bz up to a maximum concentration of 50 μM. After incubation, the culture medium was replaced to remove the tested compounds and PMM were infected for 2 h with trypomastigote forms of *T. cruzi* (Y strain, M.O.I. 10 parasites:1 cell). Then, cultures were rinsed to remove the non-internalized parasites and incubated for 48 h at 37°C with RPMI culture medium. ii) *Posttreatment*: PMM were infected for 2 h with *T. cruzi* (Y strain, M.O.I. 10 parasites:1 cell), rinsed, and incubated for 24 h at 37°C. PMM were then incubated for 48 h at 37°C with increasing concentrations (up to 50 μM) of the peptides and Bz.

The effect of the peptides on intracellular forms of *T. cruzi* present in CM was performed as follows: *i) pretreatment*: CM cultures were incubated for 24 h with different concentrations of the peptides and Bz (up to 50 μM). Then, the cultures were rinsed to remove the compounds and infected for 24 h with bloodstream trypomastigote forms of *T. cruzi* (Y strain, M.O.I. 10 parasites:1 cell). After infection, the samples were rinsed to remove non-internalized parasites and incubated for 48 h at 37°C/5% CO_2. *ii) Posttreatment*: CM were infected with bloodstream trypomastigote forms (Y strain, M.O.I. 10:1), and after 24 h, the cultures were washed to remove non-internalized parasites and incubated for 48 h at 37°C/5% CO_2 with increasing concentrations of peptides (up to 50 μM).

After the different assays, PMM and CM were rinsed with phosphate-buffered saline (PBS) and fixed with Bouin solution. Then, the samples were stained with Giemsa for quantification (under light microscopy) of the percentage of infected host cells, the number of parasites per cell to calculate the infection index (multiplication between these two factors). Infected cultures not subjected to the treatments were used as negative controls (Guedes da Silva et al., 2016).

All assays were performed in duplicates in at least two individual assays (Timm et al., 2014; Guedes-da-Silva et al., 2016).

The Activity of the Peptides on Bloodstream Trypomastigote Forms

Bloodstream trypomastigotes (Y strain) were incubated with the tested peptides and Bz up to a concentration of 100 μM. After 2 and 24 h of incubation at 37°C, the number of live parasites (identified by their characteristic morphology and movement) was determined under a light microscope by quantification in a Neubauer chamber to determine the EC_{50} values. Controls were performed with parasites kept under the same conditions, in the absence of peptides (de Araújo et al., 2019).

In-vitro studies represent the analysis of two individual assays performed in duplicates.

Effect of Peptides Upon Experimental Mouse *Trypanosoma cruzi* Infection

Male Swiss Webster mice (18–20 g, 4–5 weeks of age) obtained from the animal facilities of the Institute of Science and Biomodels Technology (ICTB) FIOCRUZ were housed at a maximum of five per cage, kept in a specific-pathogen-free room at 20°C to 24°C under a 12-h light and 12-h dark cycle, and provided sterilized water and chow *ad libitum*. Male mice were used as previous findings showed that they are more vulnerable to experimental infection than females and thus more suitable for therapeutic screenings (Guedes et al., 2015). The animals were acclimated for 7 days before starting the experiments. Infection was performed by intraperitoneal (i.p.) injection of 10^4 bloodstream trypomastigotes (Y strain). *Trypanosoma cruzi*-infected mice were treated intraperitoneally with 0.1 ml of the tested peptides for up to 10 consecutive days, starting at 5 dpi, which corresponds to (in this experimental model) the parasitemia onset. Only mice with positive parasitemia were used in the infected groups. Benznidazole at 100 mg/kg/day (as the optimal dose) was run in parallel. Peptides were freshly prepared in sterile and distilled water, dosing according to the body weight of the animals. The experimental animal groups were divided as follows: uninfected (uninfected and untreated), untreated (infected and treated with vehicle only), treated with Bz (infected and treated with daily doses of 0.1 ml at 100 mg/kg, by gavage), and treated with peptides (infected and treated with daily doses of 0.1 ml of each peptide at 10 mg/kg). Parasitemia was performed individually by direct counting of the parasite in the blood (5 μl) under a light microscope. Mice were weighed once a week to monitor possible changes in body weight. Mortality was checked daily up to 30 days after treatment and expressed as the percentage of accumulated mortality (% CM) (Ferreira de Almeida Fiuza et al., 2018). *In-vivo* studies were performed twice using five animals per group ($n = 5$).

Ethics Statement

All procedures were carried out in accordance with the guidelines established by FIOCRUZ Committee of Ethics on Animal Experimentation (CEUA) number L-038/2017.

Statistical Analysis

The statistical analysis was performed by analysis of variance (ANOVA), the data for the different assays were combined, and the significance was set at a p-value of ≤0.05 (Guedes-da-Silva et al., 2016).

RESULTS

Cytotoxic Effect of the Peptides on Mammalian Host Cells

Considering the importance of identifying non-toxic agents, the cytotoxic effect of the peptides on PMM was assessed using the alamarBlue test. The findings demonstrated that the tested peptides did not induce loss of cellular viability when PMM were incubated for 48 h (up to 500 μM), while Bz gave LC_{50} value = 333 ± 165 μM (**Table 1**).

Effect of the Peptides Upon Infection of PMM by *Trypanosoma cruzi*

The activity of the peptides and Bz upon the infection of PMM with *T. cruzi* [Y strain, discrete typing unit (DTU II)] was evaluated by counting the number of intracellular parasites and the percentage of infected host cells to determine the infection index (II) of Giemsa-stained samples (**Figure 2**). The assays were performed under two different protocols, namely, pre- and posttreatment, by the addition of the tested peptides before and after the establishment of the infection to verify their potential effect directly on the host cells and against the intracellular parasites, respectively (**Tables 2**, **3**). The previous treatment of PMM with PepA and PepB resulted in lower parasite levels as compared with untreated samples, reaching decreases of 62% ($p = 0.027$) and 49% ($p = 0.119$), respectively, while PepC and Bz gave smaller (30% and 22%) and non-significant drops ($p = 0.684$ and $p = 0.799$), respectively (**Tables 2**, **3**). After the establishment of the infection, PepA and PepB induced a non-significant effect on the parasite load, reaching 36% ($p = 0.169$) and 48% ($p = 0.621$) of decreases, respectively, while Bz reached 98% of decline ($p = 0.066$) (**Table 2**).

Effect of the Peptides Upon Infection of CM by *Trypanosoma cruzi*

The activity of PepA and PepB was additionally investigated using primary cultures of mouse cardiac cells infected with the Y strain. As depicted in **Table 4**, both peptides only caused modest and non-significant ($p > 0.05$) reductions in parasitism of CM, reaching maximum values of 35% inhibition of infection rates at the highest concentration (50 μM), while Bz resulted in 96% of decline (**Table 4**).

TABLE 1 | Determination of the cytotoxicity profile (LC_{50} values) of peptides (PepA, PepB, and PepC) and benznidazole (Bz) on the primary culture of peritoneal mouse macrophages (PMM).

	LC_{50} values (mean ± SD/μM)[a]
Bz	333 ± 165
PepA	>500
PepB	>500
PepC	>500

[a]*Analysis represents two individual assays performed in triplicates.*

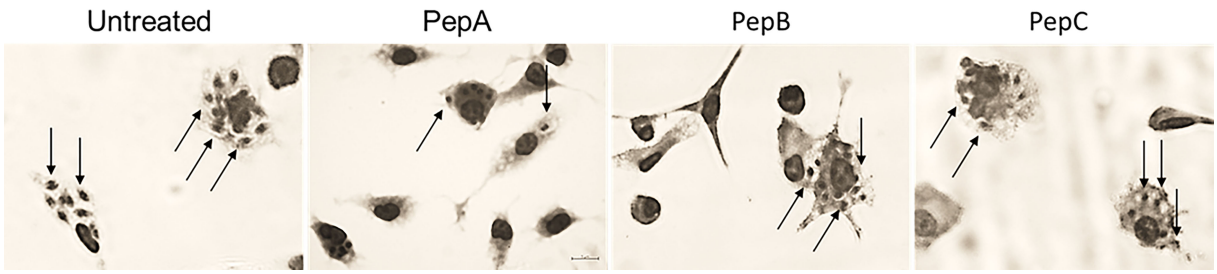

FIGURE 2 | Light microscopy images of peritoneal mouse macrophages pretreated with PepA, PepB, and PepC at 50 μM before infection with *Trypanosoma cruzi*. **(A)** Untreated, **(B)** PepA, **(C)** PepB, and **(D)** PepC. Arrows: intracellular parasites.

TABLE 2 | Activity of peptide A (PepA), peptide B (PepB), and benznidazole (Bz) on *in-vitro* infection of peritoneal mouse macrophages (PMM) by *Trypanosoma cruzi* (Y strain) submitted to pre- and posttreatment protocols.

	Infection index (mean ± SD) (% reduction)[a]	
	Pre-treatment	**Post-treatment**
Untreated	109 ± 16	272 ± 178
Bz	ND	6.5 ± 5.9 (98)*
PepA	41 ± 19 (62)**	174 ± 166 (36)[#]
PepB	56 ± 24 (49)[#]	140 ± 108 (48)[#]

Mean ± SD of the infection index (% of reduction).
ND, not determined.
[a]*Analysis of two individual assays performed in duplicates.*
**p > 0.066; **p = 0.027; [#]p > 0.05.*

TABLE 3 | Activity of peptide C (PepC) and benznidazole (Bz) on *in-vitro* infection of peritoneal mouse macrophages (PMM) by *Trypanosoma cruzi* (Y strain) using pretreatment protocol: mean ± SD of the infection index (% of reduction).

	Infection index (mean ± SD) (% reduction)[a]
Untreated	229 ± 174
PepC	160 ± 113 (30)[#]
Bz	178 ± 176 (22)[#]

[a]*Analysis of two individual assays performed in duplicates.*
[#]*p > 0.05.*

Effect of the Peptides on Bloodstream Forms of *Trypanosoma cruzi*

To check the potential direct effect of the peptides upon the other relevant form of *T. cruzi* to mammalian infections, the activity of the peptides was assayed upon extracellular bloodstream trypomastigotes (Y strain) through light microscopy. The findings demonstrated that all peptides were inactive against bloodstream forms (EC_{50} > 100 μM), while Bz achieved likely potency (EC_{50} value = 12 μM) (**Table 5**).

Effect of the Peptides *In Vivo*

Finally, *in-vivo* assays were conducted to explore the potential therapeutic effect of the peptides upon a mouse model of acute *T. cruzi* infection (Swiss mice infected with the Y strain), under administration for 5–10 consecutive days with 10 mg/kg/day, *via* the intraperitoneal route, starting at the parasitemia onset (5 dpi).

TABLE 4 | Activity of peptides A and B and benznidazole (Bz) on *in-vitro* infection of cardiac cell cultures by *Trypanosoma cruzi* (Y strain) using pre- and posttreatment with peptides (50 μM) and Bz (5.5 μM) used as a reference drug.

	Infection index (mean ± SD) (% reduction)[a]	
	Pre-treatment	**Post-treatment**
Untreated	378 ± 113	394 ± 162
Bz	386 ± 56 (0)[#]	14.57 ± 7 (96)*
PepA	288 ± 112 (24)[#]	320.8 ± 154 (19)[#]
PepB	325 ± 86 (14)[#]	253.9 ± 141 (35)[#]

Reduction of the CM infection by T. cruzi: mean ± SD of the infection index (% of reduction).
[a]*Analysis of two individual assays performed in duplicates.*
**p = 0.0107; [#]p > 0.05.*

Our findings (**Figures 3A, B**) show that all peptides displayed a maximum of 23% of parasitemia decline (8 dpi), while Bz (optimal dose of 100 mg/kg/day) fully suppressed (>99%) the parasitemia at 8 dpi, corresponding to the parasitemia peak (**Figure 3B**). Also, the ponderal curve demonstrates that all peptides were unable to protect against weight loss induced by *T. cruzi* infection, which was clearly reverted during Bz administration (**Figure 3C**). Indeed, only the reference drug gave 100% of animal survival, while all peptides reached 100% of cumulative death as soon as at 15 dpi, similar to the vehicle-treated mice group (**Figure 3D**).

DISCUSSION

The peptide with CTHRSSVVC sequence (PepA) mimics the CD163 and TNF-α tripeptide "RSS" motif. The CD163 receptor

TABLE 5 | The biological effect of the peptides and benznidazole (EC_{50} values at μM) against bloodstream trypomastigotes of *Trypanosoma cruzi* (Y strain) after 2 and 24 h of incubation at 37°C.

	EC_{50} values (mean ± SD/μM)[a]	
	2 h	**24 h**
Bz	–	12
PepA	>100	>100
PepB	>100	>100
PepC	>100	>100

[a]*Analysis of two individual assays performed in duplicates.*

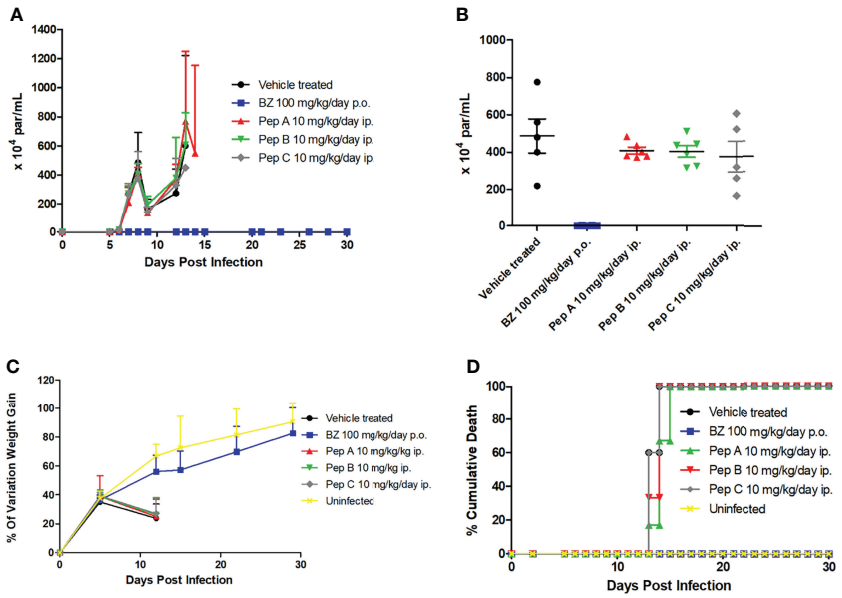

FIGURE 3 | Effect of peptides and benznidazole upon a mouse model of acute *Trypanosoma cruzi* infection. **(A)** Parasitemia curve, **(B)** data dispersion of blood parasitism at 8 days postinfection, **(C)** ponderal curve, and **(D)** cumulative mortality.

is present on monocytes, macrophages, and neutrophils, acting as a regulator of acute-phase processes and modulating aspects of the inflammatory response and the establishment of infections (Etzerodt et al., 2014; Silva et al., 2016). Hence, due to previous reports regarding the theranostic role of PepA, our aim was to evaluate its effect upon *T. cruzi* experimental infection *in vitro* and *in vivo*. Besides PepA, two other sequences were assessed: one that maintains the "RS" region (PepB) and another that maintains all the amino acids in scrambled order to the original sequence (PepC). As CD163 is present in professional phagocytes, these peptides were screened in PMM by means of distinct protocols exploring the potential cytotoxic profile on mammalian cells as well as their effect on *T. cruzi* infection before (pretreatment) and after parasite interaction (posttreatment). Our data showed that all peptides showed a non-toxic profile, which is a desirable characteristic for new drug candidates (Gupta et al., 2015).

PepA and PepB reduced the infection indexes of *T. cruzi*-infected PMM reaching a statistically significant (p = 0.027) maximum decline of 62% when the CTHRSSVVC sequence was added prior to parasite interaction. Accordingly, PepC, the one with scrambled sequence, only reached a non-significant decrease of 30% when added prior to protozoan infection, arguing in favor of the specificity of the RS motif present in PepA and PepB, possibly triggering a microbicidal response induced by the RS sequence region. On the other hand, the lack of activity of the peptides on the trypomastigote forms suggests that the effect of PepA and PepB is on PMM metabolism rather than on the parasite itself due to their inability to lyse bloodstream forms.

No major effect was noticed when cardiac cell cultures were used as host cells, supporting the hypothesis that the sequence region "RS" of PepA and PepB may selectively activate professional phagocytes such as PMM by an immunomodulatory pathway. The lack of therapeutic activity against bloodstream trypomastigotes was also corroborated by *in-vivo* approaches demonstrating only a mild reduction of the parasitemia in mice treated with the peptides after *T. cruzi* infection. Although the "RSS" motif is a conserved sequence present only in human and monkey CD163, its soluble form (sCD163) is likewise detectable in mouse serum and is present in TNF-α (Etzerodt et al., 2014; Riethmueller et al., 2016; Zunke and Rose-John, 2017). Macrophages are notoriously heterogeneous. They can adopt a spectrum of phenotypes from the anti-inflammatory M2-type state (CD163) to the pro-inflammatory M1-type state (TNF-α). However, the inflammatory phenotype of the M1 versus M2 macrophage is not constant, which probably reflects the plasticity of monocyte-derived cells in response to microenvironmental changes (Sica et al., 2006; Moghaddam et al., 2018). In this context, their potential biological effect may depend on how the peptide will be presented for specific binding to occur and where they will bind. Since *T. cruzi* infection stimulates the activation of both M1 and M2 macrophages (Zanluqui et al., 2015), further studies will be necessary to evaluate the mode of action of PepA and PepB on *T. cruzi* experimental infection. In fact, in addition to CD163, the RSS motif is present in TNF-α and a soluble CD163 exists in mice, and further studies are necessary to reveal the mode of action of the peptides. These studies would include measurements of different inflammatory mediators *in vitro* besides evaluating the response upon the infection of M1 and M2 macrophage populations as well as the use of distinct *in-vivo* models and regimens (e.g., pretreatment of mice with peptide before parasite inoculation of murine models of acute and chronic infection). Moreover, other

factors must be considered during the experimental assays such as peptide stability *in vivo*, levels of macrophage subpopulations, and different types and kinetics of inflammation in the acute and chronic models of *T. cruzi* infection (Silva et al., 2016; Fernandes et al., 2021; Kovacs et al., 2022).

The bulk of our findings suggests that the non-toxic profile of PepA and PepB along with their ability to diminish PMM parasitism *in vitro* justifies additional studies aiming to open new perspectives for alternative therapies for CD.

DATA AVAILABILITY STATEMENT

The raw data supporting the conclusions of this article will be made available by the authors, without undue reservation.

ETHICS STATEMENT

All procedures were carried out in accordance with the guidelines established by FIOCRUZ Committee of Ethics on Animal Experimentation (CEUA) number L-038/2017.

AUTHOR CONTRIBUTIONS

GL contributed to the *in-vitro* and *in-vivo* assays and wrote and edited the entire manuscript. DB contributed to the *in-vivo* assays and analyzed the data. AM contributed to the *in-vivo* assays. RS provided the peptides and reviewed the manuscript. AL provided the peptides and reviewed the manuscript. MS was responsible for the project and methodology design, analyzed the data, and edited and reviewed the manuscript. All authors contributed to the article and approved the submitted version.

FUNDING

The Carlos Chagas Filho Foundation for Research Support of the State of Rio de Janeiro (FAPERJ), National Council for Scientific and Technological Development (CNPq), Oswaldo Cruz Foundation, PAEF/CNPq/FIOCRUZ, PDTIS, and CAPES funded this study. MS is a research fellow from CNPq and CNE.

ACKNOWLEDGMENTS

The authors would like to thank to Dr. Alexis Murillo Carrasco, Dr. Lucas Freitas de Freitas, and Ludmila F. de A Fiuza (M.Sc.).

REFERENCES

Batista, D. G., Batista, M. M., de Oliveira, G. M., do Amaral, P. B., Lannes-Vieira, J., Britto, C. C., et al. (2010). Arylimidamide DB766, A Potential Chemotherapeutic Candidate for Chagas' Disease Treatment. *Antimicrobial Agents Chemother* 54 (7), 2940–2952. doi: 10.1128/AAC.01617-09

Benvenuti, L. A., Roggério, A., Cavalcanti, M. M., Nishiya, A. S., and Levi, J. (2017). An Autopsy-Based Study of Trypanosoma Cruzi Persistence in Organs of Chronic Chagasic Patients and its Relevance for Transplantation. *Transplant. Infect. Dis.* 19 (6), e12783. doi: 10.1111/tid.12783

Chatelain, E. (2017). Chagas Disease Research and Development: Is There Light at the End of the Tunnel? *Comput. Struct. Biotechnol. J.* 15, 98–103. doi: 10.1016/j.csbj.2016.12.002

de Araújo, J. S., García-Rubia, A., Sebastián-Pérez, V., Kalejaiye, T. D., da Silva, P. B., Fonseca-Berzal, C. R., et al. (2019). Imidazole Derivatives as Promising Agents for the Treatment of Chagas Disease. *Antimicrobial Agents Chemother* 63 (4), e02156–e02118. doi: 10.1128/AAC.02156-18

de Araújo, J. S., da Silva, C. F., Batista, D. G. J., Nefertiti, A., de Almeida Fiuza, L. F., Fonseca-Berzal, C. R., et al. (2020). Efficacy of Novel Pyrazolone Phosphodiesterase Inhibitors in Experimental Mouse Models of Trypanosoma Cruzi. *Antimicrobial Agents Chemother* 64 (9), e00414–20. doi: 10.1128/AAC.00414-20

Etzerodt, A., Rasmussen, M. R., Svendsen, P., Chalaris, A., Schwarz, J., Galea, I., et al. (2014). Structural Basis for Inflammation-Driven Shedding of CD163 Ectodomain and Tumor Necrosis Factor-α in Macrophages. *J. Biol. Chem.* 289 (2), 778–788. doi: 10.1074/jbc.M113.520213

Fabriek, B. O., Bruggen, R. V., Deng, D. M., Ligtenberg, A. J. M., Nazmi, K., Schornagel, K., et al. (2009). The Macrophage Scavenger Receptor CD163 Functions as an Innate Immune Sensor for Bacteria. *Blood* 113 (4), 887–892. doi: 10.1182/blood-2008-07-167064

Fernandes, B.. (2021). Development of PET Tracers for M2-Macrophages. *Univ. Groningen*, 1–174. doi: 10.33612/diss.194780714

Ferreira de Almeida Fiuza, L., Peres, R. B., Simões-Silva, M. R., da Silva, P. B., Batista, D. G. J., da Silva, C. F., et al. (2018). Identification of Pyrazolo[3,4-E][1,4]Thiazepin Based CYP51 Inhibitors as Potential Chagas Disease Therapeutic Alternative: *In Vitro* and *In Vivo* Evaluation, Binding Mode Prediction and SAR Exploration. *Eur. J. Med Chem.* 149, 257–268. doi: 10.1016/j.ejmech.2018.02.020

Guedes-da-Silva, F. H., Batista, D. G. J., Meuser, M. B., Demarque, K. C., Fulco, T., de Araújo, J. S., et al. (2016). *In Vitro* and *In Vivo* Trypanosomicidal Action of Novel Arylimidamides Against Trypanosoma Cruzi. *Antimicrobial Agents Chemother* 60, 2425–2434. doi: 10.1128/AAC.01667-15

Guedes, F. H., Batista, D. G. J., da Silva, C. F., Meuser, M. B., Simões-Silva, M. R., de Araújo, J. S., et al. (2015). Antimicrob Agents Chemother. *American Society for Microbiology* 59, 12, 7564–7570. doi: 10.1128/AAC.01294-15

Gupta, S., Kapoor, P., Chaudhary, K., Gautam, A., Kumar, R., Raghava, G. O. S., et al. (2015). 'Antimicrob Agents Chemother', in *Computational Peptidology*, vol. pp . Eds. P. Zhou and J. Huang (New York, NY: Springer New York (Methods in Molecular Biology), 143–157. doi: 10.1007/978-1-4939-2285-7_7

Kovacs, L., Davis, R. A., Ganguly, T., Chammas, R., and Sutcliffe, J. L. (2022). Repurposing an Atherosclerosis Targeting Peptide for Tumor Imaging. *BioMed. Pharmacother.* 145, 112469. doi: 10.1016/j.biopha.2021.112469

Lidani, K. C. F., Andrade, F. A., Bavia, L., Damasceno, F. S., Beltrame, M. H., Messias-Razão, I. J., et al. (2019). Chagas Disease: From Discovery to a Worldwide Health Problem. *Front. Public Health* 7. doi: 10.3389/fpubh.2019.00166

Meirelles, M. N., de Araújo-Jorge, T. C., Miranda, C. F., de Souza, W., and Barbosa, H. S. (1986). Interaction of Trypanosoma Cruzi With Heart Muscle Cells: Ultrastructural and Cytochemical Analysis of Endocytic Vacuole Formation and Effect Upon Myogenesis *In Vitro*. *Eur. J. Cell Biol.* 41 (2), 198–206.

Moghaddam, A. S., Mohammadian, S., Vazini, H., Taghadosi, M., Esmaeili, A. S., Mardani, F., et al. (2018). Macrophage Plasticity, Polarization and Function in Health and Disease. *J. Cell Physiol* 233, 6425–6440. doi: 10.1002/jcp.26429

Riethmueller, S., Ehlers, J. C., Lokau, J., Dusterhöft, S., Knittler, K., Dombrowsky, G., et al. (2016). Cleavage Site Localization Differentially Controls Interleukin-6 Receptor Proteolysis by ADAM10 and ADAM17. *Sci. Rep* 6, 25550. doi: 10.1038/srep25550

Sales Junior, P. A., Molina, I., Murta, S. M. F., Sánchez-Montalvá, A., Salvador, F., Corrêa-Oliveira, R., et al. (2017). Experimental and Clinical Treatment of Chagas Disease: A Review. *Am. J. Trop. Med. Hygiene* 97 (5), 1289–1303. doi: 10.4269/ajtmh.16-0761

Santos, C. C., Zhang, H., Batista, M. M., de Oliveira, G. M., Demarque, K. C., Silva Gomes, N., et al. (2020). *In Vitro* and *In Vivo* Evaluation of an Adamantyl-Based Phenyl Sulfonyl Acetamide Against Cutaneous Leishmaniasis Models of Leishmania Amazonensis. *Antimicrobial Agents Chemother* 64 (12), e01188–e01120. doi: 10.1128/AAC.01188-20

Scarim, C. B., Jornada, D. H., Chelucci, R. C., de Almeida, L., Santos, J. L., Chung, H. C., et al. (2018). Current Advances in Drug Discovery for Chagas Disease. *Eur. J. Med Chem.* 155, 824–838. doi: 10.1016/j.ejmech.2018.06.040

Sica, A., Schioppa, T., Mantovani, A., and Allavena, P. (2006). Tumour-Associated Macrophages Are a Distinct M2 Polarised Population Promoting Tumour Progression: Potential Targets of Anti-Cancer Therapy. *Eur. J. Cancer* 42 (6), 717–727. doi: 10.1016/j.ejca.2006.01.003

Silva, R. A., Giordano, R. J., Gutierrez, P. S., Rocha, V. Z., Rudnicki, M., Kee, P., et al. (2016). CTHRSSVVC Peptide as a Possible Early Molecular Imaging Target for Atherosclerosis. *Int. J. Mol. Sci.* 17 (9), 1383. doi: 10.3390/ijms17091383

Simões-Silva, M. R., De Araújo, J. S., Peres, R. B., da Silva, P. B., Batista, M. M., De Azevedo, L. D., et al. (2019). Repurposing Strategies for Chagas Disease Therapy: The Effect of Imatinib and Derivatives Against Trypanosoma Cruzi. *Parasitology* 146 (8), 1006–1012. doi: 10.1017/S0031182019000234

Soeiro, M. N. C. (2022). Perspectives for a New Drug Candidate for Chagas Disease Therapy. *Memórias Do Instituto Oswaldo Cruz* 117, e220004. doi: 10.1590/0074-02760220004

Soeiro, M. N. C., and de Castro, S. L. (2009). Trypanosoma Cruzi Targets for New Chemotherapeutic Approaches. *Expert Opin. Ther. Targets* 13 (1), 105–121. doi: 10.1517/14728220802623881

Soeiro, M. N. C., and de Castro, S. L. (2011). Screening of Potential Anti-Trypanosoma Cruzi Candidates: *In Vitro* and *In Vivo* Studies. *Open Med Chem. J.* 5, 21–30. doi: 10.2174/1874104501105010021

Timm, B. L., da Silva, P. B., Batista, M. M., Guedes da Silva, F. H., da Silva, C. F., Tidwell, R. R., et al. (2014). *In Vitro* and *In Vivo* Biological Effects of Novel Arylimidamide Derivatives Against Trypanosoma Cruzi. *Antimicrobial Agents Chemother* 58 (7), 3720–3726. doi: 10.1128/AAC.02353-14

Vieira, J. L., Távora, F. R. F., Sobral, M. G. V., Vasconcelos, G. G., Almeida, G. P. L., Fernandes, J. R., et al. (2019). Chagas Cardiomyopathy in Latin America Review. *Curr. Cardiol. Rep.* 21 (2), 8. doi: 10.1007/s11886-019-1095

WHO (2022) *World Health Organization*. Available at: https://www.who.int/news-room/fact-sheets/detail/chagas-disease-(american-trypanosomiasis) (Accessed 9 February 2022).

Zanluqui, N. G., Wowk, P. F., and Pinge-Filho, P. (2015). Macrophage Polarization in Chagas Disease. *J Clin Cell Immunol* 1–6. doi: 10.4172/2155-9899.1000317

Zunke, F., and Rose-John, S. (2017). The Shedding Protease ADAM17: Physiology and Pathophysiology. *Biochim. Biophys. Acta* 1864 (11 Pt B), 2059–2070. doi: 10.1016/j.bbamcr.2017.07

Conflict of Interest: The authors declare that the research was conducted in the absence of any commercial or financial relationships that could be construed as a potential conflict of interest.

Publisher's Note: All claims expressed in this article are solely those of the authors and do not necessarily represent those of their affiliated organizations, or those of the publisher, the editors and the reviewers. Any product that may be evaluated in this article, or claim that may be made by its manufacturer, is not guaranteed or endorsed by the publisher.

frontiers | Frontiers in Cellular and Infection Microbiology

MINI REVIEW
published: 30 June 2022
doi: 10.3389/fcimb.2022.910854

Role of the Complement System in the Modulation of T-Cell Responses in Chronic Chagas Disease

María Belén Caputo[1], *Josefina Elias*[1], *Gonzalo Cesar*[1], *María Gabriela Alvarez*[2], *Susana Adriana Laucella*[1,2] *and María Cecilia Albareda*[1]*

[1] Investigation Department, Instituto Nacional de Parasitología Dr. Fatala Chaben, Buenos Aires, Argentina, [2] Chagas Section, Hospital Interzonal General de Agudos Eva Perón, Buenos Aires, Argentina

Chagas disease, caused by the intracellular pathogen *Trypanosoma cruzi*, is the parasitic disease with the greatest impact in Latin America and the most common cause of infectious myocarditis in the world. The immune system plays a central role in the control of *T. cruzi* infection but at the same time needs to be controlled to prevent the development of pathology in the host. It has been shown that persistent infection with *T. cruzi* induces exhaustion of parasite-specific T cell responses in subjects with chronic Chagas disease. The continuous inflammatory reaction due to parasite persistence in the heart also leads to necrosis and fibrosis. The complement system is a key element of the innate immune system, but recent findings have also shown that the interaction between its components and immune cell receptors might modulate several functions of the adaptive immune system. Moreover, the findings that most of immune cells can produce complement proteins and express their receptors have led to the notion that the complement system also has non canonical functions in the T cell. During human infection by *T. cruzi*, complement activation might play a dual role in the acute and chronic phases of Chagas disease; it is initially crucial in controlling parasitemia and might later contributes to the development of symptomatic forms of Chagas disease due to its role in T-cell regulation. Herein, we will discuss the putative role of effector complement molecules on T-cell immune exhaustion during chronic human *T. cruzi* infection.

Keywords: *Trypanosoma cruzi*, chagas' disease, T cell, anaphylatoxins, exhaustion

OPEN ACCESS

Edited by:
Alberto Enrique Paniz Mondolfi, Icahn School of Medicine at Mount Sinai, United States

Reviewed by:
Kathryn Jones, Baylor College of Medicine, United States

***Correspondence:**
María Cecilia Albareda
mcalbareda@gmail.com

Specialty section:
This article was submitted to Clinical Microbiology, a section of the journal Frontiers in Cellular and Infection Microbiology

Received: *01 April 2022*
Accepted: *26 May 2022*
Published: *30 June 2022*

Citation:
Caputo MB, Elias J, Cesar G, Alvarez MG, Laucella SA and Albareda MC (2022) Role of the Complement System in the Modulation of T-Cell Responses in Chronic Chagas Disease. Front. Cell. Infect. Microbiol. 12:910854. doi: 10.3389/fcimb.2022.910854

INTRODUCTION

In an acute infection in which the antigen is totally eliminated, long-lived memory T cells are generated and can be maintained by homeostatic mechanisms regardless of the presence of antigen. In contrast, in the context of chronic infection, the antigen-specific T cells that are generated depend on the presence of the antigen to proliferate, do not respond to homeostatic mechanisms, and lose many of their effector capabilities, raising concerns about the establishment of "true" memory pathogen-specific T cells. This state is called immune exhaustion, and the earliest evidence suggesting the presence of this process was provided by studies using a mouse model of chronic

lymphocytic choriomeningitis virus (LCMV) (Gallimore et al., 1998); since then, it has been found to commonly occur during numerous human chronic viral (Boni et al., 2007; Kahan et al., 2015) and bacterial infections (Behar et al., 2014) and, more recently, in protozoan infections, including malaria, *Trypanosoma cruzi* and toxoplasmosis (Gigley et al., 2012; Rodrigues et al., 2014). Immune exhaustion also occurs in noninfectious environments, such as tumors, where tumor antigens are persistently expressed (Ahmadzadeh et al., 2009; Crespo et al., 2013).

Immune exhaustion of T cells is characterized by the progressive and hierarchical loss of effector functions associated with the increased expression of inhibitory receptors, altered gene expression of key transcription factors, cellular metabolic disorders, loss of the homeostatic response to the T-cell cytokines IL-7 and IL-15 and changes in the expression of pro- and anti-apoptotic factors. Finally, the process can culminate with the physical deletion of antigen-specific T lymphocyte clones (Zajac et al., 1998; Gallimore et al., 1998; Doering et al., 2012). Production of cytokine IL-2 and proliferative capacity are the first effector functions to be lost in T cells, while the capacity to produce IFN-γ is the last effector function to be lost (Moskophidis et al., 1993; Oxenius et al., 1998; Welsh, 2001; Wherry et al., 2003). However, exhausted T cells are still important for controlling the host–pathogen equilibrium in a chronic infection (Schmitz et al., 1999). In addition to the T-cell compartment, the innate immune system is affected during chronic infections (Zuniga et al., 2015; Greene and Zuniga, 2021). The complement system, which is a key effector of innate immune responses in acute infections, has also been shown to be involved in the modulation of adaptive immune responses (Ricklin et al., 2010).

The immune system is central to the control of *Trypanosoma cruzi* infection; when it is not sufficient, the parasite load and inflammation, and therefore, the potential for tissue damage, increases (Tarleton et al., 1994). Our group has shown that persistent infection by *T. cruzi* induces exhaustion of *T. cruzi*-specific T-cell responses, which is also reflected by a high degree of differentiation and activation of T cells in the circulation of subjects chronically infected with the parasite (Laucella et al., 2004; Albareda et al., 2006; Alvarez et al., 2008; Albareda et al., 2009; Albareda et al., 2013; Albareda et al., 2015).

In recent decades, much knowledge has been gained about the complexity of the complement system, which has more than just a defense role in the circulation during acute infections and is related to complement-mediated intracellular and autocrine regulation involved in the modulation of the innate and adaptive immune responses. Increased levels of complement anaphylatoxins in subjects with chronic *T. cruzi* infection have been reported (Ndao et al., 2010) but whether the complement system has an immunoregulatory role in T-cell exhaustion during chronic Chagas disease remains unknown. Understanding the interaction between complement molecules and the T-cell response is important in the setting of a chronic infection. In this minireview, we will discuss the putative role of effector complement molecules on the T-cell immune exhaustion during chronic human *T. cruzi* infection.

DEVELOPMENT OF T-CELL RESPONSES AND IMMUNE EXHAUSTION IN CHRONIC HUMAN *TRYPANOSOMA CRUZI* INFECTION

Chagas disease, caused by the intracellular pathogen *Trypanosoma cruzi*, is the parasitic disease in Latin America with the highest impact and is the most common cause of infectious myocarditis in the world (WHO, 2018). The infection is naturally transmitted by blood-feeding Reduviid insects, but transmission by oral contamination, transplacental transmission and transmission by blood transfusion/tissue transplantation are also possible. The main reason that Chagas disease has been described as having an autoimmune etiology is that detection of the parasites is difficult, but there is an emerging consensus that the persistence of parasites is the primary cause of cumulative tissue damage in chronic Chagas disease (Tarleton, 2003). Since *T. cruzi* presents two different anatomical development stages in the mammalian host, trypomastigotes in the bloodstream and amastigotes in the cytoplasm of the infected cells, immune control of the parasite requires the generation of both innate and adaptive immune responses. However, even in cases in which those immune responses are sufficient to control the acute infection, the parasite is not completely cleared, resulting in a decade-long infection in most cases (Tarleton, 2007). The persistence of these inflammatory responses may eventually result in the tissue damage that is found in subjects chronically infected with *T. cruzi* (Tarleton, 2001). These data also support the hypothesis that stimulation of an effective set of immune responses that efficiently limit the parasite load in tissues should result in less severe disease.

One of the reasons why the inflammatory process might be exacerbated in the more severe forms of the disease is that *T. cruzi*-specific T-cell responses become less effective due to the process of immune exhaustion (Laucella et al., 2004; Albareda et al., 2006; Albareda et al., 2015; Lasso et al., 2015; Egui et al., 2015; Ferreira et al., 2017). It has been shown that cells producing only one cytokine (i.e., monofunctional T cells) in response to *T. cruzi* antigens is common in adults with chronic Chagas disease (Laucella et al., 2004; Lasso et al., 2015; Mateus et al., 2015), while polyfunctional T cells are often found in children who have shorter-term infections (Albareda et al., 2013). We have demonstrated that the impairment of parasite-specific T-cell responses is inversely correlated with the severity of the disease (Laucella et al., 2004; Albareda et al., 2006; Alvarez et al., 2008) and increases with the length of the infection (Albareda et al., 2013).

We have shown that higher frequencies of IFN-γ-producing T cells specific for *T. cruzi* are detected in subjects chronically infected with *T. cruzi* without or with mild clinical symptoms compared to subjects in the more severe stages of the disease. On the other hand, IL-2-secreting T cells are infrequent in chronic infections regardless of clinical status (Laucella et al., 2004; Albareda et al., 2006; Alvarez et al., 2008). This functional profile of IFN-γ-only secreting T cells, characteristic of effector memory T cells and generally associated with long-term antigen

persistence and exhausted T cells (Harari et al., 2006), is consistent with other features of exhausted T cells found in subjects with long-term *T. cruzi* infections, such as the increased frequency of fully differentiated memory T cells, a high rate of apoptosis, high expression of inhibitory receptors, alterations in IL7/IL7R axis and high dependence on the presence of antigen for T-cell maintenance (Albareda et al., 2006; Laucella et al., 2009; Argüello et al., 2012; Lasso et al., 2015; Albareda et al., 2015; Natale et al., 2018). It is important to note that even though these T cells might be effective in controlling the infection in subjects chronically infected with *T. cruzi*, as long as the efficiency of the immune response declines, the ability to control the parasite burden without increasing the level of tissue damage appears to be diminished.

FUNCTIONS OF THE COMPLEMENT SYSTEM

Regardless of the pathway used (classical, alternative and lectin pathways) the activation of the complement system results in the generation of the C3 and C5 convertases which are cleaved into the main effectors molecules, the C3a and C5a anaphylatoxins and the opsonins C3b and C5b. The C3a and C5a molecules induce pleiotropic effector functions by binding to their specific receptors C3aR and C5aR1/2, respectively (Klos et al., 2009), C5b leads to the formation of the membrane attack component (MAC) and C3b is related to the phagocytosis of the opsonized targets (Ricklin et al., 2010), The balance between the activation and inhibition of the complement system is essential to protect cells from damage induced by an indiscriminate level of immune response. Complement activation is finely regulated by complement regulatory proteins (Cregs), including soluble (C1 inhibitor, factor H, and C4b-binding protein) and membrane-associated (CD46, CD55, CR1, and CD59) proteins, which regulate the activation of the complement cascade, mainly at the C3 convertase stage (Kim and Song, 2006; Zipfel and Skerka, 2009; Ricklin et al., 2016; Arbore et al., 2017).

The complement system is usually thought of as a serum circulating and membrane-bound protein system where the liver is the main source of their components and the main function is the detection and elimination of circulating pathogens as part of the innate immune response (Ricklin et al., 2010). However, the findings that most of immune cells can produce complement proteins and express their receptors have led to the notion that the complement system also has non canonical functions in the adaptive immune response (Klos et al., 2009; Ricklin et al., 2010; Killick et al., 2018). This intracellular complement, was named as complosome to set it apart from the liver-derived and serum-circulating complement system (Killick et al., 2018). Complement molecules might act indirectly or directly on T cells, either promoting or inhibiting immune responses (Heeger and Kemper, 2012; Clarke and Tenner, 2014; Liszewski et al., 2017; Moro-García et al., 2018; West et al., 2018).

Regarding the indirect effects, signals delivery after the activation of the C3aR, C5aR by the binding of C3a and C5a, respectively, induce the maturation of the APC (i.e. dendritic, macrophages, and monocytes) by the secretion of interleukin IL-12, upregulation of the major histocompatibility class II necessary for the induction of a good Th1 response (Kemper and Atkinson, 2007). In contrast, the binding of the C3R by the inactivated form C3b (iC3b) on the APCs activates the production of the regulatory cytokines IL-10 and TGF-b which act as a negative regulators of T-cell responses (**Figure 1**; Sohn et al., 2003). In relation to the direct effects of the complement system on the T-cell function, following antigen stimulation C3a and C3b are translocated to the T-cell membrane where they engage their receptors, C3aR and the costimulatory CD46 (West et al., 2018), respectively. These interactions mediates the cellular metabolic reprogramming of T cells by the induction of the mTOR program involved in the upregulation of the aerobic glycolysis and oxidative phosphorylation process necessary for the induction of the Th1 response (Figue 1; Liszewski et al., 2017; West et al., 2018). Additionally, there is downregulation of the membrane-bound complement negative regulator CD55 further promoting the differentiation into Th1 effector cells (Lalli et al., 2007). On the other hand, the activation of the complement receptor 1 (CR1) in T cells might inhibit IL-2 production, and proliferation, and promote the secretion of IL-10 leading to a shut-down of the T-cell response (**Figure 1**).

The complement system is also involved in T-cell homeostasis through the binding of C3b to CD46 promoting the expression of the IL7R (CD127) (Wofford et al., 2008; Carrette and Surh, 2012; Kolev et al., 2014; Clarke and Tenner, 2014). There is a basal metabolic activity of the intracellular C3a/C5a and receptor recycling pathway that promote T-cell survival *via* a low level activation of mTOR (**Figure 1**; West and Kemper, 2019).

In summary, these data support the interplay between complement effector molecules and their receptors on APCs and T cells which might influence the outcome of T-cell responses in the context of chronic Chagas disease and the mechanism of T-cell exhaustion.

POSSIBLE ROLES OF THE COMPLEMENT SYSTEM IN T-CELL EXHAUSTION IN CHRONIC CHAGAS DISEASE

The majority of people infected with *T. cruzi* remain asymptomatic throughout their lives, and parasite-host interactions seem to play a crucial role in the development of the disease. It is thought that inflammation in the heart develops over years from indolent, low-grade processes that depend, at least in part, on the few parasites that persist in the heart (Bonney et al., 2019), inducing constant activation of the immune system. Few studies have addressed the role of the complement system in the chronic phase of *T. cruzi* infection. A study by Aiello et al. (2002) using frozen myocardial samples from chronic Chagas disease patients with cardiomyopathy found that the presence of *T. cruzi* parasites in heart necropsies was associated with increased complement activation and MAC deposition

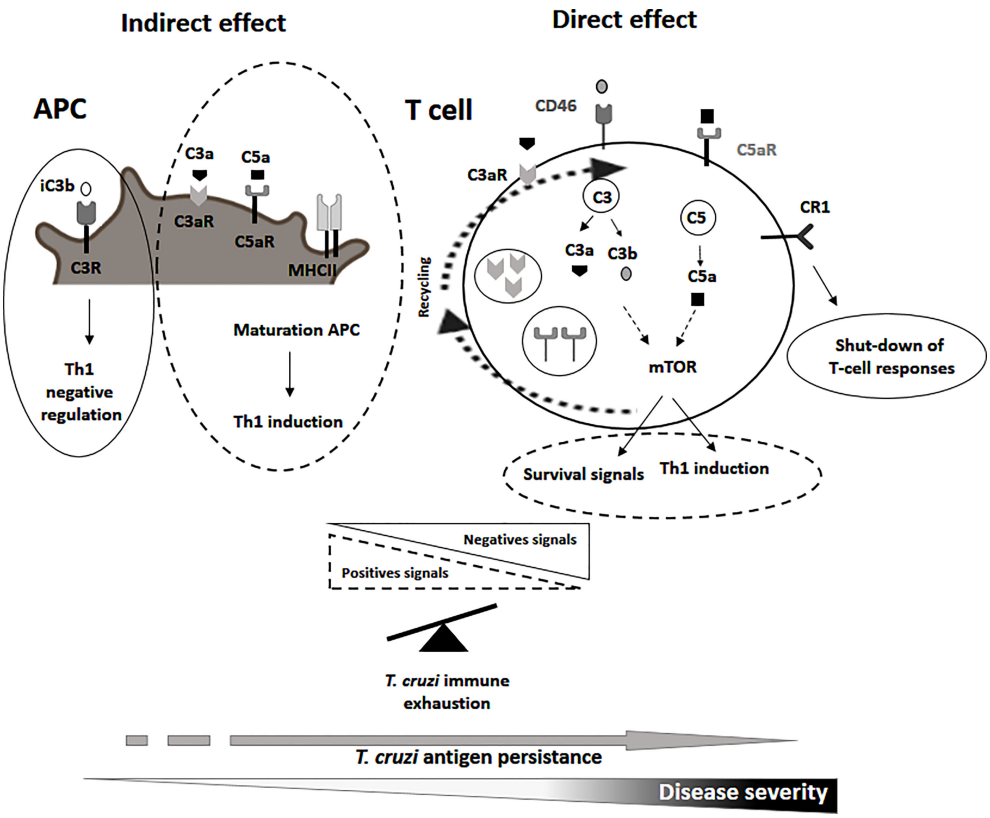

FIGURE 1 | Representative scheme of the non canonical functions of the complement molecules in the putative roles on T-cell immune exhaustion during chronic human *T. cruzi* infection. Possible roles of the C3a, C3b, C5a, their receptors and complement receptor 1 and CD46 in T-cell exhaustion process are indicated. Dashed lines indicate positive signals involved in the maturation of APC, induction of a Th1 response or T-cell survival. Complete lines indicate negative signals involved in the control of a Th1 response.

Thus, the release of effector complement molecules with canonical functions might contribute to the development of symptomatic forms of chronic infection due to their proinflammatory effect and also impact in the continuous inflammatory reaction due to parasite persistence in the heart that leads to necrosis and fibrosis in subjects chronically infected with the parasite. (Boldt et al., 2011; Weitzel et al., 2012; Luz et al., 2016). In contrast, other studies have described increased levels of C3a in the sera of subjects with asymptomatic chronic Chagas disease supporting a positive role of the complement system in chronic *T. cruzi* infection (Ndao et al., 2010).

An exacerbation of the negative regulatory mechanisms or inappropriate activation of positive signals induced by the non-canonical functions of the complement system might participate in the process of T-cell exhaustion in chronic Chagas disease by a shut-down of *T. cruzi*-specific T-cell responses. A deficiency in the maturation of the APC, a low activation of the mTOR pathway or the CD46 signaling by a deficient expression of C3aR, C5aR,C3a, C3b and C5a, might induce a poor Th1 response. An imbalance of complement-mediated negative over positive signals would further inhibit T-cell responses (**Figure 1**). Homeostatic T-cell survival might be also compromised by a downregulation of C3aR, C5aR, C3a, C3b and C5a (Le Friec et al., 2012; Clarke and Tenner, 2014).

A better understanding of the regulatory mechanisms of the complement system in T-cell responses might provide new insight in this chronic parasitic disease.

AUTHOR CONTRIBUTIONS

All authors listed have contributed in the preparation and organization of the work, and approved it for publication. All authors contributed to the article and approved the submitted version.

FUNDING

This work was supported by the Scientific and Technological Research Fund (FONCyT), Argentina (PICT 2019-00157 to MCA). MCA and SLA are members of the Scientific Career, CONICET, Argentina. MBC and GC are CONICET Ph.D. fellows. JE is a fellow of the Scientific and Technological Research Fund (FONCyT), Argentina.

REFERENCES

Ahmadzadeh, M., Johnson, L. A., Heemskerk, B., Wunderlich, J. R., Dudley, M. E., White, D. E., et al. (2009). Tumor Antigen-Specific CD8 T Cells Infiltrating the Tumor Express High Levels of PD-1 and are Functionally Impaired. *Blood* 114 (8), 1537–1544. doi: 10.1182/blood-2008-12-195792

Aiello, V. D., Reis, M. M., Benvenuti, L. A., Higuchi, M., Ramires, J. A., and Halperin, J. A. (2002). A Possible Role for Complement in the Pathogenesis of Chronic Chagasic Cardiomyopathy. *J. Pathol.* 197 (2), 224–229. doi: 10.1002/path.1095

Albareda, M. C., De Rissio, A. M., Tomas, G., Serjan, A., Alvarez, M. G., Viotti, R., et al. (2013). Polyfunctional T Cell Responses in Children in Early Stages of Chronic *Trypanosoma Cruzi* Infection Contrast With Monofunctional Responses of Long-Term Infected Adults. *PLoS Negl. Trop. Dis.* 7 (12), e2575. doi: 10.1371/journal.pntd.0002575

Albareda, M. C., Laucella, S. A., Alvarez, M. G., Armenti, A. H., Bertochi, G., Tarleton, R. L., et al. (2006). Trypanosoma Cruzi Modulates the Profile of Memory CD8+ T Cells in Chronic Chagas' Disease Patients. *Int. Immunol.* 18 (3), 465–471. doi: 10.1093/intimm/dxh387

Albareda, M. C., Olivera, G. C., Laucella, S. A., Alvarez, M. G., Fernandez, E. R., Lococo, B., et al. (2009). Chronic Human Infection With Trypanosoma Cruzi Drives CD4+ T Cells to Immune Senescence. *J. Immunol.* 183 (6), 4103–4108. doi: 10.4049/jimmunol.0900852

Albareda, M. C., Perez-Mazliah, D., Natale, M. A., Castro-Eiro, M., Alvarez, M. G., Viotti, R., et al. (2015). Perturbed T Cell IL-7 Receptor Signaling in Chronic Chagas Disease. *J. Immunol.* 194 (8), 3883–3889. doi: 10.4049/jimmunol.1402202

Alvarez, M. G., Postan, M., Weatherly, D. B., Albareda, M. C., Sidney, J., Sette, A., et al. (2008). HLA Class I-T Cell Epitopes From Trans-Sialidase Proteins Reveal Functionally Distinct Subsets of CD8+ T Cells in Chronic Chagas Disease. *PLoS Negl. Trop. Dis.* 2 (9), e288. doi: 10.1371/journal.pntd.0000288

Arbore, G., Kemper, C., and Kolev, M. (2017). Intracellular Complement - the Complosome - in Immune Cell Regulation. *Mol. Immunol.* 89, 2–9. doi: 10.1016/j.molimm.2017.05.012

Argüello, R. J., Albareda, M. C., Alvarez, M. G., Bertocchi, G., Armenti, A. H., Vigliano, C., et al. (2012). Inhibitory Receptors are Expressed by Trypanosoma Cruzi-Specific Effector T Cells and in Hearts of Subjects With Chronic Chagas Disease. *PLoS One* 7 (5), e35966. doi: 10.1371/journal.pone.0035966

Behar, S. M., Carpenter, S. M., Booty, M. G., Barber, D. L., and Jayaraman, P. (2014). Orchestration of Pulmonary T Cell Immunity During Mycobacterium Tuberculosis Infection: Immunity Interruptus. *Semin. Immunol.* 26 (6), 559–577. doi: 10.1016/j.smim.2014.09.003

Boldt, A. B., Luz, P. R., and Messias-Reason, I. J. (2011). MASP2 Haplotypes are Associated With High Risk of Cardiomyopathy in Chronic Chagas Disease. *Clin. Immunol.* 140 (1), 63–70. doi: 10.1016/j.clim.2011.03.008

Boni, C., Fisicaro, P., Valdatta, C., Amadei, B., Di Vincenzo, P., Giuberti, T., et al. (2007). Characterization of Hepatitis B Virus (HBV)-Specific T-Cell Dysfunction in Chronic HBV Infection. *J. Virol.* 81 (8), 4215–4225. doi: 10.1128/JVI.02844-06

Bonney, K. M., Luthringer, D. J., Kim, S. A., Garg, N. J., and Engman, D. M. (2019). Pathology and Pathogenesis of Chagas Heart Disease. *Annu. Rev. Pathol.* 14, 421–447. doi: 10.1146/annurev-pathol-020117-043711

Carrette, F., and Surh, C. D. (2012). IL-7 Signaling and CD127 Receptor Regulation in the Control of T Cell Homeostasis. *Semin. Immunol.* 24 (3), 209–217. doi: 10.1016/j.smim.2012.04.010

Clarke, E. V., and Tenner, A. J. (2014). Complement Modulation of T Cell Immune Responses During Homeostasis and Disease. *J. Leukoc. Biol.* 96 (5), 745–756. doi: 10.1189/jlb.3MR0214-109R

Crespo, J., Sun, H., Welling, T. H., Tian, Z., and Zou, W. (2013). T Cell Anergy, Exhaustion, Senescence, and Stemness in the Tumor Microenvironment. *Curr. Opin. Immunol.* 25 (2), 214–221. doi: 10.1016/j.coi.2012.12.003

Doering, T. A., Crawford, A., Angelosanto, J. M., Paley, M. A., Ziegler, C. G., and Wherry, E. J. (2012). Network Analysis Reveals Centrally Connected Genes and Pathways Involved in CD8+ T Cell Exhaustion Versus Memory. *Immunity* 37 (6), 1130–1144. doi: 10.1016/j.immuni.2012.08.021

Egui, A., Thomas, M. C., Carrilero, B., Segovia, M., Alonso, C., and Marañón, C. (2015). Differential Phenotypic and Functional Profiles of TcCA-2 -Specific Cytotoxic CD8+ T Cells in the Asymptomatic Versus Cardiac Phase in Chagasic Patients. *PLoS One* 10 (3), e0122115. doi: 10.1371/journal.pone.0122115

Ferreira, L. R., Ferreira, F. M., Nakaya, H. I., Deng, X., Cândido, D. D., de Oliveira, L. C., et al. (2017). Blood Gene Signatures of Chagas Cardiomyopathy With or Without Ventricular Dysfunction. *J. Infect. Dis.* 215 (3), 387–395. doi: 10.1093/infdis/jiw540

Gallimore, A., Glithero, A., Godkin, A., Tissot, A. C., Plückthun, A., Elliott, T., et al. (1998). Induction and Exhaustion of Lymphocytic Choriomeningitis Virus-Specific Cytotoxic T Lymphocytes Visualized Using Soluble Tetrameric Major Histocompatibility Complex Class I-Peptide Complexes. *J. Exp. Med.* 187 (9), 1383–1393. doi: 10.1084/jem.187.9.1383

Gigley, J. P., Bhadra, R., Moretto, M. M., and Khan, I. A. (2012). T Cell Exhaustion in Protozoan Disease. *Trends Parasitol.* 28 (9), 377–384. doi: 10.1016/j.pt.2012.07.001

Greene, T. T., and Zuniga, E. I. (2021). Type I Interferon Induction and Exhaustion During Viral Infection: Plasmacytoid Dendritic Cells and Emerging COVID-19 Findings. *Viruses* 13 (9), 1839. doi: 10.3390/v13091839

Harari, A., Dutoit, V., Cellerai, C., Bart, P. A., Du Pasquier, R. A., and Pantaleo, G. (2006). Functional Signatures of Protective Antiviral T-Cell Immunity in Human Virus Infections. *Immunol. Rev.* 211, 236–254. doi: 10.1111/j.0105-2896.2006.00395.x

Heeger, P. S., and Kemper, C. (2012). Novel Roles of Complement in T Effector Cell Regulation. *Immunobiology* 217 (2), 216–224. doi: 10.1016/j.imbio.2011.06.004

Kahan, S. M., Wherry, E. J., and Zajac, A. J. (2015). T Cell Exhaustion During Persistent Viral Infections. *Virology* 479–480, 180–193. doi: 10.1016/j.virol.2014.12.033

Kemper, C., and Atkinson, J. P. (2007). T-Cell Regulation: With Complements From Innate Immunity. *Nat. Rev. Immunol.* 7 (1), 9–18. doi: 10.1038/nri1994

Killick, J., Morisse, G., Sieger, D., and Astier, A. L. (2018). Complement as a Regulator of Adaptive Immunity. *Semin. Immunopathol.* 40 (1), 37–48. doi: 10.1007/s00281-017-0644-y

Kim, D. D., and Song, W. C. (2006). Membrane Complement Regulatory Proteins. *Clin. Immunol. Orlando Fla.* 118 (2-3), 127–136. doi: 10.1016/j.clim.2005.10.014

Klos, A., Tenner, A. J., Johswich, K. O., Ager, R. R., Reis, E. S., and Köhl, J. (2009). The Role of the Anaphylatoxins in Health and Disease. *Mol. Immunol.* 46 (14), 2753–2766. doi: 10.1016/j.molimm.2009.04.027

Kolev, M., Le Friec, G., and Kemper, C. (2014). Complement–tapping Into New Sites and Effector Systems. *Nat. Rev. Immunol.* 14 (12), 811–820. doi: 10.1038/nri3761

Lalli, P. N., Strainic, M. G., Lin, F., Medof, M. E., and Heeger, P. S. (2007). Decay Accelerating Factor can Control T Cell Differentiation Into IFN-Gamma-Producing Effector Cells *via* Regulating Local C5a-Induced IL-12 Production. *J. Immunol.* 179 (9), 5793–5802. doi: 10.4049/jimmunol.179.9.5793

Lasso, P., Mateus, J., Pavía, P., Rosas, F., Roa, N., Thomas, M. C., et al. (2015). Inhibitory Receptor Expression on CD8+ T Cells Is Linked to Functional Responses Against Trypanosoma Cruzi Antigens in Chronic Chagasic Patients. *J. Immunol.* 195 (8), 3748–3758. doi: 10.4049/jimmunol.1500459

Laucella, S. A., Mazliah, D. P., Bertocchi, G., Alvarez, M. G., Cooley, G., Viotti, R., et al. (2009). Changes in Trypanosoma Cruzi-Specific Immune Responses After Treatment: Surrogate Markers of Treatment Efficacy. *Clin. Infect. Dis.* 49 (11), 1675–1684. doi: 10.1086/648072

Laucella, S. A., Postan, M., Martin, D., Hubby Fralish, B., Albareda, M. C., Alvarez, M. G., et al. (2004). Frequency of Interferon- Gamma -Producing T Cells Specific for Trypanosoma Cruzi Inversely Correlates With Disease Severity in Chronic Human Chagas Disease. *J. Infect. Dis.* 189 (5), 909–918. doi: 10.1086/381682

Le Friec, G., Sheppard, D., Whiteman, P., Karsten, C. M., Shamoun, S. A., Laing, A., et al. (2012). The CD46-Jagged1 Interaction is Critical for Human TH1 Immunity. *Nat. Immunol.* 13 (12), 1213–1221. doi: 10.1038/ni.2454

Liszewski, M. K., Elvington, M., Kulkarni, H. S., and Atkinson, J. P. (2017). Complement's Hidden Arsenal: New Insights and Novel Functions Inside the Cell. *Mol. Immunol.* 84, 2–9. doi: 10.1016/j.molimm.2017.01.004

Luz, P. R., Miyazaki, M. I., Chiminacio Neto, N., Padeski, M. C., Barros, A. C., Boldt, A. B., et al. (2016). Genetically Determined MBL Deficiency Is Associated With Protection Against Chronic Cardiomyopathy in Chagas

Disease. *PLoS Negl. Trop. Dis.* 10 (1), e0004257. doi: 10.1371/journal.pntd.0004257

Mateus, J., Lasso, P., Pavia, P., Rosas, F., Roa, N., Valencia-Hernández, C. A., et al. (2015). Low Frequency of Circulating CD8+ T Stem Cell Memory Cells in Chronic Chagasic Patients With Severe Forms of the Disease. *PLoS Negl. Trop. Dis.* 9 (1), e3432. doi: 10.1371/journal.pntd.0003432

Moro-García, M. A., Mayo, J. C., Sainz, R. M., and Alonso-Arias, R. (2018). Influence of Inflammation in the Process of T Lymphocyte Differentiation: Proliferative, Metabolic, and Oxidative Changes. *Front. Immunol.* 9. doi: 10.3389/fimmu.2018.00339

Moskophidis, D., Lechner, F., Pircher, H., and Zinkernagel, R. M. (1993). Virus Persistence in Acutely Infected Immunocompetent Mice by Exhaustion of Antiviral Cytotoxic Effector T Cells. *Nature* 362 (6422), 758–761. doi: 10.1038/362758a0

Natale, M. A., Cesar, G., Alvarez, M. G., Castro Eiro, M. D., Lococo, B., Bertocchi, G., et al. (2018). Trypanosoma Cruzi-Specific IFN-γ-Producing Cells in Chronic Chagas Disease Associate With a Functional IL-7/IL-7R Axis. *PloS Negl. Trop. Dis.* 12 (12), e0006998. doi: 10.1371/journal.pntd.0006998

Ndao, M., Spithill, T. W., Caffrey, R., Li, H., Podust, V. N., and Perichon, R. (2010). Identification of Novel Diagnostic Serum Biomarkers for Chagas' Disease in Asymptomatic Subjects by Mass Spectrometric Profiling. *J. Clin. Microbiol.* 48 (4), 1139–1149. doi: 10.1128/JCM.02207-09

Oxenius, A., Zinkernagel, R. M., and Hengartner, H. (1998). Comparison of Activation Versus Induction of Unresponsiveness of Virus-Specific CD4+ and CD8+ T Cells Upon Acute Versus Persistent Viral Infection. *Immunity* 9 (4), 449–457. doi: 10.1016/s1074-7613(00)80628-7

Ricklin, D., Hajishengallis, G., Yang, K., and Lambris, J. D. (2010). Complement: A Key System for Immune Surveillance and Homeostasis. *Nat. Immunol.* 11 (9), 785–797. doi: 10.1038/ni.1923

Ricklin, D., Reis, E. S., and Lambris, J. D. (2016). Complement in Disease: A Defence System Turning Offensive. *Nat. Rev. Nephrol.* 12 (7), 383–401. doi: 10.1038/nrneph.2016.70

Rodrigues, V., Cordeiro-da-Silva, A., Laforge, M., Ouaissi, A., Akharid, K., Silvestre, R., et al. (2014). Impairment of T Cell Function in Parasitic Infections. *PloS Negl. Trop. Dis.* 8 (2), e2567. doi: 10.1371/journal.pntd.0002567

Schmitz, J. E., Kuroda, M. J., Santra, S., Sasseville, V. G., Simon, M. A., Lifton, M. A., et al. (1999). Control of Viremia in Simian Immunodeficiency Virus Infection by CD8+ Lymphocytes. *Science* 283 (5403), 857–860. doi: 10.1126/science.283.5403.857

Sohn, J. H., Bora, P. S., Suk, H. J., Molina, H., Kaplan, H. J., and Bora, N. S. (2003). Tolerance is Dependent on Complement C3 Fragment Ic3b Binding to Antigen-Presenting Cells. *Nat. Med.* 9, 206–212. doi: 10.1038/nm814

Tarleton, R. L. (2001). Parasite Persistence in the Aetiology of Chagas Disease. *Int. J. Parasitol.* 31 (5-6), 550–554. doi: 10.1016/s0020-7519(01)00158-8

Tarleton, R. L. (2003). Chagas Disease: A Role for Autoimmunity? *Trends Parasitol.* 19 (10), 447–451. doi: 10.1016/j.pt.2003.08.008

Tarleton, R. L. (2007). Immune System Recognition of *Trypanosoma Cruzi*. *Curr. Opin. Immunol.* 19 (4), 430–434. doi: 10.1016/j.coi.2007.06.003

Tarleton, R. L., Sun, J., Zhang, L., and Postan, M. (1994). Depletion of T-Cell Subpopulations Results in Exacerbation of Myocarditis and Parasitism in Experimental Chagas' Disease. *Infect. Immun.* 62 (5), 1820–1829. doi: 10.1128/iai.62.5.1820-1829.1994

Weitzel, T., Zulantay, I., Danquah, I., Hamann, L., Schumann, R. R., Apt, W., et al. (2012). Mannose-Binding Lectin and Toll-Like Receptor Polymorphisms and Chagas Disease in Chile. *Am. J. Trop. Med. Hyg.* 86 (2), 229–232. doi: 10.4269/ajtmh.2012.11-0539

Welsh, R. M. (2001). Assessing CD8 T Cell Number and Dysfunction in the Presence of Antigen. *J. Exp. Med.* 193 (5), F19–F22. doi: 10.1084/jem.193.5.f19

West, E. E., and Kemper, C. (2019). Complement and T Cell Metabolism: Food for Thought. *Immunometabolism. 1(T Cell Metab. Reprogramming)* 20, (1) e190006. doi: 10.20900/immunometab20190006

West, E. E., Kolev, M., and Kemper, C. (2018). Complement and the Regulation of T Cell Responses. *Annu. Rev. Immunol.* 36, 309–338. doi: 10.1146/annurev-immunol-042617-053245

Wherry, E. J., Blattman, J. N., Murali-Krishna, K., van der Most, R., and Ahmed, R. (2003). Viral Persistence Alters CD8 T-Cell Immunodominance and Tissue Distribution and Results in Distinct Stages of Functional Impairment. *J. Virol.* 77 (8), 4911–4927. doi: 10.1128/jvi.77.8.4911-4927.2003

WHO (2018) *Chagas Disease (American Trypanosomiasis) World Health Organization*. Available at: http://www.who.int/news-room/fact-sheets/detail/chagas-disease-(american-trypanosomiasis).

Wofford, J. A., Wieman, H. L., Jacobs, S. R., Zhao, Y., and Rathmell, J. C. (2008). IL-7 Promotes Glut1 Trafficking and Glucose Uptake *via* STAT5-Mediated Activation of Akt to Support T-Cell Survival. *Blood* 111 (4), 2101–2111. doi: 10.1182/blood-2007-06-096297

Zajac, A. J., Blattman, J. N., Murali-Krishna, K., Sourdive, D. J., Suresh, M., Altman, J. D., et al. (1998). Viral Immune Evasion Due to Persistence of Activated T Cells Without Effector Function. *J. Exp. Med.* 188 (12), 2205–2213. doi: 10.1084/jem.188.12.2205

Zipfel, P. F., and Skerka, C. (2009). Complement Regulators and Inhibitory Proteins. *Nat. Rev. Immunol.* 9 (10), 729–740. doi: 10.1038/nri2620

Zuniga, E. I., Macal, M., Lewis, G. M., and Harker, J. A. (2015). Innate and Adaptive Immune Regulation During Chronic Viral Infections. *Annu. Rev. Virol.* 2 (1), 573–597. doi: 10.1146/annurev-virology-100114-055226

Conflict of Interest: The authors declare that the research was conducted in the absence of any commercial or financial relationships that could be construed as a potential conflict of interest.

Publisher's Note: All claims expressed in this article are solely those of the authors and do not necessarily represent those of their affiliated organizations, or those of the publisher, the editors and the reviewers. Any product that may be evaluated in this article, or claim that may be made by its manufacturer, is not guaranteed or endorsed by the publisher.

frontiers | Frontiers in Cellular and Infection Microbiology

ORIGINAL RESEARCH
published: 05 July 2022
doi: 10.3389/fcimb.2022.855119

Miltefosine and Benznidazole Combination Improve Anti-*Trypanosoma cruzi In Vitro* and *In Vivo* Efficacy

Julián Ernesto Nicolás Gulin[1,2], *Margarita María Catalina Bisio*[1,3], *Daniela Rocco*[1], *Jaime Altcheh*[1], *María Elisa Solana*[4,5] *and Facundo García-Bournissen*[1,6*]

[1] *Instituto Multidisciplinario de Investigaciones en Patologías Pediátricas (IMIPP), Consejo Nacional de Investigaciones Científicas y Tecnológicas (CONICET)-Gobierno de la Ciudad de Buenos Aires (GCBA), Servicio de Parasitología y Enfermedad de Chagas, Hospital de Niños "Dr. Ricardo Gutiérrez, Ministerio de Salud, Buenos Aires, Argentina,* [2] *Instituto de Investigaciones Biomédicas (INBIOMED), Facultad de Medicina Universidad de Buenos Aires (UBA) – CONICET, Buenos Aires, Argentina,* [3] *Instituto Nacional de Parasitología (INP) 'Dr. Mario Fatala Chaben'-Administración Nacional de Laboratorios e Institutos de Salud (ANLIS) 'Dr. Carlos G. Malbrán', CONICET, Buenos Aires, Argentina,* [4] *Instituto de Microbiología y Parasitología Médica (IMPaM), Universidad de Buenos Aires, Buenos Aires, Argentina,* [5] *Departamento de Ciencias Básicas, Universidad Nacional de Luján, Buenos Aires, Argentina,* [6] *Division of Pediatric Clinical Pharmacology, Department of Pediatrics, Schulich School of Medicine & Dentistry, University of Western Ontario, London, ON, Canada*

Drug repurposing and combination therapy have been proposed as cost-effective strategies to improve Chagas disease treatment. Miltefosine (MLT), a synthetic alkylphospholipid initially developed for breast cancer and repositioned for leishmaniasis, is a promising candidate against *Trypanosoma cruzi* infection. This study evaluates the efficacy of MLT as a monodrug and combined with benznidazole (BZ) in both *in vitro* and *in vivo* models of infection with *T. cruzi* (VD strain, DTU TcVI). MLT exhibited *in vitro* activity on amastigotes and trypomastigotes with values of IC_{50} = 0.51 µM (0.48 µM; 0,55 µM) and LC_{50} = 31.17 µM (29.56 µM; 32.87 µM), respectively. Drug interaction was studied with the fixed-ration method. The sum of the fractional inhibitory concentrations (ΣFICs) resulted in ∑FIC= 0.45 for trypomastigotes and ∑FIC= 0.71 for amastigotes, suggesting *in vitro* synergistic and additive effects, respectively. No cytotoxic effects on host cells were observed. MLT efficacy was also evaluated in a murine model of acute infection alone or combined with BZ. Treatment was well tolerated with few adverse effects, and all treated animals displayed significantly lower mean peak parasitemia and mortality than infected non-treated controls ($p<0.05$). The *in vivo* studies showed that MLT led to a dose-dependent parasitostatic effect as monotherapy which could be improved by combining with BZ, preventing parasitemia rebound after a stringent immunosuppression protocol. These results support MLT activity in clinically relevant stages from *T. cruzi*, and it is the first report of positive interaction with BZ, providing further support for evaluating combined schemes using MLT and exploring synthetic alkylphospholipids as drug candidates.

Keywords: Chagas disease, *Trypanosoma cruzi*, miltefosine, benznidazole, drug combination chemotherapy, drug repositioning

OPEN ACCESS

Edited by:
Vilma G. Duschak, Consejo Nacional de Investigaciones Científicas y Técnicas (CONICET), Argentina

Reviewed by:
Frederick S. Buckner, University of Washington, United States
Fabiane Matos Dos Santos, Federal University of Espírito Santo, Brazil
Higo Fernando Santos Souza, University of São Paulo, Brazil
Victor Monteon, Autonomous University of Campeche, Mexico

***Correspondence:**
Facundo García-Bournissen
facugb1@gmail.com

Specialty section:
This article was submitted to Parasite and Host, a section of the journal Frontiers in Cellular and Infection Microbiology

Received: *14 January 2022*
Accepted: *16 May 2022*
Published: *05 July 2022*

Citation:
Gulin JEN, Bisio MMC, Rocco D, Altcheh J, Solana ME and García-Bournissen F (2022) Miltefosine and Benznidazole Combination Improve Anti-Trypanosoma cruzi In Vitro and In Vivo Efficacy. Front. Cell. Infect. Microbiol. 12:855119. doi: 10.3389/fcimb.2022.855119

INTRODUCTION

Chagas disease, caused by the hemoflagellate *Trypanosoma cruzi*, is considered a neglected tropical disease due to the scarcity of safe and effective treatments [1]. Current therapeutic options are limited to nifurtimox (NFX) and benznidazole (BZ), both developed over 40 years ago.

Etiological treatment during the acute stage results in high rates of parasitemia clearance and serological negativity, while treatment success during the chronic phase is currently arguable. Adverse events are usual, especially in adults, forcing treatment discontinuation (Pérez-Molina and Molina, 2018).

Despite the urgent need to develop safer drugs, the pharmaceutical industry has shown limited interest in research for new chemical entities, probably due to the socioeconomic condition of most affected patients (Paulino et al., 2005).

Drug repurposing (*i.e.*, the study of drugs already developed and tested for other diseases) (Chatelain and Ioset, 2011) and combination therapy arise as cost-effective strategies to fill the gap in the drug discovery pipeline (Keenan et al., 2013a; Andrews et al., 2014). Additionally, a positive drug combination increases drug efficacy by targeting multiple metabolic pathways, minimizing the risk of drug resistance, and reducing the frequency and intensity of dose-dependent adverse reactions (Field et al., 2017).

Initially developed for treating skin metastases in breast tumors, miltefosine (MLT), also known as hexadecylphosphocholine, is the first and to date only oral drug for visceral and cutaneous leishmaniasis (Dorlo et al., 2012). Extensive experience with MLT in leishmaniasis clinical trials suggests an excellent safety profile for patients, including pediatric patients, with low to moderate adverse events (Singh et al., 2006; Mbui et al., 2019). Still, some concerns remain regarding MLT effects on the gastrointestinal tract and potential teratogenicity (Dorlo et al., 2012).

MLT is considered a protein kinase B (PKB) inhibitor with a key role in intracellular signaling for cell viability (Dorlo et al., 2012). However, the mechanisms of action related to its anti-protozoal activity are not fully clarified yet. Some evidence suggests an inhibitory effect on phosphatidylcholine and sphingomyelin synthesis, triggering apoptosis (Maya et al., 2007; Apt, 2010) or inhibiting the mitochondrial cytochrome c oxidase and altering the organelle membrane (Dorlo et al., 2012; Ghosh et al., 2013). Similarly, it was proposed that MLT inhibits the parasite phosphatidylcholine biosynthesis through the transmethylation pathway (Lira et al., 2001).

Recently, it was proposed that MLT targeted the sphingosine-activated plasma membrane directly Ca^{+2} channel, both on *Leishmania donovani* and *T. cruzi*, affecting the intracellular calcium homeostasis (Benaim et al., 2020).

Previous reports indicated that MLT exhibits both *in vitro* (Croft et al., 1996; Santa-Rita et al., 2000) and *in vivo* activity (Saraiva et al., 2002; Martinez-Peinado et al., 2021) against *T. cruzi*.

[1] https://www.who.int/chagas/en/. Last access: Dec. 12, 2021.

However, *in vivo* efficacy was evaluated by different monotherapy treatment schemes and cure criteria hampering the assessment of the MLT ability to eradicate *T. cruzi* infection. Therefore, we conducted a set of *in vitro* and *in vivo* experiments based on previous guidelines (Romanha et al., 2010) to evaluate MLT efficacy alone and in combination with BZ.

MATERIALS AND METHODS

In Vitro Studies

Cell culture

Vero-C76 cells (obtained from Asociación Banco Argentino de Células, an ATCC-certified cell bank) were cultured in T25 or T75 flasks with RPMI-1640 medium (Life Technologies Corporation, Grand Island, New York, USA) at 37°C in an atmosphere of 5% CO_2, supplemented with 2.5 g/L sodium bicarbonate and 5% fetal bovine serum (FBS) (Natocor, Córdoba, Argentina) and penicillin (100 UI/mL) - streptomycin (50 μg/mL) or gentamicin (25 μg/mL).

Parasite Strain

The VD strain of *T. cruzi* (DTU TcVI) was previously characterized (Gulin et al., 2018), and it was used throughout these studies. Bloodstream trypomastigotes were obtained from infected CF-1 outbred mice at parasitemia peak, isolated as previously described (Brossas et al., 2017), and maintained in cell culture for *in vitro* assays or used directly for *in vivo* studies.

Trypanocidal Activity

The trypanocidal activity was assayed on cell culture-derived trypomastigotes. Experiments were carried out in 96-well microplates containing 10^6 parasites/mL, in 100 μL as final volume. Serially diluted (160-0.156 μM) pure drugs (MLT, BZ, and NFX) were added to the wells, and the plates were incubated at 37°C for 24 h. After incubation, reduction in *T. cruzi* viability was determined by counting motile trypomastigotes in Kova International, Inc., Garden Grove, CA, USA. Each drug concentration was evaluated in triplicate, and control cultures were maintained without the drug. The lytic concentration 50% (LC_{50}), defined as the drug concentration that resulted in a 50% reduction compared to the untreated control, was estimated by non-linear regression analysis plotting the percentage of viable trypomastigotes against the log of drug concentration (Rodrigues et al., 2014).

Inhibition of Trypomastigotes Egress Test

Egress of trypomastigote forms from host cells was used as an indirect method to assess the arrest of amastigote development. Vero C-76 cells, plated at a density of 10^4 cells/well in 96-well plates, were infected with 10^6 parasites/mL and incubated at 37°C and 5% CO_2 for 24 h. The wells were washed with PBS 1X to remove non-attached parasites, and the infected cell cultures were treated with serially diluted (160-0.156 μM) pure drugs (MLT, BZ, NFX) by triplicate. Control cell cultures were maintained without treatment. Trypomastigotes' egress from host cells was evaluated

on the 5th day post-infection (dpi) as previously described (Polanco-Hernández et al., 2012). The number of parasites egressed was determined by counting viable trypomastigotes in the supernatant using the KOVA Glasstic slides®. The inhibitory concentration 50% (IC_{50}), defined as the drug concentration resulting in a 50% reduction of trypomastigotes' egress from infected cells, was estimated by non-linear regression analysis plotting the percentage of viable trypomastigotes against the log of drug concentration (da Silva et al., 2010; Polanco-Hernández et al., 2012).

Determination of Cytotoxicity

Vero C-76 cells were plated at a density of 10^4 cells in 96-wells plates and maintained at 37°C in an atmosphere of 5% CO_2 overnight. Then, they were incubated in the presence of the compounds in serially diluted concentrations (160-0.156 μM). Each drug concentration was evaluated in triplicate, and control cultures were maintained without the drug. After 5 days, plates were washed and 100 μL of RPMI-5% SFB with 10% of a 3 mM resazurin solution (Sigma Aldrich, Saint Louis, MO, USA), were added to each well. The plate was incubated at 37°C with a 5% CO_2 atmosphere for 4 h, and the reduction of resazurin was read in an ELISA reader (Thermo Fisher Scientific Oy, Vantaa, Finland) at 570-595 nm. Optical densities were analyzed to obtain the dose-response curve and the cytotoxic concentration 50 (CC_{50}), defined as the concentration of compound that reduced the cell viability by 50% compared to untreated controls. Finally, the selectivity index (SI) was calculated as the CC_{50} for Vero cells/IC_{50} for *T. cruzi* parasites (Miranda et al., 2015).

Drug Combination Assays

In vitro tests were carried out to identify the LC_{50} and IC_{50} of each drug separately (see above). For combination studies, dilutions were made by the fixed-ratio method, where the LC_{50} or the IC_{50} of one of the drugs remained constant, and the other drug was diluted in fixed ratios of the obtained LC_{50} or IC_{50} (Fivelman et al., 2004).

To assess trypanocidal activity, tested MLT concentrations (30.85; 7.71; 1.93 μM) were added to the pre-determined LC_{50} value of BZ at a fixed concentration. Similarly, the MLT LC_{50} value was added to serially diluted BZ (9.43; 2.36; 0.59 μM).

To study the inhibitory amastigote effect, selected MLT concentrations (0.51; 0.25; 0.12; 0.06; 0.03) were added to the pre-determined BZ IC_{50} value at fixed concentration. Similarly, the MLT IC_{50} was added to serial dilutions of BZ (0.72; 0.36; 0.18; 0.09; 0.04 μM).

For both cases, the Fractional Inhibitory Concentration Index (FICI) was calculated according to Cantin and Chamberland (1993) where,

LC_{50} or IC_{50} of A in combination LC_{50} or IC_{50} of B in combination

$$\sum \text{FICI} = \frac{LC_{50}\ IC_{50}\ \text{of A in combination}}{LC_{50}\ \textit{or}\ IC_{50}\ \text{A alone}} + \frac{LC_{50}\ IC_{50}\ \text{of B in combination}}{LC_{50}\ \text{or}\ IC_{50}\ \text{B alone}}$$

LC_{50} or IC_{50} of A alone LC_{50} or IC_{50} of B alone

FICI values were interpreted as follows: ≤ 0.5, synergistic; 0.5 > 4, additive and ≥ 4 antagonistic interaction (Odds, 2003).

In Vivo Assays

Experimental Animals

Twenty-one-day-old female BALB/cJ mice (16 ± 2 grams) were purchased from the Faculty of Veterinary Sciences, University of Buenos Aires, Argentina, and housed under conventional closed barriers at Ricardo Gutiérrez Children's Hospital animal facilities (Buenos Aires, Argentina).

Animals were kept at five mice per cage in 600 cm^2 polycarbonate cages, including plastic tubes as environmental enrichment and nesting material. Animals were individually identified, and cages were properly labeled. Cages were filled with irradiated chip-bedding, which was changed once a week. Mice had access to food (Rata-Ratón Cooperación®, Buenos Aires, Argentina) and filtered water *ad libitum*. Macroenvironmental conditions included a 12:12-h light: dark cycle (starting at 6 a.m.), controlled temperature (20 ± 2°C), and humidity (55 ± 10%).

Procedures for housing and handling animals followed international guidelines for animal care and welfare (National Research Council, 2011). The study protocol was approved by the Institutional Animal Care and Use Committee from the Faculty of Veterinary Sciences (University of Buenos Aires) (Protocol #2014/04).

Infection and Treatment Schedules

Five-week-old mice were infected by intraperitoneal (ip) injection with 500 bloodstream trypomastigotes from the VD strain of *T. cruzi*. After the infection was established, mice with patent parasitemia were assigned by simply randomization to treatment groups as indicated in **Table 1** (monotherapy) and **Table 2** (combinatory therapy).

MLT (pure product provided by Laboratorio Dr. Lazar & Cía. S.A.Q. e I, Buenos Aires, Argentina) was prepared in a 100 mg/mL work solution and dissolved in sterile distilled water. BZ and NFX (Radanil, Roche, Buenos Aires, Argentina and Lampit, Bayer, Buenos Aires, Argentina) were used as reference treatments in this study. Commercial tablets were crushed and suspended in 0.25% carboxymethylcellulose solution (Sigma Aldrich, Saint Louis, MO, USA). To avoid potential pharmaceutical interactions between drugs, BZ was administered at least an hour before MLT in the combination treatment.

Treatment started immediately upon onset of parasitemia in all animals and it was administered daily for 20 consecutive days by oral route in 50 μL as final volume. Doses, length of treatment, and route of administration for monotherapy schemes were chosen based on published data (Saraiva et al., 2002; Romanha et al., 2010). For combinatory treatments, doses were carefully chosen to obtain sub-therapeutic (i.e., doses that are administered separately do not lead to parasitemia suppression) (Gulin et al., 2020) or additive effects (i.e., doses that are administered together add up to the therapeutic dose that leads to parasitemia suppression).

TABLE 1 | Effect of miltefosine, benznidazole, or nifurtimox on parasitemia parameters in BALB/cJ mice infected with *Trypanosoma cruzi* (VD strain) [a].

Treatment (mg/kg/day)	n	PPP (days)	MPR (trypomastigotes/ mL)	MPRreduction (%)	dMPR (median (range))	Parasitemia at end of treatment (28 dpi) (trypomastigotes/mL)	Survival (%)
MLT (25)	5	35.00 (9.80)^{D}	1.03x10^{6} (± 0.24x10^{6})^{A}	50.12	19 (15- 21)^{C}	1.56x10^{4} (± 3.13x10^{4})^{A}	4/5 (80)^{A}
MLT (50)	5	26.00 (2.74)^{CD}	2.20x10^{5} (± 0.53 x10^{5})^{B}	89.29	9 (9- 9)^{AB}	2.25x10^{4} (± 1.63x10^{4})^{B}	5/5 (100)^{A}
MLT (75)	5	24.20 (3.83)^{CD}	2.42x10^{5} (± 0.61x10^{5})^{B}	88.20	9 (9- 9)^{A}	2.00x10^{4} (± 1,4.3x10^{4})^{B}	5/5 (100)^{A}
MLT (100)	7	15.29 (4.07)^{BC}	7.68x10^{4} (± 6.43 x10^{4})^{B}	96.26	12 (12- 15)^{BC}	0.00 (± 0.00)^{C}	7/7 (100) ^{A}
BZ (100)	9	3.88 (2.23)^{AB}	1.46x10^{5} (± 1.15x10^{5})^{B}	92.02	11 (9- 12)^{AB}	0.00 (± 0,00)^{C}	9/9 (100)^{A}
NFX (100)	10	4.00 (4.32)^{A}	8.25x10^{4} (± 7.66 x10^{4})^{B}	95.99	9 (9- 9)^{A}	0.00 (± 0.00)^{C}	10/10 (100)^{A}
NT (—)	14	—	2.06x10^{6} (± 0.91 x10^{6})^{A}	—	17 (17- 21)^{C}	—	0/14 (0)^{B}

MLT, miltefosine. BZ, benznidazole. NFX, nifurtimox. NT, infected non-treated. PPP, patent parasitemia period. MPR, maximum parasitemia reached; dMPR, day of maximum parasitemia reached.

Female BALB/cJ mice were infected with 500 trypomastigotes of T. cruzi VD strain; treatment started at 8 dpi and was administered orally for 20 consecutive days.

Different letters indicate significant differences (Kruskal-Wallis; $p < 0.05$).

Values are expressed as mean (± standard deviation) except where indicated.

Evaluation of Treatment Response

Clinical condition, including physical appearance and behavior based on previously established parameters (Olfert and Godson, 2000), as well as body weight and temperature, were recorded weekly.

Blood parasitemia was evaluated twice a week with a hemocytometer, a technique with a detection limit of 12,500 parasites/mL. Briefly, 5 µL of blood obtained from the vein tail was diluted 1:5 in lysis buffer (Tris-NH_4Cl 0.83%, pH=7.2), and parasites were counted in a Neubauer chamber at 400X magnification.

Additional parameters were calculated to assess drug efficacy: patent parasitemia period (PPP), defined as the number of days in which parasitemia can be detected by direct observation; the maximum parasitemia reached (MPR), considered as the maximum parasitemia value achieved in each infected animal; and day of MPR (dMPR). Mortality was registered daily. Pre-established anticipated endpoints were used to avoid unnecessary pain and stress, and animals were euthanized if they fulfilled any of these criteria (i.e., 20% weight loss from initial body weight, body temperature lower than 33.5°C, or parasitemia ≥2x10^{6} trypomastigotes/mL). Euthanasia was performed with CO_2 inhalation in a saturated chamber or with sodium pentothal overdose (300 mg/kg, ip).

Cyclophosphamide-Induced Immune Suppression and Assessment of Cure

After the treatment schemes were completed, mice with negative parasitemia were submitted to an immunosuppression protocol with cyclophosphamide (CYP). CYP (Filaxis®; Martínez, Buenos Aires, Argentina) was diluted in sterile sodium chloride 0.45% and administered by ip route at 200 mg/kg once a week for 28 days. During the immunosuppression cycle, the presence of blood trypomastigotes was assessed periodically. If parasitemia did not rebound, animals were euthanized and blood, heart, and skeletal muscle samples were collected for parasite DNA quantification by qPCR and histology evaluation.

PCR Sampling and Preparation

Blood samples were obtained by submandibular vein puncture (Golde et al., 2005) and collected in sterile cryotubes with 1:3 guanidine-HCl 6M-EDTA 0.2M pH 8 buffer. Skeletal muscle from the rear legs and heart were obtained and rinsed with sterile distilled water before being collected in separate sterile cryotubes. Samples were stored at -20°C until processing.

DNA was extracted with High Pure PCR Template Preparation Kit (Roche Diagnostics GmbH, Mannheim, Germany) according to the manufacturer's protocol. To discard inhibitions, an internal amplification control (0.2 ng)

TABLE 2 | Effect of miltefosine alone or combined with benznidazole on parasitemia parameters in BALB/cJ mice infected with *Trypanosoma cruzi* (VD strain).

Treatment(mg/kg/day) Subtherapeutic regime	n	MPR(trypomastigotes/mL)	MPRreduction (%)	Survival(%)
MLT (25)	4	9.06x10^{4} (± 4.13x10^{4})^{A}	76.23^{A}	4/4 (100)^{A}
BZ (5)	4	7.8x1x10^{4} (± 3.13x10^{4})^{A}	79.51^{A}	4/4 (100)^{A}
MLT (25) + BZ (5)	4	7.81x10^{4} (± 4.49x10^{4})^{A}	79.51^{A}	4/4 (100)^{A}
NT (—)	4	3.81x10^{5} (± 1.64x10^{5})^{B}	—–	2/4 (50)^{B}
Additive regime*				
BZ (100)	8	2.17x10^{4} (± 1.30x10^{4})^{A}	94.31^{A}	8/8 (100)^{A}
MLT (50) + BZ (50)	8	3.63x10^{4} (± 1.24x10^{4})^{A}	90.49^{A}	8/8 (100)^{A}
NT	12	3.81x10^{5} (± 1.64x10^{5})^{B}	—	0/12 (0)^{B}

NT, infected non-treated. MLT, miltefosine. BZ, benznidazole. MPR, Maximum parasitemia reached.

*Female BALB/cJ mice were infected with 500 trypomastigotes of T. cruzi VD strain; treatment started at 8 dpi and was administered orally for 20 consecutive days. * Results obtained from two independent assays.*

Different letters indicate significant differences (Kruskal-Wallis; $p < 0.05$).

Values are expressed as mean (± standard deviation).

was included in each sample before starting the DNA extraction procedure (Duffy et al., 2013). Extracted DNA was quantified by spectrophotometry at 260 nm wavelength in a Nanodrop 1000 spectrophotometer (Thermo Fisher Scientific, Wilmington, DE, USA) and stored at -20°C until use.

Quantitative PCR

Amplification was performed using oligonucleotides targeted to a 166 bp *T. cruzi* satellite DNA fragment and IAC on a StepOne PCR system (Applied Biosystems, Foster City, California, USA) as described elsewhere (Duffy et al., 2013). qPCR conditions and standard parasite curve for data analysis were performed as previously described (Gulin et al., 2018). The efficiency of amplification was determined using the following calculation: Efficiency (E) = $10^{(-1/\text{slope})}$, using Step One Software 2.1 (Applied Biosystems, Foster City, California, USA).

Positive and negative blood or tissue samples and reagent controls were run in each assay. DNA extraction, mixing, and qPCR reaction were performed in separate areas to avoid contamination. The cycle threshold (Ct) allowed interpolating the parasite equivalents of each sample from the standard curve.

Tissue Samples Preparation and Histological Analysis

Segments of heart and skeletal muscle were fixed in buffered 10% formaldehyde, dehydrated, and embedded in paraffin. Then, 5 mm thick sections were stained with hematoxylin and eosin (H&E). A single-blind evaluation of the specimens was performed by light microscopy, and the parasite load was expressed as the presence or absence of amastigote nests. The degree of myocardial and skeletal muscle inflammation was scored as previously reported (Tarleton et al., 1994; Solana et al., 2012).

Statistical Analysis

For *in vivo* studies, data distribution and homoscedasticity were evaluated. If the distribution was normal and variance was uniform, analysis of variance (ANOVA) and correction for multiple comparisons with Bonferroni test, when necessary, were performed. Data with distributions other than normal were analyzed by non-parametric Kruskal-Wallis test and compared in pairs. Survival analysis was performed using the Kaplan-Meier test.

In all cases, p-values <0.05 were considered statistically significant. Statistical analyses for *in vivo* tests were performed with InfoStat/P 2014 program, while analysis of the *in vitro* data and graphics were prepared with GraphPad Prism 5.03 (GraphPad Software, San Diego, California, USA). Values in tables and graphs are expressed in mean values with standard deviation unless otherwise indicated.

RESULTS

In Vitro Anti-*T. cruzi* Activity of MLT Alone and Combined With BZ

The *in vitro* anti-*T. cruzi* activity and cytotoxicity of MLT, BZ, and NFX alone are summarized in **Table 3**. The MLT trypanolytic effect was significantly less potent than BZ or NFX, obtaining an LC_{50} value near the high micromolar range. However, MLT exhibited an *in vitro* amastigote inhibitory activity similar to BZ and NFX.

The *in vitro* activity of MLT and BZ combination on trypomastigotes and amastigotes stages of *T. cruzi* is summarized in **Table 4**, and isobolograms are shown in **Figure 1**. The MLT and BZ association led to a significant decrease in trypomastigotes viability, assessed as a drop in the LC_{50} value. Moreover, the ΣFICI suggested that this combination would have a synergic effect on trypomastigotes lysis in culture. Similarly, the *in vitro* MLT and BZ effect on the amastigote stage reduced the IC_{50} value compared to the IC_{50} of each drug separately. Thus, the ΣFICI suggested an additive interaction.

In Vivo Evaluation of MLT as Monotherapy

Clinical Response

Mice treated with MLT exhibited slight signs of discomfort during oral administration, denoted by retching, anxious appearance, and repeated grooming of lips and cheeks immediately after treatment. These signs lasted 15-20 minutes and then the animals returned to their usual behavior. These changes were not observed in the non-treated infected group

TABLE 3 | *In vitro* activity of miltefosine, benznidazole, and nifurtimox on trypomastigote and intracellular amastigote stages of *Trypanosoma cruzi* (VD strain) and their cytotoxic effects on Vero cells.

Drug	LC_{50}(Anti-trypomastigote activity)	IC_{50}(Anti-amastigote activity)	CC_{50}(Host-cell cytotoxic activity)	SI
MLT	31.17 (29.56; 32.87)	0.51 (0.48; 0,55)	57.36 (36.14; 91.05)	112
BZ	9.43 (8.62; 10.32)	0.73 (0.69; 0.77)	> 640	> 876
NFX	2.35 (2.00; 2.78)	0.15 (0.13; 0.17)	> 220	> 1.497

MLT, miltefosine. BZ, benznidazole. NFX, nifurtimox.

LC_{50}: lytic concentration 50%; drug concentration needed to reduce the trypomastigote motility by 50% compared to the infected non-treated control.

IC_{50}: inhibitory concentration 50%; drug concentration needed to reduce the intracellular amastigote development by 50% compared to the infected non-treated control.

CC_{50}, cell toxicity 50%; drug concentration capable of reducing the cell viability by 50% compared to the non-treated cell culture.

SI, selectivity index. SI, CC_{50}/IC_{50}.

Values are expressed in μM and reported as the mean concentration and the 95% confidence interval (IC95%).

TABLE 4 | *In vitro* fractional inhibitory concentration index from miltefosine and benznidazole on trypomastigotes and amastigotes stages of *Trypanosoma cruzi* (VD strain).

Combination	Trypomastigotes			Amastigotes		
	LC_{50} (μM)	FICI	∑FICI	IC_{50} (μM)	FICI	∑FICI
Fixed MLT + Variable BZ	2.845	0.17	0.46	0.34	0.38	0.71
Fixed BZ + Variable MLT	5.75	0.29		0.29	0.32	

MLT, miltefosine. BZ, benznidazole. FICI, Fractional inhibitory concentration index.

administered the same volume of vehicle (i.e., distilled water or CMC 0.25%), nor in the mice infected and treated with BZ or NFX.

Throughout MLT treatment, the mice experienced a decrease in body weight, although these differences were not statistically significant compared with the other experimental groups (**Supplementary Material**, **Figure S1.A**). In the groups treated with MLT at 50 or 75 mg/kg/day, the bodyweight remained between the initial and an average increase of 20%, while the mice treated with 100 mg/kg/day of MLT showed a marked weight decrease from 11 dpi, but they recovered at 21 dpi and increased by an average of 9.4% compared to the initial weight by the end of the treatment (28 dpi).

Body temperatures remained close to the lower limit of the normal range for the murine species, without significant differences between the treatment groups, possibly due to the wide dispersion of the obtained values (**Supplementary Material**, **Figure S1.B**).

However, the NT group showed a significant decrease in body temperature as the acute course of the infection progressed, which was accompanied by a reduction in body weight, lethargic behavior, and ruffled coat.

Treatment Response During the Acute Phase

MLT treatment led to suppressive effects on parasitemia and associated parameters in a dose-dependent manner (**Figure 2** and **Table 1**). The patent parasitemia period (PPP) was statistically different between the treatment groups ($p < 0.0001$). MLT administered at 100 mg/kg/day significantly reduced the PPP compared to MLT at 25 mg/kg/day. In contrast, groups treated with MLT or BZ at 100 mg/kg/day did not lead to significant differences in PPP during the acute phase of infection.

Moreover, treatment with MLT in doses ≥50 mg/kg/day reduced maximum parasitemia reached (MPR) without significant differences compared to the reduction achieved with BZ or NFX. Animals treated with 100 mg/kg/day of BZ, NFX, or

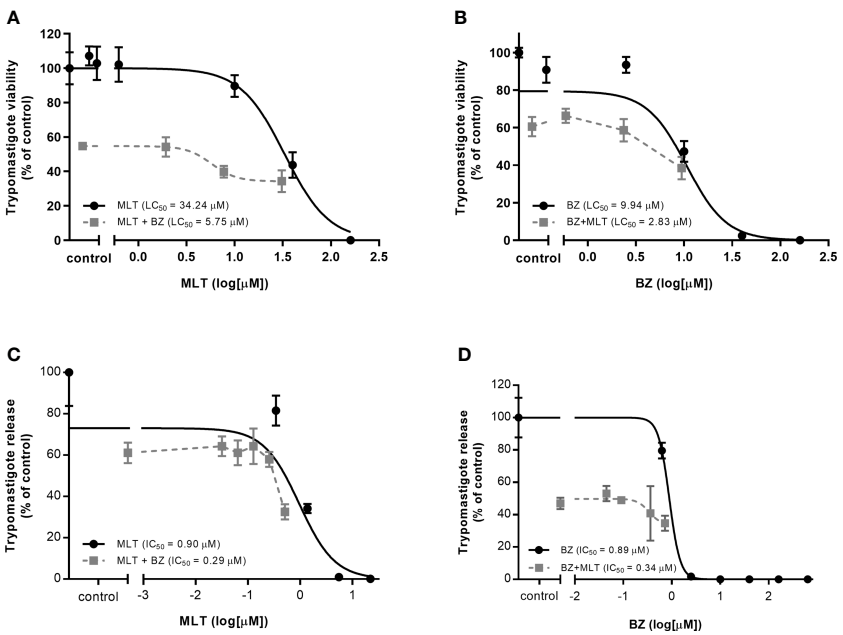

FIGURE 1 | *In vitro* activity of miltefosine (MLT) and benznidazole (BZ) combination on **(A-B)** trypomastigotes and intracellular amastigote development **(C-D)** of *Trypanosoma cruzi* (VD strain). **(A)** LC_{50} value from BZ combined with variable concentrations of MLT.**(B)** LC_{50} value from MLT combined with variable concentrations of BZ. **(C)** IC_{50} value from BZ combined with variable concentrations of MLT. **(D)** IC_{50} value from MLT combined with variable concentrations of BZ. Values are expressed in μM and reported as the mean concentration and the 95% confidence interval (IC95%).

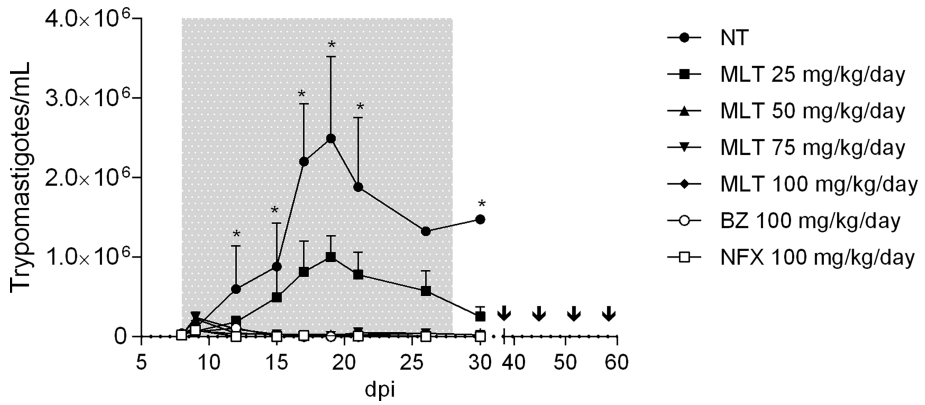

FIGURE 2 | Effect of miltefosine, benznidazole, or nifurtimox on parasitemia course in BALB/cJ mice infected with *Trypanosoma cruzi* (VD strain). Values are expressed as mean trypomastigotes/mL (± SD) in peripheral blood from experimental groups according to the days after infection (dpi). Mice were inoculated with 500 trypomastigotes of the VD strain of *Trypanosoma cruzi*, and treatment started at parasitemia onset (8th dpi). During treatment and up to 10 days post-treatment, parasitemia was evaluated by fresh blood examination (FBE) to determine parasitemia rebound. Animals with negative parasitemia were submitted to immunosuppression consisting of four doses of cyclophosphamide (CYP; 200 mg/kg; ip route), separated by one week. Parasitemia was evaluated during the CYP cycle and up to 7 days after the last dose. The asterisks indicate significant differences compared to NT and MLT 25 mg/kg/day groups (Kruskal-Wallis, $p < 0.05$). Grey shading indicates the treatment period. Arrows indicate CYP administration cycle. NT, infected non-treated. MLT, miltefosine. BZ, benznidazole. NFX, nifurtimox.

MLT had undetectable blood trypomastigotes at the end of the treatment (**Figure 2**).

Administration of MLT at doses ≥50 mg/kg/day prevented mortality in 100% of the mice. Groups treated with MLT at any dose, BZ or NFX, were statistically more likely to survive than NT controls ($p<0.0001$ for log-rank Mantel-Cox test).

Assessment of Parasitological Cure

At the end of the treatment, at least one mouse from groups receiving MLT at 25, 50, and 75 mg/kg/day exhibited patent parasitemia (1/4, 4/5, and 4/5, respectively). Conversely, all mice treated with 100 mg/kg/day of MLT, BZ, or NFX had negative parasitemia by optical microscopy. Through the following 10 days, parasitemia remained negative in all animals, regardless of the treatment previously administered.

The CYP immunosuppression cycle was initiated 10 days after treatment completion. The parasitemia rebound occurred throughout the follow-up period in all animals from MLT treated groups, usually between the second and fourth CYP dose.

Animals from BZ and NFX groups displayed parasitemia rebound in 44% (4/9) and 60% (6/10) of cases, respectively. qPCR on blood samples yielded the same positivity rate as microscopy.

Histopathology

Inflammation scoring in skeletal muscle samples was significantly different between treatment groups ($p= 0.0025$) (**Supplementary Material**, **Figure S2.A**). Inflammation in skeletal muscle was significantly lower in animals treated with MLT at 50 mg/kg/day than the NT group, similarly to animals treated with BZ or NFX. The other MLT doses studied had a wide range of variability in inflammation scores. Regarding the inflammation degree in the myocardium, there were no significant differences among treatment groups (**Supplementary Material**, **Figure S2.B**). The proportion of animals with amastigote nests was significantly higher in the NT group than in other treatment groups, in skeletal and myocardial muscle (Chi-square, p=0.0003 and 0.0044, respectively). No significant differences were detected between the groups receiving MLT, BZ, or NFX, both in skeletal muscle and myocardium (**Figure 3**). Microphotographs of representative skeletal and cardiac muscle samples from different treatment groups can be observed as **Supplementary Material** (**Figures S3**, **S4**, respectively).

In Vivo Evaluation of MLT Combined With BZ

Clinical Response

Similar to the monotherapy trials, MLT administration in combined regimes produced a significant variation of the average weight gain from day 13 post-infection (6 days of treatment), with a decrease relative to the initial weight of between 10 and 15% in the animals treated with the MLT and BZ combination, which was then partially reversed toward the end of treatment. However, the initial weight was not recovered. Body temperature values were close to the lower limit of the normal range for the species recorded, without significant differences between the treatment groups (**Supplementary Material**, **Figures S5**, **S6**).

Treatment Response

During the acute course of the infection, treatments lead to a significant decrease in parasitemia. MLT and BZ administration in sub-therapeutic doses given separately or in combination diminished the MPR between 76.23 to 79.51%, which was significantly higher in the NT infected group compared to the treatment groups ($p < 0.01$) (**Table 2**). Likewise, administration of sub-therapeutic doses of MLT and BZ alone or in combination prevented mortality (**Supplementary Material**, **Figures S7**).

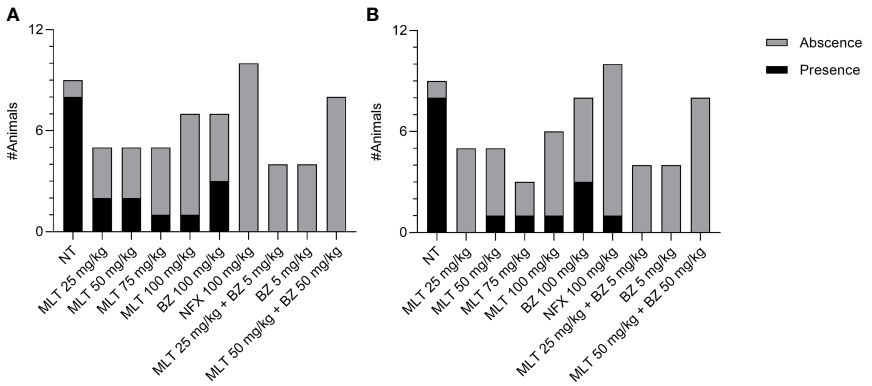

FIGURE 3 | Effect of miltefosine (alone or in combined regimes), benznidazole, or nifurtimox on amastigote nest burden in BALB/cJ mice infected *Trypanosoma cruzi*, (VD strain). Mice with the presence or absence of amastigote nests in skeletal muscle **(A)** and heart samples **(B)**. NT, infected non-treated. MLT, miltefosine. BZ, benznidazole. NFX, nifurtimox.

For the additive treatment regime, the combination of BZ +MLT at half the effective doses (i.e., 50 mg/kg/day each) significantly reduced MPR compared to NT animals, but there were no significant differences when compared with the group receiving BZ 100 mg/kg/day. Finally, 100% of the mice treated with MLT either alone or combined with BZ survived (**Supplementary Material, Figure S8**).

Assessment of Parasitological Cure

The treatment with sub-therapeutic doses of MLT or BZ, alone or in combination, was not able to eliminate circulating parasites and therefore the estimated parasitic load by qPCR was not significantly different (**Table 5**).

Regarding the additive treatment regime, mice receiving BZ at 100 mg/kg/day or MLT+BZ at 50 mg/kg/day showed negative parasitemia by fresh blood examination after 20 consecutive days of treatment. The experimental groups were kept under observation from that moment and the following 10 days, and parasitemia remained negative in all subjects, regardless of the administered treatment.

After that period, the immunosuppression cycle started in all mice (CYP, 200 mg/kg/week, ip route). Mice initially treated with MLT+BZ exhibited negative parasitemia at the end of the immunosuppression cycle, while only one animal from group BZ (100 mg/kg/day) showed parasitemia rebound.

Later, blood qPCR showed that 3/8 animals treated with BZ 100 mg/kg/day presented detectable non-quantifiable DNA. Whereas only one mouse treated with MLT+BZ combination exhibited detectable but non-quantifiable parasitic DNA in blood after immunosuppression (**Table 5**). Parasitic DNA was detected in low quantity in skeletal and cardiac muscle samples, and it could not be quantified with the previously established curve. The proportion of positive samples in skeletal and cardiac muscle was not statistically significant between treatment groups (**Table 5**).

TABLE 5 | Effect of miltefosine alone or combined with benznidazole at different sub-therapeutic or additive regimes on parasite burden at the end of the treatment in BALB/cJ mice infected with *Trypanosoma cruzi* (VD strain).

Treatment(mg/kg/day)	n	+FBE	qPCR					
			+Blood after CYP	Parasite Eq/mL blood	+BloodbeforeCYP	ParasiteEq/mL	+SkeletalMuscle	+CardiacMuscle
Subtherapeutic regime								
MLT (25)	4	4/4	4/4	4.099 (± 4.240)	ND	ND	ND	ND
BZ (5)	4	4/4	4/4	2.856 (± 2.275)	ND	ND	ND	ND
MLT (25) + BZ (5)	4	4/4	4/4	1.553 (± 2.154)	ND	ND	ND	ND
NT	1	1/1	1/1	163.734	ND	ND	ND	ND
Additive regime*								
BZ (100)	8	1/8	2/8 (2*)	NQ	3/8 (3*)	NQ	5/8 (1*)	4/8 (1*)
MLT (50) + BZ (50)	8	0/8	0/8	NQ	1/8 (1*)	NQ	4/8 (1*)	3/8 (2*)

MLT, miltefosine. BZ, benznidazole. NT, infected non-treated. CYP, cyclophosphamide (200 mg/kg; ip).
+FBE, positive parasitemia result in fresh blood examination at the end of the treatment.
+SkM, positive result for qPCR assay in skeletal muscle.
+CM, positive result for qPCR assay in cardiac muscle.
NQ, not quantifiable sample.
ND, not determined.
**Includes positive but not quantifiable samples.*

Histopathology

Regarding the combinatory therapy, inflammation scores in skeletal muscle and cardiac muscle were not significantly different among treatment groups. A scarce inflammatory infiltrate was observed, assigning scores ranging from 0 to 3 for skeletal muscle and between 0 and 2 for cardiac muscle, with no significant differences (**Supplementary Material**, **Figure S2.A**, **S2.B**). Moreover, amastigotes nests could not be recorded in any sample from treatment groups (**Figure 3**). Microphotographs of representative skeletal and cardiac muscle samples from different treatment groups can be observed as Supplementary Material (**Figure S3**, **S4**, respectively).

DISCUSSION

MLT is a lipophospholipid analog developed originally as an antineoplastic agent (Dorlo et al., 2012). Based on previous *in vitro* and *in vivo* studies and results from oncology clinical trials, MLT was repositioned for visceral and cutaneous leishmaniasis treatment. Since its registration in 2002, MLT remains the only oral drug available for leishmaniasis (Reimão et al., 2020).

MLT and other alkyl-lipophospholipids have proven activity on *T. cruzi* (Croft et al., 1996; Luna et al., 2009). Our results support the MLT effect on inhibiting amastigote development *in vitro* and the low efficacy on trypomastigote stage (Croft et al., 1996; Santa-Rita et al., 2000). Moreover, MLT high selectivity index suggests a specific antiparasitic mechanism of action without affecting the host cell.

To date, only three studies have assessed the *in vivo* efficacy of MLT (Croft et al., 1996; Saraiva et al., 2002; Martinez-Peinado et al., 2021) in mice models of acute infection. While Croft et al. observed transient parasitemia suppression without a curative effect or reduction of mortality in mice treated for 5 days at up to 30 mg/kg/day by oral route, Saraiva et al. reported parasitic sterilization in all mice treated with 25 mg/kg/day, determined by direct blood observation at 120 dpi and spleen culture for 15 days. Recently, Martinez-Peinado et al. studied MLT efficacy by giving 30 mg/kg/day for 10 days, using the Brazil strain expressing firefly luciferase, which yielded statistical differences in luciferase activity compared to infected non-treated mice.

It is well known that several experimental variables affect the infection course and the main outcomes in animal models of *T. cruzi* infection (Chatelain and Konar, 2015), and their heterogeneity make difficult the direct comparison between results.

In this work, we evaluated the *in vivo* efficacy of MLT using state-of-the-art methodology based on previous guidelines for drug screening (Romanha et al., 2010) by using qPCR and immunosuppression cycle to elucidate the possible reemergence of parasites from tissues.

The murine model of acute infection with *T. cruzi* was previously standardized (Gulin et al., 2018), using the VD strain (TcVI), originally isolated from a patient infected by a congenital route. This model becomes relevant since mother-to-child infection is the main transmission mode in vector-free areas within and outside Latin America (Carlier et al., 2019). Furthermore, the VD strain displays high parasitemia levels and mortality rates in infected non-treated mice and a moderate BZ and NFX effect to eradicate the infection.

Despite a temporary animal discomfort observed in MLT oral administration, the treatment was well tolerated by the animals. Also, the weight loss and ruffled fur agree with previously reported effects (Saraiva et al., 2002). The body weight loss could be explained by the gastrointestinal discomfort caused by MLT at all assayed doses, an adverse effect widely reported in clinical trials (Jha et al., 1999; Sundar et al., 2002).

As described by Saraiva et al., the parasitemia course throughout the acute phase of infection was not suppressed with 25 mg/kg/day of MLT. However, in our infection model, the days of patent parasitemia and the MPR were lowered in a dose-dependent manner by MLT, and the 100 mg/kg/day dose was able to reduce blood trypomastigotes circulation to undetectable levels by optical microscopy.

When administered alone, MLT at lower doses leads to a parasitemia reduction, and this could be explained in part due to the widespread drug distribution and the slow clearance rate. In mice, oral MLT is absorbed slowly but extensively and accumulates mainly in the kidneys, liver, and lungs (Breiser et al., 1987). Clinical pharmacokinetic studies indicate that, due to its prolonged half-life, MLT accumulates during treatment reaching a steady-state concentration in the last week of a 28-day treatment schedule (Kip et al., 2018).

Although the drug failed to produce parasitic sterilization, it was able to maintain the burden of amastigotes at low levels, which was reactivated by CYP-induced immunosuppression. Moreover, animals treated with MLT showed lower rates of amastigote nests in the myocardium and in skeletal muscle compared to NT, which could be explained by the MLT extensive distribution in these tissues, as previously documented in mice and rats (Breiser et al., 1987; Marschner et al., 1992).

Failure to reach parasitological sterilization was also detected in a percentage of the animals treated with BZ or NFX. These results coincide with the previously published characterization of the VD strain (Gulin et al., 2018), and with other *T. cruzi* strains from the same DTU, usually classified as BZ-sensitive (Fernández et al., 2010; Keenan et al., 2013b).

MLT effect on *Leishmania* spp. was also studied in combination with reference drugs or with repositioned compounds. *In vitro* additive synergism with sodium stibogluconate and *in vivo* potentiate synergism potentiation combined with paromomycin or amphotericin B were reported (Seifert and Croft, 2006). Costa et al. also reported the parasiticidal effect of efavirenz on *L. infantum* and a lower IC_{50} adding MLT (Costa et al., 2016).

The combined effect of MLT with other compounds on *T. cruzi* viability was previously described by *in vitro* combination with ketoconazole, both on trypomastigotes and intracellular amastigotes (Santa-Rita et al., 2005). However, this is the first study of the anti-*T cruzi* effect of the MLT and BZ combination.

The analysis of the MLT+BZ *in vitro* combination suggests a synergistic effect on trypomastigotes viability and an additive interaction on intracellular amastigote development. This

association was not evaluated previously, although similar *in vitro* interactions were reported when combining MLT with paromomycin (de Morais-Texeira et al., 2014) or nitazoxanide (Mesquita et al., 2014) on *Leishmania* spp.

We furthered the evaluation of the MLT and BZ association on a murine model of acute infection with *T. cruzi*. MLT+BZ combination at sub-therapeutic doses could not achieve an effect different from that obtained with the drugs separately. However, it decreased parasite loads in blood and prevented mortality in treated mice. Nevertheless, MLT+BZ at half the total dose (i.e., 50mg/kg) produced negative parasitemia and prevented the reactivation after the immunosuppression protocol.

The qPCR yielded disparate results in target organs such as skeletal muscle and myocardium in both experimental groups, with detection of parasitic DNA in low-loading or even non-quantifiable cases. These results could then question qPCR as a method to establish parasitological cure in cases where *T. cruzi* DNA is not detected in the blood.

Residual DNA in tissues and phagocytic cells has been reported in experimentally infected mice treated with BZ and considered cured by different methods (Guarner et al., 2001; Martins et al., 2008), which would indicate the presence of non-viable parasites or even cross-contamination with parasitic DNA.

However, recently described spontaneous dormancy in *T. cruzi* (Sánchez-Valdéz et al., 2018) could also explain the presence of parasitic DNA in tissues due to the non-replicative amastigote stage in the absence of bloodstream trypomastigotes, which would deserve further investigation to fully understand therapeutic failure both in preclinical studies and clinical trials.

Although our results demonstrate the inability of MLT to achieve a complete parasitological cure in an acute murine model of *T. cruzi* infection, the positive interaction with BZ both *in vitro* and *in vivo* opens a promising alternative in drug repurposing and combinatory therapy approach for Chagas disease treatment. MLT and other synthetic alkylphospholipids arise as drug candidates for combined treated schemes and serve as chemical scaffolds for new compound entities.

DATA AVAILABILITY STATEMENT

The raw data supporting the conclusions of this article will be made available by the authors, without undue reservation.

ETHICS STATEMENT

The animal study was reviewed and approved by Institutional Animal Care and Use Committee from the Faculty of Veterinary Sciences (University of Buenos Aires) (Protocol #2014/04).

AUTHOR CONTRIBUTIONS

JENG: Writing - original draft, Writing -review & editing, Investigation, Validation, Formal analysis. MMCB: Writing -review & editing, Investigation, Validation, Formal analysis. DR and MES: Investigation, Validation, Formal analysis. JA: Conceptualization, Methodology, Funding acquisition, Resources, Supervision. FG-B: Conceptualization, Methodology, Writing - review & editing, Funding acquisition, Resources, Supervision. All authors contributed to the article and approved the submitted version.

FUNDING

This work was supported by Agencia Nacional de Promoción de la Investigación, el Desarrollo Tecnológico y la Innovación, Ministerio de Ciencia y Técnica, Argentina (Grant: Proyectos de Investigación Científica y Tecnológica PICTO-GLAXO 2012-035).

ACKNOWLEDGMENTS

We would like to thank Dr. Daniel Lombardo (Universidad de Buenos Aires, Facultad de Ciencias Veterinarias) for providing support in histology samples preparation and images acquisition.

SUPPLEMENTARY MATERIAL

The Supplementary Material for this article can be found online at: https://www.frontiersin.org/articles/10.3389/fcimb.2022.855119/full#supplementary-material

REFERENCES

Andrews, K., Fisher, G., and Skinner-Adams, T. (2014). Drug Repurposing and Human Parasitic Protozoan Diseases. *Int. J. Parasitol. Drugs Drug Resist.* 4, 95–111. doi: 10.1016/j.ijpddr.2014.02.002

Apt, W. (2010). Current and Developing Therapeutic Agents in the Treatment of Chagas Disease. *Drug Des. Devel. Ther.* 4, 243–253. doi: 10.2147/dddt.s8338

Benaim, G., Paniz-Mondolfi, A., Sordillo, E., and Martinez-Sotillo, N. (2020). Disruption of Intracellular Calcium Homeostasis as a Therapeutic Target Against Trypanosoma Cruzi. *Front. Cell Infect. Microbiol.* 10. doi: 10.3389/fcimb.2020.00046

Breiser, A., Kim, D., Fleer, E., Damenz, W., Drube, A., Berger, M., et al. (1987). Distribution and Metabolism of Hexadecylphosphocholine in Mice. *Lipids* 22, 925–926. doi: 10.1007/BF02535556

Brossas, J., Gulin, J., Bisio, M., Chapelle, M., Marinach-Patrice, C., Bordessoules, M., et al. (2017). Secretome Analysis of Trypanosoma Cruzi by Proteomics Studies. *PloS One* 12, e0185504. doi: 10.1371/journal.pone.0185504

Cantin, L., and Chamberland, S. (1993). *In Vitro* Evaluation of the Activities of Azithromycin Alone and Combined With Pyrimethamine Against Toxoplasma Gondii. *Antimicrob. Agents Chemother.* 37, 1993–1996. doi: 10.1128/AAC.37.9.1993

Carlier, Y., Altcheh, J., Angheben, A., Freilij, H., Luquetti, A. O., Schijman, A. G., et al. (2019). Congenital Chagas Disease: Updated Recommendations for Prevention, Diagnosis, Treatment, and Follow-Up of Newborns and Siblings, Girls, Women of Childbearing Age, and Pregnant Women. *PloS Negl. Trop. Dis.* 13, 1–9. doi: 10.1371/journal.pntd.0007694

Chatelain, E., and Ioset, J. (2011). Drug Discovery and Development for Neglected Diseases: The DNDi Model. *Drug Des. Devel. Ther.* 5, 175–181. doi: 10.2147/DDDT.S16381

Chatelain, E., and Konar, N. (2015). Translational Challenges of Animal Models in Chagas Disease Drug Development: A Review. *Drug Des. Devel. Ther.* 19, 4807–4823. doi: 10.2147/DDDT.S90208

Costa, S., Machado, M., Cavadas, C., and do Céu Sousa, M. (2016). Antileishmanial Activity of Antiretroviral Drugs Combined With Miltefosine. *Parasitol. Res.* 115, 3881–3887. doi: 10.1007/s00436-016-5153-8

Croft, S., Snowdon, D., and Yardley, V. (1996). The Activities of Four Anticancer Alkyllysophospholipids Against Leishmania Donovani, Trypanosoma Cruzi and Trypanosoma Brucei. *J. Antimicrob. Chemother.* 38, 1041–1047. doi: 10.1093/jac/38.6.1041

da Silva, C., da Silva, P., Batista, M., Daliry, A., Tidwell, R., and Soeiro, M. N. (2010). The Biological *In Vitro* Effect and Selectivity of Aromatic Dicationic Compounds on Trypanosoma Cruzi. *Mem. Inst. Oswaldo. Cruz.* 105, 239–245. doi: 10.1590/S0074-02762010000300001

de Morais-Texeira, E., Gallupo, M., Fonseca Rodrigues, L., Romanha, A., and Rabello, A. (2014). *In Vitro* Interaction Between Paromomycin Sulphate and Four Drugs With Leishmanicidal Activity Against Three New World Leishmania Species. *J. Antimicrob. Chemother.* 69, 150–154. doi: 10.1093/jac/dkt318

Dorlo, T., Balasegaram, M., Beijnen, J., and de Vries, P. (2012). Miltefosine: A Review of its Pharmacology and Therapeutic Efficacy in the Treatment of Leishmaniasis. *J. Antimicrob. Chemother.* 67, 2576–2597. doi: 10.1093/jac/dks275

Duffy, T., Cura, C., Ramirez, J., Abate, T., Cayo, N., Parrado, R., et al. (2013). Analytical Performance of a Multiplex Real-Time PCR Assay Using TaqMan Probes for Quantification of Trypanosoma Cruzi Satellite DNA in Blood Samples. *PloS Negl. Trop. Dis.* 7, e2000. doi: 10.1371/journal.pntd.0002000

Fernández, M., González-Cappa, S., and Solana, M. (2010). Trypanosoma Cruzi : Immunological Predictors of Benznidazole Efficacy During Experimental Infection. *Exp. Parasitol.* 124, 172–180. doi: 10.1016/j.exppara.2009.09.006

Field, M., Horn, D., Fairlamb, A., Ferguson, M., Gray, D., Read, K., et al. (2017). Anti-Trypanosomatid Drug Discovery: An Ongoing Challenge and a Continuing Need. *Nat. Rev. Microbiol.* 15, 217–231. doi: 10.1038/nrmicro.2016.193

Fivelman, Q., Adagu, I., and Warhurst, D. (2004). Modified Fixed-Ratio Isobologram Method for Studying *In Vitro* Interactions Between Atovaquone and Proguanil or Dihydroartemisinin Against Drug-Resistant Strains of Plasmodium Falciparum. *Antimicrob. Agents Chemother.* 48, 4097–4102. doi: 10.1128/AAC.48.11.4097-4102.2004

Ghosh, M., Roy, K., and Roy, S. (2013). Immunomodulatory Effects of Antileishmanial Drugs. *J. Antimicrob. Chemother.* 68, 2834–2838. doi: 10.1093/jac/dkt262

Golde, W., Gollobin, P., and Rodriguez, L. (2005). A Rapid, Simple, and Humane Method for Submandibular Bleeding of Mice Using a Lancet. *Lab. Anim.* 34, 39–43. doi: 10.1038/laban1005-39

Guarner, J., Bartlett, J., Zaki, S., Colley, D., Grijalva, M., and Powell, M. (2001). Mouse Model for Chagas Disease: Immunohistochemical Distribution of Different Stages of Trypanosoma Cruzi in Tissues Throughout Infection. *Am. J. Trop. Med. Hyg.* 65, 152–158. doi: 10.4269/ajtmh.2001.65.152

Gulin, J., Bisio, M., Rocco, D., Altcheh, J., Solana, M., and García-Bournissen, F. (2018). Molecular and Biological Characterization of a Highly Pathogenic Trypanosoma Cruzi Strain Isolated From a Patient With Congenital Infection. *Exp. Parasitol.* 186, 50–58. doi: 10.1016/j.exppara.2018.02.002

Gulin, J., Eagleson, M., López-Muñoz, R., Solana, M., Altcheh, J., and García-Bournissen, F. (2020). *In Vitro* and *In Vivo* Activity of Voriconazole and Benznidazole Combination on Trypanosoma Cruzi Infection Models. *Acta Trop.* 211. doi: 10.1016/j.actatropica.2020.105606

Jha, T., Sundar, S., Thakur, C., Bachmann, P., Karbwang, J., Fischer, C., et al. (1999). Miltefosine, an Oral Agent, for the Treatment of Indian Visceral Leishmaniasis. *N. Engl. J. Med.* 341, 1795–1800. doi: 10.1056/NEJM199912093412403

Keenan, M., Alexander, P., Chaplin, J., Abbott, M., Diao, H., Wang, Z., et al. (2013a). Selection and Optimization of Hits From a High-Throughput Phenotypic Screen Against Trypanosoma Cruzi. *Futur. Med. Chem.* 5, 1733–1752. doi: 10.4155/fmc.13.139

Keenan, M., Chaplin, J., Alexander, P., Abbott, M., Best, W., Khong, A., et al. (2013b). Two Analogues of Fenarimol Show Curative Activity in an Experimental Model of Chagas Disease. *J. Med. Chem.* 56, 10158–10170. doi: 10.1021/jm401610c

Kip, A., Schellens, J., Beijnen, J., and Dorlo, T. (2018). Clinical Pharmacokinetics of Systemically Administered Antileishmanial Drugs. *Clin. Pharmacokinet.* 57, 151–176. doi: 10.1007/s40262-017-0570-0

Lira, R., Contreras, L., Rita, R., and Urbina, J. (2001). Mechanism of Action of Anti-Proliferative Lysophospholipid Analogues Against the Protozoan Parasite Trypanosoma Cruzi: Potentiation of *In Vitro* Activity by the Sterol Biosynthesis Inhibitor Ketoconazole. *J. Antimicrob. Chemother.* 47, 537–546. doi: 10.1093/jac/47.5.537

Luna, K., Hernández, I., Rueda, C., Zorro, M., Croft, S., and Escobar, P. (2009). *In Vitro* Susceptibility of Trypanosoma Cruzi Strains From Santander, Colombia, to Hexadecylphosphocholine (Miltefosine), Nifurtimox and Benznidazole. *Biomédica* 29, 448–455 http://www.scielo.org.co/pdf/bio/v29n3/v29n3a13.pdf

Marschner, N., Kötting, J., Eibl, H., and Unger, C. (1992). Distribution of Hexadecylphosphocholine and Octadecyl-Methyl-Glycero-3-Phosphocholine in Rat Tissues During Steady-State Treatment. *Cancer Chemother. Pharmacol.* 31, 18–22. doi: 10.1007/BF00695989

Martinez-Peinado, N., Cortes-Serra, N., Sherman, J., Rodriguez, A., Bustamante, J., Gascon, J., et al. (2021). Identification of Trypanosoma Cruzi Growth Inhibitors With Activity *In Vivo* Within a Collection of Licensed Drugs. *Microorganisms* 9. doi: 10.3390/microorganisms9020406

Martins, H., Figueiredo, L., Valamiel-Silva, J., Carneiro, C., Machado-Coelho, G., Vitelli-Avelar, D., et al. (2008). Persistence of PCR-Positive Tissue in Benznidazole-Treated Mice With Negative Blood Parasitological and Serological Tests in Dual Infections With Trypanosoma Cruzi Stocks From Different Genotypes. *J. Antimicrob. Chemother.* 61, 1319–1327. doi: 10.1093/jac/dkn092

Maya, J., Cassels, B., Iturriaga-Vásquez, P., Ferreira, J., Faúndez, M., Galanti, N., et al. (2007). Mode of Action of Natural and Synthetic Drugs Against Trypanosoma Cruzi and Their Interaction With the Mammalian Host. *Comp. Biochem. Physiol. A Mol. Integr. Physiol.* 146, 601–620. doi: 10.1016/j.cbpa.2006.03.004

Mbui, J., Olobo, J., Omollo, R., Solomos, A., Kip, A., Kirigi, G., et al. (2019). Pharmacokinetics, Safety and Efficacy of an Allometric Miltefosine Regimen for the Treatment of Visceral Leishmaniasis in Eastern African Children: An Open-Label, Phase-II Clinical Trial. *Clin. Infect. Dis.* 68, 1530–1538. doi: 10.1093/cid/ciy747

Mesquita, J., Tempone, A., and Reimão, J. (2014). Combination Therapy With Nitazoxanide and Amphotericin B, Glucantime®, Miltefosine and Sitamaquine Against Leishimania (Leishmania) Infantum Intracellular Amastigotes. *Acta Trop.* 130, 112–116. doi: 10.1016/j.actatropica.2013.11.003

Miranda, C., Solana, M., Curto, M., Lammel, E., Schijman, A., and Alba Soto, C. (2015). A Flow Cytometer-Based Method to Simultaneously Assess Activity and Selectivity of Compounds Against the Intracellular Forms of Trypanosoma Cruzi. *Acta Trop.* 152, 8–16. doi: 10.1016/j.actatropica.2015.08.004

National Research Council (2011). *Guide for the Care and Use of Laboratory Animals. 8th* (The National Academies Press Washington, D.C: The National Academic Press). doi: 10.17226/12910

Odds, F. (2003). Synergy, Antagonism, and What the Chequerboard Puts Between Them. *J. Antimicrob. Chemother.* 52, 1. doi: 10.1093/jac/dkg301

Olfert, E., and Godson, D. (2000). Humane Endpoints for Infectious Disease Animal Models. *ILAR. J.* 41, 99–104. doi: 10.1093/ilar.41.2.99

Paulino, M., Iribarne, F., Dubin, M., Aguilera-Morales, S., Tapia, O., and Stoppani, A. (2005). The Chemotherapy of Chagas' Disease: An Overview. *Mini Rev. Med. Chem.* 5, 499–519. doi: 10.2174/1389557053765565

Pérez-Molina, J., and Molina, I. (2018). Chagas Disease. *Lancet* 391, 82–94. doi: 10.1016/S0140-6736(17)31612-4

Polanco-Hernández, G., Escalante-Erosa, F., García-Sosa, K., Acosta-Viana, K., Chan-Bacab, M., Sagua-Franco, H., et al. (2012). *In Vitro* and *In Vivo* Trypanocidal Activity of Native Plants From the Yucatan Peninsula. *Parasitol. Res.* 110, 31–35. doi: 10.1007/s00436-011-2447-8

Reimão, J., Pita Pedro, D., and Coelho, A. (2020). The Preclinical Discovery and Development of Oral Miltefosine for the Treatment of Visceral Leishmaniasis: A Case History. *Expert Opin. Drug Discovery* 15, 647–658. doi: 10.1080/17460441.2020.1743674

Rodrigues, J., Ueda-Nakamura, T., Corrêa, A., Sangi, D., and Nakamura, C. (2014). A Quinoxaline Derivative as a Potent Chemotherapeutic Agent, Alone or in

Combination With Benznidazole, Against Trypanosoma Cruzi. *PloS One* 9, e85706. doi: 10.1371/journal.pone.0085706

Romanha, A., Castro, S., Soeiro, M. N., Lannes-Vieira, J., Ribeiro, I., Talvani, A., et al. (2010). *In Vitro* and *In Vivo* Experimental Models for Drug Screening and Development for Chagas Disease. *Mem. Inst. Oswaldo. Cruz.* 105, 233–238. doi: 10.1590/s0074-02762010000200022

Sánchez-Valdéz, F., Padilla, A., Wang, W., Orr, D., and Tarleton, R. (2018). Spontaneous Dormancy Protects Trypanosoma Cruzi During Extended Drug Exposure. *Elife. 7* Mar 26;7:e34039 doi: 10.7554/eLife.34039

Santa-Rita, R., Lira, R., Barbosa, H., Urbina, J., and de Castro, S. (2005). Anti-Proliferative Synergy of Lysophospholipid Analogues and Ketoconazole Against Trypanosoma Cruzi (Kinetoplastida: Trypanosomatidae): Cellular and Ultrastructural Analysis. *J. Antimicrob. Chemother.* 55, 780–784. doi: 10.1093/jac/dki087

Santa-Rita, R., Santos Barbosa, H., Meirelles, M., and de Castro, S. (2000). Effect of the Alkyl-Lysophospholipids on the Proliferation and Differentiation of Trypanosoma Cruzi. *Acta Trop.* 75, 219–228. doi: 10.1016/s0001-706x(00)00052-8

Saraiva, V., Gibaldi, D., Previato, J., Mendonça-Previato, L., Bozza, M., Freire-De-Lima, C., et al. (2002). Proinflammatory and Cytotoxic Effects of Hexadecylphosphocholine (Miltefosine) Against Drug-Resistant Strains of Trypanosoma Cruzi. *Antimicrob. Agents Chemother.* 46, 3472–3477. doi: 10.1128/AAC.46.11.3472-3477.2002

Seifert, K., and Croft, S. (2006). *In Vitro* and *In Vivo* Interactions Between Miltefosine and Other Antileishmanial Drugs. *Antimicrob. Agents Chemother.* 50, 73–79. doi: 10.1128/AAC.50.1.73-79.2006

Singh, U., Prasad, R., Mishra, O., and Jayswal, B. (2006). Miltefosine in Children With Visceral Leishmaniasis: A Prospective, Multicentric, Cross-Sectional Study. *Indian J. Pediatr.* 73, 1077–1080. doi: 10.1007/BF02763048

Solana, M., Ferrer, M., Novoa, M., Song, W., and Gómez, R. (2012). Decay-Accelerating Factor 1 Deficiency Exacerbates Trypanosoma Cruzi-Induced Murine Chronic Myositis. *Muscle Nerve* 46, 582–587. doi: 10.1002/mus.23347

Sundar, S., Jha, T., Thakur, C., Engel, J., Sindermann, H., Fischer, C., et al. (2002). Oral Miltefosine for Indian Visceral Leishmaniasis. *N. Engl. J. Med.* 347, 1739–1746. doi: 10.1056/NEJMoa021556

Tarleton, R., Sun, J., Zhang, L., and Postan, M. (1994). Depletion of T-Cell Subpopulations Results in Exacerbation of Myocarditis and Parasitism in Experimental Chagas' Disease. *Infect. Immun.* 62, 1820–1829. doi: 10.1128/iai.62.5.1820-1829.1994

Conflict of Interest: The authors declare that the research was conducted in the absence of any commercial or financial relationships that could be construed as a potential conflict of interest.

Publisher's Note: All claims expressed in this article are solely those of the authors and do not necessarily represent those of their affiliated organizations, or those of the publisher, the editors and the reviewers. Any product that may be evaluated in this article, or claim that may be made by its manufacturer, is not guaranteed or endorsed by the publisher.

frontiers | Frontiers in Cellular and Infection Microbiology

ORIGINAL RESEARCH
published: 06 July 2022
doi: 10.3389/fcimb.2022.907043

Structural New Data for Mitochondrial Peroxiredoxin From *Trypanosoma cruzi* Show High Similarity With Human Peroxiredoxin 3: Repositioning Thiostrepton as Antichagasic Drug

Lucio Rivera-Santiago, Ignacio Martínez, Ruben Arroyo-Olarte, Paulina Díaz-Garrido, Roberto I. Cuevas-Hernandez and Bertha Espinoza *

Departamento de Inmunología, Instituto de Investigaciones Biomédicas, Universidad Nacional Autónoma de México, Ciudad de México, México

OPEN ACCESS

Edited by:
Vilma G. Duschak, Consejo Nacional de Investigaciones Científicas y Técnicas (CONICET), Argentina

Reviewed by:
Wilfredo Quiñones, Universidad de Los Andes (Venezuela), Venezuela
Miguel A. Chiurillo, University of Cincinnati, United States

***Correspondence:**
Bertha Espinoza
besgu@iibiomedicas.unam.mx

Specialty section:
This article was submitted to Parasite and Host, a section of the journal Frontiers in Cellular and Infection Microbiology

Received: *29 March 2022*
Accepted: *27 May 2022*
Published: *06 July 2022*

Citation:
Rivera-Santiago L, Martínez I, Arroyo-Olarte R, Díaz-Garrido P, Cuevas-Hernandez RI and Espinoza B (2022) Structural New Data for Mitochondrial Peroxiredoxin From Trypanosoma cruzi Show High Similarity With Human Peroxiredoxin 3: Repositioning Thiostrepton as Antichagasic Drug. Front. Cell. Infect. Microbiol. 12:907043. doi: 10.3389/fcimb.2022.907043

Trypanosoma cruzi, the causal agent of Chagas disease, has peroxiredoxins (PRXs) expressed in all stages of the parasite and whose function is to detoxify oxidizing agents, such as reactive oxygen species (ROS). These proteins are central for the survival and replication of the parasite and have been proposed as virulence factors. Because of their importance, they have also been considered as possible therapeutic targets, although there is no specific drug against them. One of them, the mitochondrial PRX (TcMPX), is important in the detoxification of ROS in this organelle and has a role in the infectivity of *T. cruzi*. However, their structural characteristics are unknown, and possible inhibitors have not been proposed. The aim was to describe in detail some structural characteristics of TcMPX and compare it with several PRXs to find possible similarities and repositioning the antibiotic Thiostrepton as a potential inhibitor molecule. It was found that, in addition to the characteristic active site of a 2-cys PRX, this protein has a possible transmembrane motif and motifs involved in resistance to hyper oxidation. The homology model suggests a high structural similarity with human PRX3. This similarity was corroborated by cross-recognition using an anti-human PRX antibody. In addition, molecular docking showed that Thiostrepton, a potent inhibitor of human PRX3, could bind to TcMPX and affect its function. Our results show that Thiostrepton reduces the proliferation of *T. cruzi* epimastigotes, cell-derived trypomastigotes, and blood trypomastigotes with low cytotoxicity on Vero cells. We also demonstrated a synergic effect of Thriostepton and Beznidazol. The convenience of seeking treatment alternatives against *T. cruzi* by repositioning compounds as Thiostrepton is discussed.

Keywords: *Trypanosoma cruzi*, mitochondrial peroxiredoxin, bioinformatic analysis, repositioning Thiostrepton, trypanocidal activity

INTRODUCTION

The protozoan *T. cruzi* is the etiologic agent of the Chagas disease (American trypanosomiasis), one of the major causes of morbidity and mortality in many countries of Latin America. Because of human migrations, Chagas disease is emerging in other regions (Europe and the United States principally), and it is estimated that 6 to 7 million people are currently infected worldwide (WHO, 2021). *T. cruzi* infects two hosts, the insect vector, a member of the Reduviidae family, and mammals such as humans. During its life cycle within these hosts, the parasite faces oxidant stress. When a vector feeds on a mammal infected with blood trypomastigotes, they travel to the posterior intestine. Large amounts of hemoglobin produced by food are degraded to heme (Nogueira et al., 2015), increasing the production of reactive oxygen species (ROS), which can eliminate the parasite. Another critical component in generating ROS within the vector is the prophenoloxidase present in hemolymph and hemocytes. It participates in melanization, phagocytosis, and encapsulation of parasites (Machado-Silva et al., 2016) and the production of intermediates of ROS and reactive nitrogen species. When the vector feeds on its host, it detects near the suction area, and the host can enter the parasite due to micro-abrasions in the skin caused by scratching. Once *T. cruzi* enters to the host, it interacts with several elements of the immune response like macrophages or neutrophils, which can potentially eliminate it through ROS such as superoxide anion ($O^{2\cdot-}$), hydrogen peroxide (H_2O_2), and peroxynitrite ($ONOO^-$). The host–parasite relationship has resulted in that *T. cruzi* developed effective mechanisms of evasion and resistance to the immune system as well as efficient antioxidant machinery. The peroxiredoxins (PRXs) are proteins responsible for inactivating ROS, organic peroxides, peroxynitrites, and peroxynitrous acid, which generate an oxidizing environment for the parasite (Perkins et al., 2015).

In *T. cruzi*, five PRXs that are found in specific organelles have been reported: cytosolic PRX (TcCPX), mitochondrial PRX (TcMPX), ascorbate-dependent heme peroxidase present in the endoplasmic reticulum (TcAPX), glutathione peroxidase I present in the glycosome (TcGPXI), and glutathione peroxidase II present in the endoplasmic reticulum (TcGPXII) (Wilkinson et al., 2000).

The mitochondrial enzyme TcMPX is one of the most studied, and it belongs to the typical 2-Cys PRXs, with a molecular weight of ~25 kDa. TcMPX concentrates on the kinetoplast, indicating that its main function is to protect the mitochondrial genome from peroxide-mediated damage (Wilkinson et al., 2000). Furthermore, this enzyme interacts with other molecules such as tryparedoxin II during oxidative stress conditions (Dias et al., 2018). It has been demonstrated that the overexpression of TcMPX protects *T. cruzi* against a wide range of peroxynitrites derived from immune cells and increases the resistance to H_2O_2, corroborating its participation as an antioxidant defense mechanism (Piacenza et al., 2008). In addition, during *T. cruzi* differentiation, there is an increase of TcMPX expression in trypomastigotes (infective stage) compared with epimastigotes (non-infective stage), analyzed in several *T. cruzi* strains (Piacenza et al., 2009). Furthermore, there is a correlation between virulence and the expression levels of these proteins, which could facilitate the establishment of the parasite in the host and resistance to drugs such as Nifurtimox (NF) (Piñeyro et al., 2008; Specker et al., 2022). Finally, TcMPX has a role as a partner of several proteins important for cellular metabolism (Peloso et al., 2016). Therefore, TcMPX has been proposed as an attractive candidate for the development of anti–*T. cruzi* drugs (Wilkinson et al., 2000). However, to date, no studies have been published addressing this possibility *in vivo*, *in vitro*, or *in silico*. In the present work, TcMPX from two *T. cruzi* strains were sequenced and a phylogenetic study was done. An *in silico* analysis was also carried out, and TcMPX structural properties were deduced from a model generated by homology. Finally, the role of a potential inhibitor of TcMPX on the proliferation of *T. cruzi*, cytotoxicity on Vero cells, and synergic effect with Beznidazol (BZ) were evaluated, and its possible role as a therapeutic drug is discussed.

MATERIALS AND METHODS

Parasites and DNA Extraction

Epimastigotes of Mexican TcI Qro (TBAR/MX/0000/Queretaro) and Ninoa (MHOM/MX/1994/Ninoa) strains were cultured as previously described (López-Olmos et al., 1998). Cell-derived trypomastigotes of Qro strain were obtained from Vero cells previously infected as described (Rodríguez-Hernández et al., 2019). Infected cells were cultured in 75-cm^2 flasks instead using Dulbecco's Modified Eagle's Medium (DMEM), pH 7.2, plus 10% Fetal Bovine Serum (FBS), glutamine (2 mg/ml), penicillin (100 units/ml), and streptomycin (100 mg/ml), in a humidified 5% CO_2 atmosphere at 37°C. For maintenance, confluent cultures cells were washed with 5 mM Ethylenediaminetetraacetic acid (EDTA), incubated for 5 min with trypsin (1 mg/ml), diluted, and re-plated. Blood trypomastigotes were obtained from Balb/c mice infected with the Qro strain. Maintenance was performed by bleeding mice every 18–20 days and infecting healthy 8-week-old female mice with 1×10^5 parasites intraperitoneally. Genomic DNA extraction of epimastigotes was performed with the phenol-chloroform technique, using 20 ml of logarithmic phase parasite culture (60×10^6 parasites/ml) (Macedo et al., 1992). Nucleic acid integrity was analyzed by 1% agarose gel electrophoresis, and its concentration and purity were assessed using a NanoDrop 1000 (Thermo Fisher Scientific, Waltham, MA, USA). The DNA was kept at −20°C until used.

PCR and TcMPX Sequencing

The Polymerase Chain Reaction (PCR) to amplify TcMPX was performed using 200 ng of DNA, and specific primers were designed using the software *Primer1* (http://primer1.soton.ac.uk/primer1.html): TcMPX-Fw (5′-ATGTTTCGTCGTATGGCCG-3′) and TcMPX-Rv (5′-TCATGCGTTTTTCTCAAAATATTCA-3′). The conditions employed were as follows: 5 U Platinum™ Pfx enzyme (Invitrogen, Massachusetts, USA), 10 mM of each primer, and 4 mM $MgCl_2$. One initial step of 94°C for 3 min, 35 cycles (30 s

at 94°C, 30 s at 60°C, and 45 s at 68°C), and a final elongation step (5 min at 68°C). The amplicons obtained (330-bp fragment) were purified using the innuPREP DOUBLEpure Kit (Analytik Jena, Jena, Germany). They were sequenced in the Laboratorio de Secuenciación Genómica de la Biodiversidad y de la Salud (UNAM) with the Sanger technique, using a 3500xL genetic analyzer (Applied Biosystems, Massachusetts, USA). The obtained sequences for Qro and Ninoa were analyzed using the software Chromas. The consensus sequence was determined using the software Bioedit. Finally, the two sequences were uploaded to the GenBank as QroMPX (accession number QKE53461.1) and NinoaMPX (QKE53460.1).

Phylogenetic and Comparative Analysis

The molecular weight, isoelectric point, and net charge were determined using the software Pepstats 6.6.0 (http://www.ebi.ac.uk/Tools/services/web). The conserved domain-based prediction was performed with the online software SMART (Simple Modular Architecture Research Tool) (http://smart.embl-heidelberg.de/). For the comparative analysis, several sequences of mitochondrial PRXs from different organisms were obtained from GenBank and Protein Data Bank (PDB) (**Supplementary Table 1**). The alignment of the sequences was performed using the software ClustalW. The phylogeny was established by Neighbor-Joining (NJ) analysis, and the bootstrap statistical method (10,000 replicates) was performed with MEGA 7.0. The calculation of the genetic distances was carried out by p-distance. Only the positions with coverage greater than or equal to 95% were considered. The resulting phylogenetic trees were visualized with FigTree V1.4.3 (http://tree.bio.ed.ac.uk/software/figtree). For the identification of conserved amino acids residues and functional motifs, multiple alignments of PRXs were performed using T-coffee (https://www.ebi.ac.uk/Tools/msa/tcoffee/). The prediction of transmembrane helices in QroMPX proteins was done using TMHMM 2.0 software (https://services.healthtech.dtu.dk/service.php?TMHMM-2.0).

TcMPX Homology Modeling

The homology modeling of QroMPX was performed by two different platforms: SWISS-MODEL (https://swissmodel.expasy.org/interactive) and Phyre2 (http://www.sbg.bio.ic.ac.uk/phyre2/). The resulting models were visualized and compared with PyMol Molecular Graphics System version 2.4.0 (Janson et al., 2017). In addition, the steric arrangement of the amino acids residues and the reliability of the protein structure was validated by the software Procheck, whereas the general rate of error frequencies was established using the software ERRAT. Both software are included in the package SAVES v6.0 (https://saves.mbi.ucla.edu/).

Immunodetection by Western Blot Using a Commercial Antibody

As described above, epimastigotes of *T. cruzi* Qro strain were cultured for four days. The parasites were harvested and heat-lysed at 100°C for 5 min in lysis buffer (12% Sodium Dodecyl Sulfate (SDS), 10 mM Hepes, pH 7.0). The protein was quantified with the DC Protein Assay Kit (Bio-Rad, California, USA). Then, 12 μg of the protein were separated by electrophoresis in a 12% SDS-Polyacrylamide Gel Electrophoresis (PAGE) and blotted to nitrocellulose membrane. Western blot (WB) analysis was performed by anti-PRX IgG1 B-11 (1:2,000) (137222, Santa Cruz Biotechnology, Texas, USA) as primary antibody and anti-Mouse IgG-Peroxidase (1:4000) (A-9044, Sigma Aldrich, Missouri, USA) as a secondary antibody. The WB was revealed by the addition of 3,3-diaminobenzidine (D5637, Sigma Aldrich, Missouri, USA).

Molecular Docking With TS

To explore the possible interaction between QroMPX and Thiostrepton (TS), we performed an *in silico* molecular docking study using AutoDock Vina (ADV) 1.1.2 on Mac Os X System (Trott and Olson, 2010). The receptors used for this analysis were the QroMPX model obtained by homology and human PRX3 (PDB 5JCG). Receptors and TS ligand (PDB ID: 2L2W) were prepared and converted to *.PDBQT files in AutoDockTools 1.5.6 (Sanner, 1999). Protein preparation was performed using a standard protocol consisting of the removal of co-crystallized ligands and water molecules; polar hydrogens were added, and Kollman charges for all receptor atoms were computed to assess hydrogen-bonding interactions. All the other parameters were kept at their default settings. The TS ligand was docked at each receptor using a grid box: 60 Å × 60 Å × 60 Å centered at the midpoint between the Cα of the peroxidatic and resolutive cysteines (C_P and C_R, respectively). That is, grid center for PRX3: X = 5.865 Å, Y = −27.873 Å, and Z = −27.243 Å; and grid center for QroMPX: X = 23.17 Å, Y = 23.233 Å, and Z = −3.844 Å. The docking algorithm of ADV was used to find the best complex between ligand and protein. A maximum of 20 conformers were considered for each ligand, and the complex with the most favorable free binding energy was selected for analyzing the interactions and the binding mode between the PRXs and TS with MGLTools 1.5.6 and Discovery Studio Visualizer v21 software.

TS Activity on *T. cruzi*

TS (Sigma, T8902), a human PRX3 inhibitor used in anti-cancer therapies, was tested for its ability to *T. cruzi* damage. Epimastigotes (2×10^6) were seeded in 96-well plates (200 μl per well) and incubated at 28°C in the presence or absence of several concentrations of TS (1–40 μM) for 24 and 48 h. Benznidazole (BZ, 25 μM) or vehicle (Dymethyl sulfoxide (DMSO) 0.5%) were included as positive and negative controls, respectively. Then, the parasite number in the culture was counted in a Neubauer hemocytometer and reported as a growth percentage. Each condition was evaluated in duplicate in three independent assays. Analysis by one-way ANOVA with Tukey's multiple comparison was done using GraphPad Prism version 5 for Windows. The mean lethal concentration (IC_{50}) of TS to eliminate 50% of the parasites present in the culture was calculated as previously described (Martínez et al., 2013).

Supernatants containing cell-derived trypomastigotes were collected from Vero cells infected with Qro strain by centrifugation at 3,000×g for 20 min and resuspended in complete DMEM medium (Invitrogen, USA). Parasites were counted by microscopic observation using a Neubauer hemocytometer and adjusted to 2×10^6/ml. Parasites were seeded

(100 µl per well) in duplicates in a 96-well microplate, in presence or absence of several concentrations of TS and BZ as above, and incubated at 37°C, with 5% of CO_2 for 24 h as reported previously for other compounds (Adessi et al., 2022). Parasite number was counted as described above. Each condition was evaluated in duplicate in two independent assays. Blood trypomastigotes were obtained as described in Section 2.1. Parasites were counted and blood was diluted with DMEM medium to reach $2x10^6$ trypomastigotes/ml as described previously (Sánchez Alberti et al., 2022). These parasites were incubated with TS, like cell-derived trypomastigotes. Parasite number was counted as described above and reported as the percent of parasites. Each condition was evaluated in duplicate in three independent experiments. Statistical analysis was done as reported for epimastigotes.

Cell Cytotoxicity Assay on Vero Cells

Vero cells were maintained in DMEM medium supplemented with 10% FBS and reseeding 1/6 of the total culture content every third day. Cytotoxicity produced by TS was evaluated using 3-[4,5-dimethylthiazol-2-yl]-2,5 diphenyl tetrazolium bromide (MTT) assay. Briefly, Vero cells were seeded in a 96-well plate (5,000 per well) and allowed to adhere for 12 h. Then, the medium was removed, and 200 µl of DMEM was added in the absence or presence of TS at concentrations of 2.5 to 40 µM for further 24 h. Next, the medium was removed, and three washes with PBS were performed. Then, 200 µl of DMEM was added in the presence of MTT at 0.8 mg/ml (Sigma, USA) and incubated for 4 h at 37°C. The medium was removed, and the formazan salt was solubilized using 120 µl of DMSO. Absorbance was recorded in a microplate reader with a wavelength of 595 nm and a filter of 655 nm as reference. Three independent assays with duplicates of each condition were performed. Data were plotted and analyzed by one-way ANOVA using GraphPad Prism software.

Synergy Effect Between TS and BZ

To evaluate the synergistic effect of TS and BZ, first, we calculated the BZ IC_{50} on cell-derived trypomastigotes; we incubated the parasites with several concentrations of BZ (0.39–50 µM) for 24 h. The IC_{50} was calculated as 0.96 ± 0.04 (**Supplementary Figure 3**). Then, we used the BZ IC_{50} in synergy assays with TS. Cell-derived trypomastigotes (2×10^5) were seeded in 96-well plates (100 µl per well) and incubated at 37°C with 5% of CO_2 in the presence or absence of several concentrations of TS (1.25–10 µM) and BZ at 1.0 µM for 24 h. Parasites in the culture were counted in a Neubauer hemocytometer and reported as parasite percent. Three independent assays with duplicates of each condition were performed. Using GraphPad Prism software, data were plotted and analyzed by non-linear regression with Kolmogorov–Smirnov posttest.

RESULTS

QroMPX and NinoaMPX Sequences Analysis

The QroMPX and NinoaMPX have the same nucleotide sequences and do not show differences in their protein sequences (data not shown). Both TcMPX have a predicted size of 226 aa, a molecular weight of 25.5 kDa, an isoelectric point of 7.65, and a net electric charge of 2. A NJ analysis was performed to establish the phylogeny of both proteins. The topology of the obtained tree shows that both sequenced proteins belong to the trypanosomatids clade. Both protein sequences are very similar to the other from *T. cruzi* because tree topology shows a comb structure, characteristic of sequences that are highly similar to each other (**Figure 1A**).

Multiple Alignments and Functional Motifs Identification

Because of the high identity between QroMPX and NinoaMPX, we decided to work only with the QroMPX as a representative molecule. Multiple alignments were performed with other MPX (including the best-known human PRX3) to establish the presence of functional motifs in the sequence. This analysis showed a percentage of 48%–63% of similarity between QroMPX and the other proteins. In addition, the peroxidatic cysteine (Cp81) and resolving cysteine (C_R204) from the catalytic site are almost the same in all PRX. However, the second catalytic site in QroMPX has two amino acid changes (IPC instead of VCP). This is one of the notable differences between QroMPX and the myochondrial tryparedoxin TXNII from *T. cruzi* that does preserve the VCP sequence at the C-terminus. Adjacent to the C_R (C204) are present two amino acids (N205 y P211) and GGLG and YF motifs, involved in events of hyper oxidation on several PRXs (**Figure 1B**).

QroMPX Homology Modeling

The models generated by homology in the two platforms used were very similar (**Supplementary Figure 1A**). Furthermore, a similarity was observed between the amino acid sequence Y67 to S89 of QroMPX with a transmembrane motif described in *B. xylophilus*. Because of this, an analysis was carried out to establish the probability that QroMPX is a transmembrane protein, and the probability is 0.014. Therefore, there is no enough evidence to say that QroMPX can be a transmembranal protein under this analysis. The validation of the model using the Ramachandran plot showed that 90.2% of the amino acids are in the favorable region, indicating good reliability of the structure. The ERRAT plot showed a quality factor of 95.7%, indicating a good model quality. Thus, the model was representative with seven parallel and antiparallel β-sheets, and five α-helices of different lengths (**Figure 2A**). The resulting modeling in all the servers suggests that the template for our target protein (QroMPX) was the human PRX3. The structural similarity between both proteins is highlighted when they are overlapped (**Figure 2B**). The molecular modeling showed that QroMPX monomers could interact forming an interface type B to generate homodimers (**Supplementary Figure 2A**). They could be formed by the interaction of the β7 sheets from each subunit (**Supplementary Figure 2B**). By assembling five dimers, the formation of oligomers (decamers) was also modeled (**Supplementary Figure 2C**), and the electric charges in the oligomer show that the negative charges are preferably

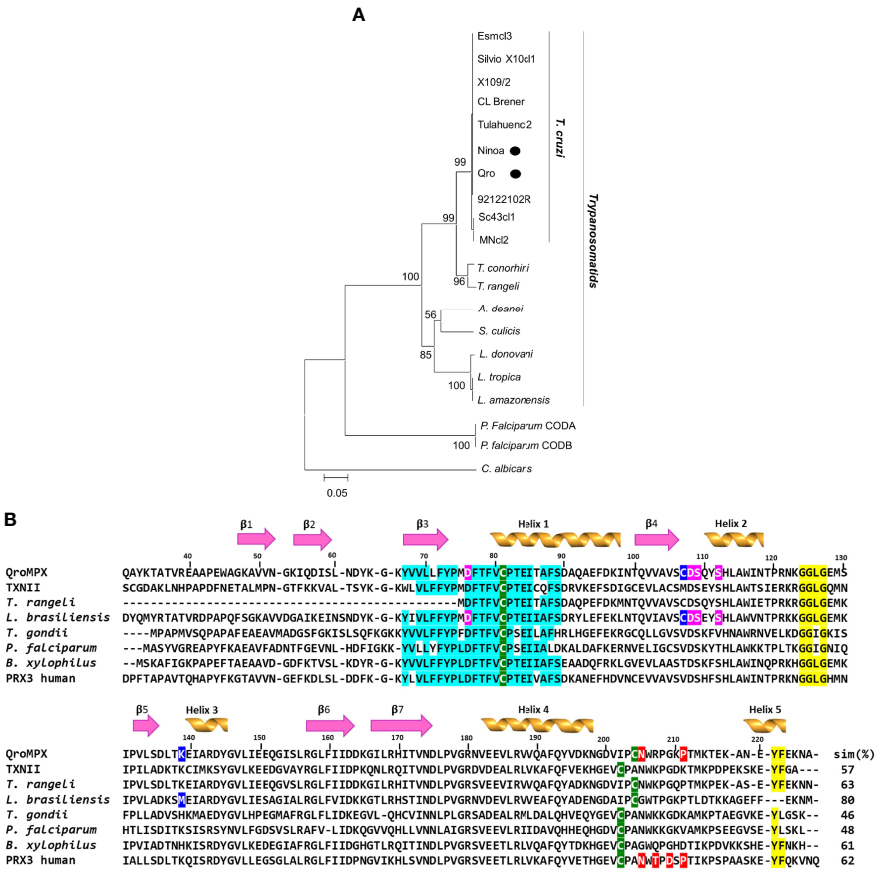

FIGURE 1 | Phylogeny of QroMPX and NinoaMPX and alignment with other mitochondrial PRXs. **(A)** The phylogeny was inferred using the Neighbor-Joining method. The percentage of replicate trees in which the associated taxa clustered together in the bootstrap test (10,000 replicates) are shown next to the nodes. The evolutionary distances were computed using the p-distance method and are in the units of the number of amino acid differences per site (scale bar). The analysis involved 20–amino acid sequences. All positions with less than 95% coverage were eliminated. The sequences of TcMPX from Mexican strains Qro and Ninoa (●) were grouped in the clade of trypanosomatids, close to other T. cruzi strains. **(B)** The sequences were aligned as indicated in materials and methods. Beta sheets (1–7) and a-helix are indicated on the corresponding sequence. The numbering corresponds to the position of the amino acids in the sequence of QroMPX. The cysteines of the catalytic site are indicated in green background. The motifs involved in susceptibility (yellow background) and resistance (red background) to hyperoxidation are also indicated. The transmembrane sequence identified in *B. xylophilus* (ABW81468.1) and the identical amino acids in the other sequences are indicated in cyan. The amino acids that interact with divalent cations (pink background) and those that stabilize the binding (blue background) identified in *L. brasiliensis* (XP_001562236.1) are also indicated in QroMPX. The first 30 amino acids of the QroMPX and *L. brasiliensis* sequences were cut to facilitate alignment. The other sequences used were from *T. cruzi* (TXNII, PDB 4LLR), *T. rangeli* (ESL05855.1), *T. gondii* (AAG25678.2), *P. falciparum* (BAA97121.1), and human PRX3 (PDB 5JCG). At the end of each sequence, the percentage of similarity (sim%) with QroMPX is indicated.

distributed inside the structure (**Supplementary Figure 2D**) as reported in other PRXs.

The C_P (C81) from a QroMPX monomer could be associated with the C_R (C204) from the adjacent monomer. In this conformational structure, C_P is surrounded by the catalytic triad formed by the amino acid residues P74, T78, and R157, close to the motifs GGLG and YF, whereas C_R is close to the amino acid residues N205 and P211 (**Figure 2C**). The location of the amino acid around the catalytic site is very similar to the human PRX3 (**Figure 2D**).

Similarity Between QroMPX and PRX3

Because of the observed similarity between human PRX3 and QroMPX, it was decided to test whether a commercial anti-PRX antibody that recognizes the former could also recognize the *T. cruzi* protein because the amino acid sequence recognized by the commercial antibody is very similar in both proteins (**Figure 3A**). The commercial antibody recognized in a *T. cruzi* total protein extract a protein with molecular weight close to that predicted from TcMPX (**Figure 3B**). Interestingly, when modeling the recognition site in the QroMPX dimer, it was observed that a region of the sequence is exposed on the surface of the molecules, which could facilitate the recognition of these structures by commercial antibodies (**Figure 3C**).

TS-QroMPX Docking

Because QroMPX and human PRX3 are structurally similar, there is a possibility that QroMPX was susceptible to PRX3

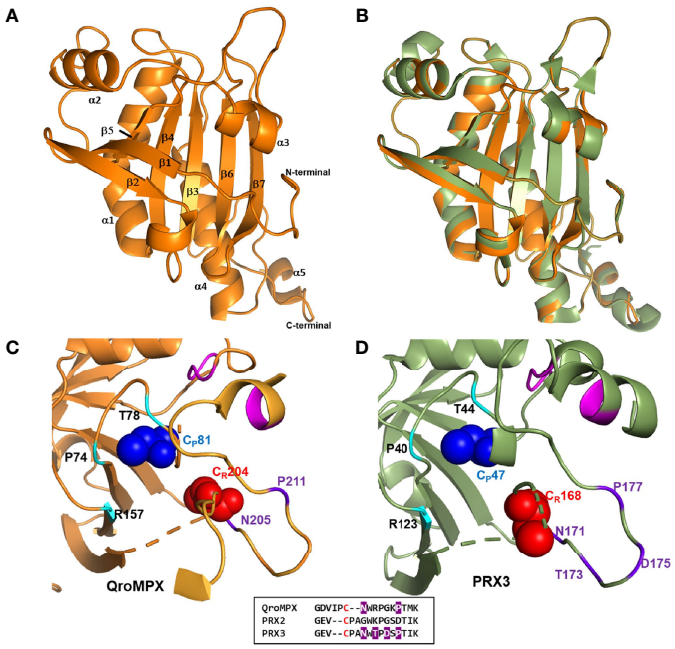

FIGURE 2 | QroMPX tertiary structure model. Modeling was performed as indicated in Materials and Methods. **A)** Monomer of the protein. Alpha-helices and beta sheets are indicated with the corresponding numbering. **B)** Overlap of QroMPX (orange) and human PRX3 (PDB 5JCG, green). **C)** The amino acids surrounding the peroxidatic (CP) and resolutive (CR) cysteine are shown for QroMPX. The GGLG and YF motifs are indicated in pink. The catalytic triad (PTR) is indicated in cyan. The amino acids that could participate in the resistance to hyper oxidation are shown in purple. The comparison of these amino acids in the sequences of QroMPX (QKE461.1), human PRX2 (ABB02182.1), and human PRX3 (PDB 5JCG) are shown in the lower box (in red resolutive cysteines, in purple amino acids involved in resistance to hiperoxidation). **D)** The position of the amino acids around the catalytic site in human PRX3 are shown with the same colors as in C.

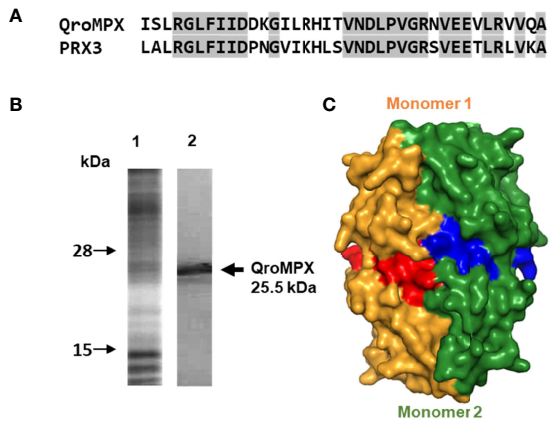

FIGURE 3 | Recognition of QroMPX by anti-human PRX3 antibody. **(A)** Shared sequence between QroMPX and PRX3 recognized by a commercial antibody. Identical amino acids are shaded. **(B)** Western blot was performed as indicated in materials and methods. The total parasite protein transferred (lane 1, Coomassie Blue stain) and the recognition of QroMPX by the commercial anti-PRX antibody (lane 2). **(C)** Model showing the regions on the surface of each QroMPX monomer (red and blue) that can be recognized by the antibody.

inhibitors such as the antibiotic TS. To explore this hypothesis, we performed an in silico molecular docking study. Our computational model considered a stable conformation of minimum energy for the protein QroMPX obtained by homology and for PRX3 obtained from the PDB (5JCG). To eliminate bias from the rigid nature of the receptor in our model, we used one monomer of each protein for ligand-receptor interaction analysis, because the ligand (TS) would be physically hindered by its bulk. Therefore, our results showed that TS has an affinity for the catalytic site, particularly, the resolutive-cysteine (C_R) in PRX3 (**Figure 4A**). Something similar was observed in the TS-QroMPX interaction model in which, in addition to the resolutive cysteine, the amino acids V38, H170, T172, N174, N181, R187, I202, CR204, and M213 are involved, with a $\Delta G = 7.0$ kCal/mol (**Figure 4B**). These results suggest that TS has a high probability of binding to cysteines in the catalytic domain of QroMPX and interfering with their biological activity.

TS Activity on *T. cruzi*

To establish whether TS could reduce the growth of *T. cruzi* as it does with some cancer cells, epimastigotes were incubated in the presence of this compound for 24 and 48 h. It was observed that TS reduced the number of parasites only at 48 h of incubation at concentrations of 20 and 40 μM (**Figure 5A**). The IC_{50} value was established at 40 ± 7.5 μM.

It was observed that TS has a high trypanocidal effect on the infective state of *T. cruzi* because, at 24 h, more than 50% of the cell-derived trypomastigotes had been eliminated with less than 5 μM of the compound (**Figure 5B**). The IC_{50} value was

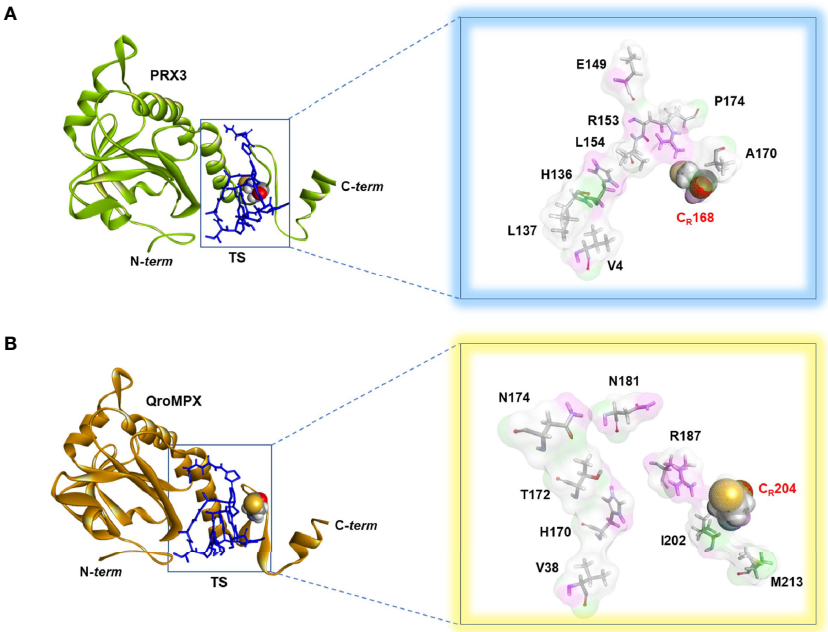

FIGURE 4 | TS-PRX3 and TS-QroMPX Docking. **(A)** Binding mode between TS (blue sticks) and human PRX3 (green). The amino acids (sticks format) and cysteine resolutive (ball format) involved in the interaction are shown in the box. **(B)** Binding mode between TS (blue sticks) and QroMPX (orange). The amino acids (sticks format) and cysteine resolutive (ball format) involved in the interaction are shown in the box.

calculated at 4.5 ± 0.7 μM. On the other hand, blood trypomastigotes were also sensitive to the effect of TS because, with 20 μM of TS, more than 65% of the parasites were eliminated from the culture (**Figure 5C**). The IC_{50} value was calculated at 11 ± 2.6 μM. No morphological damage was observed at optical microscopy. Preliminary experiments show no effect on intracellular amastigotes at 24 h of incubation with several TS concentrations.

Cytotoxicity Effect of Ts on Vero Cells

A significant decrease in the metabolic activity of Vero cells was observed in the presence of TS, but this was not greater than 25%, even at the highest TS concentration used (40 μM). The IC_{50} for Vero cells is greater than 40 μM, but it could not be established, so the selectivity index could not be calculated. The cytotoxicity of TS on Vero cells was moderate since between 62% and 72% of the cells maintained their metabolic activity (**Figure 5D**).

Synergic Effect Between TS and BZ

Because of the trypanocidal effect of TS on *T. cruzi* trypomastigotes, we evaluate a possible synergic effect with BZ. Using the combination of 1.25 μM TS and 1.0 μM BZ, a 46.66% presence of parasites was observed. By contrast, 79.14% of parasites were observed with TS alone at the same concentration. Similar results were observed with 2.5 μM TS and 1.0 μM BZ because 39.38% of parasites were found versus 58.57% with TS alone. There were no significant differences comparing 5 and 10 μM TS alone or with BZ (**Figure 6**).

DISCUSSION

There are no effective vaccines or drugs against T. cruzi, and the available drugs (NF and BZ) have low efficacy to treat the chronic phase of this disease and cause several side effects (Lascano et al., 2020). With the purpose to find new therapeutic targets, metabolic and defense pathways in *T. cruzi* have been studied in recent years. The detoxification of ROS is one of the main mechanisms implicated in the survival of the parasite, and for this reason, antioxidant enzymes have been considered as good therapeutic targets (González-Chávez et al., 2015).

The TcMPX have received particular attention due to their role as partner of several important proteins for cellular metabolism, as well as a virulence factor by protecting *T. cruzi* against NF effect, macrophage-derived peroxynitrite, and avoiding redox imbalance by ROS during mitochondrial energy generation (Piacenza et al., 2008; Piacenza et al., 2009; Peloso Ede et al., 2011; Piacenza et al., 2013; Peloso et al., 2016; Specker et al., 2022). In this study, the TcMPX from Querétaro and Ninoa Mexican *T. cruzi* strains were sequenced and analyzed *in silico*. The phylogenetic analysis showed that they are highly conserved proteins among *T. cruzi* strains, which suggests that variations in the sequence could affect their function and compromise the viability of *T. cruzi*. In addition, TcMPX is a single copy gene (Yeo et al., 2011). These reasons make it an attractive therapeutic target. However, to date, no inhibitor has been reported for this protein.

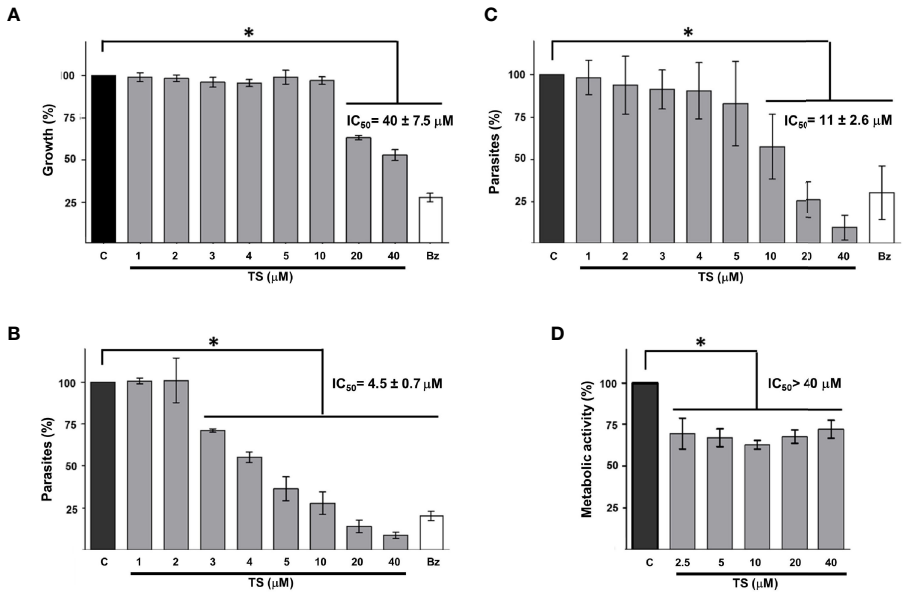

FIGURE 5 | Tripanocidal effect of TS. Epimastigotes **(A)**, cell-derived trypomastigotes **(B)**, blood trypomastigotes **(C)**, and Vero cells cytotoxicity **(D)** were incubated in the presence or absence of TS at the indicated micromolar concentrations. Parasite number was established by counting at 48 h **(A)** or 24 h **(B, C)** of incubation. Metabolic activity was measured using MTT assay at 24 h **(D)**. The results are presented as media ± standard deviation. Bz (25 µM) was used as a positive control. Media without TS **(C)** was used as control. Statistically significant differences are indicated with an asterisk ($p < 0.05$).

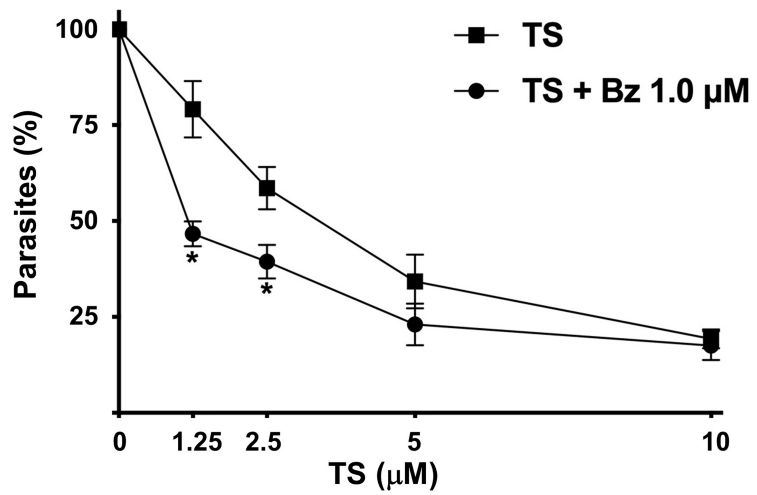

FIGURE 6 | Synergic effect of TS and Bz. Cell-derived trypomastigotes were incubated in the presence of different concentrations of TS alone or in combination with 1.0 µM Bz. Parasite number was established by counting in a Neubauer chamber after 24 h of drugs incubation. The results are presented as media ± standard deviation. Statistically significant differences are indicated with an asterisk ($p < 0.001$).

When comparing the sequence from QroMPX with other PRX previously characterized, we find that it shares 57% similarity with mitochondrial peroxidase (TXNII) reported in *T. cruzi* with which it interacts in oxidative stress conditions (Dias et al., 2018). Although both QroMPX and TXNII are mitochondrial, their similarity percentage is lower than that between QroMPX and human PRX2 and PRX3. This explains why homology modeling pointed to human PRX3 as temperate.

In addition, it was observed that the similarity is higher with MPX from other trypanosomatids (*L. brasiliensis* or *T. rangeli*) and human PRX3. This similarity of more than 60% in the sequence and highly similar spatial disposition of the QroMPX

3D model with PRX3 could suggest a similar function for both proteins, like an increase in its expression during heat stress events as has been shown for human PRX3 (Tchouagué et al., 2019). Although specific analysis showed that Qro MPX is unlikely to be a transmembrane protein, the presence of a sequence that has been proposed as a transmembranal domain in other PRXs opens the possibility that this protein may be secreted by *T. cruzi* or actively transported to the extracellular environment, probably to counteract ROS produced by the host, as proposed for other PRXs of trypanosomatids (Cuervo et al., 2009; Gadelha et al., 2013). It has been proposed that the PRX from *B. xylophylus* could use this motif to be transported across the intracellular membranes by ABC transporters (Li et al., 2011). This possibility cannot yet be ruled out for QroMPX and should be explored in the future. The possibility that this protein can be transported across the mitochondrial membrane or interact with it during cellular events has not been described and still needs to be explored as reported for other PRXs (Sasagawa et al., 2001; Choi et al., 2005). However, for the moment, we propose that it could be in soluble form as other mitochondrial and chloroplast PRXs (Flohé and Harris, 2007).

In the QroMPX sequence, the presence of GGLG and YF motifs was observed, which have been associated with the susceptibility of some PRXs to be hyper oxidated, leading to their inactivation (Cox et al., 2009). The QroMPX reported in this study is the first to be reported in *T. cruzi* with the presence of these structural motifs.

In addition, the molecular modeling showed that QroMPX monomers could interact by its β7-sheets, forming an interface type B to generate homodimers, as it was exemplified for other 2-cys PRXs (Poole and Nelson, 2016). In these structures, the C_P (C81) from a monomer could be associated with the C_R (C204) from the adjacent monomer. In this conformational structure, the arrangement of the GGLG and YF motifs and the catalytic triad (P74, T78, and R157) around the catalytic site are very similar to the human PRX3. This would facilitate the hyper oxidation of the molecule, but the presence and position of the amino acids N205 and P211 close to C_R (C204) indicate that QroMPX could be partially resistant to this phenomenon because the resistance to over-oxidation events in PRX3 is given by the presence of four amino acids (NTDP) in a similar position close to the C_R (Cox et al., 2009). Homology modeling also suggests that dimers can assemble into oligomers.

On other hand, several PRXs from protozoa have been proposed as therapeutic targets using molecules that inhibit it, which leads to a reduction in the resistance to oxidative stress (Haraldsen et al., 2009; König et al., 2011). Because of the similarity between QroMPX and PRX3, as well as the arrangement of the active site cysteines and the amino acids that surround them, it is very probable that QroMPX will be susceptible to the same inhibitors as PRX3. This feature can be used to reposition molecules that are currently therapeutic in humans. Several iron chelator molecules such as triapine, auranofin, and cisplatin reduce the presence of human PRX3 and have a pharmacological use in the treatment of some types of cancer (Myers, 2016). It would be interesting to test whether these molecules affect the *T. cruzi* proliferation or viability. Another molecule is TS, an excellent inhibitor of PRX3 that interacts with the active site cysteines, and this molecule also induces an oxidative stress condition in several types of cancer cells and is used as a treatment to reduce cell growth (Nelson et al., 2021). TS and some derivatives have shown good activity against protozoa as *Babesia* and *Plasmodium* sp. but have not been tested against other protozoa such as *T. cruzi* (Aminake et al., 2011; Aboulaila et al., 2012).

Docking analysis suggested that TS could bind to the resolutive-cysteine in the catalytic site, but we do not rule out the possibility that both cysteines are involved because the functional unit of PRX is dimeric in a biological environment (Poole and Nelson, 2016). Likewise, because of the similarity found in the amino acid sequence (>55%) between QroMPX and TXNII, it is highly probable that TS also interacts with this protein, and the inhibition of both PRXs could be related to a synergistic effect.

When we incubated epimastigotes of *T. cruzi* for 48 h in the presence of TS, a reduction in the multiplication of the parasite in the culture was observed, without obvious morphological changes in the remaining parasites. In addition, cell-derived trypomastigotes and blood trypomastigotes (both infective) were susceptible to the trypanocidal effect of TS, but in a shorter time and with a lower drug concentration. At 24 h of incubation with different concentration of TS, no significant differences with respect to control groups were observed in intracellular amastigotes. Longer incubation time periods and combination with other drugs should be investigated in future works.

Previously, it has been shown that disrupting the electron transport chain in *T. cruzi* epimastigotes inhibits growth (Aldunate et al., 1986). The interaction between TS and QroMPX could interrupt the electron transport chain involved in the mitochondrial antioxidant network, leading to growth inhibition. On the other hand, it was very important to observe that *T. cruzi* trypomastigotes are more susceptible to the trypanocidal effect of TS because they are the ones that infect mammalian hosts, including humans. It has previously been shown that trypomastigotes from several strains of *T. cruzi* have two to six times more TcMPX than epimastigotes, so it has been proposed that it is one of the important enzymes for maintaining redox balance during energy generation in the infective stage (Piacenza et al., 2009; Gadelha et al., 2013). In addition, it has been reported that mitochondrial activity is greater in trypomastigotes than in epimastigotes, with the consequent production of H_2O_2 (Gonçalves et al., 2011). Because of this abundance of the protein and its biological role, it would be expected that when it is inhibited by TS, the effects would be faster and stronger on trypomastigotes than epimastrigotes, which is consistent with the IC_{50} differences observed.

TS IC_{50} values for cell-derived trypomastigotes (4.5 μM) and blood trypomastigotes (11 μM) are lower than those concentration used for healthy human cells. We observed that the IC_{50} of TS on Vero cells is greater than 40 μM, which is higher than the solubility limit of the compound. Similar results have been reported for human epidermal melanocytes at 24 h (Qiao et al., 2012).

TS can be used in combination with the classical treatment against Chagas disease. We compare the synergic effect of TS and BZ in trypomastigotes to reduce the concentration of both compounds, and we observed a significant reduction in the parasite number with the lowest TS-BZ combination used. Intriguingly, at high doses, we do not find synergic effect; further work should be done to address this phenomenon.

Therefore, the results obtained are promising, and they could be improved by making modifications to TS to make it more specific to PRX or by searching for similar molecules with higher selectivity.

Furthermore, the possibility of using TS in an animal model of infection with *T. cruzi*, as well as the mechanism of action, should be explored. In addition, the repositioning of this molecule, which is currently used in the human treatment of some oncological diseases, can be an alternative for a better Chagas disease treatment.

CONCLUSIONS

The results reported in the present work suggest that TcMPX from *T. cruzi* has a high similarity with human PRX3, so this characteristic could be exploited to evaluate its susceptibility to inhibitors and their derivatives that are currently used for therapeutic purposes, such as TS that was found that reduced the growth of the parasite by a mechanism that could involve the change in the mitochondrial metabolism of *T. cruzi*.

DATA AVAILABILITY STATEMENT

The datasets presented in this study can be found in online repositories. The names of the repository/repositories and accession number(s) can be found in the article/**Supplementary Material**.

ETHICS STATEMENT

The animal study was reviewed and approved by the Comite para el Cuidado y Uso de Animals de Laboratorio following the recommendation of the Ethical Code of the Instituto de Investigaciones Biomédicas, UNAM (https://www.biomedicas.unam.mx/wp-content/pdf/intranet/reglamentos/codigo-etico-iibo.pdf?x88126).

AUTHOR CONTRIBUTIONS

LR-S, IM, and BE designed the experiments. LR-S and RA-O sequenced the proteins. LR-S, PD-G, and IM performed homology modeling and bioinformatic analysis. LR-S and RC-H performed the molecular docking. LR-S and IM carried out the trypanocidal activity assays. LR-S, IM, and BE wrote the manuscript. All authors contributed to the article and approved the submitted version.

FUNDING

BE acknowledges the financial support of DGAPA-PAPIIT, UNAM-IN206620, NUATEI-IIB 2019-2021, and CONACYT (CB) 160671.

ACKNOWLEDGMENT

Lucio Rivera-Santiago is a doctoral student from the Programa de Doctorado en Ciencias Biomédicas, Universidad Nacional Autónoma de México (UNAM) and has received CONACyT fellowship 266855 and the support of the Carlos Espinosa Fuentes Trust. Authors are grateful to Patricia de la Torre from Instituto de Investigaciones Biomédicas for the support on the sequencing and to Beatriz Ruiz-Villafan for providing the TS.

SUPPLEMENTARY MATERIAL

The Supplementary Material for this article can be found online at: https://www.frontiersin.org/articles/10.3389/fcimb.2022.907043/full#supplementary-material

REFERENCES

Aboulaila, M., Munkhjargal, T., Sivakumar, T., Ueno, A., Nakano, Y., Yokoyama, M., et al. (2012). Apicoplast-Targeting Antibacterials Inhibit the Growth of *Babesia* Parasites. *Antimicrob. Agents Chemother.* 56 (6), 3196–3206. doi: 10.1128/aac.05488-11

Adessi, T. G., Ana, Y., Stempin, C. C., García, M. C., Bisogno, F. R., Nicotra, V. E., et al. (2022). Psilostachyins as Trypanocidal Compounds: Bioguided Fractionation of *Ambrosia Tenuifolia* Chemically Modified Extract. *Phytochemistry* 194, 113014. doi: 10.1016/j.phytochem.2021.113014

Aldunate, J., Ferreira, J., Letelier, M. E., Repetto, Y., and Morello, A. (1986). T-Butyl-4-Hydroxyanisole, a Novel Respiratory Chain Inhibitor. Effects on *Trypanosoma Cruzi* Epimastigotes. *FEBS Lett.* 195 (1-2), 295–297. doi: 10.1016/0014-5793(86)80180-6

Aminake, M. N., Schoof, S., Sologub, L., Leubner, M., Kirschner, M., Arndt, H. D., et al. (2011). Thiostrepton and Derivatives Exhibit Antimalarial and Gametocytocidal Activity by Dually Targeting Parasite Proteasome and Apicoplast. *Antimicrob. Agents Chemother.* 55 (4), 1338–1348. doi: 10.1128/aac.01096-10

Choi, M. H., Sajed, D., Poole, L., Hirata, K., Herdman, S., Torian, B. E., et al. (2005). An Unusual Surface Peroxiredoxin Protects Invasive *Entamoeba Histolytica* From Oxidant Attack. *Mol. Biochem. Parasitol.* 143 (1), 80–89. doi: 10.1016/j.molbiopara.2005.04.014

Cox, A. G., Pearson, A. G., Pullar, J. M., Jönsson, T. J., Lowther, W. T., Winterbourn, C. C., et al. (2009). Mitochondrial Peroxiredoxin 3 is More Resilient to Hyperoxidation Than Cytoplasmic Peroxiredoxins. *Biochem. J.* 421 (1), 51–58. doi: 10.1042/bj20090242

Cuervo, P., De Jesus, J. B., Saboia-Vahia, L., Mendonça-Lima, L., Domont, G. B., and Cupolillo, E. (2009). Proteomic Characterization of the Released/Secreted Proteins of *Leishmania (Viannia) Braziliensis* Promastigotes. *J. Proteomics* 73 (1), 79–92. doi: 10.1016/j.jprot.2009.08.006

Dias, L., Peloso, E. F., Leme, A. F. P., Carnielli, C. M., Pereira, C. N., Werneck, C. C., et al. (2018). *Trypanosoma Cruzi* Tryparedoxin II Interacts With Different

Peroxiredoxins Under Physiological and Oxidative Stress Conditions. *Exp. Parasitol.* 184, 1–10. doi: 10.1016/j.exppara.2017.10.015

Flohé, L., and Harris, J. R. (2007). Introduction. History of the Peroxiredoxins and Topical Perspectives. *Subcell. Biochem.* 44, 1–25. doi: 10.1007/978-1-4020-6051-9_1

Gadelha, F. R., Gonçalves, C. C., Mattos, E. C., Alves, M. J., Piñeyro, M. D., Robello, C., et al. (2013). Release of the Cytosolic Tryparedoxin Peroxidase Into the Incubation Medium and a Different Profile of Cytosolic and Mitochondrial Peroxiredoxin Expression in H2O2-Treated *Trypanosoma Cruzi* Tissue Culture-Derived Trypomastigotes. *Exp. Parasitol.* 133 (3), 287–293. doi: 10.1016/j.exppara.2012.12.007

Gonçalves, R. L., Barreto, R. F., Polycarpo, C. R., Gadelha, F. R., Castro, S. L., and Oliveira, M. F. (2011). A Comparative Assessment of Mitochondrial Function in Epimastigotes and Bloodstream Trypomastigotes of *Trypanosoma Cruzi*. *J. Bioenerg. Biomembr.* 43 (6), 651–661. doi: 10.1007/s10863-011-9398-8

González-Chávez, Z., Olin-Sandoval, V., Rodíguez-Zavala, J. S., Moreno-Sánchez, R., and Saavedra, E. (2015). Metabolic Control Analysis of the *Trypanosoma Cruzi* Peroxide Detoxification Pathway Identifies Tryparedoxin as a Suitable Drug Target. *Biochim. Biophys. Acta* 1850 (2), 263–273. doi: 10.1016/j.bbagen.2014.10.029

Haraldsen, J. D., Liu, G., Botting, C. H., Walton, J. G., Storm, J., Phalen, T. J., et al. (2009). Identification of Conoidin a as a Covalent Inhibitor of Peroxiredoxin II. *Org. Biomol. Chem.* 7, 3040–3048. doi: 10.1039/b901735f

Janson, G., Zhang, C., Prado, M. G., and Paiardini, A. (2017). PyMod 2.0: Improvements in Protein Sequence-Structure Analysis and Homology Modeling Within PyMOL. *Bioinformatics* 33 (3), 444–446. doi: 10.1093/bioinformatics/btw638

König, J., Wyllie, S., Wells, G., Stevens, M. F., Wyatt, P. G., and Fairlamb, A. H. (2011). Antitumor Quinol PMX464 is a Cytocidal Anti-Trypanosomal Inhibitor Targeting Trypanothione Metabolism. *J. Biol. Chem.* 286 (10), 8523–8533. doi: 10.1074/jbc.M110.214833

Lascano, F., García Bournissen, F., and Altcheh, J. (2020). Review of Pharmacological Options for the Treatment of Chagas Disease. *Br. J. Clin. Pharmacol.* 88 (2), 383–402. doi: 10.1111/bcp.14700

Li, Z., Liu, X., Chu, Y., Wang, Y., Zhang, Q., and Zhou, X. (2011). Cloning and Characterization of a 2-Cys Peroxiredoxin in the Pine Wood Nematode, Bursaphelenchus Xylophilus, a Putative Genetic Factor Facilitating the Infestation. *Int. J. Biol. Sci.* 7 (6), 823–836. doi: 10.7150/ijbs.7.823

López-Olmos, V., Pérez-Nasser, N., Piñero, D., Ortega, E., Hernandez, R., and Espinoza, B. (1998). Biological Characterization and Genetic Diversity of Mexican Isolates of *Trypanosoma Cruzi*. *Acta Trop.* 69 (3), 239–254. doi: 10.1016/s0001-706x(97)00131-9

Macedo, A. M., Martins, M. S., Chiari, E., and Pena, S. D. (1992). DNA Fingerprinting of *Trypanosoma Cruzi*: A New Tool for Characterization of Strains and Clones. *Mol. Biochem. Parasitol.* 55 (1-2), 147–153. doi: 10.1016/0166-6851(92)90135-7

Machado-Silva, A., Cerqueira, P. G., Grazielle-Silva, V., Gadelha, F.R., Peloso, E., Teixeira, S. M., et al. (2016). How *Trypanosoma Cruzi* Deals With Oxidative Stress: Antioxidant Defence and DNA Repair Pathways. *Mutat. Res. Rev. Mutat. Res.* 767, 8–22. doi: 10.1016/j.mrrev.2015.12.003

Martínez, I., Nogueda, B., Martínez-Hernández, F., and Espinoza, B. (2013). Microsatellite and Mini-Exon Analysis of Mexican Human DTU I *Trypanosoma Cruzi* Strains and Their Susceptibility to Nifurtimox and Benznidazole. *Vector. Borne. Zoonotic. Dis.* 13 (3), 181–187. doi: 10.1089/vbz.2012.1072

Myers, C. R. (2016). Enhanced Targeting of Mitochondrial Peroxide Defense by the Combined Use of Thiosemicarbazones and Inhibitors of Thioredoxin Reductase. *Free Radic. Biol. Med.* 91, 81–92. doi: 10.1016/j.freeradbiomed.2015.12.008

Nelson, K. J., Messier, T., Milczarek, S., Saaman, A., Beuschel, S., Gandhi, U., et al. (2021). Unique Cellular and Biochemical Features of Human Mitochondrial Peroxiredoxin 3 Establish the Molecular Basis for its Specific Reaction With Thiostrepton. *Antioxidants. (Basel).* 10 (2), 150. doi: 10.3390/antiox10020150

Nogueira, N. P., Saraiva, F. M., Sultano, P. E., Cunha, P. R., Laranja, G. A., Justo, G. A., et al. (2015). Proliferation and Differentiation of *Trypanosoma Cruzi* Inside Its Vector Have a New Trigger: Redox Status. *PloS One* 10 (2), e0116712. doi: 10.1371/journal.pone.0116712

Peloso, E. F., Dias, L., Queiroz, R. M., Leme, A. F., Pereira, C. N., Carnielli, C. M., et al. (2016). *Trypanosoma Cruzi* Mitochondrial Tryparedoxin Peroxidase is Located Throughout the Cell and its Pull Down Provides One Step Towards the Understanding of its Mechanism of Action. *Biochim. Biophys. Acta* 1864 (1), 1–10. doi: 10.1016/j.bbapap.2015.10.005

Peloso Ede, F., Vitor, S. C., Ribeiro, L. H., Piñeyro, M. D., Robello, C., and Gadelha, F. R. (2011). Role of *Trypanosoma Cruzi* Peroxiredoxins in Mitochondrial Bioenergetics. *J. Bioenerg. Biomembr.* 43 (4), 419–424. doi: 10.1007/s10863-011-9365-4

Perkins, A., Nelson, K. J., Parsonage, D., Poole, L. B., and Karplus, P. A. (2015). Peroxiredoxins: Guardians Against Oxidative Stress and Modulators of Peroxide Signaling. *Trends Biochem. Sci.* 40 (8), 435–445. doi: 10.1016/j.tibs.2015.05.001

Piacenza, L., Peluffo, G., Alvarez, M. N., Kelly, J. M., Wilkinson, S. R., and Radi, R. (2008). Peroxiredoxins Play a Major Role in Protecting *Trypanosoma Cruzi* Against Macrophage- and Endogenously-Derived Peroxynitrite. *Biochem. J.* 410 (2), 359–368. doi: 10.1042/bj20071138

Piacenza, L., Peluffo, G., Alvarez, M. N., Martínez, A., and Radi, R. (2013). *Trypanosoma Cruzi* Antioxidant Enzymes as Virulence Factors in Chagas Disease. *Antioxid. Redox Signal* 19 (7), 723–734. doi: 10.1089/ars.2012.4618

Piacenza, L., Zago, M. P., Peluffo, G., Alvarez, M. N., Basombrio, M. A., and Radi, R. (2009). Enzymes of the Antioxidant Network as Novel Determiners of *Trypanosoma Cruzi* Virulence. *Int. J. Parasitol.* 39 (13), 1455–1464. doi: 10.1016/j.ijpara.2009.05.010

Piñeyro, M. D., Parodi-Talice, A., Arcari, T., and Robello, C. (2008). Peroxiredoxins From *Trypanosoma Cruzi:* Virulence Factors and Drug Targets for Treatment of Chagas Disease? *Gene* 408 (1-2), 45–50. doi: 10.1016/j.gene.2007.10.014

Poole, L. B., and Nelson, K. J. (2016). Distribution and Features of the Six Classes of Peroxiredoxins. *Mol. Cells* 39 (1), 53–59. doi: 10.14348/molcells.2016.2330

Qiao, S., Lamore, S. D., Cabello, C. M., Lesson, J. L., Muñoz-Rodriguez, J. L., and Wondrak, G. T. (2012). Thiostrepton is an Inducer of Oxidative and Proteotoxic Stress That Impairs Viability of Human Melanoma Cells But Not Primary Melanocytes. *Biochem. Pharmacol.* 83 (9), 1229–1240. doi: 10.1016/j.bcp.2012.01.027

Rodríguez-Hernández, K. D., Martínez, I., Agredano-Moreno, L. T., Jiménez-García, L. F., Reyes-Chilpa, R., and Espinoza, B. (2019). Coumarins Isolated From *Calophyllum Brasiliense* Produce Ultrastructural Alterations and Affect *In Vitro* Infectivity of *Trypanosoma Cruzi*. *Phytomedicine* 61, 152827. doi: 10.1016/j.phymed.2019.152827

Sánchez Alberti, A., Beer, M. F., Cerny, N., Bivona, A. E., Fabian, L., Morales, C., et al. (2022). *In Vitro, in Vivo*, and *in Silico* Studies of Cumanin Diacetate as a Potential Drug Against *Trypanosoma Cruzi* Infection. *ACS Omega.* 7 (1), 968–978. doi: 10.1021/acsomega.1c05560

Sanner, M. F. (1999). Python: A Programming Language for Software Integration and Development. *J. Mol. Graph. Model.* 17 (1), 57–61.

Sasagawa, I., Matsuki, S., Suzuki, Y., Iuchi, Y., Tohya, K., Kimura, M., et al. (2001). Possible Involvement of the Membrane-Bound Form of Peroxiredoxin 4 in Acrosome Formation During Spermiogenesis of Rats. *Eur. J. Biochem.* 268 (10), 3053–3061. doi: 10.1046/j.1432-1327.2001.02200.x

Specker, G., Estrada, D., Radi, R., and Piacenza, L. (2022). *Trypanosoma Cruzi* Mitochondrial Peroxiredoxin Promotes Infectivity in Macrophages and Attenuates Nifurtimox Toxicity. *Front. Cell Infect. Microbiol.* 12. doi: 10.3389/fcimb.2022.749476

Tchouagué, M., Grondin, M., Glory, A., and Averill-Bates, D. (2019). Heat Shock Induces the Cellular Antioxidant Defenses Peroxiredoxin, Glutathione and Glucose 6-Phosphate Dehydrogenase Through Nrf2. *Chem. Biol. Interact.* 310, 108717. doi: 10.1016/j.cbi.2019.06.030

Trott, O., and Olson, A. J. (2010). AutoDock Vina: Improving the Speed and Accuracy of Docking With a New Scoring Function, Efficient Optimization, and Multithreading. *J. Comput. Chem.* 31 (2), 455–461. doi: 10.1002/jcc.21334

WHO (2021). *Chagas disease (also known as American trypanosomiasis)*. (Fact Sheet, World Health Organization, WHO). Consulted August 2, 2021.

Wilkinson, S. R., Temperton, N. J., Mondragon, A., and Kelly, J. M. (2000). Distinct Mitochondrial and Cytosolic Enzymes Mediate Trypanothione-Dependent Peroxide Metabolism in *Trypanosoma Cruzi*. *J. Biol. Chem.* 275 (11), 8220–8225. doi: 10.1074/jbc.275.11.8220

Yeo, M., Mauricio, I. L., Messenger, L. A., Lewis, M. D., Llewellyn, M. S., Acosta, N., et al. (2011). Multilocus Sequence Typing (MLST) for Lineage Assignment and High Resolution Diversity Studies in. *Trypanosoma. cruzi. PloS Negl. Trop. Dis.* 5 (6), e1049. doi: 10.1371/journal.pntd.0001049

Conflict of Interest: The authors declare that the research was conducted in the absence of any commercial or financial relationships that could be construed as a potential conflict of interest.

Publisher's Note: All claims expressed in this article are solely those of the authors and do not necessarily represent those of their affiliated organizations, or those of the publisher, the editors and the reviewers. Any product that may be evaluated in this article, or claim that may be made by its manufacturer, is not guaranteed or endorsed by the publisher.

frontiers | Frontiers in Cellular and Infection Microbiology

ORIGINAL RESEARCH
published: 07 July 2022
doi: 10.3389/fcimb.2022.890709

The Role of the Na^+/Ca^{2+} Exchanger in Aberrant Intracellular Ca^{2+} in Cardiomyocytes of Chagas-Infected Rodents

Jose R. Lopez[1], *Nancy Linares*[2], *Jose A. Adams*[3] *and Alfredo Mijares*[2]*

[1] Department of Research, Mount Sinai, Medical Center, Miami, FL, United States, [2] Centro de Biofísica y Bioquímica, Instituto Venezolano de Investigaciones Científicas, Caracas, Venezuela, [3] Division of Neonatology, Mount Sinai, Medical Center, Miami, FL, United States

OPEN ACCESS

Edited by:
Vilma G. Duschak,
Consejo Nacional de Investigaciones Científicas y Técnicas (CONICET), Argentina

Reviewed by:
Veronica Jimenez,
California State University, Fullerton, United States
Sergio Schenkman,
Federal University of São Paulo, Brazil

***Correspondence:**
Alfredo Mijares
mijaresa@gmail.com

Specialty section:
This article was submitted to Parasite and Host, a section of the journal Frontiers in Cellular and Infection Microbiology

Received: 06 March 2022
Accepted: 03 June 2022
Published: 07 July 2022

Citation:
Lopez JR, Linares N, Adams JA and Mijares A (2022) The Role of the Na^+/Ca^{2+} Exchanger in Aberrant Intracellular Ca^{2+} in Cardiomyocytes of Chagas-Infected Rodents. Front. Cell. Infect. Microbiol. 12:890709. doi: 10.3389/fcimb.2022.890709

Chagas disease is produced by the parasite *Trypanosoma cruzi (T. cruzi)*, which is the leading cause of death and morbidity in Latin America. We have shown that in patients with Chagas cardiomyopathy, there is a chronic elevation of diastolic Ca^{2+} concentration ($[Ca^{2+}]_d$), associated with deterioration to further address this issue, we explored the role Na^+/Ca^{2+} exchanger (NCX). Experiments were carried out in noninfected C57BL/6 mice and infected with blood-derived trypomastigotes of the *T. cruzi* Y strain. Anesthetized mice were sacrificed and the cardiomyocytes were enzymatically dissociated. Diastolic $[Ca^{2+}]$ ($[Ca^{2+}]_d$) was measured using Ca^{2+} selective microelectrodes in cardiomyocytes from control mice (CONT) and cardiomyocytes from *T. cruzi* infected mice in the early acute phase (EAP) at 20 dpi, in the acute phase (AP) at 40 dpi, and in the chronic phase (CP) at 120 dpi. $[Ca^{2+}]_d$ was 1.5-times higher in EAP, 2.6-times in AP, and 3.4-times in CP compared to CONT. Exploring the reverse mode activity of NCX, we replaced extracellular Na^+ in equivalent amounts with N-methyl-D-glucamine. Reduction of $[Na^+]_e$ to 65 mM caused an increase in $[Ca^{2+}]_d$ of 1.7 times in cardiomyocytes from CONT mice, 2 times in EAP infected mice, 2.4 times in AP infected mice and 2.8 in CP infected mice. The Na^+ free solution caused a further elevation of $[Ca^{2+}]_d$ of 2.5 times in cardiomyocytes from CONT, 2.8 times in EAP infected mice, 3.1 times in AP infected mice, and 3.3 times in CP infected mice. Extracellular Ca^{2+} withdrawal reduced $[Ca^{2+}]_d$ in both CONT and cardiomyocytes from Chagas-infected mice and prevented the increase in $[Ca^{2+}]_d$ induced by Na^+ depletion. Preincubation with 10μM KB-R7943 or in 1μM YM-244769 reduced $[Ca^{2+}]_d$ in cardiomyocytes from infected mice, but not control mice. Furthermore, both NCX blockers prevented the increase in $[Ca^{2+}]_d$ associated with exposure to a solution without Na^+. These results suggest that Ca^{2+} entry through the reverse NCX mode plays a significant role in the observed $[Ca^{2+}]_d$ dyshomeostasis in Chagas infected cardiomyocytes. Additionally, NCX inhibitors may be a viable therapeutic approach for treating patients with Chagas cardiomyopathy.

Keywords: chagas disease, Na/Ca exchanger, cardiomyopathy, *Trypanosoma cruzi* (T cruzi), calcium

INTRODUCTION

Chagas disease, caused by the protozoan *Trypanosoma cruzi* (*T. cruzi*), affects approximately eight million people in the poorest areas of Central and South America. The prevalent form of transmission of *T. cruzi* to humans is contact with contaminated feces/urine of the invertebrate vector during a blood meal. However, human infection through blood transfusion, organ transplantation and oral. (Bern et al., 2008) and oral transmission due to ingestion of contaminated fruit juices (Alarcon De Noya et al., 2010) have been reported. Chagas disease is characterized by a varied clinical scenario that evolves from an acute phase, often asymptomatic or oligosymptomatic, to a chronic phase that can manifest as indeterminate, cardiac, or digestive forms (Echavarria et al., 2021). Most infected people develop cardiac conditions characterized by ventricular arrhythmias, heart blocks, heart failure, thromboembolic phenomena, and sudden death (Rassi et al., 2010; Teixeira et al., 2011; Echavarria et al., 2021; http://www.who.int/mediacentre/factsheets/fs340/en/, 2021).

Calcium is a central player in the regulation of cardiac contractility, and its intracellular concentration is maintained through the interaction of Ca^{2+} transport mechanisms and diastolic leak mediated by the ryanodine receptor (Shannon et al., 2003; Bers and Ginsburg, 2007; Bers, 2014; Freichel et al., 2017; Smith and Eisner, 2019). In healthy cardiomyocytes, the diastolic Ca^{2+} concentration ($[Ca^{2+}]_d$) is in the range of 100-120 nM (Marban et al., 1980; Lopez et al., 2011; Mijares et al., 2014; Mijares et al., 2020). We have demonstrated dysregulation of $[Ca^{2+}]_d$ in cardiomyocytes isolated from Chagas patients, which is correlated with the patient's clinical condition (Lopez et al., 2011). Furthermore, this diastolic disturbance of $[Ca^{2+}]$ appears to be associated with alterations in the regulation of the intracellular messenger inositol 1,4,5-trisphosphate (Lopez et al., 2011; Mijares et al., 2020).

NCX is a bidirectional high-capacity transporter that represents the primary way of Ca^{2+} extrusion in excitable cells (Blaustein and Lederer, 1999; Aronsen et al., 2013). It can import 3 Na^+ into the cell in exchange for 1 Ca^{2+} (forward mode) or drive the efflux of 3 Na^+ in exchange for 1 Ca^{2+} (reverse mode) across the plasma membrane (Bers and Ginsburg, 2007). The direction of NCX (forward or reverse) depends on the internal and external concentration of both Na^+ and Ca^{2+} and the membrane potential (Bers, 2000). NCX works almost exclusively in the forward mode (Ca^{2+} extrusion) in normal cardiomyocytes, driven primarily by the elevated subsarcolemmal $[Ca^{2+}]$. Elevated diastolic $[Na^+]$ ($[Na^+]_d$) could change the direction of the fluxes to a more significant influx of Ca^{2+} and fewer Ca^{2+} effluxes, resulting in increased intracellular $[Ca^{2+}]$. However, the dynamic of NCX can be altered in pathophysiological situations such as heart failure, arrhythmia, ischemia-reperfusion injury, and hypertrophy (Bers and Despa, 2006). Recently, Santos-Miranda et al. (Santos-Miranda et al., 2021) reported a cellular arrhythmogenic profile in chronic Chagas cardiomyopathy, which was sensitive to Ni^{2+} and NCX blocker SEA0400, indicating the involvement of NCX.

In the present study, we evaluated the activity of NCX in cardiomyocytes from control and Chagas infected mice. We showed that NCX activity is enhanced in cardiomyocytes from *T. cruzi*-infected mice compared to control cardiomyocytes and that the reverse mode of NCX contributes to intracellular Ca^{2+} dyshomeostasis observed in cardiomyocytes from infected mice.

MATERIAL AND METHODS

Animals

Homozygous male C57BL/10 with a bodyweight of 25 ± 0.45 g. and 12 weeks of age were housed at constant temperature (24 C) and a 12 h light/12 h dark cycle, with free access to water and fed a commercial pelletized diet.

Trypanosoma cruzi Infection

Mice were randomly divided into two groups: **Group A** (Control) that were not inoculated with *T. cruzi* and **Group B** (infected mice) were infected intraperitoneally with $5x10^{-2}$ blood-form trypomastigotes of the Y strain of *T. cruzi* (O'Daly et al., 1984). The Y strain of *T. cruzi* was originally obtained from patients in Brazil and was kindly provided by Dr. Jose O'Daly, who has maintained the strain over the years through serial passages in homozygous C57B1/6 mice. Parasitemia was monitored by counting the number of parasites/5 μl of blood obtained from the tail vein of infected mice. A positive parasitemia was found in all inoculated animals on days 12-15 post-infection (dpi). Non-infected and infected anesthetized (ketamine/xylazine) mice were sacrificed by cervical dislocation at 20 (early acute phase), 40 (acute phase), and 120-dpi (chronic phase), and the cardiomyocytes were enzymatically dissociated.

Isolation of Cardiomyocytes and Inclusion Criteria

Control and infected mice were anesthetized (ketamine 100 mg/kg/xylazine 5 mg/Kg) and hearts were rapidly removed, attached to a cannula, and mounted on a Langendorff reverse coronary perfusion system for the enzymatic dissociation of ventricular cardiomyocytes (Liao and Jain, 2007). Only Ca^{2+} tolerant cardiomyocytes with rod-shaped, well-defined striation spacing and a resting sarcomere length of ≥1.75 μm (Wussling et al., 1987) were used and studied within 4-6 h after isolation. The isolation procedure was carried out at 37°C.

Ca^{2+} and Na^+ Selective Microelectrodes

Double-barreled Ca^{2+} and Na^+ selective microelectrodes were prepared as previously described (Eltit et al., 2013). Each ion-selective microelectrode was individually calibrated before and after the determination of $[Ca^{2+}]_d$ and the $[Na^+]_d$ as previously described (Mijares et al., 2014). Ca^{2+} selective microelectrodes with a Nernstian response between pCa3 and pCa7 (30.5 mV/pCa units at 37°C) and Na^+ selective microelectrodes with Nernstian responses between 100 and 10 mM $[Na^+]_e$, and an adequate response (40–45 mV) between 10 and 1 mM $[Na^+]_e$ were used experimentally (Lopez et al., 1983; Lopez et al., 2000; Eltit et al., 2013). The Ca^{2+}- and Na^+-microelectrode response was not affected by any of the drugs used in the present study.

Recording of Diastolic Calcium and Sodium Concentrations

Isolated cardiomyocytes from control mice and *T. cruzi* infected mice were impaled with double-barrel Ca^{2+} or Na^+ microelectrodes to measure $[Ca^{2+}]_d$ and $[Na^+]_d$, respectively, and potentials were recorded using a high impedance electrometer (WPI 773 electrometer, FL, USA) as previously described (Lopez et al., 2000; Lopez et al., 2017). The potential of the 3M KCl microelectrode barrel (Vm) was electronically subtracted from the potential recorded by the Ca^{2+} selective barrel (V_{Ca}) to produce a differential Ca^{2+} specific potential (V_{CaE}) that represents the cardiomyocyte $[Ca^{2+}]_d$. A similar approach was used to produce the specific Na^+ potential (V_{NaE}), which represents the cardiomyocyte $[Na^+]_d$. The potentials were acquired at a frequency of 1,000 Hz with the AxoGraph software (version 4.6; Axon Instruments, CA, USA) and stored in a computer for further analysis.

Individual cardiomyocyte measurements of $[Ca^{2+}]_d$ and $[Na^+]_d$ from control and infected mice were accepted when there was ***i)*** an abrupt drop to a steady level of Vm equal to or more negative than -80 mV in healthy cells and -70 mV in unhealthy cardiomyocytes; ***ii)*** a stable recording of Vm and V_{Ca} potentials or Vm and V_{Na} potentials for more than 60 seconds and an abrupt return to baseline at the exit of the microelectrode from the cell. Vm was used as a biological indicator of the integrity of cardiomyocyte sarcolemma in real-time; therefore, any cardiomyocytes with a recorded Vm <-70 mV were discarded. These criteria were not met in 18% of total impalements performed in cardiomyocytes from control mice and 41% in infected mouse cardiomyocytes.

Reverse Mode NCX Protocol

The effect of NCX (reverse mode) on $[Ca^{2+}]_d$ in cardiomyocytes from control and infected mice was determined by preincubating cardiomyocytes in a solution in which $[Na^+]e$ was partially or completely removed (see solutions below) and replaced by *N*-methyl-D-glucamine hydrochloride. Measurements of $[Ca^{2+}]_d$ were carried out before and after incubation in low Na^+ solutions.

Equilibrium Potentials

The equilibrium potentials for Ca^{2+} (E_{Ca}) and Na^+ (E_{Na}) were calculated using the Nernst equation (E_{ion}= RT/zF x ln $[ion]_i$/ $[ion]_e$) and $[Ca^{2+}]_d$ and $[Na^+]_d$ obtained in cardiomyocytes from CONT and infected mice in EAP, AP, and CP. The equilibrium potential of the Na^+/Ca^{2+} exchanger (E_{NCX}) was estimated using the following equation: $E_{NCX} = 3E_{Na} - 2E_{Ca}$ (with a stoichiometry of 3:1), where E_{Na} and E_{Ca} are the equilibrium potentials of Na^+ and Ca^{2+} obtained from the Nernst equation.

Solutions

All solutions were made with ultrapure water supplied by a Milli-Q system (Millipore, Bedford, MA). The Tyrode solution had the following composition (in mM): 130 NaCl, 5 KCl, 2.5 $CaCl_2$, 1 $MgCl_2$, 20 $NaHCO_3$, 0.33 NaH_2PO_4, and 10 glucose gassed with 95% O_2 and 5% CO_2, pH 7.4. A low- or Na^+-free solution was prepared by the partial or total withdrawal of $[Na^+]_e$, and replacement by an equivalent amount of impermeable cation *N*-methyl-D-glucamine (NMG) hydrochloride to maintain osmolarity. A Ca^{2+}-free solution was prepared, omitting $CaCl_2$ and adding 1 mM of EGTA and 2 mM of $MgCl_2$. Solutions 2-(2-(4-nitrobenzyloxy-phenyl-ethyl-isothiourea methanesulfonate (KB-R7943) and N- (3-aminobenzyl) -6- 4- [(3-fluorobenzyl-oxy] phenoxy nicotinamide (YM-244769) were made by adding the desired concentration of the reagent to the Tyrode solution. All experiments were carried out at 37°C.

Statistical Analysis

Experimental results are expressed as means ± SD; n_{mice} represents the number of mice used and n_{cells} the number of successful measurements in cardiomyocytes isolated from CONT and infected mice used for statistical analysis. Data were analyzed using one-way analysis of variance ANOVA for repeated measures, followed by Tukey's multiple comparison tests to determine significance. A $p<0.05$ was considered significant. GraphPad Prism 9 (GraphPad Software, CA, USA) was used for statistical analysis.

RESULTS

$[Ca^{2+}]_d$ and $[Na^+]_d$ in Ventricular Cardiomyocytes of Chagasic Rodents

We previously reported a significant elevation in $[Ca^{2+}]_d$ in cardiomyocytes obtained from patients with chronic Chagas cardiomyopath, which was related to the extent of their cardiac dysfunction (Lopez et al., 2011; Mijares et al., 2020). **Figure 1** shows representative records of simultaneous measurement of Vm and $[Ca^{2+}]_d$ in a single cardiomyocyte isolated from (**A**) CONT mice, (**B**) EAP-infected mice (20 dpi), (**C**) AP-infected mice (40 dpi), and (**D**) CP-infected mice (120 dpi). The cardiomyocytes of Chagas-infected mice showed partial depolarization and increased $[Ca^{2+}]_d$, which aggravated as a function of days after infection. The mean Vm and $[Ca^{2+}]_d$ in quiescent cardiomyocytes from CONT mice were 81 ± 1 mV and 122 ± 3 nM. Respectively. In cardiomyocytes from EAP-infected mice, Vm was 78 ± 1.7 mV and $[Ca^{2+}]_d$ 194 ± 23 nM ($p<0.001$ compared to CONT cardiomyocytes); in cardiomyocytes from AP-infected mice, Vm was 76 ± 1.6 mV and $[Ca^{2+}]_d$ 320 ± 38 nM ($p<0.001$ compared to CONT cardiomyocytes) and in cardiomyocytes from CP-infected mice, Vm was 72 ± 1.8 mV and $[Ca^{2+}]_d$ 470 ± 43 nM ($p<0.001$ compared to CONT cardiomyocytes) (**Figures 2A, B**).

Similar differences in $[Na^+]_d$ were obtained in the measurements carried out in quiescent cardiomyocytes of Chagas-infected mice at different phases of infection. In cardiomyocytes from CONT mice $[Na^+]_d$ was 8 ± 0.2 mM; In cardiomyocytes from EAP-infected mice $[Na^+]_d$ was 9.4 ± 0.7 mM ($p<0.001$ compared to CONT cardiomyocytes); In cardiomyocytes from AP-infected mice $[Na^+]_d$ was 13.9 ± 0.8 mM ($p<0.001$ compared to CONT cardiomyocytes); and in cardiomyocytes from CP-infected mice $[Na^+]_d$ was 15.9 ± 1 mM ($p<0.001$ compared to CONT cardiomyocytes) (**Figure 2C**).

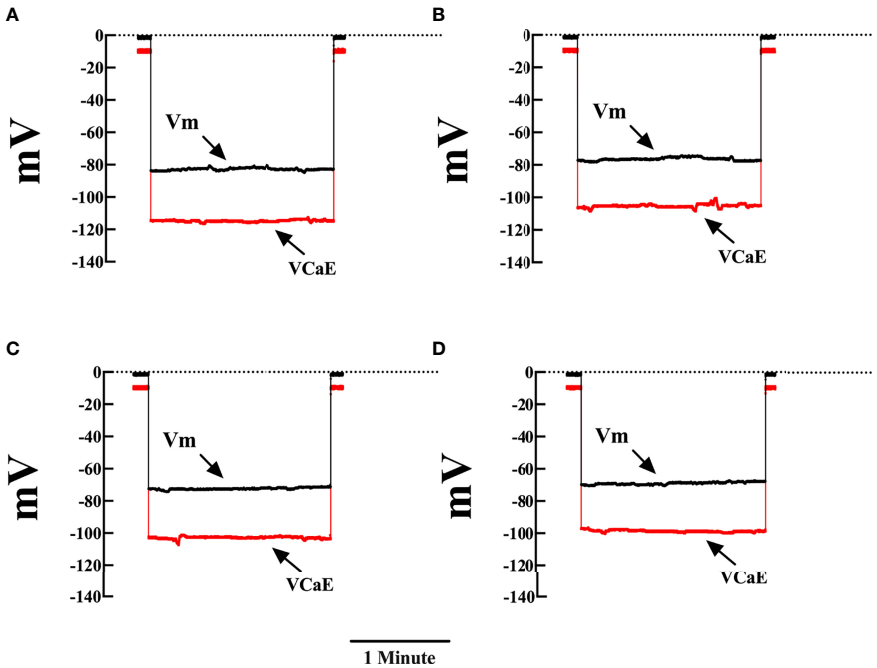

FIGURE 1 | Representative measurements of Vm and $[Ca^{2+}]_d$ in cardiomyocytes from control and Chagas infected mice. Simultaneous measurements of membrane potential (Vm) and $[Ca^{2+}]_d$ **(A)** Cardiomyocyte from control mice (Vm was -82 mV and $[Ca^{2+}]_d$ 122 nM). **(B)** Cardiomyocyte from EAP-infected mice (Vm was -76mV and $[Ca^{2+}]_d$ 200 nM). **(C)** Cardiomyocyte from AP-infected mice (Vm was -73 mV and $[Ca^{2+}]_d$ 312 nM). **(D)** Cardiomyocyte from CP-infected mice (Vm was -69 mV and $[Ca^{2+}]_d$ 414 nM). Vm, resting membrane potential and V_{Cae}, specific calcium potential; CONT, control mice; EAP, infected mice in the early acute phase; AP, infected mice in the acute phase; and CP, infected mice in the chronic phase. Calibration bar = 1 minute.

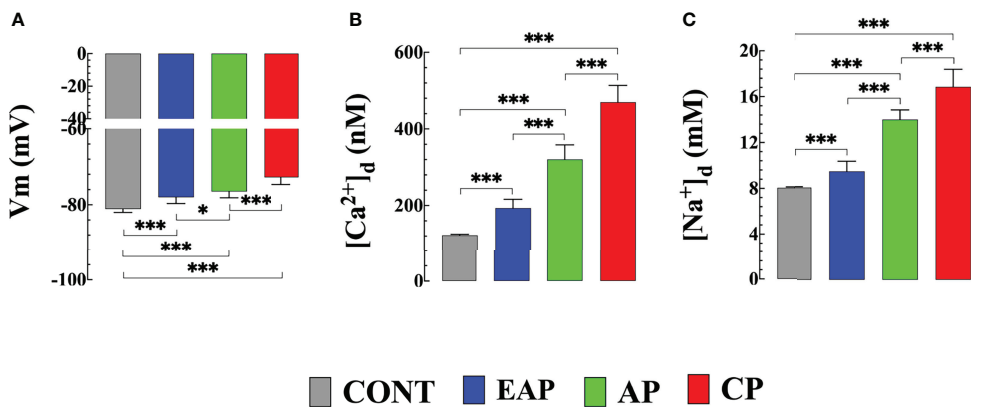

FIGURE 2 | Resting membrane potential, diastolic $[Ca^{2+}]$ and $[Na^+]$ in cardiomyocytes from control and Chagas infected mice. **(A)** The resting membrane potential, **(B)** $[Ca^{2+}]_d$, and **(C)** $[Na^+]_d$ were measured in quiescent cardiomyocytes from CONT mice (n_{cells}=24 and n_{mice}=3), EAP-infected mice (n_{cells}=19 and n_{mice}=3), AP-infected mice (n_{cells}=21 and n_{mice}=3) and CP-infected mice (n_{cells}=18 and n_{mice}=5). Data are expressed as means ± S.D. Statistical analysis was performed using one-way ANOVA, followed by Tukey's multiple comparison tests, $^*p < 0.05$; $^{***}p < 0.001$. CONT, control mice; EAP, early acute phase of infected mice; AP, acute phase of infected mice; and CP, chronic phase of infected mice.

Removal of $[Na^+]_e$ Increased $[Ca^{2+}]_d$ in Cardiomyocytes

In a separate set of experiments, the reverse mode activity of NCX (Ca^{2+} entry in exchange for Na^+ leaving the cell) was studied in quiescent cardiomyocytes isolated from control and infected mice by incubation in a solution in which Na^+ was replaced in equivalent amounts by NMG. $[Ca^{2+}]_d$ was measured before and after incubation with a low or Na^+ free solution. The

reduction of $[Na^+]_e$ to 65 mM caused an increase in $[Ca^{2+}]_d$ in CONT cardiomyocytes to 212 ± 27 nM, in cardiomyocytes from EAP-infected mice to 400 ± 24 nM, in cardiomyocytes from AP infected mice to 790 ± 62 nM, and cardiomyocytes from CP-infected mice to 1,320 ± 137 nM (p<0.001 compared to cardiomyocytes from CONT, EAP, AP and CP-infected mice bathed in normal $[Na^+]_e$) (**Figure 3**).

Incubation in Na^+ free solution caused a further increase in $[Ca^{2+}]_d$ in control and cardiomyocytes from infected mice. In CONT cardiomyocytes $[Ca^{2+}]_d$ increased significantly to 309 ± 42 nM, in cardiomyocytes from EAP-infected mice to 540 ± 69 nM, from AP-infected mice to 1,016 ± 64 nM, and from CP-infected mice to 1,523 ± 62 nM respectively (p<0.001 compared to cardiomyocytes from CONT, and EAP-, AP- and CP- infected mice bathed in normal $[Na^+]_e$). (**Figure 3**). The sustained increase $[Ca^{2+}]_d$ was maintained as long as Na^+ was absent from the bath solution and reversed when Na^+ was reintroduced into the Tyrode solution, except for cardiomyocytes from CP-infected mice where an irreversible elevation $[Ca^{2+}]_d$ associated with contracture was observed.

Removal of Extracellular Ca^{2+} Prevents the Increase in $[Ca^{2+}]_d$ Induced by Na^+ Depletion

In a different set of experiments, we explored the contribution of the Ca^{2+} influx to the elevation of $[Ca^{2+}]_d$ elicited by the withdrawal of Na^+ in quiescent cardiomyocytes from control and infected mice. Cardiomyocytes were incubated for 10 minutes in a Ca^{2+}-free solution prior to the withdrawal of Na^+ (see solutions). Incubation in a Ca^{2+}-free solution significantly reduced $[Ca^{2+}]_d$ to 98 ± 5 nM in cardiomyocytes from CONT mice (p<0.001 compared to CONT cardiomyocytes in normal $[Ca^{2+}]_e$), to 100 ± 11 nM in cardiomyocytes from EAP-infected mice (p<0.001 compared to EAP cardiomyocytes in normal $[Ca^{2+}]_e$), to 123 ± 14 nM cardiomyocytes from AP-infected mice (p<0.001 compared to AP cardiomyocytes in normal $[Ca^{2+}]_e$), and to 136 ± 11 nM in cardiomyocytes from CP-infected mice (p<0.001 compared to CP cardiomyocytes in normal $[Ca^{2+}]_e$). (**Figure 4**). Elevation of $[Ca^{2+}]_d$ induced by withdrawal of Na^+ was abolished in the absence of extracellular Ca^{2+} in all cardiomyocyte groups (**Figure 4**).

Equilibrium Potentials

Using the Nernst equation and the actual values $[Ca^{2+}]_d$ and $[Na^+]_d$ found in the present study, the estimated E_{Ca} in cardiomyocytes from CONT mice was +133 mV, in cardiomyocytes from EAP-infected mice was +127 mV, in cardiomyocytes from AP-infected mice was +119 mV, and in cardiomyocytes from CP-infected mice were +116 mV. While the estimated E_{Na} in cardiomyocytes isolated from CONT mice was +74 mV, EAP-infected mice was +70 mV, AP-

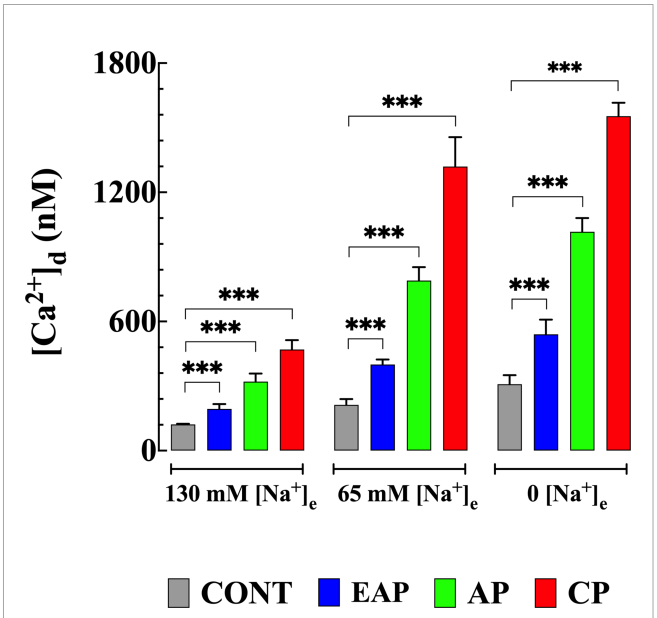

FIGURE 3 | Effects of reduction in $[Na^+]_e$ on $[Ca^{2+}]_d$ in cardiomyocytes from control and Chagas infected mice. $[Ca^{2+}]_d$ was measured before and after cardiomyocyte treatments with solutions in which $[Na^+]_e$ was partially or completely replaced with NMG. $[Ca^{2+}]_d$ was determined in quiescent cardiomyocytes from CONT mice (n_{cells}=13-24 and n_{mice}=4), EAP-infected mice (n_{cells}=12-19 and n_{mice}=5), AP-infected mice (n_{cells}=12-21 and n_{mice}=5) and CP-infected mice (n_{cells}=6-18 and n_{mice}=9). Data are expressed as means ± S.D. Statistical analysis was performed as described above, ***p < 0.001. CONT, control mice; EAP, early acute phase of infected mice; AP, acute phase of infected mice; and CP, chronic phase of infected mice.

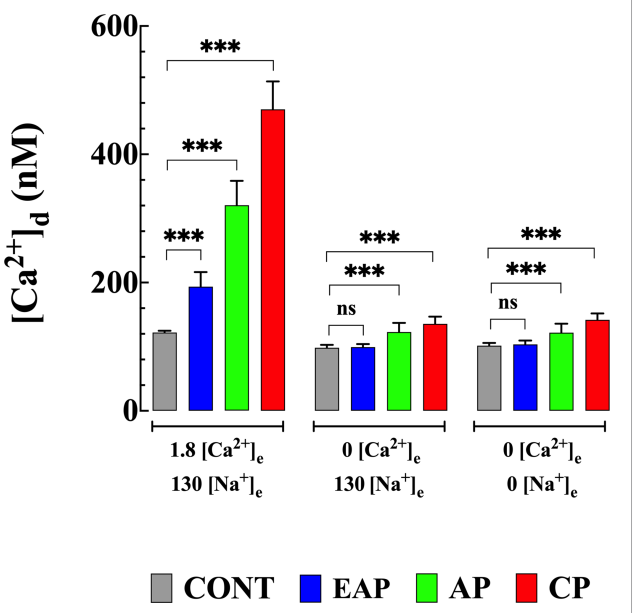

FIGURE 4 | Effect extracellular Ca^{2+} on Na^+ depletion-induced elevation of $[Ca^{2+}]_d$. $[Ca^{2+}]_d$ was measured in cardiomyocytes from CONT, EAP-, AP-, and CP-infected mice in normal Tyrode, Ca^{2+}-free Tyrode solution, and Ca^{2+} and Na^+ free Tyrode solution. $[Ca^{2+}]_d$ was determined in quiescent cardiomyocytes from CONT (n_{cells}=16-24 and n_{mice}=4), EAP-infect mice (n_{cells}=15-19 and n_{mice}=5), AP-infect mice (n_{cells}=18-21 and n_{mice}=6) and CP-infect mice (n_{cells}=15-18 and n_{mice}=8). Data are expressed as mean ± S.E. Statistical analysis was performed as described above, *** p < 0.001. CONT, control mice; EAP, early acute phase of infected mice; AP, acute phase of infected mice; and CP, chronic phase of infected mice. ns, no significant.

infected mice was +59 mV, and CP-infected mice was +56 mV. The equilibrium potential of the Na^+/Ca^{2+} exchanger (E_{NCX}) was -44 mV in cardiomyocytes from CONT, -46 mV from EA-infected mice, -61 mV from AP-infected mice, and –64 mV from CP-infected mice, respectively.

KB-R7943 and YM-244769 Reduced $[Ca^{2+}]_d$ and Prevented the Elevation of Ca^{2+} Induced by the Na^+ Free Solution

To determine the mechanisms involved in the elevation of $[Ca^{2+}]_d$ caused by exposure to Na^+ free medium, quiescent cardiomyocytes from control and infected mice were incubated in KB-R7943, a nonspecific blocker of the NCX reverse mode, which modified Na^+ dependent binding (Iwamoto et al., 1996; Akabas, 2004). Cardiomyocyte preincubation with 10 μM KB-R7943 for 10 minutes significantly reduced $[Ca^{2+}]_d$ and inhibited the increase in $[Ca^{2+}]_d$ induced by the solution without Na^+ (**Figure 5A**). KB-R7943 reduced $[Ca^{2+}]_d$ to 152 ± 16 nM in cardiomyocytes from EAP-infected mice, to 186 ± 21 nM from AP-infected mice, and 258 ± 30 nM from CP-infected mice (**Figure 5A**). No significant effect was observed in cardiomyocytes from CONT mice (116 ± 5 nM*)*. Preincubation with KB-R7943 prevented the elevation of $[Ca^{2+}]_d$ caused by the Na^+ free solution in cardiomyocytes of control and infected mice (compare **Figures 3**,**5A**).

Due to the lack of specificity of KB-R7943 (Abramochkin and Vornanen, 2014), we also examined the effects of YM-244769, a high-affinity blocker of the NCX reverse mode (Iwamoto and Kita, 2006). Incubation with 1 μM YM-244769 for 10 minutes reduced $[Ca^{2+}]_d$ to 176 ± 20 nM in cardiomyocytes from EAP-infected mice, to 254 ± 19 nM from AP-infected mice, and to 336 ± 32 nM from CP-infected mice. YM-244769 did not significantly reduce $[Ca^{2+}]_d$ in cardiomyocytes of CONT and EAP-infected mice. YM-244769 fully inhibited the elevation of $[Ca^{2+}]_d$ induced by the Na^+ free solution in CONT cardiomyocytes and infected mice (compare **Figures 3**, **5B**).

DISCUSSION

Cardiac alterations are a severe and recurrent complication related to Chagas disease and represent the most common causes of heart failure and sudden death in Latin America (Velasco and Morillo, 2020). The present study reinforces our previous finding that progressive deterioration of cardiac function in Chagas cardiomyopathy is associated with defective intracellular Ca^{2+} regulation. In this report, we demonstrate, for the first time, that ventricular cardiomyocytes from rodents infected with *T. cruzi* show a partial depolarization associated with aberrant $[Ca^{2+}]_d$ and $[Na^+]_d$, which aggravated with endpoint after infection (chronic>acute>early acute). Furthermore, we provide evidence that chagasic infection enhances the reverse mode of NCX, causing an elevation of $[Ca^{2+}]_d$, which is not mediated by membrane depolarization.

Calcium is essential in the regulation of cardiac contractility, and defective intracellular Ca^{2+} homeostasis plays an vital role in the pathogenesis of diverse cardiac diseases (Houser and Margulies, 2003; Lopez et al., 2011; Uryash et al., 2021a; Uryash et al., 2021b). $[Ca^{2+}]_d$ is regulated by several mechanisms that controls Ca^{2+} influx-efflux and intracellular reuptake that allow the maintenance of $[Ca^{2+}]$ within a physiological range (~100 nM) (Lopez et al., 2011; Mijares et al., 2014; Mijares et al., 2020). The $[Ca^{2+}]_d$ values obtained from CONT cardiomyocytes are in agreement with previous estimates obtained from humans (Lopez et al., 2011; Mijares et al., 2020) and non-human ventricular myocytes (Mijares et al., 2014; Uryash et al., 2021a; Uryash et al., 2021b) using Ca^{2+}-selective microelectrodes and fluorescent Ca^{2+} indicator (Piacentino et al., 2003). The abnormal $[Ca^{2+}]_d$ in cardiomyocytes from infected mice (chronic>acute>early acute) agree with a similar dysfunction observed in cardiomyocytes obtained from Chagas patients and could potentially promote arrhythmias, similar to those observed

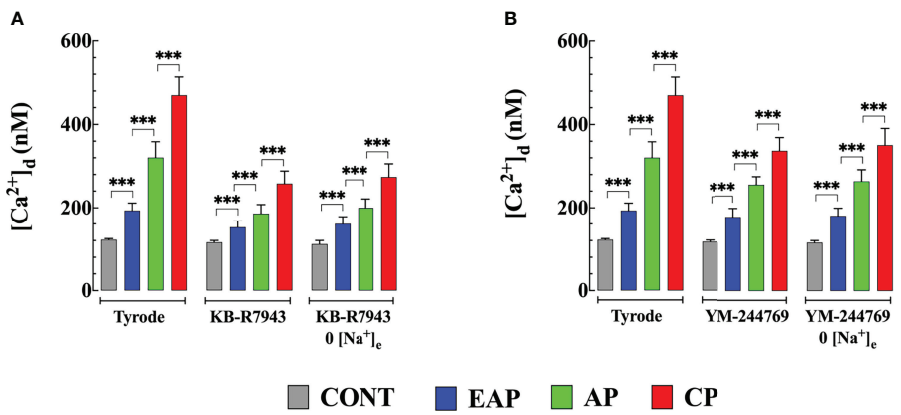

FIGURE 5 | NCX blockers inhibited Na^+ withdraw-induced $[Ca^{2+}]_d$ increases in cardiomyocytes from control and Chagas infected mice. **(A)** Effects of KB-R7943 and **(B)** YM-244769 on $[Ca^{2+}]_d$ increases caused by Na^+ removal. $[Ca^{2+}]_d$ was determined in (i) normal Tyrode solution (ii) after 10 min of incubation with 10 μm KB-R7943) or 1 μM YM-244769 and (iii) after incubation, either KB-R7943 in Na^+ free solution or YM-244769 in Na^+ free solution. Experiments were carried out in cardiomyocytes from CONT (n_{cells}=15-24 and n_{mice}=6), EAP (n_{cells}=12-19 and n_{mice}=8), AP (n_{cells}=13-21 and n_{mice}=8) and CP cardiomyocytes (n_{cells}=11-18 and n_{mice}=9). Data are expressed as mean ± S.E. Statistical analysis was performed as described above, ***$p < 0.001$. CONT: control mice; EAP: early acute phase of infected mice; AP: acute phase of infected mice; and CP: chronic phase of infected mice.

in patients with Chagas cardiomyopathy (Benziger et al., 2017; Almeida et al., 2018).

Normal resting $[Na^+]_d$ in cardiomyocytes is in the range of 7-8 mM (Gray et al., 2001; Mijares et al., 2014), while in cardiomyocytes from infected mice, it was higher (CP>EP>AEP). Intracellular $[Na^+]$ is mainly regulated in cardiac myocytes by Na^+/K^+-ATPase, Na^+/Ca^{2+} exchange, Na^+ channels, and amiloride-sensitive Na^+/H^+ exchanger (Everts et al., 1992; Blaustein and Lederer, 1999; Bers et al., 2003). An elevated $[Na^+]_d$, as found in Chagas-infected mice cardiomyocytes, could change the balance of fluxes through NCX to favor a greater inflow of Ca^{2+} (reverse mode) (Blaustein and Lederer, 1999), contributing to intracellular Ca^{2+} overload as observed in Chagas-infected mice cardiomyocytes. Furthermore, it is plausible that the partial depolarization observed in cardiomyocytes from infected mice (chronic>acute>early acute) may be related to diastolic Na^+ overload. Unfortunately, we did not explore whether the elevation of $[Na^+]_d$ in cardiomyocytes from infected mice was related to an increased influx or decreased efflux of Na^+; therefore, no conclusions can be drawn.

Sodium-calcium exchange is the major Ca^{2+} efflux mechanism of ventricular cardiomyocytes. NCX mediates an electrogenic exchange of 3 Na^+ for 1 Ca^{2+}, which can occur in the forward (Ca^{2+} extrusion–Na^+ entry) or in the reverse (Ca^{2+} entry– Na^+ extrusion) mode (Blaustein and Lederer, 1999; Bers, 2000; Bers, 2002). In this study, we provide evidence for the first time of an enhancement in the reverse mode function of NCX in cardiomyocytes from infected mice (chronic>acute>early acute). The increase in $[Ca^{2+}]_d$ mediated by NCX was not associated with membrane depolarization and was dependent on extracellular $[Ca^{2+}]$ and $[Na^+]$ in all cardiomyocytes. Therefore, changes in NCX could contribute to intracellular Ca^{2+} overload, but could also contribute to the arrhythmogenesis observed in Chagas patients (Stein et al. 2018). The elevation of $[Ca^{2+}]_d$ was prevented in cardiomyocytes from control and infected mice by removing extracellular Ca^{2+} and reversed when Na^+ was reintroduced into the bath, except for cardiomyocytes from CP-infected mice, where the removal of Na^+ (partially or completely) produced irreversible contraction and cell death (40% in 65 mM $[Na^+]e$ and 82% in Na^+ free solution, respectively).

The mode in which NCX operates is dependent on the Na^+ and Ca^{2+} gradients across the sarcolemma, as well as the membrane potential, following a driving force equal to $E_m - E_{Na/Ca}$ (where $E_{Na/Ca} = 3E_{Na} - 2E_{Ca}$ with E_{Na} and E_{Ca} represent the equilibrium potentials of Na^+ and Ca^{2+}, respectively) (Bers and Ginsburg, 2007). If the driving force for $3Na^+$ is greater than $1Ca^{2+}$ in the cell (3:1 Na^+/Ca^{2+} stoichiometry), the NCX will transport Na^+ into the cell and take Ca^{2+} out (forward mode). On the other hand, if under another set of conditions (altered membrane potential, ionic gradients, or post-translational modifications), the driving force for $3Na^+$ is less than that for $1Ca^{2+}$ in the cell, then the electrochemical gradient of Ca^{2+} will become the dominant inward driving force (reverse mode) (Bers and Ginsburg, 2007). The intracellular ionic changes in cardiomyocytes from infected mice modified the driving force ($E_m - E_{Na/Ca}$) by 5 mV in cardiomyocytes from EAP-infected mice, 22 mV in cardiomyocytes from AP-infected mice, and 29 mV in cardiomyocytes from CP-infected mice.

KB-R7943 significantly reduced $[Ca^{2+}]_d$ by 1.3 times in cardiomyocytes from EAP-infected mice, 1.7 times in AP-infected mice, and 1.8 times in CP-infected mice, suggesting that the elevation of $[Ca^{2+}]_d$ observed in cardiomyocytes of Chagas infected mice was due in part to an influx of Ca^{2+} mediated by NCX in its reverse mode. On the contrary, in cardiomyocytes from CONT mice, KB-R7943 did not modify $[Ca^{2+}]_d$, indicating that in healthy quiescent cardiomyocytes, NCX in its reverse mode does not contribute significantly to $[Ca^{2+}]_d$. Furthermore, KB-R7943 prevented the elevation of $[Ca^{2+}]_d$ induced by Na^+ withdrawal in cardiomyocytes from CONT and cardiomyocytes from infected mice. The involvement of NCX in the pathophysiology of Chagas disease is consistent with the recent publication by Santos-Miranda et al. (Santos-Miranda et al., 2021), which found the contribution of NCX as a cellular arrhythmogenic substrate in isolated cardiomyocytes from infected mice with the Colombian strain of *T. cruzi*. However, the effect of KB-R7943 on $[Ca^{2+}]_d$ must be considered with caution due to the lack of selectivity, since the NCX blocker also affects voltage-gated Na^+ and Ca^{2+} channels, inward rectifying K^+ channels in cardiac cells (Watano et al., 1996).

YM-244769 is a potent and highly selective NCX blocker that up to 1 μM (dose used in the present study) preferentially inhibits the reverse mode of NCX, with no effect on the forward mode (Iwamoto and Kita, 2006). YM-244769 significantly reduced $[Ca^{2+}]_d$ by 1.3 times in cardiomyocytes from AP- and 1.4 times from CP-infected mice. YM-244769 did not significantly reduce $[Ca^{2+}]_d$ in cardiomyocytes from CONT and EAP-infected mice, suggesting that the contribution of NCX to $[Ca^{2+}]_d$ is negligible. The effect of YM-244769 on $[Ca^{2+}]_d$ cardiomyocytes was small compared to KB-R7943, which is consistent with the fact that YM-244769 is a more specific NCX blocker and that KB-R7943 can act on other Ca^{2+} entry pathways. Furthermore, YM-244769 blocked the observed elevation of $[Ca^{2+}]_d$ caused by the Na^+ free solution in all cardiomyocytes. Together, these data strongly support the hypothesis that Ca^{2+} entry mediated by the reverse NCX mode plays a significant role in $[Ca^{2+}]_d$ dyshomeostasis observed in cardiomyocytes isolated from Chagas infected mice during acute and chronic stages of infection. The fact that KB-R7943 or YM-244769 did not normalize $[Ca^{2+}]_d$ in cardiomyocytes from infected mice suggests the existence of additional Ca^{2+} pathways that appear to be altered due to Chagas infection.

Conclusions

These results provide, for the first time, evidence that NCX plays an important role in aberrant diastolic $[Ca^{2+}]$ observed in cardiomyocytes from infected mice (chronic>acute>early acute). These novel findings may open a new therapeutic approach to improve cardiac function in patients suffering from chronic Chagas cardiomyopathy because there is still no effective treatment. Unfortunately, Chagas cardiomyopathy remains largely ignored despite its medical and social relevance.

Study Limitations

Despite the novelty of this study, some limitations should be pointed out. We did not determine whether the elevation of $[Na^+]_d$ in cardiomyocytes from infected mice could be related to an increased influx or decreased efflux of Na^+. Furthermore, the expression of NCX and other proteins involved in intracellular Ca^{2+} regulation were not studied.

DATA AVAILABILITY STATEMENT

The original contributions presented in the study are included in the article/supplementary material. Further inquiries can be directed to the corresponding author.

ETHICS STATEMENT

The animal study was reviewed and approved by Care and Use Handbook of Laboratory Animals published by the US National Institute of Health (NIH publication No. 85-23, revised 1996) and approved by the Institutional Animal Care (IACUC) and Use Committees.

AUTHOR CONTRIBUTIONS

JRL: Designed research, performed the experiments, and analyzed the data; NL: Performed the experiments; JAA: Designed research; AM: Designed research, and analyzed the data. All authors contributed to manuscript revision, read, and approved the submitted version.

FUNDING

This work was supported by the Florida Heart Research Foundation.

ACKNOWLEDGMENTS

The author thanks Dr. Jose O'Daly for kindly giving us the *T cruzi*-infected mice.

REFERENCES

Abramochkin, D. V., and Vornanen, M. (2014). Inhibition of the Cardiac ATP-Dependent Potassium Current by KB-R7943. *Comp. Biochem. Physiol. A Mol. Integr. Physiol.* 175, 38–45. doi: 10.1016/j.cbpa.2014.05.005

Akabas, M. H. (2004). Na+/Ca2+ Exchange Inhibitors: Potential Drugs to Mitigate the Severity of Ischemic Injury. *Mol. Pharmacol.* 66, 8–10. doi: 10.1124/mol.104.000232.

Alarcon De Noya, B., Diaz-Bello, Z., Colmenares, C., Ruiz-Guevara, R., Mauriello, L., Zavala-Jaspe, R., et al. (2010). Large Urban Outbreak of Orally Acquired Acute Chagas Disease at a School in Caracas, Venezuela. *J. Infect. Dis.* 201, 1308–1315. doi: 10.1086/651608

Almeida, B. C. S., Carmo, A., Barbosa, M. P. T., Silva, J., and Ribeiro, A. L. P. (2018). Association Between Microvolt T-Wave Alternans and Malignant Ventricular Arrhythmias in Chagas Disease. *Arq. Bras. Cardiol.* 110, 412–417. doi: 10.5935/abc.20180056

Aronsen, J. M., Swift, F., and Sejersted, O. M. (2013). Cardiac Sodium Transport and Excitation-Contraction Coupling. *J. Mol. Cell Cardiol.* 61, 11–19. doi: 10.1016/j.yjmcc.2013.06.003

Benziger, C. P., Do Carmo, G. A. L., and Ribeiro, A. L. P. (2017). Chagas Cardiomyopathy: Clinical Presentation and Management in the Americas. *Cardiol. Clin.* 35, 31–47. doi: 10.1016/j.ccl.2016.08.013

Bern, C., Montgomery, S. P., Katz, L., Caglioti, S., and Stramer, S. L. (2008). Chagas Disease and the US Blood Supply. *Curr. Opin. Infect. Dis.* 21, 476–482. doi: 10.1097/QCO.0b013e32830ef5b6

Bers, D. M. (2000). Calcium Fluxes Involved in Control of Cardiac Myocyte Contraction. *Circ. Res.* 87, 275–281. doi: 10.1161/01.RES.87.4.275

Bers, D. M. (2002). Cardiac Excitation-Contraction Coupling. *Nature* 415, 198–205. doi: 10.1038/415198a

Bers, D. M. (2014). Cardiac Sarcoplasmic Reticulum Calcium Leak: Basis and Roles in Cardiac Dysfunction. *Annu. Rev. Physiol.* 76, 107–127. doi: 10.1146/annurev-physiol-020911-153308

Bers, D. M., Barry, W. H., and Despa, S. (2003). Intracellular Na+ Regulation in Cardiac Myocytes. *Cardiovasc. Res.* 57, 897–912. doi: 10.1016/S0008-6363(02)00656-9

Bers, D. M., and Despa, S. (2006). Cardiac Myocytes Ca2+ and Na+ Regulation in Normal and Failing Hearts. *J. Pharmacol. Sci.* 100, 315–322. doi: 10.1254/jphs.CPJ06001X

Bers, D. M., and Ginsburg, K. S. (2007). Na : Ca Stoichiometry and Cytosolic Ca-Dependent Activation of NCX in Intact Cardiomyocytes. *Ann. N. Y. Acad. Sci.* 1099, 326–338. doi: 10.1196/annals.1387.060

Blaustein, M. P., and Lederer, W. J. (1999). Sodium/calcium Exchange: Its Physiological Implications. *Physiol. Rev.* 79, 763–854. doi: 10.1152/physrev.1999.79.3.763

Echavarria, N. G., Echeverria, L. E., Stewart, M., Gallego, C., and Saldarriaga, C. (2021). Chagas Disease: Chronic Chagas Cardiomyopathy. *Curr. Probl. Cardiol.* 46, 100507. doi: 10.1016/j.cpcardiol.2019.100507

Eltit, J. M., Ding, X., Pessah, I. N., Allen, P. D., and Lopez, J. R. (2013). Nonspecific Sarcolemmal Cation Channels are Critical for the Pathogenesis of Malignant Hyperthermia. *FASEB J.* 27, 991–1000. doi: 10.1096/fj.12-218354

Everts, M. E., Ording, H., Hansen, O., and Nielsen, P. A. (1992). Ca(2+)-ATPase and Na(+)-K(+)-ATPase Content in Skeletal Muscle From Malignant Hyperthermia Patients. *Muscle Nerve* 15, 162–167. doi: 10.1002/mus.880150206

Freichel, M., Berlin, M., Schurger, A., Mathar, I., Bacmeister, L., Medert, R., et al. (2017). "TRP Channels in the Heart," in *Neurobiology of TRP Channels*. Ed. T. L. R. Emir(Boca Raton (FL: CRC Press/Taylor & Francis), 149–185.

Gray, R. P., Mcintyre, H., Sheridan, D. S., and Fry, C. H. (2001). Intracellular Sodium and Contractile Function in Hypertrophied Human and Guinea-Pig Myocardium. *Pflugers Arch.* 442, 117–123. doi: 10.1007/s004240000512

Houser, S. R., and Margulies, K. B. (2003). Is Depressed Myocyte Contractility Centrally Involved in Heart Failure? *Circ. Res.* 92, 350–358.

Http://Www.Who.Int/Mediacentre/Factsheets/Fs340/En/. (2021).

Iwamoto, T., and Kita, S. (2006). YM-244769, a Novel Na+/Ca2+ Exchange Inhibitor That Preferentially Inhibits NCX3, Efficiently Protects Against Hypoxia/Reoxygenation-Induced SH-SY5Y Neuronal Cell Damage. *Mol. Pharmacol.* 70, 2075–2083. doi: 10.1124/mol.106.028464

Iwamoto, T., Watano, T., and Shigekawa, M. (1996). A Novel Isothiourea Derivative Selectively Inhibits the Reverse Mode of Na+/Ca2+ Exchange in Cells Expressing NCX1. *J. Biol. Chem.* 271, 22391–22397. doi: 10.1074/jbc.271.37.22391

Liao, R., and Jain, M. (2007). Isolation, Culture, and Functional Analysis of Adult Mouse Cardiomyocytes. *Methods Mol. Med.* 139, 251–262. doi: 10.1007/978-1-59745-571-8_16

Lopez, J. R., Alamo, L., Caputo, C., Dipolo, R., and Vergara, S. (1983). Determination of Ionic Calcium in Frog Skeletal Muscle Fibers. *Biophys. J.* 43, 1–4. doi: 10.1016/S0006-3495(83)84316-1

Lopez, J. R., Contreras, J., Linares, N., and Allen, P. D. (2000). Hypersensitivity of Malignant Hyperthermia-Susceptible Swine Skeletal Muscle to Caffeine is Mediated by High Resting Myoplasmic [Ca2+]. *Anesthesiology* 92, 1799–1806. doi: 10.1097/00000542-200006000-00040

Lopez, J. R., Espinosa, R., Landazuru, P., Linares, N., Allen, P., and Mijares, A. (2011). [Dysfunction of Diastolic [Ca(2)(+)] in Cardiomyocytes Isolated From Chagasic Patients]. *Rev. Esp. Cardiol.* 64, 456–462.

Lopez, J. R., Kolster, J., Zhang, R., and Adams, J. (2017). Increased Constitutive Nitric Oxide Production by Whole Body Periodic Acceleration Ameliorates Alterations in Cardiomyocytes Associated With Utrophin/Dystrophin Deficiency. *J. Mol. Cell Cardiol.* 108, 149–157. doi: 10.1016/j.yjmcc.2017.06.004

Marban, E., Rink, T. J., Tsien, R. W., and Tsien, R. Y. (1980). Free Calcium in Heart Muscle at Rest and During Contraction Measured With Ca2+ -Sensitive Microelectrodes. *Nature* 286, 845–850. doi: 10.1038/286845a0

Mijares, A., Altamirano, F., Kolster, J., Adams, J. A., and Lopez, J. R. (2014). Age-Dependent Changes in Diastolic Ca(2+) and Na(+) Concentrations in Dystrophic Cardiomyopathy: Role of Ca(2+) Entry and IP3. *Biochem. Biophys. Res. Commun.* 452, 1054–1059. doi: 10.1016/j.bbrc.2014.09.045

Mijares, A., Espinosa, R., Adams, J., and Lopez, J. R. (2020). Increases in [IP3]i Aggravates Diastolic [Ca2+] and Contractile Dysfunction in Chagas' Human Cardiomyocytes. *PLoS Negl. Trop. Dis.* 14, e0008162. doi: 10.1371/journal.pntd.0008162

O'Daly, J. A. , Simonis, S. , de Rolo, N. , and Caballero, H. (1984). Suppression of Humoral Immunity and Lymphocyte Responsiveness During Experimental Trypanosoma Cruzi Infections. *Rev. Inst. Med. Trop.* 26(2):67–77. doi: 10.1590/s0036-46651984000200001

Piacentino, V.3rd, Weber, C. R., Chen, X., Weisser-Thomas, J., Margulies, K. B., Bers, D. M., et al. (2003). Cellular Basis of Abnormal Calcium Transients of Failing Human Ventricular Myocytes. *Circ. Res.* 92, 651–658. doi: 10.1161/01.RES.0000062469.83985.9B

Rassi, A.Jr., Rassi, A., and Marin-Neto, J. A. (2010). Chagas Disease. *Lancet* 375, 1388–1402. doi: 10.1016/S0140-6736(10)60061-X

Santos-Miranda, A., Joviano-Santos, J. V., Sarmento, J. O., Costa, A. D., Soares, A. T. C., Machado, F. S., et al. (2021). A Novel Substrate for Arrhythmias in Chagas Disease. *PloS Negl. Trop. Dis.* 15, e0009421. doi: 10.1371/journal.pntd.0009421

Shannon, T. R., Pogwizd, S. M., and Bers, D. M. (2003). Elevated Sarcoplasmic Reticulum Ca2+ Leak in Intact Ventricular Myocytes From Rabbits in Heart Failure. *Circ. Res.* 93, 592–594. doi: 10.1161/01.RES.0000093399.11734.B3

Smith, G. L., and Eisner, D. A. (2019). Calcium Buffering in the Heart in Health and Disease. *Circulation* 139, 2358–2371. doi: 10.1161/CIRCULATIONAHA.118.039329

Stein, C., Migliavaca, C. B., Colpani, V., Rosa, P. R., Sganzerla, D., Giordani, N. E., et al. (2018). Amiodarone for arrhythmia in patients with Chagas disease: A systematic review and individual patient data meta-analysis. *PLoS Negl Trop Dis* 12 (8), e0006742. doi: 10.1371/journal.pntd.0006742

Teixeira, A. R., Hecht, M. M., Guimaro, M. C., Sousa, A. O., and Nitz, N. (2011). Pathogenesis of Chagas' Disease: Parasite Persistence and Autoimmunity. *Clin. Microbiol. Rev.* 24, 592–630. doi: 10.1128/CMR.00063-10

Uryash, A., Mijares, A., Esteve, E., Adams, J. A., and Lopez, J. R. (2021a). Cardioprotective Effect of Whole Body Periodic Acceleration in Dystrophic Phenotype Mdx Rodent. *Front. Physiol.* 12, 658042. doi: 10.3389/fphys.2021.658042

Uryash, A., Mijares, A., Flores, V., Adams, J. A., and Lopez, J. R. (2021b). Effects of Naringin on Cardiomyocytes From a Rodent Model of Type 2 Diabetes. *Front. Pharmacol.* 12, 719268. doi: 10.3389/fphar.2021.719268

Velasco, A., and Morillo, C. A. (2020). Chagas Heart Disease: A Contemporary Review. *J. Nucl. Cardiol.* 27, 445–451. doi: 10.1007/s12350-018-1361-1

Watano, T., Kimura, J., Morita, T., and Nakanishi, H. (1996). A Novel Antagonist, No. 7943, of the Na+/Ca2+ Exchange Current in Guinea-Pig Cardiac Ventricular Cells. *Br. J. Pharmacol.* 119, 555–563. doi: 10.1111/j.1476-5381.1996.tb15708.x

Wussling, M., Schenk, W., and Nilius, B. (1987). A Study of Dynamic Properties in Isolated Myocardial Cells by the Laser Diffraction Method. *J. Mol. Cell Cardiol.* 19, 897–907. doi: 10.1016/S0022-2828(87)80618-1

Conflict of Interest: The authors declare that the research was conducted in the absence of any commercial or financial relationships that could be construed as a potential conflict of interest.

Publisher's Note: All claims expressed in this article are solely those of the authors and do not necessarily represent those of their affiliated organizations, or those of the publisher, the editors and the reviewers. Any product that may be evaluated in this article, or claim that may be made by its manufacturer, is not guaranteed or endorsed by the publisher.

frontiers | Frontiers in Cellular and Infection Microbiology

ORIGINAL RESEARCH
published: 14 July 2022
doi: 10.3389/fcimb.2022.944748

The Use of AlphaFold for *In Silico* Exploration of Drug Targets in the Parasite *Trypanosoma cruzi*

Albert Ros-Lucas[1*], *Nieves Martinez-Peinado*[1*], *Jaume Bastida*[2], *Joaquim Gascón*[1,3] *and Julio Alonso-Padilla*[1,3*]

[1] Barcelona Institute for Global Health (ISGlobal), Hospital Clinic - University of Barcelona, Barcelona, Spain, [2] Departament de Biologia, Sanitat i Medi Ambient, Facultat de Farmàcia i Ciències de l'Alimentació, Universitat de Barcelona, Barcelona, Spain, [3] CIBERINFEC, ISCIII—CIBER de Enfermedades Infecciosas, Instituto de Salud Carlos III, Madrid, Spain

OPEN ACCESS

Edited by:
Gustavo Benaim,
Fundación Instituto de Estudios Avanzados (IDEA), Venezuela

Reviewed by:
Marcelo A. Comini,
Institut Pasteur de Montevideo, Uruguay
Alexis Mendoza-León,
Universidad Central de Venezuela, Venezuela

***Correspondence:**
Albert Ros-Lucas
albert.ros@isglobal.org
Nieves Martinez-Peinado
nieves.martinez@isglobal.org
Julio Alonso-Padilla
julio.a.padilla@isglobal.org

Specialty section:
This article was submitted to Parasite and Host, a section of the journal Frontiers in Cellular and Infection Microbiology

Received: 15 May 2022
Accepted: 23 June 2022
Published: 14 July 2022

Citation:
Ros-Lucas A, Martinez-Peinado N, Bastida J, Gascón J and Alonso-Padilla J (2022) The Use of AlphaFold for In Silico Exploration of Drug Targets in the Parasite Trypanosoma cruzi. Front. Cell. Infect. Microbiol. 12:944748. doi: 10.3389/fcimb.2022.944748

Chagas disease is a devastating neglected disease caused by the parasite *Trypanosoma cruzi*, which affects millions of people worldwide. The two anti-parasitic drugs available, nifurtimox and benznidazole, have a good efficacy against the acute stage of the infection. But this is short, usually asymptomatic and often goes undiagnosed. Access to treatment is mostly achieved during the chronic stage, when the cardiac and/or digestive life-threatening symptoms manifest. Then, the efficacy of both drugs is diminished, and their long administration regimens involve frequently associated adverse effects that compromise treatment compliance. Therefore, the discovery of safer and more effective drugs is an urgent need. Despite its advantages over lately used phenotypic screening, target-based identification of new anti-parasitic molecules has been hampered by incomplete annotation and lack of structures of the parasite protein space. Presently, the AlphaFold Protein Structure Database is home to 19,036 protein models from *T. cruzi*, which could hold the key to not only describe new therapeutic approaches, but also shed light on molecular mechanisms of action for known compounds. In this proof-of-concept study, we screened the AlphaFold *T. cruzi* set of predicted protein models to find prospective targets for a pre-selected list of compounds with known anti-trypanosomal activity using docking-based inverse virtual screening. The best receptors (targets) for the most promising ligands were analyzed in detail to address molecular interactions and potential drugs' mode of action. The results provide insight into the mechanisms of action of the compounds and their targets, and pave the way for new strategies to finding novel compounds or optimize already existing ones.

Keywords: chagas disease, *trypanosoma cruzi*, drug discovery, AlphaFold, target deconvolution

INTRODUCTION

Chagas disease, caused by the parasite *Trypanosoma cruzi*, is a potentially life-threatening disease with several socioeconomic, environmental and public health issues (World Health Organization, 2022). It is endemic in Latin America where it exerts its highest burden. Moreover, owing to migration in recent decades, it has spread to other non-endemic regions becoming a global health

issue. Approximately 6-7 million people worldwide are infected with *T. cruzi*, and 10,000 people die annually from such infection (World Health Organization, 2022). Its acquisition occurs by vector, congenital, iatrogenic or oral routes (World Health Organization, 2022). Once infected, individuals go through a short (4-8 weeks) acute phase that is characterized for the appearance of non-specific mild symptoms or an absence of symptomatology which makes it go undiagnosed. Then, the disease progresses to a chronic phase which can be silent for life or, in 30-40% of the patients, manifest with cardiac and/or digestive alterations that can lead to the formation of mega-syndromes and death if untreated (Prata, 2001).

For the last 50 years, the nitroheterocyclic drugs benznidazole (BNZ) and nifurtimox (NFX) have been the only drugs available to treat Chagas disease. BNZ and NFX are prodrugs that act through the formation of free radicals and electrophilic metabolites generated when its nitro group is reduced to an amino group by the action of nitro-reductases (Wilkinson et al., 2008). Both drugs have shown to be effective when administered to early infections and are well tolerated by infants (Prata, 2001). However, their efficacy diminishes at the chronic stage and the appearance of toxic side effects usually leads to treatment interruption (Alonso-Padilla et al., 2019). Thus, there is an urgent need for new drugs for Chagas disease.

Drug development is a long and expensive process handicapped by high attrition rates. In the drug discovery cascade, compounds are first evaluated through *in vitro* assays prior its evaluation at preclinical and clinical trials. At this early stage, two strategies are typically undertaken to identify hit compounds: target-based or whole cell phenotypic assays (Martínez-Peinado et al., 2020). The latest are usually preferred over target-based approaches as those represent a more holistic insight with higher translational rate to *in vivo* efficacy assessment (Martínez-Peinado et al., 2020). However, phenotypic approaches usually require additional steps to identify the molecular target, not just for elucidating the mechanism of action, but also to aid in the rational design of the drug and allow efficient structure-activity relationship (SAR) studies (Terstappen et al., 2007). The process to identify the molecular target, termed target deconvolution, may entail expression cloning-based methods, protein microarrays, RNAi/CRISPR screening or radioactive compound-binding assays, among others (Kubota et al., 2019). However, these experiments are time- and resource-extensive, and computational alternatives commonly known as *in silico* target prediction or molecular docking studies have gained considerable attention in last years (Kubota et al., 2019). This is particularly the case in Neglected Tropical Diseases (NTDs) drug discovery research, like that for Chagas disease, where developmental costs must be kept necessarily low due to the scarce funds available. Notably, these computational strategies have been strengthened thanks to the increasing availability of pathogen sequences and genome-scale functional datasets (Crowther et al., 2010).

Chagas disease, as other NTDs, suffers from a lack of well-characterized and validated targets that has hampered drug development (Chatelain and Ioset, 2018). Among *T. cruzi* identified targets there are the following enzymes: triosephosphate isomerase (TIM), sterol 14α-demethylase (CYP51), dihydroorotate dehydrogenase (DHODH), cruzipain, trypanothione reductase (TR), superoxide dismutase (Fe-SOD), pteridine reductase (PTR) and dihydrofolate reductasethymidylate synthase (DHFR-TS) (Beltran-Hortelano et al., 2022). Interestingly, the recent failure of posaconazole, inhibitor of *T. cruzi* CYP51, in clinical trials has highlighted the challenge of molecular target validation for Chagas drug development; and such target could ultimately be validated if associated with a curative profile (Chatelain and Ioset, 2018).

AlphaFold is a recently developed software for the prediction of protein 3D structures from their genetic sequence (Jumper et al., 2021). The AlphaFold Protein Structure Database has the entire human proteome, as well as the entire proteomes of other 20 widely studied organisms such as *Escherichia coli, Trypanosoma brucei* or *T. cruzi*. Specifically, it is home to 19,036 protein models from *T. cruzi* (Varadi et al., 2022). Thus, it has emerged as a very valuable tool to predict potential targets and hypothesize mechanisms of action of known compounds. In this proof-of-concept work, we have used docking-based inverse virtual screening with AlphaFold *T. cruzi* protein models to find prospective targets for a pre-selected list of compounds with known anti-trypanosomal activity in clinical trials or in chronic *in vivo* models of *T. cruzi* infection. The goal is to assess the usefulness of AlphaFold models for *in silico* drug discovery pipelines, as well as computationally validating the targets described for this list of compounds.

METHODS

Generation of the *T. cruzi* library of potential targets

First, a list of genes of interest was created from the TryTrip database (Aslett et al., 2010; Amos et al., 2022). All genes from *T. cruzi* CL Brener Esmeraldo-like strain, member of the pathogenic Discrete Typing Unit II (DTU II), were searched. We further selected genes which expression was above the 10% percentile in any of the samples of the three experiments where trypomastigote or amastigote samples were available (Smircich et al., 2015; Li et al., 2016; Belew et al., 2017). Additionally, genes were also selected if at least one peptide was detected in any of the two mass spectrometry proteomic experiments for trypomastigotes and/or amastigotes (Atwood et al., 2005; Marchini et al., 2011). Genes without a UniProtKB ID were discarded, since the AlphaFold Protein Structure Database only contains models with an entry in UniProtKB (The UniProt Consortium, 2021).

All protein models in PDB format for the *T. cruzi* CL Brener proteome were downloaded from the AlphaFold Protein Structure Database downloads section on October 20th 2021 as a compressed tar file. Models with a UniProtKB ID that did not match any of the selected genes were discarded. Selected genes without a model were a consequence of their products' length being larger than 2,700 residues, and since AlphaFold models were not available for such lengths, these were discarded too. Conversion to the pdbqt format used for docking was done with Open Babel (O'Boyle et al., 2011), adding hydrogens with a pH of 7.4 and using the Gasteiger method to add partial charges. Binding pocket prediction was performed using P2Rank (Krivák and Hoksza, 2018) with standard settings. Pockets

with a probability score (as given by P2Rank) above 0.1 were considered as candidates for binding sites. For each model, the pocket with the highest probability score was selected as the binding site. Structures without predicted pockets, or predicted pockets with a probability score below 0.1, were discarded.

In order to assess the global model quality, the predicted Local Distance Difference Test (pLDDT) (Mariani et al., 2013) score of each α-carbon was extracted from the PDB files, and the proportion of residues with a pLDDT score above 70 (described as the threshold for good backbone prediction) (Tunyasuvunakool et al., 2021) was calculated. Only models with at least half of its total residues with a pLDDT score above 70 were considered for docking. Additionally, to assess the local quality of the binding pocket, the residues predicted to be part of the pocket by P2Rank were considered. Only models in which at least half of the residues in the pocket had a pLDDT score above 90 were kept. This stricter threshold is given by the fact that residues with a pLDDT score above 90 can be interpreted as having very high quality and correct side-chain orientation (Tunyasuvunakool et al., 2021). Finally, the Predicted Aligned Error (PAE) of the pocket residues was also analyzed. To do so, the mean PAE of each residue of the pocket (as specified by P2Rank) with the rest of the residues of the pocket was calculated, and the overall mean PAE was obtained. Any model with a mean pocket PAE above 5 Å was discarded.

Identification of the list of ligands

In order to select suitable ligands, we undertook a search of publications in PubMed/MEDLINE and ClinicalTrials.gov databases. Searches in ClinicalTrials.gov were performed in January 2022 under the search term [Chagas disease]. We selected only those drugs in clinical trials with previously reported anti-*T. cruzi* activity (**Table S1**). Searches in PubMed/MEDLINE were performed from September to November 2021 and were restricted to publications published between 2015 and 2021. The search terms used were [*Trypanosoma cruzi*] AND [Drug] OR [Compound] OR [Natural product]. We performed a manual revision to select those that included anti-*T. cruzi* activity *in vivo* and prioritized those compounds that had inhibited the parasite equally or superior to the reference drug BNZ in a chronic model of the infection (**Table S2**). For those that were the result of chemical synthesis, we maintained the number of the compound reported in each publication and added a number from one to six to avoid name repetitions and to differentiate them (**Table S2**). Ligand structures were downloaded from PubChem (Kim et al., 2021) as 3D SDF files where possible, otherwise they were downloaded either as 2D SDF files or drawn using Avogadro (Hanwell et al., 2012). For the latter two, the final 3D conformation was obtained by using Avogadro's Auto Optimization tool, using the UFF force field with 4 steps per update and the Steepest Descent algorithm until the energy differential (dE) fell below 0.001 for several seconds. Conversion to pdbqt format was also done using Open Babel, assigning charges using the Gasteiger method. For compounds C8-3 and C26-6, this method proved to be unsuccessful due to having selenium atoms, for which the EEM method was used instead. The size of the binding box for each ligand was optimized according to Feinstein and Brylinski (Feinstein and Brylinski, 2015), using a radius of gyration to box side ratio of 0.35, and rounding up to the nearest integer. The radius of gyration for each ligand was calculated using the Python RDKit (Landrum et al., 2021) library Descriptors3D module.

Docking of targets to their described ligands

Docking simulations were performed using AutoDock Vina 1.1.2 (Trott and Olson, 2009). The exhaustiveness parameter was set to 8, and the energy range to 2. The search box center was chosen from the P2Rank predictions, and its size was calculated for each ligand as described above. For each receptor and ligand pair, ten docking repetitions were done with different random seeds. The best mode for each pair was chosen from the lowest docking energy of all the repetitions. This resulted in a matrix of n ligands by m receptors, with the best possible energy for each pair. To normalize results, a receptor-average Z-score matrix was calculated (Yang et al., 2009). For this, each value of the binding energy matrix was substituted by a Z-score using the formula:

$$Z_{ij} = \left(X_{ij} - \bar{X}_i\right)/SD_i;$$

where X_{ij} is the binding energy as given by AutoDock Vina for the receptor i and ligand j pair, $\bar{X}_i$ is the mean binding energy of receptor i, and SD_i is the standard deviation for receptor i. Positive X_{ij} values were ignored and considered as missing. The top 3% scored receptors in the Z-score combined matrix were chosen as the best putative receptors for each ligand. Results were visualized using PyMol (Schrödinger, 2015).

RESULTS AND DISCUSSION

The final list of selected genes from TriTryp encompassed 7,988 entries filtered out of the 10,596 *T. cruzi* CL Brener Esmeraldo-like genes available. From these, 7,810 had a protein model available. A total of 5,088 models had a predicted binding site available, and after discarding models with low quality, given by low pLDDT scores or high PAE, only 1,819 models rested available for docking predictions (**Figure 1**). Our search and selection of ligands (as described in Methods) returned 16 compounds for the docking simulations (**Table 1**), 6 from clinical trials (**Figure 2**) and 10 from chronic models of infection (**Figure 3**). In total, 363,800 docking simulations were performed by AutoDock Vina, doing 10 repetitions for each receptor-ligand pair. Some ligands performed quicker than others, being the computation speed inversely proportional to their number of atoms and rotatable bonds. The lowest binding energy for each pair was selected as the best binding mode. Thus, the binding energy matrix generated contained 1,819 rows (receptors) and 16 columns (ligands) (**Table S3**). The average binding energy for each ligand, as well as their docking box edge size are shown in **Table 1**. The binding energy matrix was then normalized to a Z-score matrix using each receptor's average binding energy and standard deviation (**Table S4**), and filtered to

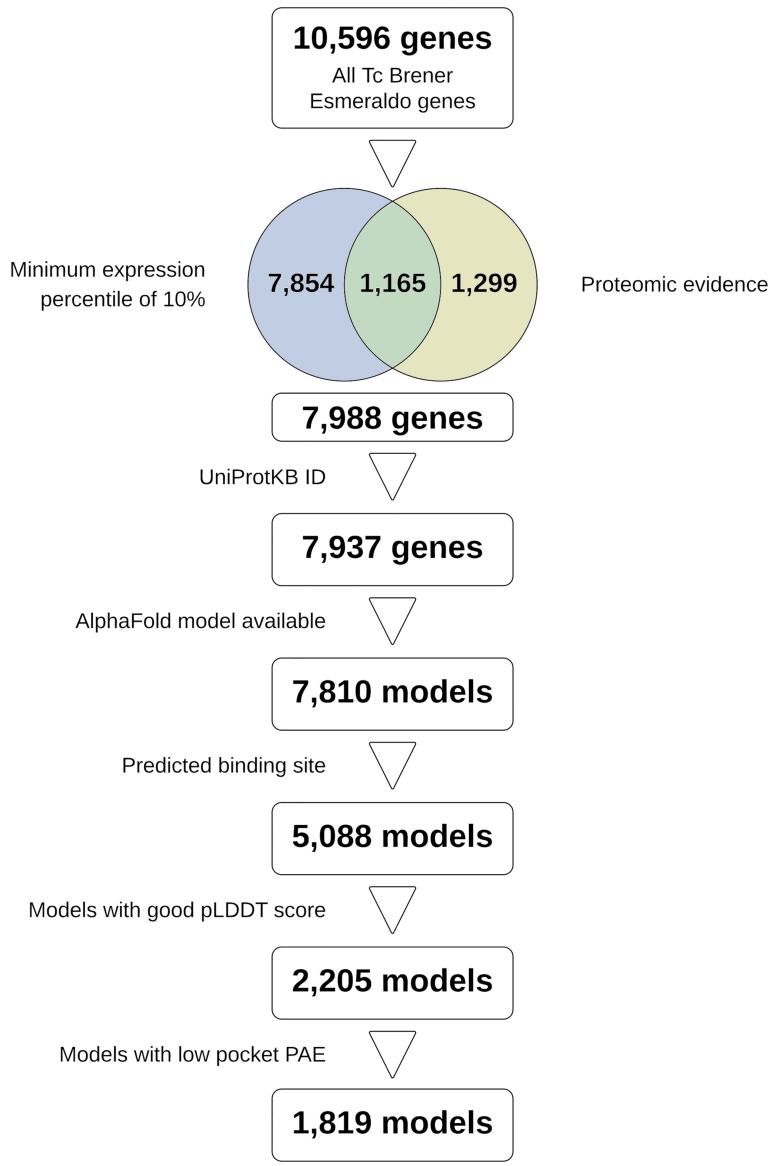

FIGURE 1 | Study flowchart summarizing the steps followed to reach the models used in docking. Figure made in Lucidchart.

only keep the top 3% binders for each ligand as their putative receptors (**Table S5**).

Taking a closer look at the compounds from clinical trials and good activity *in vivo*, and comparing their top binders with existing literature records, we found that some of them indeed have their experimentally validated receptors inside their corresponding top 3% putative receptors. In the following subsections we describe the results obtained with each class of inhibitors evaluated.

Ergosterol biosynthesis inhibitors

Posaconazole is widely described to act upon the *T. cruzi* ergosterol biosynthesis pathway by inhibiting the CYP family enzyme lanosterol 14-alpha demethylase (TcCLB.510101.50, UniProtKB Q7Z1V1) (Lepesheva et al., 2011). In our analysis, we retrieved that same target in position 32 out of 54 in the top 3% receptors (targets) of posaconazole. While it would have been expected to find it in a higher position, its relatively low placement could be attributed to the fact that, as a CYP family member, the binding site of lanosterol 14-alpha demethylase contains a heme cofactor. This group directly interacts with posaconazole as seen in PDB structure 3K1O (Lepesheva et al., 2010). Even though AlphaFold models correctly predict the binding site of cofactors, they do not contain these molecules, which poses a certain limitation to their use in *in silico* docking. Advances to compensate for this have been made. For example, the yet unpublished AlphaFill (Hekkelman et al., 2021) can transfer cofactors from PDB into AlphaFold models based on

TABLE 1 | List of compounds used in this study.

Compound	Box size	Mean predicted binding energy (kcal/mol)	Described target
Benznidazole	10 Å	-7.07	Nitroreductase
Nifurtimox	12 Å	-6.91	Nitroreductase
Fexinidazole	13 Å	-6.50	Nitroreductase
Posaconazole	20 Å	-7.35	Ergosterol biosynthesis
Ravuconazole	14 Å	-7.59	Ergosterol biosynthesis
Amiodarone	13 Å	-6.39	Calcium homeostasis
GNF6702	16 Å	-8.87	Proteasome
NFOH	12 Å	-6.29	Nitroreductase
Clofazimine	15 Å	-7.51	Cruzipain
Benidipine	13 Å	-7.92	Cruzipain
Compound 9-1	16 Å	-7.33	FeSOD
Compound 16-2	11 Å	-7.05	Mitochondria
Compound 8-3	16 Å	-7.60	Mitochondria
Compound 7-4	15 Å	-7.00	Glycosome
Compound 9-5	14 Å	-7.33	FeSOD
Compound 26-6	13 Å	-7.04	Mitochondria

sequence and structure similarity. In this regard, the AlphaFill model for the lanosterol 14-alpha demethylase correctly displays a heme group in the expected position, which would certainly improve the binding energy of posaconazole.

Ravuconazole is another compound that has been described to target the lanosterol 14-alpha demethylase (Lepesheva et al., 2011), but for this ligand we found that the expected target enzyme was outside the top 3% selected. Ravuconazole would be expected to also interact with the heme cofactor of the enzyme, and such low ranking could thus be reasonable. The fact we retrieved it at a much lower position in the list in comparison to posaconazole might be attributed to small inaccuracies in the binding pocket, which could probably be improved by allowing AutoDock Vina to use flexible pocket residues in its docking simulations. Unfortunately, such an approach was unfeasible in the current study due to computational time limitations.

Compounds disrupting parasite calcium homeostasis

Amiodarone has been widely used to prevent arrhythmias in patients with Chagas cardiomyopathy (Stein et al., 2018). Nonetheless, it was recently described to have *in vitro* anti-parasitic activity and synergic activity with posaconazole in *in vivo* models of *T. cruzi* infection (Adesse et al., 2011; Benaim et al., 2021). Amiodarone has been described to act thought the disruption of intracellular calcium homeostasis, which has been

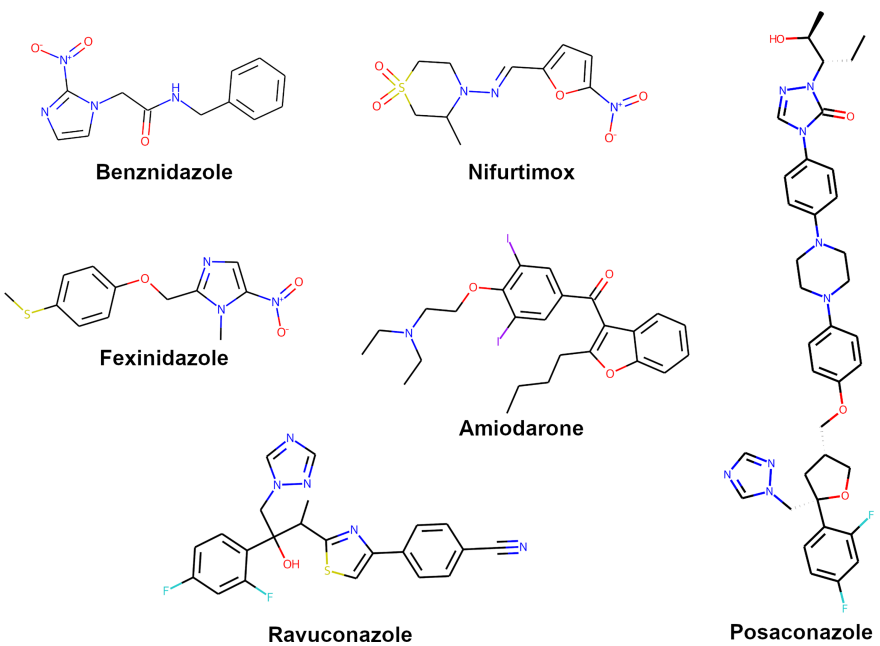

FIGURE 2 | Structures of compounds with anti-*T.cruzi* activity used in clinical trials.

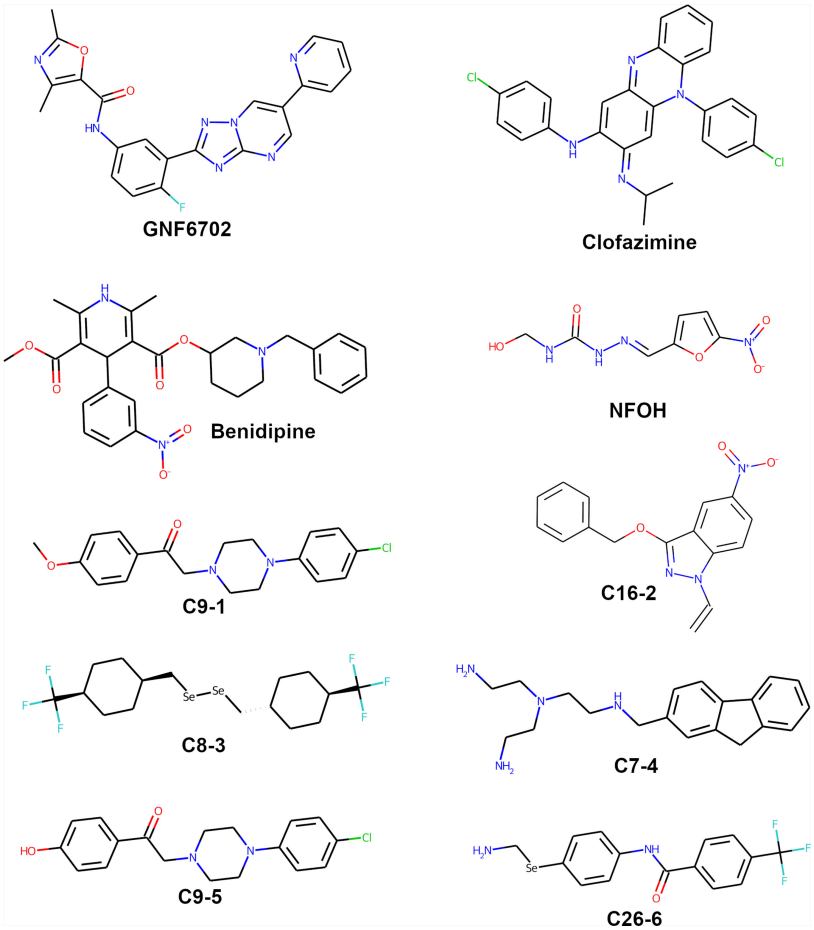

FIGURE 3 | Structures of compounds with anti-*T.cruzi* activity used in chronic experimental models of the disease.

identified as a potential therapeutic target in trypanosomatids (Benaim et al., 2021). More specifically, amiodarone collapses the mitochondrial electrochemical potential and prompts the alkalization of acidocalcisomes, increasing parasite intracellular calcium concentration (Benaim et al., 2021). In our analysis, we found the V-type proton ATPase subunit A TcCLB.509767.70 (Q4DSC7) at position 42 out of 54 in the top 3%. The V-type proton ATPase is involved in the acidification of the acidocalcisome by the uptake of H^+ (Docampo and Moreno, 2011). Thus, this ATPase could be a possible target for this drug that would correlate with that described by Benaim et al. (Benaim et al., 2021). Additionally, we found a transporter (TcCLB.506369.20, UniProtKB Q4D047) located in the acidocalcisome membrane at position 36 out of 54. Amiodarone has also been reported to inhibit the oxidosqualene cyclase, a key enzyme in ergosterol biosynthesis. However, we did not find this enzyme in the top 3% of our analysis.

Compounds activated by nitroreductase enzymes

Regarding BNZ, NFX, hydroxymethylnitrofurazone (NFOH) and fexinidazole, they are all described to be prodrugs, which upon being metabolized generate highly reactive intermediary compounds that can target many cellular components (Maya et al., 2007; Hall et al., 2011; Scarim et al., 2021). In particular, these drugs would be mainly metabolized by *T. cruzi* nitroreductase (TcCLB.510611.60, UniProtKB Q4D8D9) (Maya et al., 2007; Hall et al., 2011). However, the binding site detected by P2Rank in the AlphaFold model for this enzyme showed a high predicted aligned error (PAE), due to being formed between the N-terminal domain and the rest of the protein (**Figure 4**). This poor quality of the binding pocket prevented the model from being used in the screening, and thus it could not have been selected as a putative receptor for these ligands. Alternative enzymes that have been described to metabolize these drugs, such as dihydrolipoamide dehydrogenase, cytochrome P450

reductase, trypanothione reductase or prostaglandin F2α synthase (Hall et al., 2011), were neither selected for any of these ligands.

Iron superoxide dismutase (FeSOD) inhibitors

Another ligand that has a suggested target in the top 3% putative receptors is the Manich base-type derivative C9-1, which is described to inhibit the iron superoxide dismutase enzyme (FeSOD) with an IC_{50} value of 6.5 μM (Martín-Escolano et al., 2018b). FeSOD is a trypanosomatid-exclusive enzyme that prevents oxidative stress caused by reactive oxygen species (ROS) and that considerably differs from its human homologue (Martín-Escolano et al., 2018b). Therefore, it has been considered a desirable druggable target. A TriTryp search for superoxide dismutase (SOD) enzymes for the CL Brener Esmeraldo-like strain resulted in six enzymes with matching annotation. However, only the TcCLB.511735.60 SOD (UniProt ID Q4CUQ5) was used for docking. Superoxide dismutase enzymes FeSOD TcCLB.509775.40 (Q4DCQ3), FeSOD TcCLB.511715.10 (Q4D5A6), FeSOD TcCLB.507039.10 (Q4CVN4) and SOD TcCLB.511545.120 (Q4DMR9), which pertain to the same ortholog group, were discarded because P2Rank failed to predict their binding pockets, while SOD TcCLB.511737.3 (Q4D5Z8) was discarded due to not having transcriptomic and/or proteomic evidence. However, all six showed high structural similarity upon alignment with PyMol (data not shown). A comparison with available PDB structures for the *T. cruzi* FeSOD 4H3E and 4DVH (both from TcCLB.509775.40) showed that this enzyme is in fact a homodimer, with the binding site located between its subunits. Unfortunately, the version of AlphaFold used in the AlphaFold Protein Database currently does not support multi-chain models. Thus, one of the limitations of our pipeline is the fact that protein complexes with binding sites situated in the interaction between chains will probably not have correct predictions. Despite this

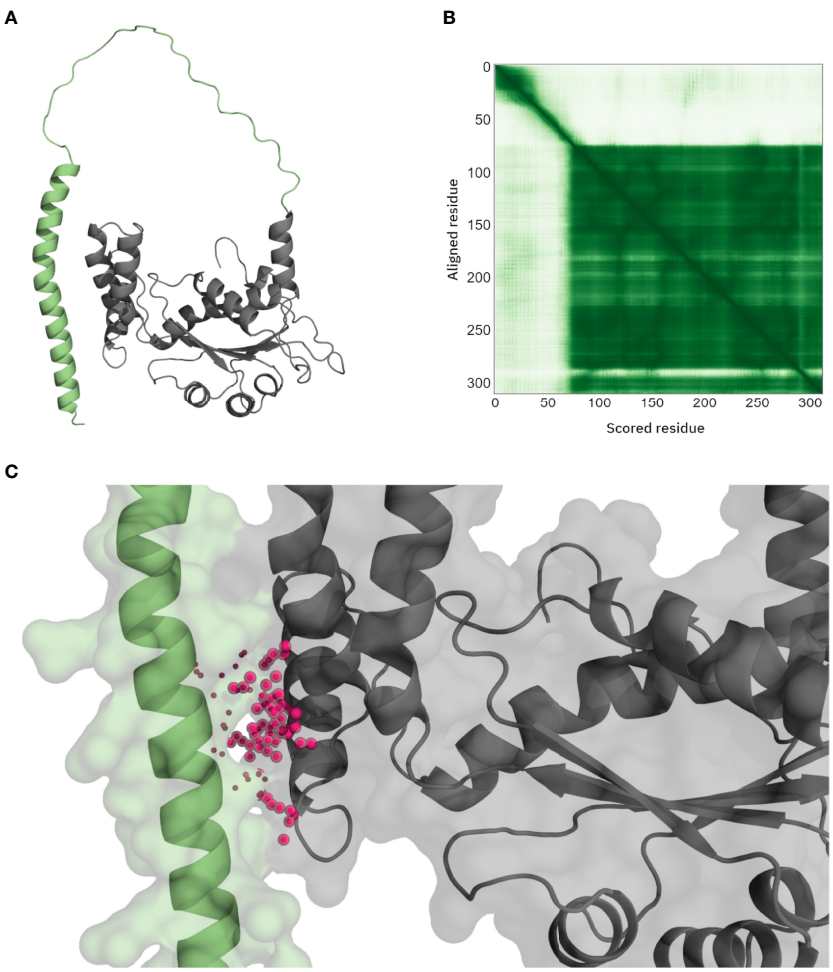

FIGURE 4 | *T. cruzi* nitroreductase AlphaFold model. The relative position of the N-terminal domain (**A**, green residues) compared with the rest of the protein has very low confidence, as seen in the Predicted Aligned Error (PAE) plot **(B)**. The predicted pocket by P2Rank falls in the interaction between this domain and the rest of the protein (**C**, purple spheres), suggesting that this pocket might be an artifact.

limitation, we found that TcCLB.511735.60 superoxide dismutase appeared in position 1 out of 55 of the best binders for C9-1, providing reliability to the methodology followed. Additionally, Manich base type-derivatives have been described as potent inhibitors of *T. cruzi* trypanothione reductase based on the ability of those compounds to interact with dithiol groups (Beltran-Hortelano et al., 2017). For C9-1, we found the trypanothione reductase (TcCLB.504507.5, Q4CMQ7) at the position 48 out of 55 in the top 3%, suggesting a multiple target for C9-1.

Upon looking at compound C9-5, which is also a Manich base-type derivative highly similar to C9-1 and also suggested to act on the FeSOD (Paucar et al., 2019), we were unable to find it in the top 3%. This might have been caused by the fact that, as described above, the FeSOD enzyme is found as a dimer, and the binding site used in the docking simulations did not reflect that reality. The only difference between these two ligands is an *O*-methyl group at one of the ends of the C9-1 molecule, where C9-5 only has a hydroxyl group. This gives C9-1 a bigger radius of gyration, and thus a larger docking box. It is possible that this allowed C9-1 to adopt a higher affinity mode in comparison to C9-5, hence the higher ranking of the FeSOD in that case.

Cruzipain inhibitors

Another two ligands considered were the cruzipain inhibitors clofazimine and benidipine (Sbaraglini et al., 2016). Cruzipain is a cysteine peptidase of *T. cruzi*, and three enzymes annotated as such were used in the docking simulations: major cysteine proteinase TcCLB.507603.270 (Q4DW02), cysteine peptidase TcCLB.506529.550 (Q4E5M4), and cysteine peptidase Tc CLB .507537.20 (Q4CV00). Cysteine peptidase TcCLB.507603.260 (Q4DW03) was discarded beforehand due to exhibiting a low mean pocket pLDDT. The docking analysis could not find any of the former three enzymes in the selected putative receptors for clofazimine and benidipine. Structural comparison of these enzymes with available cruzipain PDB structures 4PI3 and 3KKU showed that the binding site in the AlphaFold models is obstructed by residues between positions 80 and 110 approximately. UniProt annotation for cruzipain P25779 (corresponding to cysteine peptidase TcCLB.507603.260) indicates that residues 19 – 122 are in fact a propeptide, which would be cleaved in the mature protein. Thus, the cruzipain AlphaFold models we used do not reflect the reality of the protein, and the P2Rank pocket prediction could have not detected the binding site. Notwithstanding, it is interesting to find that in the top selected receptors for both ligands there are indeed other cysteine peptidases, in particular TcCLB.504107.10 calpain-like cysteine peptidase (Q4CMV9) in position 7 out of 52 for clofazimine; and TcCLB.509013.19 calpain-like cysteine peptidase (Q4CW01) and TcCLB.511527.50 cysteine peptidase (Q4D5K1) respectively in positions 32 and 38 out of 55 for benidipine. While the latter cysteine peptidase bears low sequence identity to cruzipains, its catalytic site hints to a structural similarity with them, as illustrated by the pairwise structure alignment using the TM-align algorithm of cruzipain PDB structure 4PI3 with the Q4D5K1 AlphaFold model (**Figure 5**). In particular, the catalytic triad appears to be roughly in the same positioning, Cys-His-Asn in the case of cruzipain, and Cys-His-Asp for the Q4D5K1 cysteine peptidase. It is then conceivable that benidipine would also show high affinity for this enzyme, being the binding site predicted by P2Rank located in the catalytic site. The calpain-like cysteine peptidases share some overall structural similarity to that of cruzipains; however, their catalytic site appears to be inactive, keeping the nucleophilic cysteine but without the amino acid dyad base needed to deprotonate it (**Figure 6**). Indeed, catalytically inactive calpain-like proteins are not uncommon (Dear et al., 1997; Ersfeld et al., 2005), and these might have another regulatory function in the parasite. Additionally, the binding site predicted by P2Rank for both calpain-like proteins is not located in the proximity of the catalytic site, suggesting that the inhibition by clofazimine and benidipine could be given by another mechanism.

Proteasome inhibitors

In the case of GNF6702, it is described to target the cell proteasome, specifically an allosteric site in the proteasome β4 subunit in close proximity to the catalytic site of the β5 subunit (Khare et al., 2016). A protein BLAST search in TriTryp found that the sequence corresponding to the proteasome β4 subunit described by Khare and co-workers is annotated as the β2 subunit of the *T. cruzi* CL Brener Esmeraldo-like strain (TcCLB.510287.30; UniProtKB ID Q4CU77), which was not found in the top 3% binders for GNF6702. Compared to the binding site described in the original article, which is situated adjacent to the residues F24 and I29 of the β4 subunit, near the β5 subunit, the pocket predicted by P2Rank and used in the docking was not found near those residues. Similar to the case of the FeSOD, the binding site might be formed in the junction of the two protein subunits, and so the correct binding site could not have been predicted. Nevertheless, it is noteworthy that position 1 out of 55 from GNF6702 top binders is occupied by the proteasome β3 subunit (TcCLB.506779.50, UniProtKB Q4DHA9). Mapping this subunit's model onto the *Leishmania tarentolae* proteasome structure 6QM8, it can be visualized that the β3 subunit predicted binding site is in close proximity to the actual proteasome β2 subunit, which a BLAST search confirmed it to be the *T. cruzi* CL Brener Non-Esmeraldo-like (TcCLB.508461.430, UniProtKB Q4E4R6). A superposition of the β4 Q4CU77 subunit on the β2 Q4E4R6 subunit shows that the loop containing the F24 and I29 residues of β4 subunit matches the β2 loop in proximity to the predicted β3 binding site (**Figure 7**). A possible explanation would be that this loop plays an important role in GNF6702 sensitivity, and thus the proteasome β3 subunit could be a reasonable target for this ligand.

Mitochondria-affecting compounds

In the case of compounds C16-2, C26-6 and C8-3, they are all proposed to act at the mitochondrial level. These three compounds appear to cause a bioenergetic collapse of the cell (2021a; 2021b; Martín-Escolano et al., 2018a). We found that the respiratory complex I NADH-ubiquinone oxidoreductase

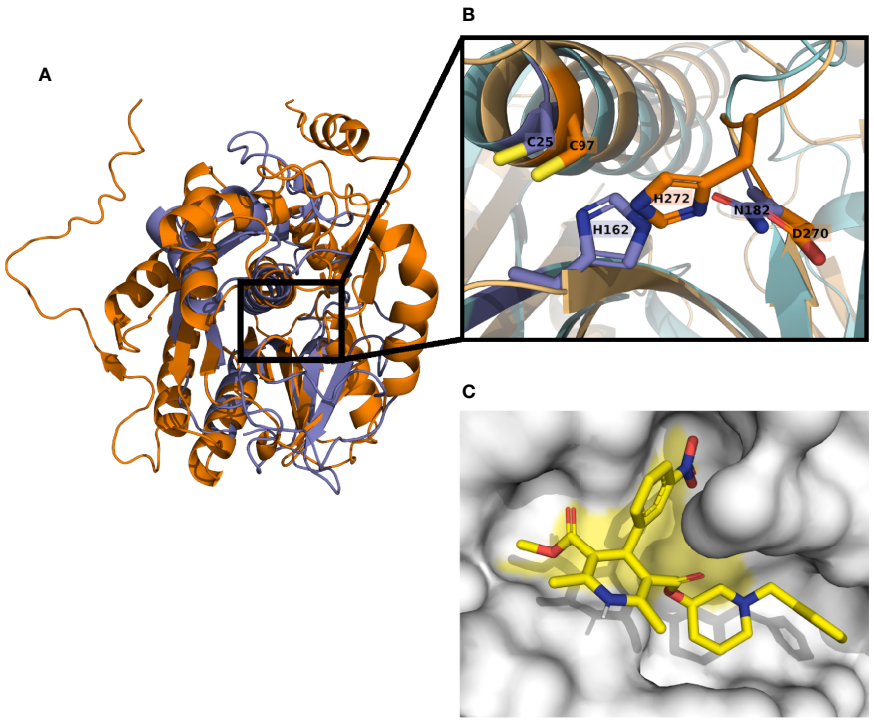

FIGURE 5 | *T. cruzi* cysteine peptidase Q4D5K1 model aligned with cruzipain structure 4PI3. Structural similarities can be appreciated between cruzipain (blue) and the cysteine peptidase Q4D5K1 (orange) **(A)**. The catalytic triad in cruzipain is composed by residues C25-H162 -N182, and aligns with the putative catalytic triad C97-H272-D270 of the cysteine peptidase **(B)**. Docking predictions show benidipine (yellow) binding in the catalytic site (yellow area) of the cysteine peptidase **(C)**.

(TcCLB.506513.190, Q4DPI1), the catalytic first step in the electron transport chain, was selected in the top 3% in both C16-2 (position 35 out of 56) and C26-6 (position 2 out of 56), which would agree with what is described about these two compounds. Besides, C16-2 is a 3-alkoxy-1-vinylindazoles compound and thus belongs to the indazole family for which information about their mechanism of action on *T. cruzi* is scant in the literature. Some works suggest that indazoles are able to lead both the formation of ROS through their nitro group and also inhibit the trypanothione reductase (Aguilera-Venegas et al., 2013). Unfortunately, we did not find any of those enzymes in the top 3% reported for these ligands. Notably, dihydroorotate dehydrogenase (fumarate) (TcCLB.508375.50, Q4D3W2) was found in position 11 (out of 56) in C26-6 and 18 (out of 56) in C16-2, and aspartate carbamoyltransferase (TcCLB.507091.50, Q4DGV1) and orotidine-5-phosphate decarboxylase/orotate phosphoribosyltransferase (TcCLB.508373.29, Q4CSV7) were respectively found in positions 3 and 24 out of 56 in C16-2. These three enzymes are involved in the pyrimidine synthesis pathway, essential for parasite survival (Inaoka et al., 2017). Thus, it could be interesting to perform inhibition studies with these enzymes in search of a possible novel mechanism of action of indazoles compounds.

For C8-3, we retrieved the ATP synthase F_1 subunit gamma (TcCLB.511145.60, Q4D1H0), mediator of the final step in the electron transport chain, selected in position 32 out of 56, which could also be the target of this compound. Interestingly, we also found trans-sialidase enzymes (TcCLB.505931.30 Q4CWF1, TcCLB.506515.29 Q4CPR9, TcCLB.508089.10 Q4CYW1 and TcCLB.509817.50 Q4CZP0) at positions 7, 8, 12 and 18 out of 56 for this same compound. C8-3 lightly resembles some benzoic acid derivatives that have been described to target the trans-sialidase protein family by another virtual screening study (Vázquez-Jiménez et al., 2021). Additionally, the presence of fluorine atoms, aside from increasing their metabolic stability and membrane permeation, could be involved in protein-ligand short contacts further increasing C8-3 binding affinity (Zhou et al., 2009).

Glycosome-affecting compounds

Finally, C7-4 is a polyamine compound based on the well-known tripodal polyamine tris(2-amimoethyl)amine moiety (Martín-Escolano et al., 2019). Martin-Escolano and co-workers performed metabolism excretion, mitochondrial membrane potential and SOD-inhibition studies in order to decipher C7-4 mechanism of action. Their results showed that C7-4 anti-*T. cruzi* activity could be related to its effect at the glycosomal level (Martín-Escolano et al., 2019). In our analysis, we found a TcCLB.507009.10 (Q4DC12) glycosomal membrane protein, also annotated as Gim5A protein, occupying position 24 out of 55 in the top selected binders. It has been described that this protein might play an important role in the parasite transition

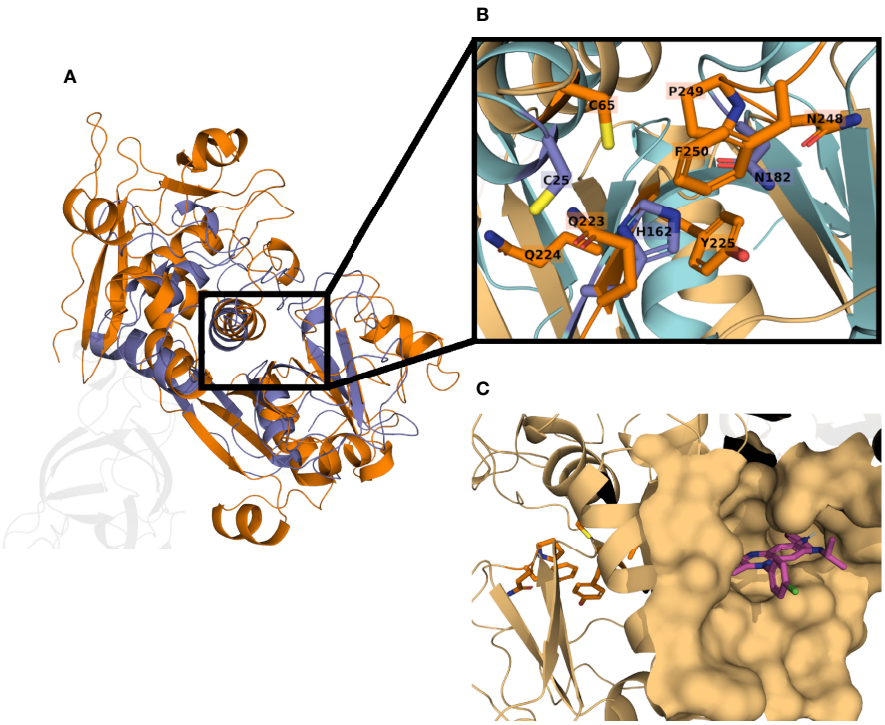

FIGURE 6 | *T. cruzi* calpain-like peptidase Q4CMV9 model aligned with cruzipain structure 4PI3. Structural similarities can be appreciated between cruzipain (blue) and the calpain-like peptidase Q4CMV9 (orange) **(A)**; unaligned residues in the C-terminal domain are shown transparent. The calpain-like peptidase shows an inactive catalytic site, lacking the basic residue, typically a histidine, necessary to deprotonate the cysteine **(B)**. The binding site of clofazimine (magenta) is located far from the inactivated catalytic site (orange residues), suggesting another mechanism of action **(C)**.

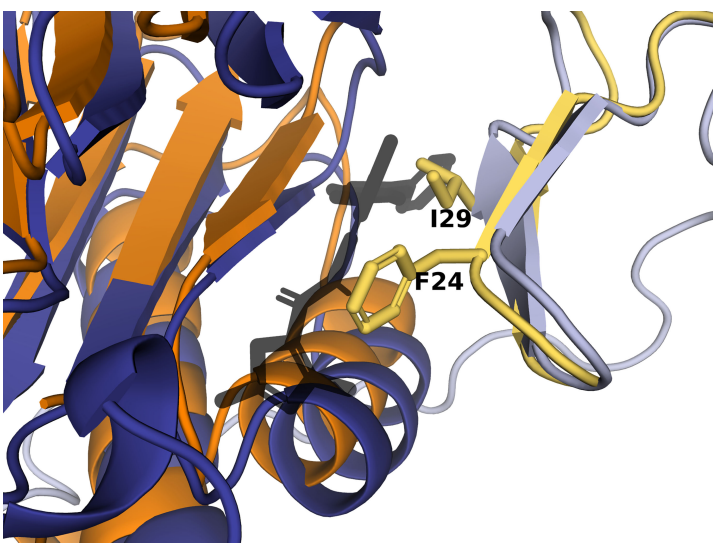

FIGURE 7 | *T. cruzi* proteasome β2 and β3 subunits superimposed with β4 and β5 subunits. The β2 (light blue) and β3 (dark blue) subunits were mapped unto the *L. tarentolae* corresponding proteasome subunits in PDB structure 6QM8. GNF6702 (dark shadow) binds with high affinity with subunit β3. The β4 (light orange) and β5 (dark orange) subunits were superposed to the β2 and β3 subunits, respectively. The β4 F24 and I29 residues, which are believed to play a role in GNF6702 sensitivity, are shown as sticks.

from proliferative to stationary phase (Avila et al., 2018). In *T. brucei*, Gim5A and Gim5B are the most abundant glycosome membrane proteins, and depletion of the latter is lethal for the bloodstream form (Maier et al., 2001). However, there is no evidence of this protein in *T. cruzi*. On the other hand, polyamines are polycationic compounds essential for the growth and function of *T. cruzi* parasites, including cellular processes like the synthesis of trypanothione (Talevi et al., 2019). The thiol-polyamine metabolism of *T. cruzi* has been previously shown to be a suitable drug target due to its unique configuration and dependency on external supply (Reigada et al., 2018; Talevi et al., 2019). We found that C7-4 targeted spermidine synthases, the enzyme that converts putrescine into spermidine, in positions 43 (TcCLB.503855.20, Q4DBH6) and 48 (TcCLB.504033.130, Q4DR69) out of 55 in the top 3%. In addition, trypanothione reductase (TcCLB.504507.5, Q4CMQ7) was found at position 53. Our docking results showed that C7-4 is allocated in the flavin adenine dinucleotide (FAD) coenzyme site of the trypanothione reductase (Garrard et al., 2000; Beltran-Hortelano et al., 2017). Specifically, the fluorene moiety of C7-4 accommodates at the catalytic site near Cys53 and Cys58 residues, similarly to other polyamine derivatives with large substituents (Garrard et al., 2000). Altogether, the previously performed *in vitro* assays and our docking results could suggest multiple targeting for this compound.

CONCLUSIONS

AlphaFold models of *T. cruzi* proteins open the way to new opportunities in drug discovery against this parasite, allowing to explore targets that have lacked structural information to date. With the aim to validate the application of this resource for computational drug screening purposes, we selected compounds with known targets or effects and launched an inverse virtual screening against the AlphaFold *T. cruzi* proteome. We found that some of the targets derived from the computational analysis successfully matched their experimentally described targets, while others showed a more nuanced result. The work performed identified some caveats of the virtual approach that must be taken into consideration. For instance, the quality of the models had a great variability between proteins, and given that precise residue positions and orientations are paramount in virtual drug screening experiments, we had to discard many of the structures from the subsequent docking simulations. Recently, a new pipeline based on AlphaFold has been developed, focused on improving the quality of models for trypanosomatids (Wheeler, 2021). This would provide very useful for "classical" virtual screening experiments, where usually just a few protein targets are studied, and so new models could be generated for these. Since models available at the AlphaFold Protein Structure Database only consider monomeric proteins, they cannot illustrate multimeric complexes and thus the binding sites formed in the interactions between subunits. This issue might be circumvented in the near future, as a new AlphaFold multimeric algorithm has been developed. On the other hand, some fine-tuning will be necessary for protein models that have post-translational modifications such as propeptides that need to be cleaved, or those proteins that have cofactors in their binding sites which must be considered to correctly predict binding affinities with ligands. Additional steps could be taken in order to further pinpoint suitable targets for a compound. For example, excluding from the top binders those proteins that are non-essential or those with multiple gene copies, and also prioritizing proteins which exert a high flux control on specific metabolic pathways (Olin-Sandoval et al., 2012). Furthermore, performing this inverse virtual screening pipeline with non-active analogs of the studied compound would also help to validate their specificity to any particular target; however, this is only doable with specific compound families and not in large-scale screenings such as the one we present here. All these steps, together with the results of phenotypic screening experiments, would help to propose a list of targets to be finally tested in an experimental setting. Despite these limitations, AlphaFold appears to be an extremely useful tool to study the 3D-space location of *Trypanosoma cruzi* proteins. Crystal structures deposited in PDB will be the gold standard, but these are scarce for neglected parasites, for which AlphaFold can contribute to fill (part of) the gap. While caution is advisable when using these models, some of them can show a high degree of quality, even comparable to PDB structures. Thus, they could be used not only for target deconvolution, but also for virtual screenings of chemical entities from diverse origin and nature in the search of new drugs to treat Chagas disease.

DATA AVAILABILITY STATEMENT

The original contributions presented in the study are included in the article/**Supplementary Material**. Further inquiries can be directed to the corresponding authors.

AUTHOR CONTRIBUTIONS

AR-L: conceptualization, methodology, software, formal analysis, investigation, writing - original draft, and visualization. NM-P: conceptualization, methodology, investigation, and writing - original draft. JB: validation and writing - review and editing. JG: validation and writing - review and editing. JA: conceptualization, validation, writing - review and editing, and supervision. All authors contributed to the article and approved the submitted version.

ACKNOWLEDGMENTS

We acknowledge support from the Spanish Ministry of Science and Innovation and State Research Agency through the "Centro de Excelencia Severo Ochoa 2019-2023" Program (CEX2018-

000806-S), and support from the Generalitat de Catalunya through the CERCA Program. This research was supported by CIBER -Consorcio Centro de Investigación Biomédica en Red- (CB 2021), Instituto de Salud Carlos III, Ministerio de Ciencia e Innovación and Unión Europea—NextGenerationEU.

SUPPLEMENTARY MATERIAL

The Supplementary Material for this article can be found online at: https://www.frontiersin.org/articles/10.3389/fcimb.2022.944748/full#supplementary-material

REFERENCES

Adesse, D., Meirelles Azzam, E., de Nazareth L. Meirelles, M., Urbina, J. A., and Garzoni, L. R. (2011). Amiodarone Inhibits *Trypanosoma Cruzi* Infection and Promotes Cardiac Cell Recovery With Gap Junction and Cytoskeleton Reassembly *In Vitro*. *Antimicrob. Agents Chemother.* 55, 203–210. doi: 10.1128/AAC.01129-10

Aguilera-Venegas, B., Olea-Azar, C., Arán, V. J., and Speisky, H. (2013). Indazoles: A New Top Seed Structure in the Search of Efficient Drugs Against *Trypanosoma Cruzi*. *Future Med. Chem.* 5, 1843–1859. doi: 10.4155/fmc.13.144

Alonso-Padilla, J., Cortés-Serra, N., Pinazo, M. J., Bottazzi, M. E., Abril, M., Barreira, F., et al. (2019). Strategies to Enhance Access to Diagnosis and Treatment for Chagas Disease Patients in Latin America. *Expert Rev. Anti-infect. Ther.* 17, 145–157. doi: 10.1080/14787210.2019.1577731

Amos, B., Aurrecoechea, C., Barba, M., Barreto, A., Basenko, E. Y., Bażant, W., et al. (2022). VEuPathDB: The Eukaryotic Pathogen, Vector and Host Bioinformatics Resource Center. *Nucleic Acids Res.* 50, D898–D911. doi: 10.1093/nar/gkab929

Aslett, M., Aurrecoechea, C., Berriman, M., Brestelli, J., Brunk, B. P., Carrington, M., et al. (2010). TriTrypDB: A Functional Genomic Resource for the Trypanosomatidae. *Nucleic Acids Res.* 38, D457–D462. doi: 10.1093/nar/gkp851

Atwood, J. A., Weatherly, D. B., Minning, T. A., Bundy, B., Cavola, C., Opperdoes, F. R., et al. (2005). The *Trypanosoma Cruzi* Proteome. *Science* 309, 473–476. doi: 10.1126/science.1110289

Avila, C. C., Mule, S. N., Rosa-Fernandes, L., Viner, R., Barisón, M. J., Costa-Martins, A. G., et al. (2018). Proteome-Wide Analysis of *Trypanosoma Cruzi* Exponential and Stationary Growth Phases Reveals a Subcellular Compartment-Specific Regulation. *Genes* 9, 413. doi: 10.3390/genes9080413

Belew, A. T., Junqueira, C., Rodrigues-Luiz, G. F., Valente, B. M., Oliveira, A. E. R., Polidoro, R. B., et al. (2017). Comparative Transcriptome Profiling of Virulent and non-Virulent *Trypanosoma Cruzi* Underlines the Role of Surface Proteins During Infection. *PloS Pathog.* 13, e1006767. doi: 10.1371/journal.ppat.1006767

Beltran-Hortelano, I., Alcolea, V., Font, M., and Pérez-Silanes, S. (2022). Examination of Multiple *Trypanosoma Cruzi* Targets in a New Drug Discovery Approach for Chagas Disease. *Bioorg. Med. Chem.* 58, 116577. doi: 10.1016/j.bmc.2021.116577

Beltran-Hortelano, I., Perez-Silanes, S., and Galiano, S. (2017). Trypanothione Reductase and Superoxide Dismutase as Current Drug Targets for *Trypanosoma Cruzi*: An Overview of Compounds With Activity Against Chagas Disease. *CMC* 24, 1066–1138. doi: 10.2174/0929867323666161227094049

Benaim, G., Paniz-Mondolfi, A. E., and Sordillo, E. M. (2021). The Rationale for Use of Amiodarone and its Derivatives for the Treatment of Chagas' Disease and Leishmaniasis. *CPD* 27, 1825–1833. doi: 10.2174/1381612826666200928161403

Chatelain, E., and Ioset, J.-R. (2018). Phenotypic Screening Approaches for Chagas Disease Drug Discovery. *Expert Opin. Drug Discovery* 13, 141–153. doi: 10.1080/17460441.2018.1417380

Crowther, G. J., Shanmugam, D., Carmona, S. J., Doyle, M. A., Hertz-Fowler, C., Berriman, M., et al. (2010). Identification of Attractive Drug Targets in Neglected-Disease Pathogens Using an In Silico Approach. *PloS Negl. Trop. Dis.* 4, e804. doi: 10.1371/journal.pntd.0000804

Dear, N., Matena, K., Vingron, M., and Boehm, T. (1997). A New Subfamily of Vertebrate Calpains Lacking a Calmodulin-Like Domain: Implications for Calpain Regulation and Evolution. *Genomics* 45, 175–184. doi: 10.1006/geno.1997.4870

Docampo, R., and Moreno, S. N. J. (2011). Acidocalcisomes. *Cell Calc.* 50, 113–119. doi: 10.1016/j.ceca.2011.05.012

Ersfeld, K., Barraclough, H., and Gull, K. (2005). Evolutionary Relationships and Protein Domain Architecture in an Expanded Calpain Superfamily in Kinetoplastid Parasites. *J. Mol. Evol.* 61, 742–757. doi: 10.1007/s00239-004-0272-8

Feinstein, W. P., and Brylinski, M. (2015). Calculating an Optimal Box Size for Ligand Docking and Virtual Screening Against Experimental and Predicted Binding Pockets. *J. Cheminform.* 7, 18. doi: 10.1186/s13321-015-0067-5

Garrard, E. A., Borman, E. C., Cook, B. N., Pike, E. J., and Alberg, D. G. (2000). Inhibition of Trypanothione Reductase by Substrate Analogues. *Org. Lett.* 2, 3639–3642. doi: 10.1021/ol0065423

Hall, B. S., Bot, C., and Wilkinson, S. R. (2011). Nifurtimox Activation by Trypanosomal Type I Nitroreductases Generates Cytotoxic Nitrile Metabolites. *J. Biol. Chem.* 286, 13088–13095. doi: 10.1074/jbc.M111.230847

Hanwell, M. D., Curtis, D. E., Lonie, D. C., Vandermeersch, T., Zurek, E., and Hutchison, G. R. (2012). Avogadro: An Advanced Semantic Chemical Editor, Visualization, and Analysis Platform. *J. Cheminform.* 4, 17. doi: 10.1186/1758-2946-4-17

Hekkelman, M. L., Vries, I., Joosten, R. P., and Perrakis, A. (2021). AlphaFill: Enriching the AlphaFold Models With Ligands and Co-Factors. *bioRxiv* 11, 26. doi: 10.1101/2021.11.26.470110

Inaoka, D. K., Iida, M., Hashimoto, S., Tabuchi, T., Kuranaga, T., Balogun, E. O., et al. (2017). Design and Synthesis of Potent Substrate-Based Inhibitors of the *Trypanosoma Cruzi* Dihydroorotate Dehydrogenase. *Bioorg. Med. Chem.* 25, 1465–1470. doi: 10.1016/j.bmc.2017.01.009

Jumper, J., Evans, R., Pritzel, A., Green, T., Figurnov, M., Ronneberger, O., et al. (2021). Highly Accurate Protein Structure Prediction With AlphaFold. *Nature* 596, 583–589. doi: 10.1038/s41586-021-03819-2

Khare, S., Nagle, A. S., Biggart, A., Lai, Y. H., Liang, F., Davis, L. C., et al. (2016). Proteasome Inhibition for Treatment of Leishmaniasis, Chagas Disease and Sleeping Sickness. *Nature* 537, 229–233. doi: 10.1038/nature19339

Kim, S., Chen, J., Cheng, T., Gindulyte, A., He, J., He, S., et al. (2021). PubChem in 2021: New Data Content and Improved Web Interfaces. *Nucleic Acids Res.* 49, D1388–D1395. doi: 10.1093/nar/gkaa971

Krivák, R., and Hoksza, D. (2018). P2Rank: Machine Learning Based Tool for Rapid and Accurate Prediction of Ligand Binding Sites From Protein Structure. *J. Cheminform.* 10, 39. doi: 10.1186/s13321-018-0285-8

Kubota, K., Funabashi, M., and Ogura, Y. (2019). Target Deconvolution From Phenotype-Based Drug Discovery by Using Chemical Proteomics Approaches. *Biochim. Biophys. Acta (BBA) - Proteins Proteomics* 1867, 22–27. doi: 10.1016/j.bbapap.2018.08.002

Landrum, G., Tosco, P., Kelley, B., Ric,, Sriniker,, Gedeck,, et al. (2021). RDKit: Open-Source Cheminformatics Software. 2021_09_2 (Q3 2021) Release. *Zenodo*. doi: 10.5281/ZENODO.5589557

Lepesheva, G. I., Hargrove, T. Y., Anderson, S., Kleshchenko, Y., Furtak, V., Wawrzak, Z., et al. (2010). Structural Insights Into Inhibition of Sterol 14α-Demethylase in the Human Pathogen *Trypanosoma Cruzi**. *J. Biol. Chem.* 285, 25582–25590. doi: 10.1074/jbc.M110.133215

Lepesheva, G. I., Villalta, F., and Waterman, M. R. (2011). "Targeting Trypanosoma Cruzi Sterol 14α-Demethylase (Cyp51)," in *Advances in Parasitology* (Elsevier: Academic Press), 65–87. doi: 10.1016/B978-0-12-385863-4.00004-6

Li, Y., Shah-Simpson, S., Okrah, K., Belew, A. T., Choi, J., Caradonna, K. L., et al. (2016). Transcriptome Remodeling in *Trypanosoma Cruzi* and Human Cells During Intracellular Infection. *PloS Pathog.* 12, e1005511. doi: 10.1371/journal.ppat.1005511

Maier, A., Lorenz, P., Voncken, F., and Clayton, C. (2001). An Essential Dimeric Membrane Protein of Trypanosome Glycosomes. *Mol. Microbiol.* 39, 1443–1451. doi: 10.1046/j.1365-2958.2001.02333.x

Marchini, F. K., Godoy, L. M. F., de Rampazzo, R. C. P., Pavoni, D. P., Probst, C. M., Gnad, F., et al. (2011). Profiling the *Trypanosoma Cruzi* Phosphoproteome. *PloS One* 6, e25381. doi: 10.1371/journal.pone.0025381

Mariani, V., Biasini, M., Barbato, A., and Schwede, T. (2013). lDDT: A Local Superposition-Free Score for Comparing Protein Structures and Models Using Distance Difference Tests. *Bioinformatics* 29, 2722–2728. doi: 10.1093/bioinformatics/btt473

Martín-Escolano, R., Aguilera-Venegas, B., Marín, C., Martín-Montes, Á., Martín-Escolano, J., Medina-Carmona, E., et al. (2018a). Synthesis and Biological *In Vitro* and *In Vivo* Evaluation of 2-(5-Nitroindazol-1-Yl)Ethylamines and Related Compounds as Potential Therapeutic Alternatives for Chagas Disease. *ChemMedChem* 13, 2104–2118. doi: 10.1002/cmdc.201800512

Martín-Escolano, R., Etxebeste-Mitxeltorena, M., Martín-Escolano, J., Plano, D., Rosales, M. J., Espuelas, S., et al. (2021a). Selenium Derivatives as Promising Therapy for Chagas Disease: *In Vitro* and *In Vivo* Studies. *ACS Infect. Dis.* 7, 1727–1738. doi: 10.1021/acsinfecdis.1c00048

Martín-Escolano, R., Molina-Carreño, D., Delgado-Pinar, E., Martin-Montes, Á., Clares, M. P., Medina-Carmona, E., et al. (2019). New Polyamine Drugs as More Effective Antichagas Agents Than Benznidazole in Both the Acute and Chronic Phases. *Eur. J. Med. Chem.* 164, 27–46. doi: 10.1016/j.ejmech.2018.12.034

Martín-Escolano, R., Molina-Carreño, D., Plano, D., Espuelas, S., Rosales, M. J., Moreno, E., et al. (2021b). Library of Selenocyanate and Diselenide Derivatives as *In Vivo* Antichagasic Compounds Targeting *Trypanosoma Cruzi* Mitochondrion. *Pharmaceuticals* 14, 419. doi: 10.3390/ph14050419

Martín-Escolano, R., Moreno-Viguri, E., Santivañez-Veliz, M., Martin-Montes, A., Medina-Carmona, E., Paucar, R., et al. (2018b). Second Generation of Mannich Base-Type Derivatives With *in Vivo* Activity Against *Trypanosoma Cruzi*. *J. Med. Chem.* 61, 5643–5663. doi: 10.1021/acs.jmedchem.8b00468

Martínez-Peinado, N., Cortes-Serra, N., Losada-Galvan, I., Alonso-Vega, C., Urbina, J. A., Rodríguez, A., et al. (2020). Emerging Agents for the Treatment of Chagas Disease: What is in the Preclinical and Clinical Development Pipeline? *Expert Opin. Invest. Drugs* 29, 947–959. doi: 10.1080/13543784.2020.1793955

Maya, J. D., Cassels, B. K., Iturriaga-Vásquez, P., Ferreira, J., Faúndez, M., Galanti, N., et al. (2007). Mode of Action of Natural and Synthetic Drugs Against *Trypanosoma Cruzi* and Their Interaction With the Mammalian Host. *Comp. Biochem. Physiol. Part A.: Mol. Integr. Physiol.* 146, 601–620. doi: 10.1016/j.cbpa.2006.03.004

O'Boyle, N. M., Banck, M., James, C. A., Morley, C., and Vandermeersch, T. (2011). And Hutchison, GOpen Babel: An Open Chemical Toolbox. *R.J. Cheminform.* 3, 33. doi: 10.1186/1758-2946-3-33

Olin-Sandoval, V., González-Chávez, Z., Berzunza-Cruz, M., Martínez, I., Jasso-Chávez, R., Becker, I., et al. (2012). Drug Target Validation of the Trypanothione Pathway Enzymes Through Metabolic Modelling. *FEBS J.* 279, 1811–1833. doi: 10.1111/j.1742-4658.2012.08557.x

Paucar, R., Martín-Escolano, R., Moreno-Viguri, E., Azqueta, A., Cirauqui, N., Marín, C., et al. (2019). Rational Modification of Mannich Base-Type Derivatives as Novel Antichagasic Compounds: Synthesis, *In Vitro* and *In Vivo* Evaluation. *Bioorg. Med. Chem.* 27, 3902–3917. doi: 10.1016/j.bmc.2019.07.029

Prata, A. (2001). Clinical and Epidemiological Aspects of Chagas Disease. *Lancet Infect. Dis.* 1, 92–100. doi: 10.1016/S1473-3099(01)00065-2

Reigada, C., Phanstiel, O., Miranda, M. R., and Pereira, C. A. (2018). Targeting Polyamine Transport in *Trypanosoma Cruzi*. *Eur. J. Med. Chem.* 147, 1–6. doi: 10.1016/j.ejmech.2018.01.083

Sbaraglini, M. L., Bellera, C. L., Fraccaroli, L., Larocca, L., Carrillo, C., Talevi, A., et al. (2016). Novel Cruzipain Inhibitors for the Chemotherapy of Chronic Chagas Disease. *Int. J. Antimicrob. Agents* 48, 91–95. doi: 10.1016/j.ijantimicag.2016.02.018

Scarim, C., Olmo, F., Ferreira, E., Chin, C., Kelly, J., and Francisco, A. (20216930). Image-Based *In Vitro* Screening Reveals the Trypanostatic Activity of Hydroxymethylnitrofurazone Against *Trypanosoma Cruzi*. *IJMS* 22 (13), 6930. doi: 10.3390/ijms22136930

Schrödinger, L. L. C. (2015). *The PyMOL Molecular Graphics System, Version 2.4.1.*

Smircich, P., Eastman, G., Bispo, S., Duhagon, M. A., Guerra-Slompo, E. P., Garat, B., et al. (2015). Ribosome Profiling Reveals Translation Control as a Key Mechanism Generating Differential Gene Expression in *Trypanosoma Cruzi*. *BMC Genomics* 16, 443. doi: 10.1186/s12864-015-1563-8

Stein, C., Migliavaca, C. B., Colpani, V., da Rosa, P. R., Sganzerla, D., Giordani, N. E., et al. (2018). Amiodarone for Arrhythmia in Patients With Chagas Disease: A Systematic Review and Individual Patient Data Meta-Analysis. *PloS Negl. Trop. Dis.* 12, e0006742. doi: 10.1371/journal.pntd.0006742

Talevi, A., Carrillo, C., and Comini, M. (2019). The Thiol-Polyamine Metabolism of *Trypanosoma Cruzi*: Molecular Targets and Drug Repurposing Strategies. *CMC* 26, 6614–6635. doi: 10.2174/0929867325666180926151059

Terstappen, G. C., Schlüpen, C., Raggiaschi, R., and Gaviraghi, G. (2007). Target Deconvolution Strategies in Drug Discovery. *Nat. Rev. Drug Discovery* 6, 891–903. doi: 10.1038/nrd2410

The UniProt Consortium (2021). UniProt: The Universal Protein Knowledgebase in 2021. *Nucleic Acids Res.* 49, D480–D489. doi: 10.1093/nar/gkaa1100

Trott, O., and Olson, A. J. (2009). AutoDock Vina: Improving the Speed and Accuracy of Docking With a New Scoring Function, Efficient Optimization, and Multithreading. *J. Comput. Chem.* 31 (2), 455–461 doi: 10.1002/jcc.21334.

Tunyasuvunakool, K., Adler, J., Wu, Z., Green, T., Zielinski, M., Žídek, A., et al. (2021). Highly Accurate Protein Structure Prediction for the Human Proteome. *Nature* 596, 590–596. doi: 10.1038/s41586-021-03828-1

Varadi, M., Anyango, S., Deshpande, M., Nair, S., Natassia, C., Yordanova, G., et al. (2022). AlphaFold Protein Structure Database: Massively Expanding the Structural Coverage of Protein-Sequence Space With High-Accuracy Models. *Nucleic Acids Res.* 50, D439–D444. doi: 10.1093/nar/gkab1061

Vázquez-Jiménez, L. K., Paz-González, A. D., Juárez-Saldivar, A., Uhrig, M. L., Agusti, R., Reyes-Arellano, A., et al. (2021). Structure-Based Virtual Screening of New Benzoic Acid Derivatives as *Trypanosoma Cruzi* Trans-Sialidase Inhibitors. *MC* 17, 724–731. doi: 10.2174/1573406416666200506084611

Wheeler, R. J. (2021). A Resource for Improved Predictions of Trypanosoma and Leishmania Protein Three-Dimensional Structure. *PloS One* 16, e0259871. doi: 10.1371/journal.pone.0259871

Wilkinson, S. R., Taylor, M. C., Horn, D., Kelly, J. M., and Cheeseman, I. (2008). A Mechanism for Cross-Resistance to Nifurtimox and Benznidazole in Trypanosomes. *Proc. Natl. Acad. Sci. U.S.A.* 105, 5022–5027. doi: 10.1073/pnas.0711014105

World Health Organization (2022) *Chagas Disease (Also Known as American Trypanosomiasis)*. Available at: https://www.who.int/news-room/fact-sheets/detail/chagas-disease-(american-trypanosomiasis) (Accessed April 28, 2022).

Yang, L., Luo, H., Chen, J., Xing, Q., and He, L. (2009). SePreSA: A Server for the Prediction of Populations Susceptible to Serious Adverse Drug Reactions Implementing the Methodology of a Chemical–Protein Interactome. *Nucleic Acids Res.* 37, W406–W412. doi: 10.1093/nar/gkp312

Zhou, P., Zou, J., Tian, F., and Shang, Z. (2009). Fluorine Bonding — How Does It Work In Protein–Ligand Interactions? *J. Chem. Inf. Model.* 49, 2344–2355. doi: 10.1021/ci9002393

Conflict of Interest: The authors declare that the research was conducted in the absence of any commercial or financial relationships that could be construed as a potential conflict of interest.

Publisher's Note: All claims expressed in this article are solely those of the authors and do not necessarily represent those of their affiliated organizations, or those of the publisher, the editors and the reviewers. Any product that may be evaluated in this article, or claim that may be made by its manufacturer, is not guaranteed or endorsed by the publisher.

frontiers | Frontiers in Cellular and Infection Microbiology

TYPE Brief Research Report
PUBLISHED 28 July 2022
DOI 10.3389/fcimb.2022.885268

OPEN ACCESS

EDITED BY
Vilma G. Duschak,
Consejo Nacional de Investigaciones Científicas y Técnicas (CONICET), Argentina

REVIEWED BY
Esteban Serra,
National University of Rosario, Argentina
Ana Lia Mazzeti,
Minas Gerais State University, Brazil

*CORRESPONDENCE
Laura Fraccaroli
lfraccaroli@fundacioncassara.org.ar
Carolina Carrillo
ccarrillo@centromilstein.org.ar

†These authors have contributed equally to this work and share first authorship

SPECIALTY SECTION
This article was submitted to Clinical Microbiology, a section of the journal Frontiers in Cellular and Infection Microbiology

RECEIVED 27 February 2022
ACCEPTED 05 July 2022
PUBLISHED 28 July 2022

CITATION
Fraccaroli L, Ruiz MD, Perdomo VG, Clausi AN, Balcazar DE, Larocca L and Carrillo C (2022) Broadening the spectrum of ivermectin: Its effect on *Trypanosoma cruzi* and related trypanosomatids. *Front. Cell. Infect. Microbiol.* 12:885268. doi: 10.3389/fcimb.2022.885268

Broadening the spectrum of ivermectin: Its effect on *Trypanosoma cruzi* and related trypanosomatids

Laura Fraccaroli[1*†], María Daniela Ruiz[1†], Virginia Gabriela Perdomo[2], Agustina Nicole Clausi[1], Darío Emmanuel Balcazar[2], Luciana Larocca[1] and Carolina Carrillo[1*]

[1]Laboratorio de Biología Molecular y Bioquímica en *Trypanosoma* cruzi y otros agentes infecciosos, CONICET for Instituto de Ciencia y Tecnología (ICT) Milstein - Consejo Nacional de Investigaciones Científicas y Tecnológicas (CONICET), Buenos Aires, Argentina, [2]Área Parasitología, Microbiología, Facultad de Ciencias Bioquímicas y Farmacéuticas, Universidad Nacional de Rosario (UNR), Rosario, Argentina, [3]Centro de Estudios Parasitológicos y Vectores (CEPAVE), CONICET - Universidad Nacional de La Plata (UNLP), La Plata, Argentina

Chagas disease is an endemic American parasitosis, caused by *Trypanosoma cruzi*. The current therapies, benznidazole (BZN) and nifurtimox (NFX), show limited efficacy and multiple side effects. Thus, there is a need to develop new trypanocidal strategies. Ivermectin (IVM) is a broad-spectrum antiparasitic drug with low human and veterinary toxicity with effects against *T. brucei* and *Leishmania* spp. Considering this and its relatively low cost, we evaluate IVM as a potential repurposed trypanocidal drug on *T. cruzi* and other trypanosomatids. We found that IVM affected, in a dose-dependent manner, the proliferation of *T. cruzi* epimastigotes as well as the amastigotes and trypomastigotes survival. The Selectivity Index for the amastigote stage with respect to Vero cells was 12. The IVM effect was also observed in *Phytomonas jma 066* and *Leishmania mexicana* proliferation but not in *Crithidia fasciculata*. On the epimastigote stage, the IVM effect was trypanostatic at 50 μM but trypanocidal at 100 μM. The assays of the drug combinations of IVM with BNZ or NFX showed mainly additive effects among combinations. *In silico* studies showed that classical structures belonging to glutamate-gated Cl channels, the most common IVM target, are absent in kinetoplastids. However, we found in the studied trypanosomatid genomes one copy for putative IMPα and IMPβ, potential targets for IVM. The putative IMPα genes (with 76% similarity) showed conserved Armadillo domains but lacked the canonical IMPβ binding sequence. These results allowed us to propose a novel molecular target in *T. cruzi* and suggest IVM as a good candidate for drug repurposing in the Chagas disease context.

KEYWORDS

Chagas disease, ivermectin, drug repurposing, trypanocidal drug, drug combination, *Trypanosoma cruzi*

Introduction

Chagas disease, caused by the protozoan parasite *Trypanosoma cruzi*, is considered a neglected tropical disease (NTD) (World Health Organization, 2015). This originally American endemic affects at least 6 million people and has been globally spread with the recent migrations (Pérez-Molina and Molina, 2018), estimating that 75 million people are at risk of contracting the disease. The social and economic impact of this disease is significant, with 14,000 annual deaths and 40,000 new cases every year (Nunes et al., 2013).

In addition to the complexity of social, economic, and biomedical issues about Chagas disease, there are only two drugs accepted for its treatment: nifurtimox (NFX) and benznidazole (BZN). Both drugs, developed 50 years ago, show very variable parasitological cure rates depending on the disease stage and present several adverse effects (Nunes et al., 2013). Thus, there is a clear need to find new therapies against Chagas disease to provide better assistance and life quality to patients and to reduce the social and economic burden associated with contagion and chronicity. A cost- and time-saving strategy to discover new trypanocidal treatments is drug repurposing, finding new therapeutic indications for drugs that are already approved for its use in humans (Bellera et al., 2013).

Ivermectin (IVM) is a broad-spectrum antiparasitic drug, initially developed to combat parasitic worms in veterinary fields (Campbell et al., 1983). It is a mixture of semisynthetic macrocyclic lactones (~80% 22,23-dihydro-avermectin B1a and ~20% 22,23-dihydro-avermectin B1b) (Crump, 2017; Deng et al., 2019). Nowadays, IVM is used mainly as an oral medication in the primary treatment of onchocerciasis, lymphatic filariasis, and strongyloidiasis infections, all caused by different nematode species (Turner and Schaeffer, 1989; Laing et al., 2017). IVM also affects arthropod ectoparasites, being used in the treatment of scabies (Thomas et al., 2015), ticks (Sheele et al., 2014), and head lice (Devore and Schutze, 2015).

In WHO massive antiparasitic-drug administration programs, it was observed that the incidence of malaria seemed to decrease in pediatric groups treated with IVM (Alout et al., 2014; Chaccour and Rabinovich, 2019). Further studies showed that IVM has presented *in vitro* and *in vivo* antimalarial effects, arresting the cell cycle and inhibiting parasite development and survival (Mendes et al., 2017; de Carvalho et al., 2019). In regard to trypanosomatids, IVM showed effects on *Leishmania* spp. in animal models and patients' therapy with cutaneous leishmaniasis (Opara and I.G, 2005; Kadir et al., 2009). IVM also showed promising results in the models of mice infected with *T. brucei* (Udensi and Fagbenro-Beyioku, 2012). Related to Chagas disease and IVM, few studies have been made, mainly centered in triatomine vectors (Dias et al., 2005; Dadé et al., 2014; Dadé et al., 2017). To our knowledge, the unique report of IVM in Chagas disease in humans was a descriptive work based on a survey conducted in a self-medicated population group living in an endemic area of Bolivia, in which IVM caused some improvements in their self-perception of Chagas disease symptoms (Forsyth, 2018).

Different mechanisms of action have been proposed to explain the IVM effect on diverse organisms. IVM potentiates the glutamate-gated Cl channel (GluCl), found in invertebrates (nematodes and arthropods) (Cully et al., 1994), resulting in the hyperpolarization of parasite neurons and muscles (Chen and Kubo, 2018). IVM also inhibits importin α/β (or "karyopherins") (Wehbe et al., 2021), a heterodimer that transports proteins to the nucleus across the nuclear complex pore; this effect has been described in the asexual blood stages of *Plasmodium falciparum* (Panchal et al., 2014).

This evidence, together with its relative low cost, make IVM an interesting drug candidate to study for Chagas disease treatment. The aim of this work was to analyze the effect of IVM on different *T. cruzi* stages and other trypanosomatids' proliferation and viability.

Materials and methods

Parasites and cell cultures

T. cruzi epimastigotes (Y, Dm28c/pLacZ, CL Brener, RA and Tulahuen 0 strains), *Phytomonas Jma 066* promastigotes, and *Crithidia fasciculata* choanomastigotes were cultured at 28°C in a Brain Heart Tryptose (BHT) medium supplemented with hemin (20 µg/ml) and *Leishmania mexicana mexicana* promastigotes (WHO strain), kindly provided by Dr. Cazzulo, were cultured at 28°C in SDM-79 (M199 media, Gibco, Grand Island, NY, USA). *T. cruzi* trypomastigotes and amastigotes were obtained from Dm28c/pLacZ epimastigotes expressing β-galactosidase, according to Alonso et al. (2021). Vero cells were maintained at 37°C and 5% CO_2 atmosphere in Dulbecco's Modified Eagle Medium (DMEM) high glucose (Gibco) supplemented with 2 mM glutamine. All media were supplemented with streptomycin (100 µg/ml) and penicillin (100 IU/ml) and 2%–10% heat-inactivated fetal bovine serum (FBS; Natocor, Córdoba, Argentina) as indicated.

Compounds and drugs

The stock solutions of the drugs (50 mM) were prepared in dimethyl sulfoxide (DMSO) for IVM (MW: 875.1, kindly provided by Pablo Cassará Laboratory), NFX (MW: 287.3, Sigma) and BZN (MW: 260.25, Sigma, Saint Louis, MO, USA). The stock solutions were diluted in culture media to obtain the working concentrations at the moment of the assay.

Effect of ivermectin on *T. cruzi* and related trypanosomatids in culture

The effect of IVM was tested after 72 h of culture, by counting the number of mobile parasites in a hemocytometer

chamber, by measuring optical density (OD) at 630 nm and by the Thiazolyl Blue Tetrazolium Bromide (MTT) assay (Frank and Pace, 1998), as indicated. For this last methodology, treated cells were incubated for 3:30 h at 28°C in the absence of light. The formed formazan was resuspended in DMSO. The absorbance was read at 570 nm using an ELISA plate reader (Cambridge Technology, Lexington, MA, USA) using wells with only media and reagents as reaction blank.

For Dm28c/pLacZ epimastigote, trypomastigote, and amastigote cultures, the proliferation was measured indirectly by the cytoplasmic β-galactosidase activity. Briefly, after the treatment with IVM, parasites were lysed and incubated with the enzyme substrate, chlorophenol red β-D-galactopyranoside. The colorimetric reaction was measured at 570 nm (Alonso et al., 2021).

Under same culture conditions, DMSO (at the highest concentration used) and NFX or BZN were used as negative and positive controls, respectively.

Mammalian cytotoxic activity

Cytotoxicity was *in vitro* tested on Vero cells treated with increasing concentrations of IVM diluted in DMEM (up to 15 µM). The plate was then incubated for 24 h at 37°C with 5% CO_2, and the MTT assay was performed as previously explained (see *Effect of ivermectin on T. cruzi and related trypanosomatids in culture*).

Cell proliferation recovery assay

Recovery assays were performed as Kessler et al. (2013). Briefly, *T. cruzi* epimastigotes were preincubated with IVM at 50 and 100 µM (four and eight times the calculated IVM $EC50_{72h}$, respectively), during different periods of time (from 30 min to 3 h). Then, parasites were washed with sterile PBS, transferred to a drug-free BHT 10% FBS medium, and incubated at 28°C. Growth recovery was monitored at days 4 and 8 by cell density in a hemocytometer chamber and OD at 630 nm.

Drug combination study

To evaluate the effect of interaction between IVM and BZN or NFX on *T. cruzi* epimastigotes, a drug combination matrix was designed to test both drugs simultaneously or in a sequential manner. For simultaneous assays, the serial dilutions of IVM (0–50 µM) were placed in the columns of a 96-well plate and increasing concentrations of the second drug (BNZ or NFX) were added in each row, and then, parasites were seeded. For sequential assays, epimastigotes were first preincubated with IVM, NFX, or BZN in the corresponding matrix concentration; after 1 h, parasites were washed and seeded in a 96-well plate and the second drug was added following the combination matrix. The final concentration of DMSO was at most 0.5%. Treated cultures, blank samples (only BHT and drugs in their maximal concentration), and negative control (parasites in 0.5% DMSO) were incubated at 28°C for 72 h, and parasite proliferation was measured by OD at 630 nm. Data were analyzed using the free software Combenefit (v. 2.021, Cambridge University, Cambridge, UK) (Di Veroli et al., 2016). Relative epimastigote proliferation obtained experimentally was compared against the predicted values according to *Bliss Independence* or *Loewe additivity* models. The synergy score calculated by the software is a positive value for a synergic effect, 0 for an additive effect (when drugs have no interaction), and negative for an antagonic effect. The results obtained were depicted in a synergy distribution plot where effects are indicated by a scale of colors and numbers, and statistical differences are marked with an asterisk.

In silico analysis

In order to postulate a possible mechanism of action of IVM in *T. cruzi*, an *in silico* study was performed, supported with bibliographic data. To search for orthologous protein sequences of importin α (IMPα) and importin β (IMPβ) in the trypanosomatids of interest (*T. cruzi, L. exicana, C. fasciculata*, and *Phytomonas* spp.) and other close-related species, TritrypDB (*Tritrypdb.org*), Uniprot (www.uniprot.org/), and National Center for Biotechnology Information (NCBI) databases were used. Sequence alignments and analysis were performed with ClustalOmega (www.ebi.ac.uk/Tools/msa/clustalo/), GeneDoc 2.7 (www.psc.edu/biomed/genedoc), and Jalview 2.11.1.2 (www.jalview.org). Protein domains were identified using PFAM (Mistry et al., 2021) and SMART (Letunic et al., 2021) online tools, both developed by EMBL-EBI.

Statistical analysis

All assays were independently performed in triplicate and data expressed as mean ± SEM. The significance of differences was evaluated with one-way analysis of variance (ANOVA) with *post-hoc* analysis using Dunnet's test. A $p < 0.05$ was considered significant. To calculate the $EC50_{24/72h}$ of the drug, normalized proliferation or viability values were plotted against the Log of drug concentration (µM) and fitted to a sigmoidal curve determined by a non-linear regression. The selectivity index (SI) was calculated as $CC50_{Vero\ cells}/EC50_{amastigotes}$. Tests were performed using the GraphPad prism version 5.00 for Windows (GraphPad Software, La Jolla, CA, USA, www.graphpad.com).

Results

Effect and specificity of ivermectin on *T. cruzi*, other related trypanosomatids and host cells

The drug effect was evaluated, as a first approach, by following epimastigote cultures during 8 days with/without increasing concentrations of IVM, NFX, and BNZ. IVM affected *T. cruzi* epimastigote proliferation in a dose-dependent manner with an $EC50_{72h}$ of 12.5 µM for the Y strain (Supplementary Figure 1) and 5.3 uM for the Dm28c strain. Other strains of *T. cruzi* (CL Brener, RA and Tulahuen 0) showed $EC50_{72h}$ values ranging from 8.1 to 9.2 µM (data not shown). These are encouraging values as they are found between those obtained for us for the reference drugs (Table 1) and in bibliography (Luna et al., 2009; Alonso et al., 2021).

The Dm28c strain expressing β-galactosidase, a quick and reproducible drug screening method, was used to evaluate the sensitivity of the trypomastigote and intracellular amastigote forms to IVM. Trypomastigotes showed an $EC50_{24h}$ of 10.4 µM, while intracellular amastigotes showed more sensitivity with an $EC50_{24h}$ of 0.3 µM (Table 1).

The IVM effect was also evaluated in trypanosomatid species related to *T. cruzi*; while it did not show effects on *C. fasciculata* (an insect trypanosomatid) under the evaluated concentrations (up to 200 µM), this drug affected the proliferation of *Phytomonas jma 066* (a plant parasite) and *L. mexicana* (a human disease–causing parasite) with an $EC50_{72h}$ of 5.7 µM and 11.7 µM, respectively (Table 1). These results show that IVM has a specific broad range of effects on the different species of trypanosomatids as it has for other human pathogens.

The IVM cytotoxic effect at 24 h in Vero cells ($CC50_{24h}$) was 3.6 µM (2.8–4.6) that, related to the $EC50_{24h}$ in amastigotes (both assays performed in similar conditions), results in a selectivity index (SI) of 12, being an SI value ≥10 commonly assumed as a promissory basal (Katsuno et al., 2015).

Effect of ivermectin in cell recovery assays in *T. cruzi* epimastigotes

To evaluate whether the effect of IVM was trypanostatic or trypanocidal, cell recovery assays were performed. The effect of a drug is considered trypanostatic when parasite proliferation recovers in a drug-free medium after a short exposure to high drug concentrations and trypanocidal when it has irreversible effects on parasite proliferation (Mosquillo et al., 2018). At 50 µM IVM (4× $EC50_{72h}$), we observed that epimastigote proliferation was recovered by removing the drug after incubation for up to 1 h, indicating a trypanostatic effect, followed by a significant slight proliferation decrease effect after 3 h treatment (Figure 1A). The assays performed with 100 µM IVM (8× $EC50_{72h}$) showed an irreversible effect of the drug on parasite proliferation, independently of the exposure time, indicating a trypanocidal effect at this concentration (Figure 1B). According to these results, IVM treatment during short periods of time can be trypanostatic or trypanocidal depending on the concentration used.

Effect of ivermectin in combination with benznidazole and nifurtimox

To study the effect of the simultaneous or sequential combination of IVM with BZN or NFX, epimastigotes were cultured in combination matrices and the obtained data were analyzed with the free software Combenefit (Di Veroli et al., 2016), in which the null hypothesis of no synergy needs to be defined in order to assess the degree of the effect. In the case of IVM+BZN and IVM+NFX, the hypothesis was that these drugs have different mechanisms of action, taking the *Bliss independence* model as the best approach (Seguel et al., 2016; Tang, 2017). When the drugs were combined simultaneously, synergy distribution heatmaps-obtained from the comparison of

TABLE 1 EC50 values (µM) of ivermectin, nifurtimox, and benznidazole were determined in *T. cruzi* (Y strain-DTU II epimastigotes; Dm28c—Discreet Typing Units (DTU) I epimastigotes, trypomastigotes, and intracellular amastigotes), *C. fasciculata* choanomastigotes, and *L. mexicana* and *Phytomonas jma 066* promastigotes.

Organism	Life cycle form	µM	IVM	NFX	BZN
***Trypanosoma cruzi* Y strain**	***Epimastigote***	$EC50_{72h}$	12.5 (9.4–16.8)	2.1 (1.2–3.5)	22.2 (16.3–30.4)
***Trypanosoma cruzi* Dm28c strain**	***Epimastigote***	$EC50_{72h}$	5.3 (3.8–7.3)	0.9 (0.6–1.5)	3.8 (1.8–8.0)
	Trypomastigote	$EC50_{24h}$	10.4 (7.0–15.5)	16.1 (7.6–33.8)	35.3 (11.3–110.1)
	Amastigote	$EC50_{24h}$	0.3 (0.2–0.6)	1.4 (0.8–2.2)	0.8 (0.4–1.7)
Leishmania mexicana	***Promastigote***	$EC50_{72h}$	9.7 (6.9–13.6)	3.8 (2.8–5)	7.9 (5.8–10.6)
Phytomonas jma 066	***Promastigote***	$EC50_{72h}$	5.7 (4.6–7.5)	1.8 (1.1–2.7)	28.5 (20.7–39.1)
Crithidia fasciculata	***Choanomastigote***	$EC50_{72h}$	ne	3.4 (1.9–5.8)	ne

ne, no effect observed.

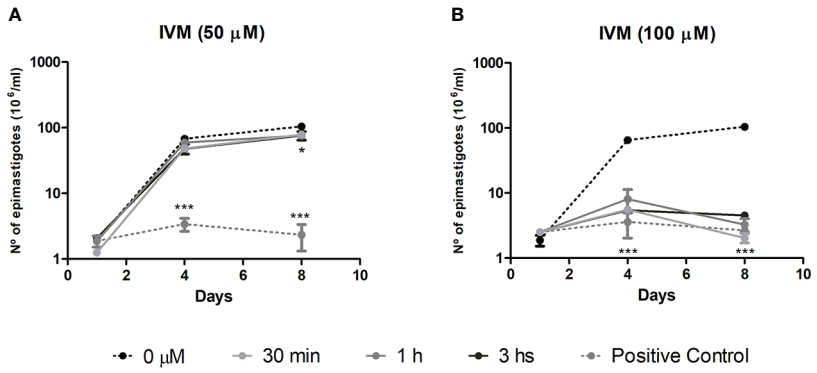

FIGURE 1
Cell proliferation recovery assay to test the effects of ivermectin (IVM) when exposed for short periods of time. *T. cruzi* epimastigotes were preincubated with **(A)** IVM 50 µM ($4xEC50_{72h}$) or **(B)** IVM 100 µM ($8xEC50_{72h}$) for 30 min, 1 or 3 h and then transferred to a drug-free medium for 8 days of culture. Untreated control: 0 µM IVM (0.5% dimethyl sulfoxide); positive control: 50 or 100 µM IVM during the 8 days of culture. Results are expressed as the number of epimastigotes (10^6)/ml, counted in a hemocytometer chamber. ***p<0.001, *p<0.05, ANOVA, Dunnett test.

experimental data with model-predicted values-showed an additive behavior in most of the concentrations. However, there were antagonistic effects at some combinations with middle and high concentrations of IVM (Figures 2A, B), and, on the other hand, some synergistic points at low concentrations of IVM-NFX were observed. In sequential assays, when IVM was preincubated for 1 h and then NFX or BZN was added, we only observed additive effects (Figures 2C, D), but when the preincubation was done with NFX or BZN, aside from additive effects, a slight antagonistic behavior at high concentrations of drugs was also observed (Figures 2E, F). Finally, we performed a control combination with NFX-BZN using the *Loewe additivity* model, based on the hypothesis that both drugs have common mechanisms of action (Tang, 2017), and the observed effects of combinations were mainly additive or antagonistic (Figure 2G).

Bioinformatic analysis of potential drug targets and mechanism of action of ivermectin in *T. cruzi*

In order to find a possible mechanism of action of IVM on *T. cruzi*, different known targets of the drug in other organisms were studied. A first search in *TritrypsDB*, performed for ligand-activated chloride channels, did not show any positive coincidence in the genome of *T. cruzi*. To verify these results, an extensive bibliographic search was performed, finding well-established phylogenetic relations between homologous genes encoding for a GluCl along the kingdoms of life (Rendon et al., 2011). Other authors, applying three independent approaches (Psi-BLAST, HMMer, and Interpro, all based on hidden Markov models), found genetic sequences that codify for pentameric ligand–gated ion channel structures from Cys-loop receptors in a wide array of protists (Jaiteh et al., 2016) that did not include kinetoplastid genomes. Then, we conclude that IVM would be acting through another mechanism in *T. cruzi*.

Another studied mechanism of IVM action is the inhibition of nuclear transport by dissociating the performed importin α/β1 (IMPα/β1) heterodimer as well as by preventing its formation (Yang et al., 2020). At the moment, there is a unique report about IMPα in *T. cruzi* (Canela-Pérez et al., 2020). In order to deepen this work, we found putative sequences of IMPα in *T. cruzi* (Gene DB: TcCLB.509965.110), *L. mexicana* (Gene DB: LmxM.29.1120), *C. fasciculata* (Gene DB: CFAC1_260031300), and *Phytomonas* spp. (Protein DB: W6KHG4). TcIMPα is present in the CL Brener strain, Esmeraldo-like and non-Esmeraldo-like haplotypes, in chromosome 32; its length is 1,602 bp, and the predicted protein has 533 aa. We also found one copy of IMPβ (Gene DB: TcCLB.504105.150). Only one variant of each protein is reported in trypanosomatids, unlike mammals in which there exists a family of IMPα and IMPβ (in humans, seven IMPα and more than 20 IMPβ), showing the relevance of the *T. cruzi* heterodimer as a potential druggable target (Wagstaff et al., 2012).

A structural characterization of the IMPα sequences was made by the alignment of these proteins with those already characterized in *Mus musculus* (UniProtKB DB: P52293), *Homo sapiens* (UniProtKB DB: P52292), and *P. falciparum* (UniProtKB DB: Q7KAV0) (Supplementary Figure 2). Each sequence was analyzed with Pfam and SMART (EMBL) in order to determine domains and relative positions. All proteins had seven-to-nine Armadillo domains (ARM), separated by a conserved glycine (Canela-Pérez et al., 2020), with each ARM being composed of three hydrophobic α-helices

10.3389/fcimb.2022.885268

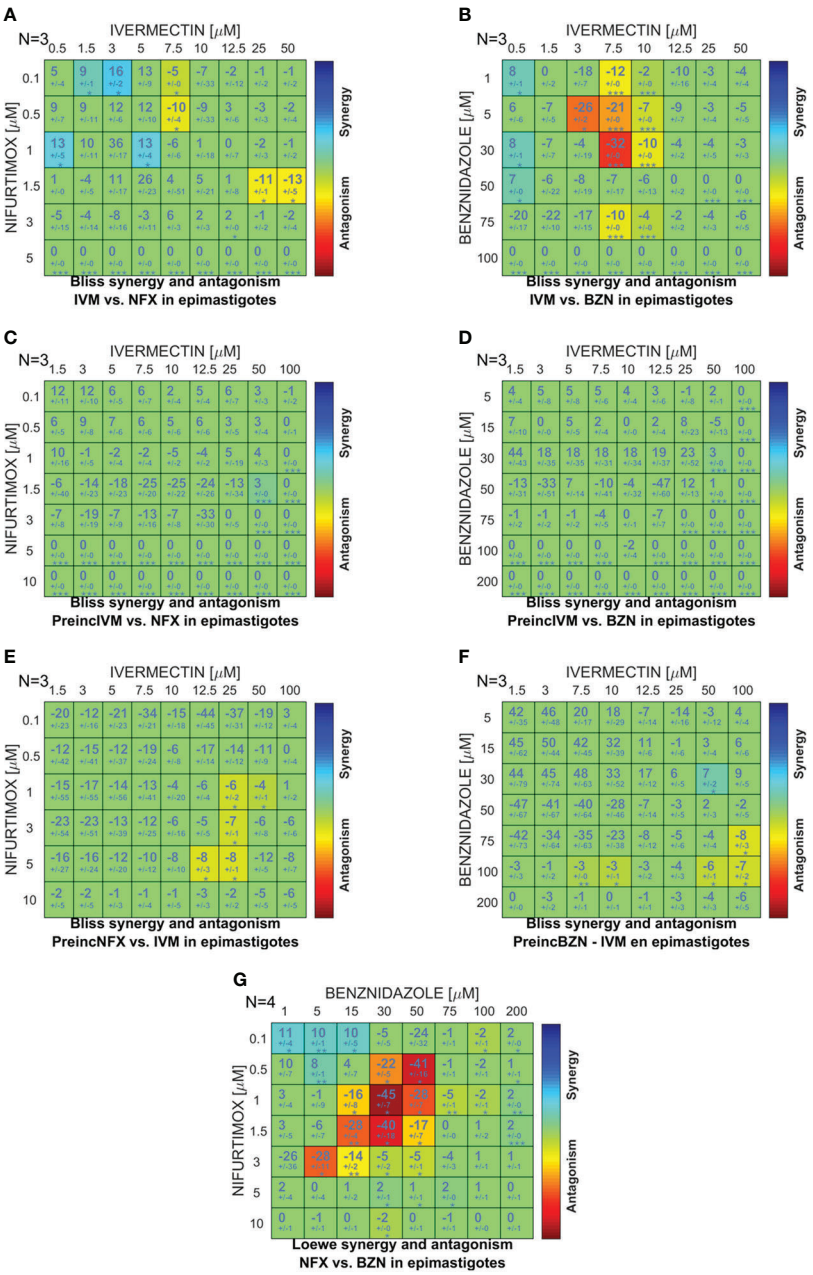

FIGURE 2
Comparison between the *in vitro* and predicted effects of drug combinations on *T. cruzi* epimastigote proliferation. A combination matrix was designed with IVM (0–50 μM) and benznidazole (BZN; 0–100 μM) or nifurtimox (NFX; 0–5 μM), and the drug combination effect was evaluated on the culture proliferation of epimastigotes at day 4. The results obtained in the *in vitro* culture assay were compared against the synergy scores predicted by applying the *Bliss independence* model for: **(A)** IVM-NFX and **(B)** IVM-BZN combined simultaneously; **(C)** IVM-NFX and **(D)** IVM-BZN with the preincubation of IVM for 1 h; **(E)** NFX-IVM and **(F)** BZN-IVM with preincubation of the trypanocidal drug for 1 h; and **(G)** by applying *Loewe additivity* model for the combination of NFX-BZN simultaneously. The scale of numbers and colors represents the type of effect obtained according to the comparison between *in vitro* and model-predicted results; the scale spans from statistically significant synergistic interaction (positive values—blue color, $p<0.01$) to statistically significant antagonism (negative values—red color, $p<0.01$).

(Cingolani et al., 1999). These repeated ARM domains end with an atypical ARM repeat (ARM9), which could be the linker with CAS exportin, and the IBB domain (Importinβ-binding domain) is found in the first 100 amino acids (N-terminal) in mammals as *H. sapiens* and *M. musculus*. In trypanosomatids, ARM repeats appear after the first 100-110 aa but there is not a typical recognizable IBB, which could be related to the presence of an IBB domain with particular characteristics (Supplementary Figure 2).

Discussion

Drug repositioning is a widely used strategy to find new treatments for Chagas disease; several of the latest clinical trials were performed with repurposed drugs as posaconazole and fosravuconazole (Field et al., 2017). With IVM being a secure broad-spectrum antiparasitic drug used in human diseases, this drug would be an attractive repurposing candidate to study. Curiously, there are few reports that tangentially relate it with some Chagas disease aspects. Here, we present the first approach to study the effects of IVM on *T. cruzi* as a potential drug for Chagas disease.

In this report, we showed that IVM affected in a dose-dependent manner the proliferation of *T. cruzi* epimastigotes-a simple model to study trypanocidal drug effects-($EC50_{72h}$= 5.3–12.5 µM in the different strains evaluated) as well as amastigote ($EC50_{24h}$=0.3 µM) and trypomastigote survival ($EC50_{24h}$=10.4 µM). As BZN and NFX, IVM resulted to be more effective against amastigote stage, but with lower EC50 values (Luna et al., 2009), arousing interest as a potential trypanocidal drug. Moreover, the SI of IVM obtained for *T. cruzi* amastigotes was 12 in agreement with the drug selection criteria for infectious diseases that establish an SI value ≥10 as a promissory limit (Katsuno et al., 2015). On the other hand, the SI of NFX and BZN reported in bibliography are very variable, with values ranging from 1.5 to over 200 according to the strain and the cell line used (González et al., 2020). Reinforcing the idea of IVM as possible therapy against *T. cruzi* in humans, published pharmacokinetic data have shown a safety profile for the human use of the oral administration of IVM without adverse side effects, reaching plasmatic concentrations in the range of the EC50 values found in this work (Guzzo et al., 2002).

IVM also inhibited the *in vitro* proliferation of *Phytomonas jma 066* and *L. mexicana*, as previously shown in *L. tropica* (Kadir et al., 2009), while *C. fasciculata* choanomastigotes resulted to be highly tolerant to IVM and BZN. Throughout our results, IVM has shown effects on a broad but specific range of trypanosomatids as it has for other human pathogens.

We found that the trypanocidal capacity of IVM depends on its concentration ($8xEC50_{72h}$) but not on the exposure time. An irreversible effect was also observed on *P. falciparum* at 25-µM IVM during 24 h of exposure (Panchal et al., 2014). Different mechanisms of cellular death (as necrosis or autophagy) could be triggered in *T. cruzi* parasites in response to drugs (Kessler et al., 2013). Moreover, the same compound can trigger different-reversible or irreversible-mechanisms according to the concentration and duration of the *stimuli*. Additionally, when the underlying mechanism of the drug is trypanostatic, parasitemia could show a relapse after antitrypanosomal chemotherapy (Ercoli and Iudice, 1980). This variable behavior of a compound is an important issue for therapy design.

In the last few years, the investigation of drug combinations has become an important strategy to combat drug resistance and reduce treatment courses in NTDs. Here, different drug combination regimens were tested *in vitro* on the epimastigote culture, finding that a simultaneous combination of IVM-BZN and IVM-NFX showed mainly additive effects; however, some combinations showed significant antagonistic or synergic effects. These effects could be explained by different described mechanisms of IVM action, including an antagonism by increasing detoxification processes induced by this drug that avoid the effects of NFX or BZN (Lespine et al., 2007; Ménez et al., 2012; Nodari et al., 2020) or a synergism by inhibiting the activity of P-gp, a member of the superfamily of transporters ABC (ATP-binding cassette), that enhances the cytotoxicity of other drugs (Furusawa et al., 2000; Landfear, 2019). As mentioned by other authors, the *in vitro* assays about the interaction between two drugs are usually the first-step studies, although the observed results do not necessarily reflect the *in vivo* effects; pharmacokinetic and host factors (as the immune response) may lead to different outcomes due to the modification of the effective exposure of the parasites to the drugs (Vincent et al., 2012).

The IMPα and IMPβ heterodimer complex, one of the IVM molecular targets, was searched in trypanosomatid genomes. One copy of each gene was detected in *T. cruzi*, *L. mexicana*, *Phytomonas* spp., and *C. fasciculata*, in agreement with previous studies (Canela-Pérez et al., 2020). Through multiple sequence alignment and structural analysis, we identified ARM domains (between seven and nine, according to the organism) while the typical IBB domain was not recognizable in these trypanosomatids.

The IMPα ARM repeat domain is relevant for the interaction with cargo proteins *via* a nuclear localization sequence (NLS), a short amino acid motif, present in cargo proteins (Yang et al., 2020). The evidence of conserved ARM domains in trypanosomatids and the *in vitro* studies showing their capacity of recognizing and binding to the NLS of *T. cruzi* (Canela-Pérez et al., 2019) suggest that this conserved mechanism of intracellular trafficking is worthy to be studied (Canela-Pérez et al., 2020).

The IBB domain, in N-terminus of IMPα, has three clusters of basic amino acid residues, and it is essential for binding to IMPβ and for efficient nuclear entry (Cingolani et al., 1999); in addition, the IBB domain can bind to the NLS-binding site of IMPα, leading to the autoinhibition of intracellular transport

(Dey and Patankar, 2018). However, most protozoans lack a typical IBB, showing an early divergence (Dey and Patankar, 2018; Mayol et al., 2020). For example, *P. falciparum*, *T. gondii*, and *G. lamblia* do not present the three conserved clusters of basic amino acids in this region, and particularly, *P. falciparum* has shown to have a reduced autoinhibition mechanism of nuclear transport (Dey and Patankar, 2018; Mayol et al., 2020).

IVM is nowadays considered a specific inhibitor of the classical transport pathway of nuclear proteins. Although little is known about nuclear transport in *T. cruzi*, IVM has been associated with the inhibition of nuclear transport by *Tc*IMPα, showing that 25 µM IVM impaired the nuclear transport of an RNA polymerase of *T. cruzi* and 250 µM IVM has an inhibitory effect on the binding ability of *Tc*IMPα to an NLS peptide (Canela-Pérez et al., 2018 and Canela-Pérez et al., 2020). The accumulating evidence about importins makes them an attractive potential druggable target to continue studying. Finally, the study of the mechanisms of action of IVM on *T. cruzi* and other trypanosomatids is relevant to understand the currently unknown aspects of the parasite biochemistry and to discover novel molecular targets with potential for trypanosomatid therapy.

Data availability statement

The raw data supporting the conclusions of this article will be made available by the authors, without undue reservation.

Author contributions

LF, MR, and CC have worked in the study design, writing, and result discussion; LF and MR have made most of the experimental work. VP has conducted the experiments in the infective stages of *T. cruzi*. AC and LL have contributed with proliferation assays and DEB with bioinformatic work and analysis. LF and CC coordinated the investigation. LF and MR contributed equally, sharing the first authorship. All authors have contributed and given approval to the final version of the manuscript.

Funding

The present work was supported by ICT Milstein - CONICET and The National Agency of Scientific and Technological Promotion (funds PICT 2015-0962 and PICT 2018-1124).

Acknowledgments

The authors would like to thank CONICET, the Argentine National Council responsible for RRHH, ANPCyT, the Argentine National Agency that funded this work, and Laboratorio Pablo Cassará for donating the ivermectin used in this work.

Conflict of interest

The authors declare that the research was conducted in the absence of any commercial or financial relationships that could be construed as a potential conflict of interest.

Publisher's note

Supplementary material

The Supplementary Material for this article can be found online at: https://www.frontiersin.org/articles/10.3389/fcimb.2022.885268/full#supplementary-material

References

Alonso, V. L., Manarin, R., Perdomo, V., Gulin, E., Serra, E., and Cribb, P. (2021). In vitro drug screening against all life cycle stages of trypanosoma cruzi using parasites expressing β-galactosidase. *J. Vis. Exp.* 5 (177), e63210. doi: 10.3791/63210

Alout, H., Krajacich, B. J., Meyers, J. I., Grubaugh, N. D., Brackney, D. E., Kobylinski, K. C., et al. (2014). Evaluation of ivermectin mass drug administration for malaria transmission control across different West African environments. *Malar. J.* 13, 417. doi: 10.1186/1475-2875-13-417

Bellera, C. L., Balcazar, D. E., Alberca, L., Labriola, C. A., Talevi, A., and Carrillo, C. (2013). Application of computer-aided drug repurposing in the search of new cruzipain inhibitors: Discovery of amiodarone and bromocriptine inhibitory effects. *J. Chem. Inf. Model.* 53, 2402–2408. doi: 10.1021/ci400284v

Campbell, W. C., Fisher, M. H., Stapley, E. O., Albers-Schonberg, G., and Jacob, T. A. (1983). Ivermectin: a potent new antiparasitic agent. *Science* 221, 823–828. doi: 10.1126/science.6308762

Canela-Pérez, I., López-Villaseñor, I., Cevallos, A. M., and Hernández, R. (2018). Nuclear distribution of the trypanosoma cruzi RNA pol I subunit RPA31 during growth and metacyclogenesis, and characterization of its nuclear localization signal. *Parasitol. Res.* 117, 911–918. doi: 10.1007/s00436-018-5747-4

Canela-Pérez, I., López-Villaseñor, I., Cevallos, A. M., and Hernández, R. (2020). Trypanosoma cruzi importin α: ability to bind to a functional classical nuclear localization signal of the bipartite type. *Parasitol. Res.* 119, 3899–3907. doi: 10.1007/s00436-020-06885-z

Canela-Pérez, I., López-Villaseñor, I., Mendoza, L., Cevallos, A. M., and Hernández, R. (2019). Nuclear localization signals in trypanosomal proteins. *Mol. Biochem. Parasitol.* 229, 15–23. doi: 10.1016/j.molbiopara.2019.02.003

Chaccour, C., and Rabinovich, N. R. (2019). Advancing the repurposing of ivermectin for malaria. *Lancet* 393, 1480–1481. doi: 10.1016/S0140-6736(18)32613-8

Chen, I.-S., and Kubo, Y. (2018). Ivermectin and its target molecules: shared and unique modulation mechanisms of ion channels and receptors by ivermectin. *J. Physiol.* 596, 1833–1845. doi: 10.1113/JP275236

Cingolani, G., Petosa, C., Weis, K., and Müller, C. W. (1999). Structure of importin-beta bound to the IBB domain of importin-alpha. *Nature* 399, 221–229. doi: 10.1038/20367

Crump, A. (2017). Ivermectin: enigmatic multifaceted 'wonder' drug continues to surprise and exceed expectations. *J. Antibiot. (Tokyo)* 70, 495–505. doi: 10.1038/ja.2017.11

Cully, D. F., Vassilatis, D. K., Liu, K. K., Paress, P. S., van der Ploeg, L. H. T., Schaeffer, J. M., et al. (1994). Cloning of an avermectin-sensitive glutamate-gated chloride channel from caenorhabditis elegans. *Nature* 371, 707–711. doi: 10.1038/371707a0

Dadé, M., Daniele, M., Marin, G., Maria Pia, S., and Mestorino, N. (2014). Ivermectin efficacy against triatoma infestans *in vivo* using hen model. *J. Pharm. Pharmacol.* 2, 353–358.

Dadé, M., Daniele, M., Mestorino, N., Dadé, M., Daniele, M., and Mestorino, N. (2017). Evaluation of the toxic effects of doramectin, ivermectin and eprinomectin against triatoma infestans using a rat model. *Biomédica* 37, 324–332. doi: 10.7705/biomedica.v34i2.3316

de Carvalho, L. P., Sandri, T. L., José Tenório de Melo, E., Fendel, R., Kremsner, P. G., Mordmüller, B., et al. (2019). Ivermectin impairs the development of sexual and asexual stages of plasmodium falciparum *In vitro*. *Antimicrob. Agents Chemother.* 63, e00085–e00019. doi: 10.1128/AAC.00085-19

Deng, Q., Xiao, L., Liu, Y., Zhang, L., Deng, Z., and Zhao, C. (2019). Streptomyces avermitilis industrial strain as cell factory for ivermectin B1a production. *Synth. Syst. Biotechnol.* 4, 34–39. doi: 10.1016/j.synbio.2018.12.003

Devore, C. D., and Schutze, G. E. (2015). Head lice. *Pediatrics* 135, e1355–e1365. doi: 10.1542/peds.2015-0746

Dey, V., and Patankar, S. (2018). Molecular basis for the lack of auto-inhibition of plasmodium falciparum importin α. *Biochem. Biophys. Res. Commun.* 503, 1792–1797. doi: 10.1016/j.bbrc.2018.07.115

Dias, J. C. P., Schofield, C. J., Machado, E. M. M., and Fernandes, A. J. (2005). Ticks, ivermectin, and experimental chagas disease. *Mem. Inst. Oswaldo Cruz* 100, 829–832. doi: 10.1590/s0074-02762005000800002

Di Veroli, G. Y., Fornari, C., Wang, D., Mollard, S., Bramhall, J. L., Richards, F. M., et al. (2016). Combenefit: an interactive platform for the analysis and visualization of drug combinations. *Bioinform. Oxf. Engl.* 32, 2866–2868. doi: 10.1093/bioinformatics/btw230

Ercoli, N., and Iudice, G. (1980). Trypanostatic drug action: its relation to relapse following chemotherapy. *Chemotherapy* 26, 218–223. doi: 10.1159/000237908

Field, M. C., Horn, D., Fairlamb, A. H., Ferguson, M. A. J., Gray, D. W., Read, K. D., et al. (2017). Anti-trypanosomatid drug discovery: an ongoing challenge and a continuing need. *Nat. Rev. Microbiol.* 15, 217–231. doi: 10.1038/nrmicro.2016.193

Forsyth, C. (2018). From lemongrass to ivermectin: Ethnomedical management of chagas disease in tropical Bolivia. *Med. Anthropol.* 37, 236–252. doi: 10.1080/01459740.2017.1360878

Frank, D. N., and Pace, N. R. (1998). RIBONUCLEASE p: Unity and diversity in a tRNA processing ribozyme. *Annu. Rev. Biochem.* 67, 153–180. doi: 10.1146/annurev.biochem.67.1.153

Furusawa, S., Shibata, H., Nishimura, H., Nemoto, S., Takayanagi, M., Takayanagi, Y., et al. (2000). Potentiation of doxorubicin-induced apoptosis of resistant mouse leukaemia cells by ivermectin. *Pharm. Pharmacol. Commun.* 6, 129–134. doi: 10.1211/146080800128735764

González, A., Becerra, N., Kashif, M., González, M., Cerecetto, H., Aguilera, E., et al. (2020). *In vitro* and in silico evaluations of new aryloxy-1,4-naphthoquinones as anti-trypanosoma cruzi agents. *Medicinal Chemistry Research* 29, 665–674. doi: 10.1007/s00044-020-02512-9

Guzzo, C. A., Furtek, C. I., Porras, A. G., Chen, C., Tipping, R., Clineschmidt, C. M., et al. (2002). Safety, tolerability, and pharmacokinetics of escalating high doses of ivermectin in healthy adult subjects. *J. Clin. Pharmacol.* 42, 1122–1133. doi: 10.1177/009127002401382731

Jaiteh, M., Taly, A., and Hénin, J. (2016). Evolution of pentameric ligand-gated ion channels: Pro-loop receptors. *PloS One* 11, e0151934–e0151934. doi: 10.1371/journal.pone.0151934

Kadir, M. A., Aswad, H. S., Al-Samarai, A. M., and Al-Mula, G. A. (2009). Comparison between the efficacy of ivermectin and other drugs in treatment of cutaneous leishmaniasis. *Iraqi J. Vet. Sci.* 23, 175-180.

Katsuno, K., Burrows, J. N., Duncan, K., Hooft van Huijsduijnen, R., Kaneko, T., Kita, K., et al. (2015). Hit and lead criteria in drug discovery for infectious diseases of the developing world. *Nat. Rev. Drug Discovery* 14, 751–758. doi: 10.1038/nrd4683

Kessler, R. L., Soares, M. J., Probst, C. M., and Krieger, M. A. (2013). Trypanosoma cruzi response to sterol biosynthesis inhibitors: Morphophysiological alterations leading to cell death. *PloS One* 8 (1), e5549. doi: 10.1371/journal.pone.0055497

Laing, R., Gillan, V., and Devaney, E. (2017). Ivermectin - old drug, new tricks? *Trends Parasitol.* 33, 463–472. doi: 10.1016/j.pt.2017.02.004

Landfear, S. M. (2019). Protean permeases: Diverse roles for membrane transport proteins in kinetoplastid protozoa. *Mol. Biochem. Parasitol.* 227, 39–46. doi: 10.1016/j.molbiopara.2018.12.006

Lespine, A., Martin, S., Dupuy, J., Roulet, A., Pineau, T., Orlowski, S., et al. (2007). Interaction of macrocyclic lactones with p-glycoprotein: Structure–affinity relationship. *Eur. J. Pharm. Sci.* 30, 84–94. doi: 10.1016/j.ejps.2006.10.004

Letunic, I., Khedkar, S., and Bork, P. (2021). SMART: recent updates, new developments and status in 2020. *Nucleic Acids Res.* 49, D458–D460. doi: 10.1093/nar/gkaa937

Luna, K. P., Hernández, I. P., Rueda, C. M., Zorro, M. M., Croft, S. L., and Escobar, P. (2009). *In vitro* susceptibility of trypanosoma cruzi strains from santander, Colombia, to hexadecylphosphocholine (miltefosine), nifurtimox and benznidazole. *Biomed. Rev. Inst. Nac. Salud* 29, 448–455.

Mayol, G. F., Revuelta, M. V., Salusso, A., Touz, M. C., and Ropolo, A. S. (2020). Evidence of nuclear transport mechanisms in the protozoan parasite giardia lamblia. *Biochim. Biophys. Acta BBA Mol. Cell Res.* 1867, 118566. doi: 10.1016/j.bbamcr.2019.118566

Mendes, A. M., Albuquerque, I. S., Machado, M., Pissarra, J., Meireles, P., and Prudêncio, M. (2017). Inhibition of plasmodium liver infection by ivermectin. *Antimicrob. Agents Chemother.* 61, e02005–e02016. doi: 10.1128/AAC.02005-16

Ménez, C., Mselli-Lakhal, L., Foucaud-Vignault, M., Balaguer, P., Alvinerie, M., and Lespine, A. (2012). Ivermectin induces p-glycoprotein expression and function through mRNA stabilization in murine hepatocyte cell line. *Biochem. Pharmacol.* 83, 269–278. doi: 10.1016/j.bcp.2011.10.010

Mistry, J., Chuguransky, S., Williams, L., Qureshi, M., Salazar, G. A., Sonnhammer, E. L. L., et al. (2021). Pfam: The protein families database in 2021. *Nucleic Acids Res.* 49, D412–D419. doi: 10.1093/nar/gkaa913

Mosquillo, M. F., Bilbao, L., Hernández, F., Tissot, F., Gambino, D., Garat, B., et al. (2018). Trypanosoma cruzi biochemical changes and cell death induced by an organometallic platinum-based compound. *Chem. Biol. Drug Des.* 92, 1657–1669. doi: 10.1111/cbdd.13332

Nodari, R., Corbett, Y., Varotto-Boccazzi, I., Porretta, D., Taramelli, D., Epis, S., et al. (2020). Effects of combined drug treatments on plasmodium falciparum: *In vitro* assays with doxycycline, ivermectin and efflux pump inhibitors. *PloS One* 15 (4), e0232171. doi: 10.1371/journal.pone.0232171

Nunes, M. C. P., Dones, W., Morillo, C. A., Encina, J. J., and Ribeiro, A. L. (2013). Council on chagas disease of the interamerican society of cardiology 2013. chagas disease: an overview of clinical and epidemiological aspects. *J. Am. Coll. Cardiol.* 62, 767–776. doi: 10.1016/j.jacc.2013.05.046

Opara, W. E. K., and I.G, A. (2005). Cutaneous leishmaniasis: A report of its treatment with mectizan in sokoto, Nigeria. *J. Med. Sci* 5, 186–188. doi: 10.3923/jms.2005.186.188

Panchal, M., Rawat, K., Kumar, G., Kibria, K. M., Singh, S., Kalamuddin, M., et al. (2014). Plasmodium falciparum signal recognition particle components and anti-parasitic effect of ivermectin in blocking nucleo-cytoplasmic shuttling of SRP. *Cell Death Dis.* 5, e994. doi: 10.1038/cddis.2013.521

Pérez-Molina, J. A., and Molina, I. (2018). Chagas disease. *Lancet* 391, 82–94. doi: 10.1016/S0140-6736(17)31612-4

Rendon, G., Kantorovitz, M. R., Tilson, J. L., and Jakobsson, E. (2011). Identifying bacterial and archaeal homologs of pentameric ligand-gated ion channel (pLGIC) family using domain-based and alignment-based approaches. *Channels Austin Tex* 5, 325–343. doi: 10.4161/chan.5.4.16822

Seguel, V., Castro, L., Reigada, C., Cortes, L., Díaz, M. V., Miranda, M. R., et al. (2016). Pentamidine antagonizes the benznidazole's effect *in vitro*, and lacks of synergy *in vivo*: Implications about the polyamine transport as an anti-trypanosoma cruzi target. *Experiment. Parasitol* 171, 23–32. doi: 10.1016/j.exppara.2016.10.007

Sheele, J. M., Ford, L. R., Tse, A., Chidester, B., Byers, P. A., and Sonenshine, D. E. (2014). The use of ivermectin to kill ixodes scapularis ticks feeding on humans. *Wilderness Environ. Med.* 25, 29–34. doi: 10.1016/j.wem.2013.09.008

Tang, J. (2017). Informatics approaches for predicting, understanding, and testing cancer drug combinations. *Methods Mol. Biol. Clifton NJ* 1636, 485–506. doi: 10.1007/978-1-4939-7154-1_30

Thomas, J., Peterson, G. M., Walton, S. F., Carson, C. F., Naunton, M., and Baby, K. E. (2015). Scabies: an ancient global disease with a need for new therapies. *BMC Infect. Dis.* 15, 250. doi: 10.1186/s12879-015-0983-z

Turner, M. J., and Schaeffer, J. M. (1989). *Mode of action of ivermectin BT - ivermectin and abamectin*. Ed. W. C. Campbell (New York, NY: Springer New York), 73–88. doi: 10.1007/978-1-4612-3626-9_5

Udensi, U. K., and Fagbenro-Beyioku, A. F. (2012). Effect of ivermectin on trypanosoma brucei brucei in experimentally infected mice. *J. Vector Borne Dis.* 49, 143.

Vincent, I. M., Creek, D. J., Burgess, K., Woods, D. J., Burchmore, R. J. S., and Barrett, M. P. (2012). Untargeted metabolomics reveals a lack of synergy between nifurtimox and eflornithine against trypanosoma brucei. *PloS Negl. Trop. Dis.* 6, e1618. doi: 10.1371/journal.pntd.0001618

Wagstaff, K. M., Sivakumaran, H., Heaton, S. M., Harrich, D., and Jans, D. A. (2012). Ivermectin is a specific inhibitor of importin α/β-mediated nuclear import able to inhibit replication of HIV-1 and dengue virus. *Biochem. J.* 443, 851–856. doi: 10.1042/BJ20120150

Wehbe, Z., Wehbe, M., Iratni, R., Pintus, G., Zaraket, H., Yassine, H. M., et al. (2021). Repurposing ivermectin for COVID-19: Molecular aspects and therapeutic possibilities. *Front. Immunol.* 12. doi: 10.3389/fimmu.2021.663586

World Health Organization (2015). Chagas disease in Latin America : an epidemiological update based on 2010 estimates. *Wkly. Epidemiol. Rec.* 90, 33–44.

Yang, S. N. Y., Atkinson, S. C., Wang, C., Lee, A., Bogoyevitch, M. A., Borg, N. A., et al. (2020). The broad spectrum antiviral ivermectin targets the host nuclear transport importin α/β1 heterodimer. *Antiviral Res.* 177, 104760. doi: 10.1016/j.antiviral.2020.104760

frontiers | Frontiers in Cellular and Infection Microbiology

TYPE Original Research
PUBLISHED 29 July 2022
DOI 10.3389/fcimb.2022.926699

OPEN ACCESS

EDITED BY
Gustavo Benaim,
Fundación Instituto de Estudios Avanzados (IDEA), Venezuela

REVIEWED BY
Alan Talevi,
National University of La Plata, Argentina
Marta Helena Branquinha,
Federal University of Rio de Janeiro, Brazil

*CORRESPONDENCE
Marcos André Vannier-Santos
marcos.vannier@ioc.fiocruz.br

SPECIALTY SECTION
This article was submitted to Clinical Microbiology, a section of the journal Frontiers in Cellular and Infection Microbiology

RECEIVED 22 April 2022
ACCEPTED 27 June 2022
PUBLISHED 29 July 2022

CITATION
Almeida-Silva J, Menezes DS, Fernandes JMP, Almeida MC, Vasco-dos-Santos DR, Saraiva RM, Viçosa AL, Perez SAC, Andrade SG, Suarez-Fontes AM and Vannier-Santos MA (2022) The repositioned drugs disulfiram/diethyldithiocarbamate combined to benznidazole: Searching for Chagas disease selective therapy, preventing toxicity and drug resistance *Front. Cell. Infect. Microbiol.* 12:926699. doi: 10.3389/fcimb.2022.926699

The repositioned drugs disulfiram/diethyldithiocarbamate combined to benznidazole: Searching for Chagas disease selective therapy, preventing toxicity and drug resistance

Juliana Almeida-Silva[1], Diego Silva Menezes[2], Juan Mateus Pereira Fernandes[1], Márcio Cerqueira Almeida[2], Deyvison Rhuan Vasco-dos-Santos[1], Roberto Magalhães Saraiva[3], Alessandra Lifsitch Viçosa[4], Sandra Aurora Chavez Perez[5], Sônia Gumes Andrade[6], Ana Márcia Suarez-Fontes[1] and Marcos André Vannier-Santos[1]*

[1]Innovations in Therapies, Education and Bioproducts Laboratory, Oswaldo Cruz Institute, Oswaldo Cruz Foundation, Rio de Janeiro, RJ, Brazil, [2]Parasite Biology Laboratory, Gonçalo Moniz Institute, Oswaldo Cruz Foundation, Salvador, BA, Brazil, [3]Laboratory of Clinical Research on Chagas Disease, Evandro Chagas Infectious Disease Institute, Oswaldo Cruz Foundation, Rio de Janeiro, RJ, Brazil, [4]Experimental Pharmacotechnics Laboratory, Department of Galenic Innovation, Institute of Drug Technology - Farmanguinhos, Oswaldo Cruz Foundation, Rio de Janeiro, RJ, Brazil, [5]Project Management Technical Assistance, Institute of Drug Technology - Farmanguinhos, Oswaldo Cruz Foundation, Rio de Janeiro, RJ, Brazil, [6]Experimental Chagas Disease Laboratory, Gonçalo Moniz Institute, Oswaldo Cruz Foundation, Salvador, BA, Brazil

Chagas disease (CD) affects at least 6 million people in 21 South American countries besides several thousand in other nations all over the world. It is estimated that at least 14,000 people die every year of CD. Since vaccines are not available, chemotherapy remains of pivotal relevance. About 30% of the treated patients cannot complete the therapy because of severe adverse reactions. Thus, the search for novel drugs is required. Here we tested the benznidazole (BZ) combination with the repositioned drug disulfiram (DSF) and its derivative diethyldithiocarbamate (DETC) upon *Trypanosoma cruzi in vitro* and *in vivo*. DETC-BZ combination was synergistic diminishing epimastigote proliferation and enhancing selective indexes up to over 10-fold. DETC was effective upon amastigotes of the BZ- partially resistant Y and the BZ-resistant Colombiana strains. The combination reduced proliferation even using low concentrations (e.g., 2.5 μM). Scanning electron microscopy revealed membrane discontinuities and cell body volume reduction. Transmission electron microscopy revealed remarkable enlargement of endoplasmic reticulum cisternae besides, dilated mitochondria with decreased electron density and disorganized kinetoplast DNA. At advanced stages, the cytoplasm

vacuolation apparently impaired compartmentation. The fluorescent probe H_2-DCFDA indicates the increased production of reactive oxygen species associated with enhanced lipid peroxidation in parasites incubated with DETC. The biochemical measurement indicates the downmodulation of thiol expression. DETC inhibited superoxide dismutase activity on parasites was more pronounced than in infected mice. In order to approach the DETC effects on intracellular infection, peritoneal macrophages were infected with Colombiana trypomastigotes. DETC addition diminished parasite numbers and the DETC-BZ combination was effective, despite the low concentrations used. In the murine infection, the combination significantly enhanced animal survival, decreasing parasitemia over BZ. Histopathology revealed that low doses of BZ-treated animals presented myocardial amastigote, not observed in combination-treated animals. The picrosirius collagen staining showed reduced myocardial fibrosis. Aminotransferase de aspartate, Aminotransferase de alanine, Creatine kinase, and urea plasma levels demonstrated that the combination was non-toxic. As DSF and DETC can reduce the toxicity of other drugs and resistance phenotypes, such a combination may be safe and effective.

KEYWORDS

Trypanosoma cruzi, disulfiram, drug combination, repositioning, Chagas disease, chemotherapy, Diethyldithiocarbamate

Introduction

At least 6-7 million people have Chagas disease (CD), mostly in Latin America (WHO - World Health Organization, 2021), where over 10% of the population is at risk of infection (Pérez-Molina and Molina, 2018). There are at least 4.6 million infected people in Brazil, which can reach 1.5% of the Brazilian population. In addition, about 70 million are at risk of infection by *Trypanosoma cruzi* (Dias et al., 2016). The parasitosis, also known as American trypanosomiasis, is already considered a public health problem on a global scale (Franco-Paredes et al., 2009; Coura and Viñas, 2010; Parker and Sethi, 2011).

CD causes economic losses in excess of U$1.2 billion/year to endemic countries in South America, in addition to more than $7 billion/year at global levels (Lee et al., 2013), including treatment and loss of productivity, not including the losses caused by infections by tourists and emigrants to North America, Europe, and Asia (Coura and Viñas, 2010) coming from South and Central America. Therefore, it can be inferred that effective drugs, besides promoting the quality of life of patients and their families, can provide considerable socioeconomic benefit.

Since CD discovery by the Brazilian researcher Carlos Chagas over a century ago, the disease is intensely studied, but only two drugs, benznidazole (BZ) and nifurtimox (NFX), are employed in CD treatment. However, BZ side effects lead to therapy discontinuation from approximately 30% of the cases up to eventually reaching 50% of the patients (Guggenbühl Noller et al., 2020). The option is NFX but a recent study (Crespillo-Andújar et al., 2018) reported that the use of NFX in patients who had been discontinued from BZ treatment still led to more than 12% of elevated toxicity, forcing physicians to permanently discontinue treatment. Therefore, there is pressing demand for the development of new drugs or therapeutic regimens for CD.

Different chemotherapy targets have been approached during the last decades (Duschak, 2011; Duschak, 2016; Beltran-Hortelano et al., 2017; Duschak, 2019; Beltran-Hortelano et al., 2022), and much was learned about the biochemistry and cell biology of *T. cruzi*, but new agents are still not in clinical use. Drug combinations may be promising for allowing dosing reduction (Bustamante et al., 2014), hampering resistance selection (Hill and Cowen, 2015), and enhancing selectivity (Zimmermann et al., 2007; Lehár et al., 2009a; Lehár et al., 2009b). In addition, drug combinations can promote effectivity of repositioning (Sun et al., 2016).

The use of repositioned drugs (approved by the FDA), with well-established data on bioavailability, safety, etc., allows accelerating drug development, significantly increasing the percentage of success, but reducing their costs (Zheng et al., 2018). Such innovations can be of great value in the therapy of neglected diseases, highly prevalent in South America, caused by parasitic protozoa (Müller and Hemphill, 2016), including CD (Palos et al., 2017).

The repositioning of a low-cost drug such as Disulfiram (DSF, Antabuse®) can be considered a "salvation" for global health care (Cvek, 2012). DSF, a drug used for the therapy of alcoholism, is

widely used and well tolerated in humans (Jørgensen et al., 2011; Sinclair et al., 2016) and is even considered less toxic than aspirin (Gessner and Gessner, 1992) and trials employing 200-250 mg/d daily or 800 mg/twice a week are regularly performed, with no reports of adverse effects (Sinclair et al., 2016). The DSF first derivative sodium diethyldithiocarbamate (DETC), also known as imuthiol, has been successfully used as an immunostimulant in HIV patients, reducing opportunistic infections (Hersh et al., 1991). DSF is used for different purposes (e.g. Kona et al., 2011), such as cancer therapy (Cvek, 2012; Meraz-Torres et al., 2020; Kannappan et al., 2021; Lu et al., 2021; Lu et al., 2022) and chemoprevention (Askgaard et al., 2014; Yang et al., 2015; Harrington et al., 2020). The DSF and/or DETC combination can enhance antitumoral activities of drugs such as cisplatin (O'Brien et al., 2012; Nechushtan et al., 2015), but diminish adverse reactions (Wysor et al., 1982; Elliott et al., 1983; Bodenner et al., 1986; Roemeling et al., 1986). In addition, DSF can overcome resistance, *via* different mechanisms (Schmidtova et al., 2019; Yang et al., 2019). The data presented here indicate that the BZ-DSF combination may comprise a promising alternative for CD therapy.

Materials and methods

Drugs

BZ (Nortec Química, Rio de Janeiro, Brazil) and DSF (Corden Pharma Bergamo S.p.A) were provided by Farmanguinhos (Fiocruz, Rio de Janeiro) and DETC was purchased from Sigma-Aldrich. Drugs were dissolved in dimethyl sulfoxide (DMSO) and stored at -20°C until use.

Parasites and mammalian cells

T. cruzi Y and the Colombiana strains epimastigote forms were maintained in LIT (Liver Infusion Trypticase) medium, supplemented with 10% fetal bovine serum (FBS), 100 µg/mL penicillin, and streptomycin at 25°C (dos Anjos et al., 2016). Cultures were harvested at the exponential growth phase. Then $5x10^5$ parasites were incubated in the presence of the isolated compounds. Trypomastigote forms were obtained by cardiac puncture, at the peak of parasitemia of infected Swiss Webster mice (Sueth-Santiago et al., 2016) and maintained through co-culture with epithelial cells, VERO, previously in Dulbecco's modified Eagle's medium (DMEM) supplemented with 10% FBS, at 37°C, 5% CO_2, as well as the amastigote form obtained after 8 days of cell infection (Monteiro et al., 2001). Axenic amastigotes were obtained from cell cultures of trypomastigotes in BHT medium incubated at 28°C, being collected after three passages of 56-64 h, in an initial concentration between $5x10^6$ cells/mL (Engel et al., 1987). Macrophages from BALB/c mice were collected by peritoneal lavage in Hank's balanced solution, seeded in 24-well plates or bottles (Falcon, New Jersey, USA), and kept at 37°C in atmosphere of 5% CO_2 in DMEM medium supplemented with 10% FBS.

Parasite-host interaction

Assays were performed using a parasite:cell ratio of 10:1, and infection quantification was performed by direct counting cultured cells Giemsa (Laborklin)-stained coverslips under light microscopy, approximately 1000 cells per coverslip. Association indices (AI) were obtained by multiplying the percentage of infected macrophages by the average number of parasites per host cell, as previously described (Martiny et al., 1996).

In vitro evaluation of trypanocidal activity and cytotoxicity

T. cruzi epimastigotes (10^7 cells/mL) incubated with DETC and BZ, to determine IC_{50} values each drug, at 24 h at 28°C, determined by the Alamar Blue assay at 570 nm and 600 nm. For the combinations, both for trypanocidal activity and for the selectivity index (10^7 Swiss Webster mouse peritoneal macrophages/mL), six fixed doses were prepared based on the IC_{50} value of the isolated drugs, in the proportions 5:0, 4:1, 3:2, 2:3, 1:4 and 0:5 (Fivelman et al., 2004). Concentration-response curves were plotted and the IC_{50} and CC_{50} values of the compounds (inhibition and cytotoxicity, respectively), alone or in combination, were calculated using GraphPad Prism, 7.

ROS detection

ROS were detected using the H_2-DCFDA probe using a confocal microscope Fluoview 1000, Olympus.

Lipid peroxidation

Lipid peroxidation was determined by the production of thiobarbituric acid (TBA) reactive substances (TBARS), by parasites incubated or not in the presence of the compounds for 24 h. Subsequently, the cells were centrifuged three times in phosphate-buffered saline (PBS). After washing, the parasites were resuspended in 200 µL PBS and 200 µL TBA at a final concentration of 1%. After homogenization, the material was incubated at 99°C for a period of 3 h and measured in a spectrophotometer at 532 nm (Menezes et al., 2006).

Thiol group measurements

The determination of the concentration of low molecular weight thiols was carried out using 5,5′-dithiobis (2-nitrobenzoic acid) (DTNB) and methanol assay after protein removal with 10% trichloro acetic acid. Subsequently, the supernatant was read in a spectrophotometer at 412 nm (Hitachi U-1100), as previously described (Sedlak and Lindsay, 1968).

Dosage of superoxide dismutase

Parasite samples untreated and treated with DETC alone and in combination with BZ, for 1 and 24 hours, were evaluated using a colorimetric method for superoxide dismutase (SOD) measurement (Sigma-Aldrich Kit-WST- SOD Assay), which is based on the generation of the radial superoxide from the xanthine-xanthine oxidase (XOD) system, where the superoxide reacts with the sample and converts the tetrazolium salt to formazan. After reactions, the measurements spectrophotometrically performed in a VersaMax at 440 nm (Moukdar et al., 2009).

Electron microscopy

Parasites were washed with PBS and fixed in Karnovsky for 24 h, at 4°C. Then, samples were post-fixed in 1% osmium tetroxide, 5 mM calcium chloride, and 0.8% potassium ferricyanide in 0.1M sodium cacodylate buffer, protected from light for 40 min at room temperature. For scanning, electron microscopy (SEM) samples were dehydrated in ethanol series, critical point-dried, mounted on stubs, gold-metalized, and observed in a JEOL 5310 scanning electron microscope. For transmission, electron microscopy (TEM) samples were dehydrated in acetone and embedded in Polybed epoxy resin (Polysciences, Inc). After 72 h at 60°C, the samples were sectioned on an ultramicrotome (Reichert, Leica), using a diamond knife (Diatome, Hatfield, PA), and the sections were collected on 300 mesh copper grids and counterstained with 3% lead citrate and 5% uranyl acetate in water. Samples were observed in a transmission electron microscope Zeiss EM 109 at 80kV, as previously described (Vannier-Santos and Lins, 2001).

In vivo infection

Swiss Webster mice were infected with Y or Colombian strain, intraperitoneally (i.p.), with 10^4 bloodstream trypomastigotes. The infected animals were divided into the following groups (15 animals per group): positive control (BZ); negative control (PBS + 1% Kolliphor); DETC + BZ combination; DSF + BZ. The therapy was initiated 5 days from the beginning of the parasitemia and carried out for 30/60 days, administered through the intragastric route (Salomão et al., 2010). Parasitemia was verified by direct microscopic, slide analysis of parasites in 5 µL of blood, and mortality rates were checked daily/weekly up to 30 days post-treatment.

Systemic toxicity

Thirty days after the end of the treatment, uninfected mice blood was collected through the brachial plexus and stored at -80°C for biochemical analysis of the enzymes: urea, for renal monitoring, total creatine kinase (CK), for evaluation of cardiac or skeletal musculature lesions, alanine aminotransferase (ALT) and aspartate aminotransferase (AST), assessment of liver damage, all being determined in whole blood by the Reflotron® reactive test strip system (Roche Diagnostics, F Hoffmann-La Roche Ltd, Basel, Switzerland) using reflectance photometry (Salomão et al., 2010).

Histopathology

Tissue samples were fixed in formaldehyde solution pH 7.2, embedded in paraffin, and 5 µm-thick sections were stained with hematoxylin and eosin (H&E) and picrosirius red to stain collagen fibers (Andrade et al., 1994).

Statistical analysis

The data obtained are representative of at least three independent experiments carried out in triplicate. Statistically significant differences were analyzed using the ANOVA test and Tukey or Dunn post-tests with $p < 0.05$, using GraphPad Prism, 7.

Results

DETC inhibited dose-dependently the axenic proliferation of epimastigote forms (Figure 1). The IC_{50} value obtained was 1.48 µM. The BZ IC_{50} observed was 2.28 µM (Table 1). The selectivity indexes revealed that the combination selectivity was increased over an order of magnitude (about 13-fold), as compared to the drug of choice, BZ. Based on the IC_{50} values obtained DETC and BZ were combined at different proportions. Isobolograms were plotted to analyze the possible synergism between BZ and DETC on the trypanocidal activity. There was synergistic activity, particularly at 3:2 and 2:3 concentration ratios (Figure 2). Afterward, we observed that 5 µM of either BZ or DETC significantly inhibited parasite growth, whereas the combination of 2.5 µM of each compound was even more effective (Figure 3). In order to approach the DETC effects upon general parasite structure, we employed scanning

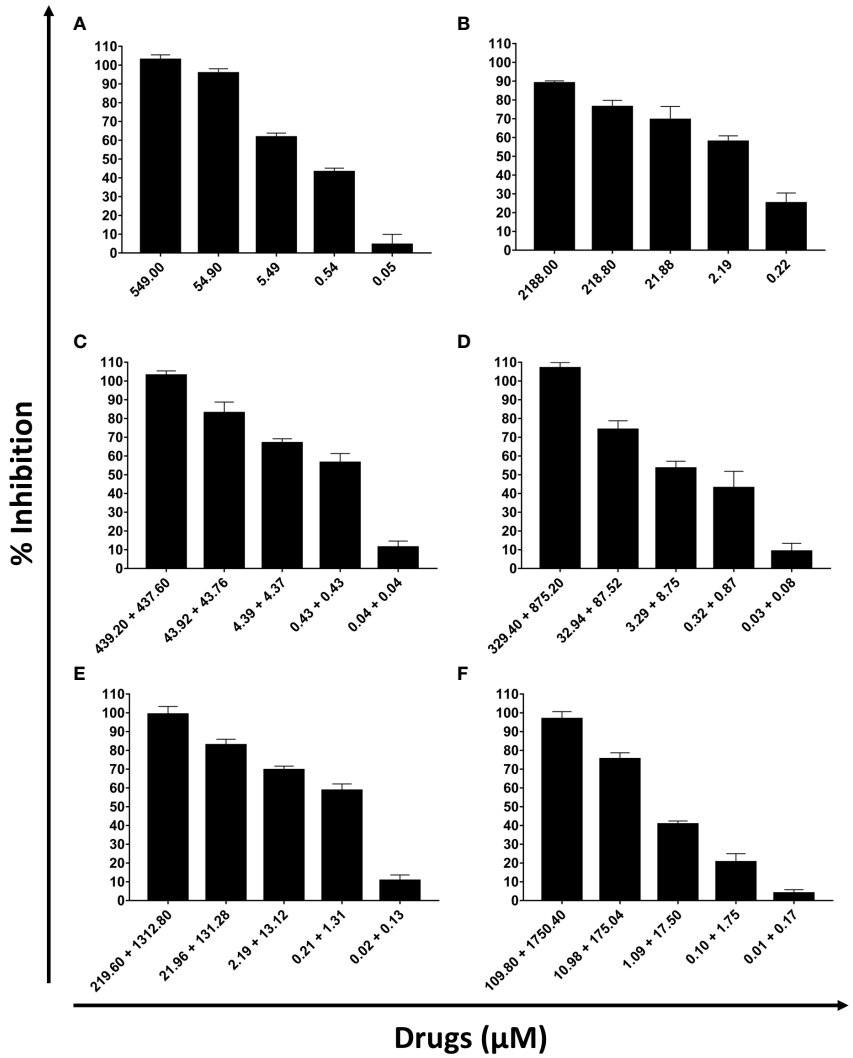

FIGURE 1
Evaluation of the activity of sodium diethyldithiocarbamate (DETC) and benznidazole (BZ) in the *in vitro* proliferation of *Trypanosoma cruzi* epimastigote forms (10^7 parasites/mL, Y strain). The proportions of the combinations were: 5 x IC_{50} DETC **(A)**; 5 x IC_{50} BZ **(B)**, 4 x IC_{50} DETC + IC_{50} BZ **(C)**, 3 x IC_{50} DETC + 2 x IC_{50} BZ **(D)**, 2 x IC_{50} DETC + 3 x IC_{50} BZ **(E)** and IC_{50} DETC + 4 x IC_{50} BZ **(F)**. After 24h incubation, the inhibitory effects were determined using Alamar Blue.

electron microscopy. DETC-treated epimastigotes were often bizarrely shaped, eventually presenting surface discontinuities and reduced cell body volume (Figure 4). We used transmission electron microscopy to determine the DTEC effects on epimastigote subcellular architecture. DETC-treated parasites displayed remarkably enlarged endoplasmic reticulum (ER) cisternae as well as reduced mitochondrial electrondensity (Figure 5). Morphometric analysis indicate the ER lumen was enhanced over 1000-fold (not shown). Some parasites displayed disorganized kinetoplast DNA and loss of cell ultrastructural compartmentation.

In order to approach reactive oxygen species (ROS) production in DETC-treated parasites, we used fluorescent probes. Incubation with DETC remarkably enhanced H_2DCFDA staining under fluorescence microscopy (Figure 6) and labeling was found in sub-cellular compartments, rather than whole cell. To evaluate the oxidative stress consequence, we measured lipoperoxidation using the TBARS assay (Figure 7). We observed that both BZ and DETC had little effect ($p > 0.05$) on lipid peroxidation, but it was significantly ($p < 0.05$) increased by their combination. Since sulfhydryl groups are largely involved in the redox regulation in trypanosomatid parasites, we measured thiol expression using the colorimetric Ellman's reaction DETC diminished thiol expression in the parasite (Figure 8). The biochemical colorimetric approach indicates that DETC produce a dose-dependent effect and that the

TABLE 1 Trypanocidal activity, cytotoxicity, and selectivity indexes of the DETC + BZ combination after 24 h of treatment.

Combination ratio (DETC : BZ)	Cytotoxicity (peritoneal cells)	*Trypanosoma cruzi* (Y) epimastigotes	Selectivity indexes
	CC_{50} (μM)	IC_{50} (μM)	
5:0	2.09	1.48	1.41
4:1	20.06	0.67	29.94
3:2	147.00	1.48	99.32
2:3	0.58	0.30	1.93
1:4	1.03	1.68	0.61
0:5	17.54	2.28	7.69

The CC_{50} and IC_{50} values of the combination were calculated from the cytotoxicity and inhibition assay, respectively, using Alamar Blue.

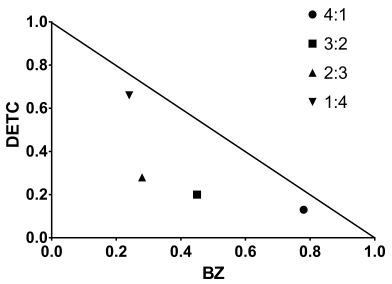

FIGURE 2
Representative isobologram demonstrating the synergistic interaction between DETC and BZ upon *T. cruzi* (Y strain) epimastigote forms, cultured for 24 h, based on IC_{50} values.

isolated compounds reduced SH levels ($p < 0.05$), but the combination was more effective ($p < 0.01$). As DETC is well-known for its SOD inhibiting capacity, we measured SOD activity *in vitro* and *in vivo*, in murine infection, before and after DETC treatment (Table 2). Interestingly, the combination was more inhibitory, and the effects *in vitro* were more pronounced.

As the Y strain is sensitive to BZ, we decided to test the DETC susceptibility of axenic amastigotes of both Y and Colombiana strains. Although the Colombiana strain, naturally resistant to BZ, was less sensitive to DETC at 0.8-3 μM ($p < 0.05$), the effects were highly significant ($p < 0.01$) at 5 μM. Both strains showed significantly decreased parasite survival in a dose-dependent manner (Figure 9).

In order to test the effects of the combination in intracellular parasites, we infected murine macrophages with blood trypomastigotes in the presence or in the absence of DETC (Figure 10). We noticed that 10 μM DETC remarkably reduced the monolayer parasite load, and a DETC-BZ combination at 5 μM concentration was equally or even more effective.

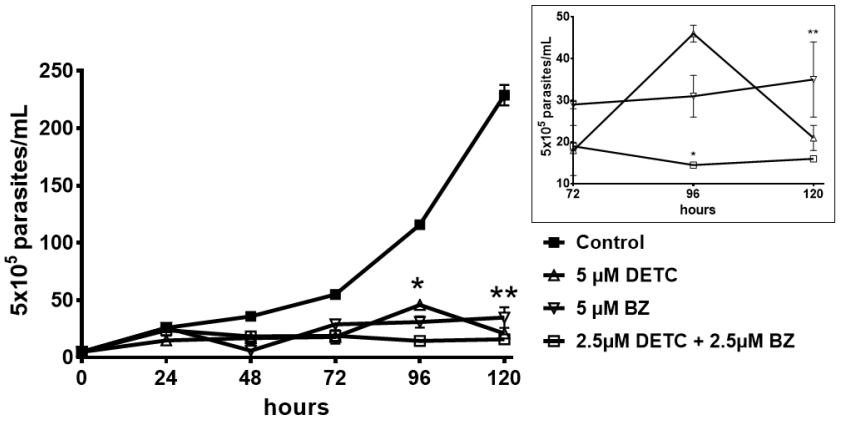

FIGURE 3
Evaluation of the *in vitro* proliferation of *T. cruzi* epimastigote forms (Y strain), challenged with DETC and BZ combined or alone. 10^5 parasites were incubated for 5 days with 5 μM DETC, 5 μM BZ and the combination of 2.5 μM each compound. The effects of the compounds were evaluated by daily quantitation of parasites by light microscopy. Inset displays 72-120 h data in a different scale. The combined drugs effectivity was significant, (*$p < 0.05$; **$p < 0.01$), despite the reduced concentrations, as compared to the parasites treated with BZ by the 2-way ANOVA. Data represent the mean ± SD (n = 3).

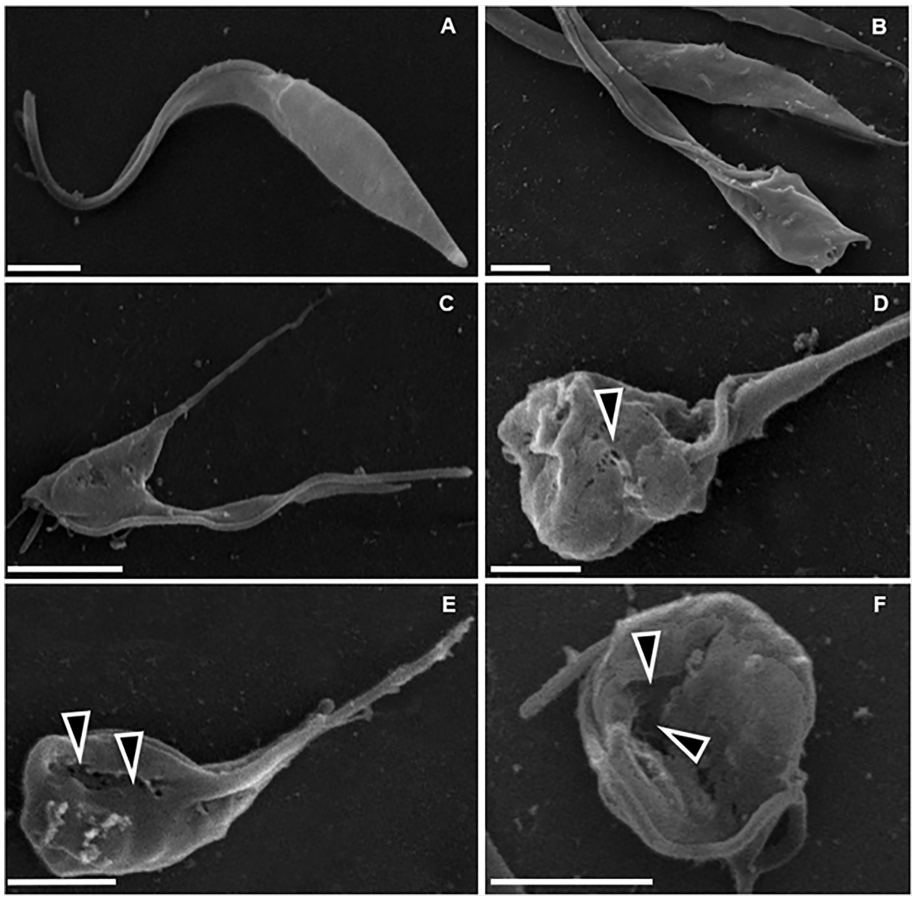

FIGURE 4
Scanning electron microscopy of *T. cruzi* epimastigote forms (Y strain). **(A)** Untreated control, showing normal parasite morphology. **B–F**) Parasites treated with 200 μM DETC for 24 h, showing cellular disorganization **(B, C)** and plasma membrane discontinuities (**D–F**, arrowheads), associated with cell body rounding and volume reduction. Bars correspond to 1 μm.

To approach the activity of the combination *in vivo*, we tested the murine infection for 30-60 days. The parasitemia of animals infected with both Y and Colombiana strains was reduced by the BZ-DSF combination (Figure 11) as compared to BZ low concentrations (20/50 mg/kg). The cumulative survival of the animas treated with the 10 mg/kg/day (each) DETC-BZ combination was increased by circa 6-fold ($p < 0.01$) as compared to BZ alone (Figure 12). We used histopathology to evaluate the murine infection. Contrary to animals treated with low BZ concentration (10 mg/kg/d) the ones incubated with the combination (10 mg/kg/d BZ + 10 mg/kg/d DETC) showed no amastigote nests in myocardium (Figure 13). The Sirus red staining was employed to assess tissue fibrosis. Animals treated with the combination displayed less, and focal fibrosis, whereas mice treated with BZ alone showed intense fibrosis staining. To evaluate the systemic toxicity of the treatments we measured the plasma levels of ALT, AST, CK, and urea. Measurements demonstrated (Figure 14) that the combination at 10 mg/kg/day (each) was not as toxic than the isolated drugs at 20 mg/kg/day.

Discussion

CD remains a major public health problem, as most of the infected people and domestic animals such as dogs, important reservoir hosts (Enriquez et al., 2014; Castillo-Neyra et al., 2015), are not treated or diagnosed (Dias et al., 2016). Since both drugs employed in CD chemotherapy are remarkably toxic (Castro and Diaz de Toranzo, 1988; Castro et al., 2006), therapy is frequently associated with severe adverse reactions, often causing treatment suspension (Levi et al., 1996; Olivera et al., 2017; Guggenbühl Noller et al., 2020; Pérez-Molina et al., 2021). Development of new safe and low-cost therapeutic alternatives is urgently required. Drug repositioning and combinations

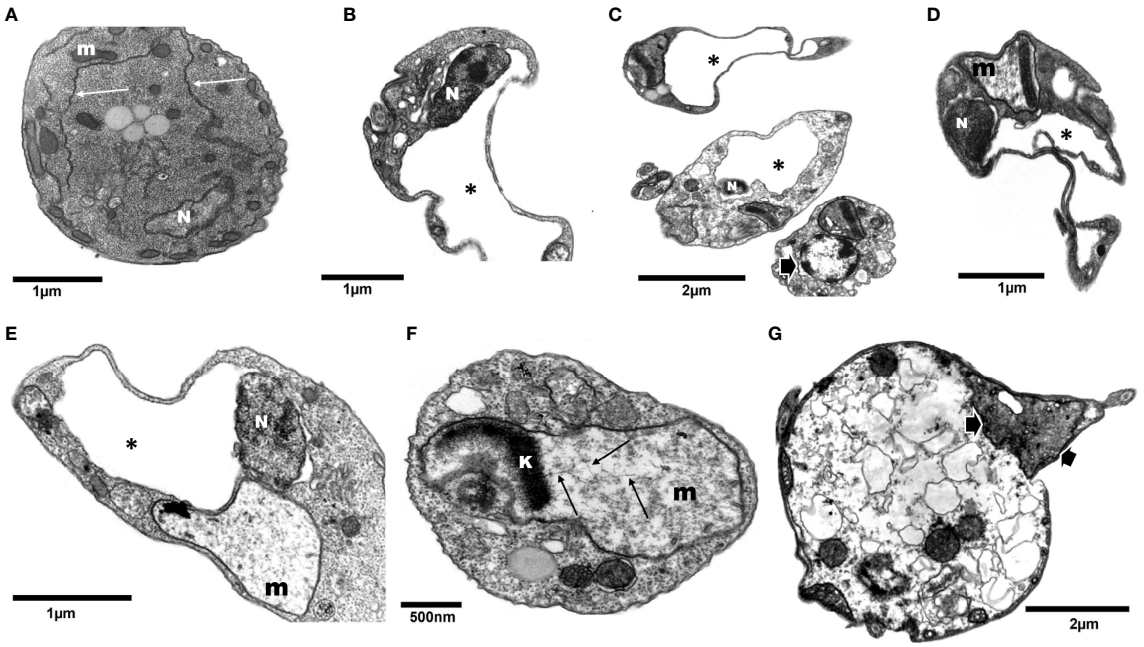

FIGURE 5
Transmission electron microscopy of *T. cruzi* epimastigotes (Y strain) incubated with 200 µM DETC for 24 h. Contrary to control cells (**A**, arrows – endoplasmic reticulum cisternae; m- mitochondria; N- nuclei), DETC treated **(B–G)** displayed remarkably enlarged endoplasmic reticulum cisternae **(B–E*)**, often replacing an even distorting nuclei **(B, C)**. Some parasites displayed electroluscent nuclear matrix with aggregated peripheral dense chromatin (**C**, arrow). Mitochondria were enlarged and generally presented reduced electrondensity **(D–F)** and eventually presenting kinetoplast (k) DNA (kDNA) disorganized fibers (**F**- arrows). Some cells displaying condensed mitochondria presenting swollen cristae (**C, G**-arrows) were also observed. In the final stage of treatment, parasites showed loss of normal compartmentation **(G)**.

comprise valuable tools for overcoming CD monotherapy limitations (e.g., Aguilera et al., 2019).

Both DETC and DSF express antiparasitic activities upon *T. cruzi* (Lane et al., 1996; de Freitas Oliveira et al., 2021; de Freitas Oliveira et al., 2022) and *Leishmania* (Khouri et al., 2010; Celes et al., 2016; Mazur et al., 2019). In macrophage cultures, DETC caused destruction of intracellular amastigotes with little effect on macrophage spreading pattern. Similarly, in the murine infection, the combination reduced parasitemia and significantly ($p < 0.001$) enhanced animal survival by circa 6-fold. Synergistic combinations can enhance selectivity (Zimmermann et al., 2007; Lehár et al., 2009a; Lehár et al., 2009b). In fact, the BZ + DETC combination was synergistic *in vitro* and *in vivo* and produced over 10-fold selectivity index increase. Such synergistic activities may be caused by the prooxidant effects of BZ (Pedrosa et al., 2001; Rigalli et al., 2016), associated with the antagonism of antioxidant defenses of DSF and that can allow dosing reduction (Bustamante et al., 2014), presumably leading to decreased adverse reactions. Besides, DSF and DETC were shown to reduce adverse reactions of other drugs (*vide supra*). Here we observed that reduced combined drug concentrations did not impair effectivity. Therefore, such combinations may lead to the development of safe and effective medications.

Since one of the major problems in CD therapy is the prompt rise of resistance, we tested the combination in axenic amastigotes as well as in infected macrophages, not only of the Y strain but also of the Colombiana one, highly drug-resistant (Andrade et al., 1985). Interestingly, both strains were sensitive to the thiocarbamates at low µM range. Drug combinations were employed for overcoming drug resistance rising but were not effective in leishmaniasis (García-Hernández et al., 2012) or malaria (Wongsrichanalai et al., 2002) and drug combinations were not effective upon drug-resistant *T. cruzi* (Bustamante et al., 2014).

CD treatment is confronted with growing frequencies of refractory cases. Over 60% of *T. cruzi* strains isolated in Colombia display some degree of BZ resistance (Mejía-Jaramillo et al., 2012) and strains isolated in the Brazilian Amazon show natural resistance to this drug (Teston et al., 2013). The rise of readily acquired (Neal and van Bueren, 1988; Mejia et al., 2012) or natural resistance (Zingales, 2018) significantly limit the therapeutic success of CD. Thus, a major relevance of the DSF + BZ stems from the potential revert drug resistance phenotypes, by inhibiting both activity (Loo et al., 2004; Sauna et al., 2004) and expression (Loo and Clarke, 2000) of p-glycoproteins, which are involved in *T. cruzi* drug resistance (Campos et al., 2013).

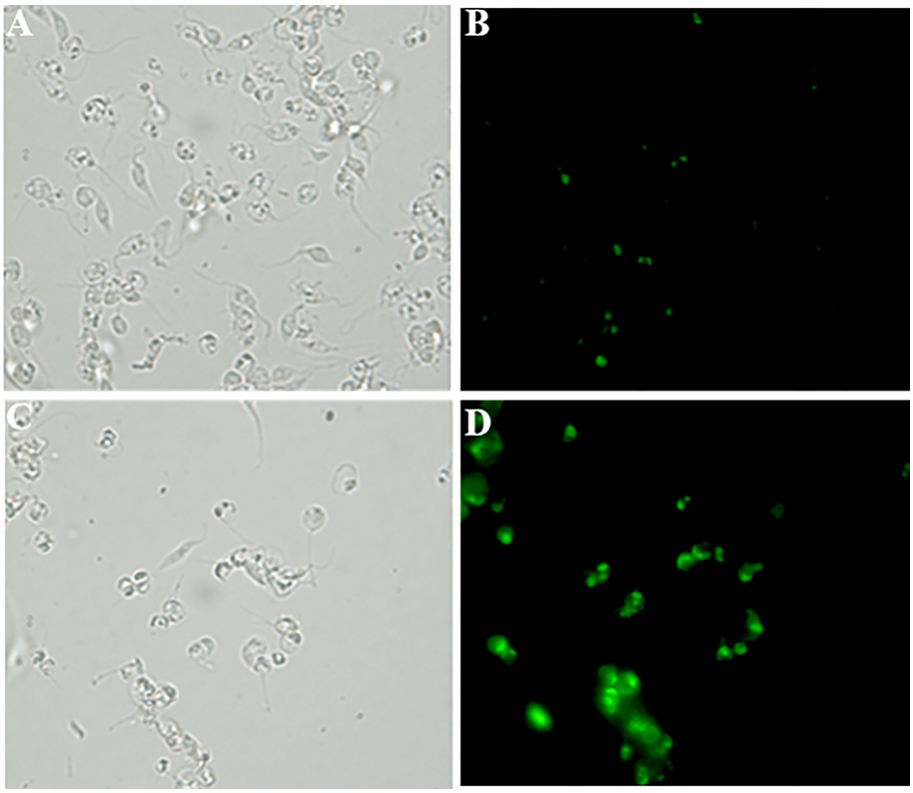

FIGURE 6
Detection of cellular reactive oxygen species (ROS) in *T. cruzi* epimastigote forms (Y strain) using the H_2DCFDA probe accessed by fluorescence microscopy **(B, D)**. **(A, B)** - Control and **(C, D)**- 10μM DETC-treated. **(A, C)** - phase contrast images. Note intense and compartmented staining in DETC-treated parasites. Magnification - 400X.

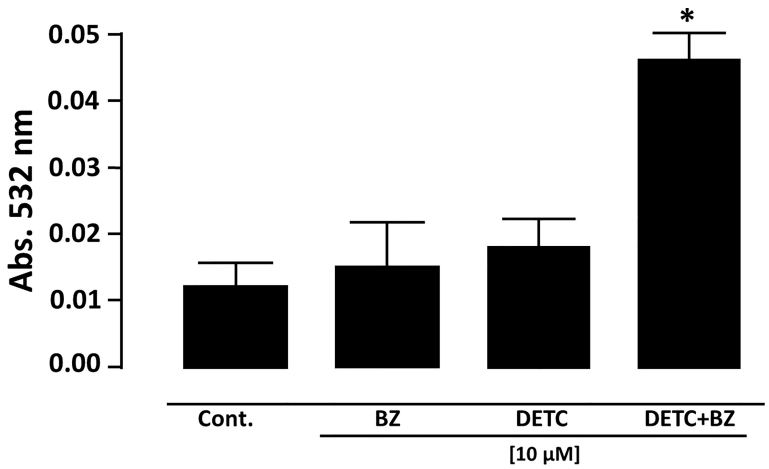

FIGURE 7
Measurement of lipid peroxidation in *T. cruzi* epimastigote forms (Y strain) by determination of thiobarbituric acid reactive substances (TBARS). Parasite cells treated with 10 μM DETC and 10 μM BZ combination for 24 h presented a significantly (*$p < 0.05$, ANOVA and Dunn's post-test) increased lipoperoxidation. Bars represent mean ± SD (n = 4).

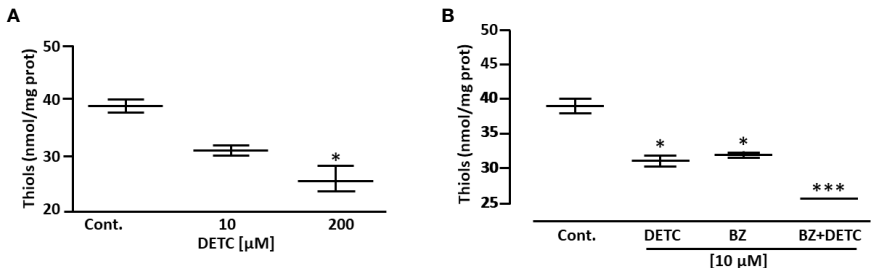

FIGURE 8
Effect of DETC and BZ on the concentration of low mol. wt. thiols of *T. cruzi* epimastigote forms (Y strain), determined colorimetrically by the Ellman reaction. DETC reduced thiol levels dose-dependently **(A)**. The DETC + BZ combination significantly potentiated thiol depletion **(B)**. Data represent mean ± SD. *$p < 0.05$ and ***$p < 0.001$ (ANOVA and Dunn's post-test; n = 5).

TABLE 2 Evaluation of *T. cruzi* superoxide dismutase (SOD) activity in presence of DETC *in vitro* and DSF *in vivo* isolated and combined to BZ.

Assay	SOD activity (U/mL)				
	Untreated (1% kolliphor)	BZ (100 μM)		DETC (100 μM)	BZ + DETC (50:50 μM)
In vitro[1] 1h	2.975	2.821		3.056	2.103**
In vitro[1] 24h	0.896	0.705		0.773*	0.734*
	Untreated (1% kolliphor)	BZ (50 mg/kg)	DSF(100 mg/kg)	BZ + DSF (50:50 mg/kg)	BZ + DSF (50:100 mg/kg)
In vivo[2]	0.059	0.059	0.058	0.063	0.052

[1]*T. cruzi* epimastigote forms (Y strain), treated or not with DETC isolated or in combination with BZ, spectrophotometrically measured.
[2]SOD activity of trypomastigote (Y strain)-infected mice treated for 3 consecutive days. * $p < 0.05$ and ** $p < 0.01$ ANOVA and Dunn's post-test (n = 3).

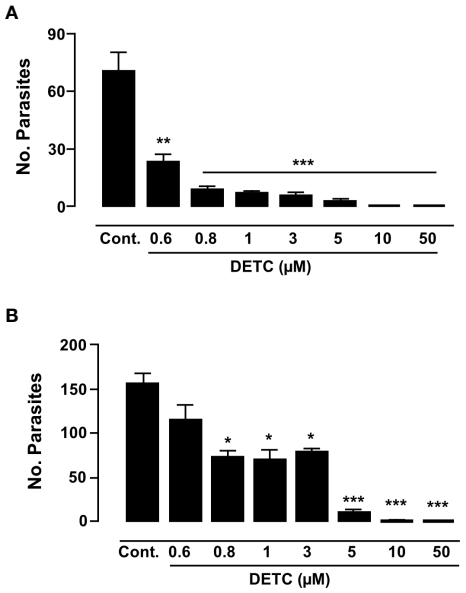

FIGURE 9
Inhibitory effect of DETC on the proliferation of *T. cruzi* amastigote forms in Y **(A)** and Colombiana **(B)** strains, after incubations of 120 h and 24 h, respectively. * $p < 0.05$, ** $p < 0.01$ and *** indicates $p < 0.001$ ANOVA and Dunn's post-test. Bars represent the mean ± SD (n=3).

Besides ABC cassette pumps (Zingales et al., 2015), natural resistance may rely on aldo-keto reductase and alcohol dehydrogenase (González et al., 2017). In this regard, it is important to notice that DSF inhibits alcohol dehydrogenase activity (Carper et al., 1987) and decreases the expression of aldo-keto reductase accessed by proteomic analysis (Yoshino et al., 2020). In addition, glutathione (GSH) forms conjugates with different drugs that are extruded by ABC transporters (Jedlitschky et al., 1994; Loe et al., 1998), so GSH and trypanothione (TSH) are implicated in detoxication of both NFX and BZ (Repetto et al., 1996). DSF can act as a glutathionylation agent (Hirschenson and Mailloux, 2021). Similarly, DETC derivatives form conjugates with GSH *via* carbamoylation (Ningaraj et al., 1998) and this reaction inhibits glutathione reductase (Miller and Blakely, 1992). *T. cruzi* ABC proteins externalize thiol-drug conjugates (da Costa et al., 2018) and inhibition of GSH and so TSH synthesis by buthionine sulfoximine (Maya et al., 2004; Faúndez et al., 2005; Vázquez et al., 2017) augments the effectivity of trypanocidal agents BZ and nifurtimox (Faúndez et al., 2005; Faúndez et al., 2008). Interestingly, DSF/DETC can diminish reduced GSH levels (Strömme, 1963; Ohno et al., 1990; Nagendra et al., 1994; Mittal et al., 2014) and GSH/TSH depletion can trigger *T. cruzi* programmed cell death (Piacenza et al., 2007). Here we observed reduced low mol. wt. thiol levels in DETC-treated

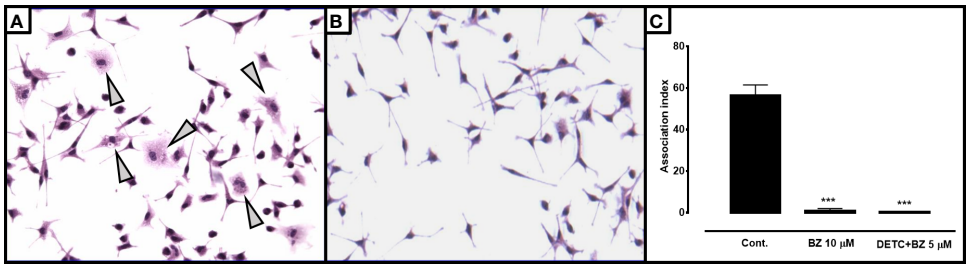

FIGURE 10
Effect of DETC alone or combined with BZ on the *T. cruzi*-macrophage interaction. BALB/c mice peritoneal macrophages were infected with Colombiana strain bloodstream trypomastigote forms 1:10 phagocyte/parasite ratio. Control cultures **(A)** showing several parasitized macrophages as well as larger number of intracellular forms per phagocyte (arrowheads) than cells treated with the combination 5 µM DETC + 5 µM BZ **(B)**. Magnification 200X. The association index in cultures treated with 10 µM BZ or the 5 µM DETC + 5 µM BZ combination after 24 hours of incubation **(C)** was significantly (***$p < 0.001$, ANOVA and Dunn's post-test) reduced. A slightly greater inhibition was observed in cultures incubated with the combination, despite the reduced concentrations. Bars represent mean ± SD.

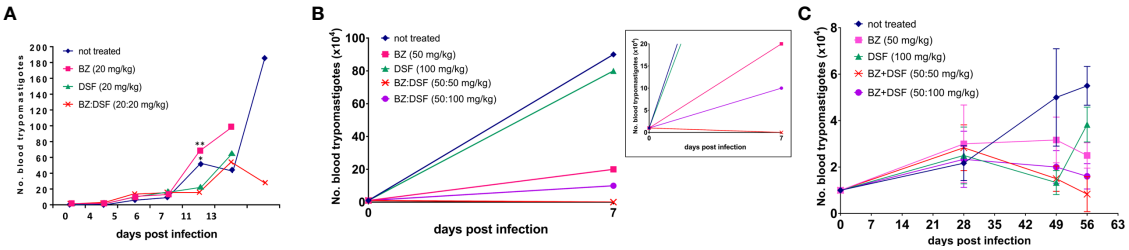

FIGURE 11
Parasitemia of Swiss Webster mice infected with *T. cruzi* blood trypomastigotes, Y strain **(A, B)** and Colombiana **(C)**. The animals were infected with 10^4 blood trypomastigotes/mL, strain Y, treated for 60 days with vehicle; low doses of BZ (20 mg/kg); DETC (20 mg/kg) or a combination of BZ + DETC (20:20 mg/kg), orally. *$p < 0.05$ and **$p < 0.01$ ANOVA test and Dunn's post-test **(A)**. Parasites treated with vehicle; BZ (50 mg/kg); DSF (50 mg/kg); combination of BZ + DSF (50:50 mg/kg); and BZ + DSF (50:100 mg/kg), administered for 10 consecutive days **(B, C**, $p > 0.05$**)**. Insert shows data in a different scale. The parasites were counted daily **(A)** or weekly **(B, C)** on Neubauer chambers and the graphs were plotted in GraphPad Prism, 7.

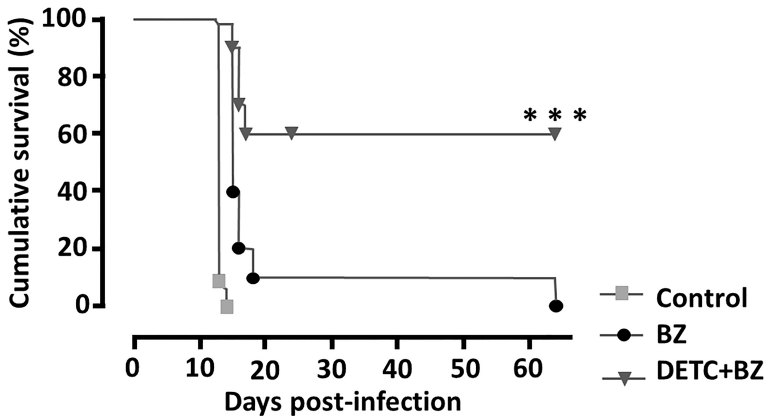

FIGURE 12
Monitoring the cumulative survival of mice infected intraperitoneally with 10^4 *T. cruzi* blood trypomastigote/mL (Y strain) of and treated with 10 mg/kg/day of DETC and BZ alone or in combination, p.o. daily for 60 consecutive days. Note that animals treated with the combination had a survival rate of 60%, whereas the group treated with BZ was 10% and the control group died on the 14^{th} day. ***$p < 0.001$ ANOVA and Tukey post-test.

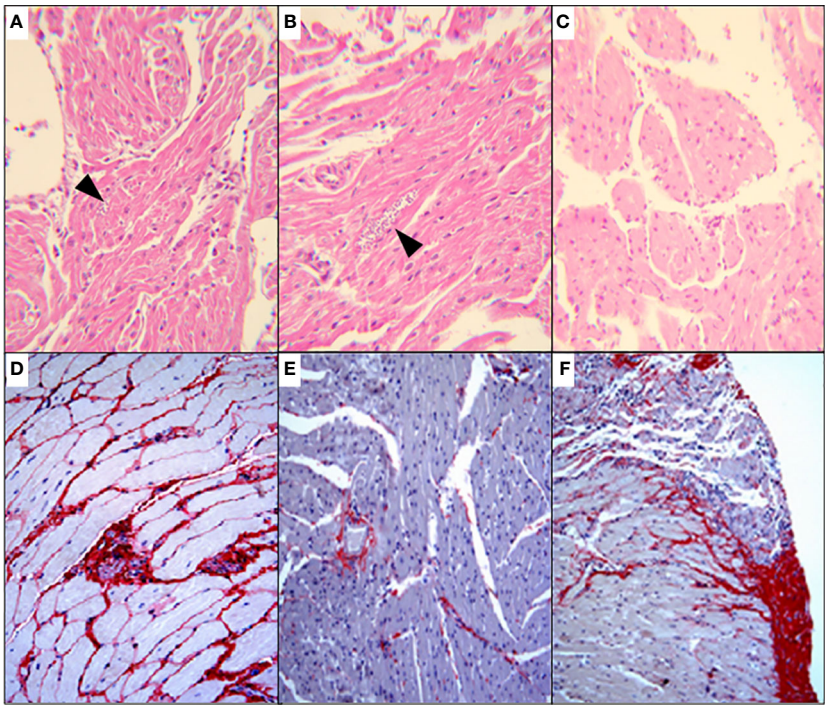

FIGURE 13
Histopathological analysis (H&E) of murine myocardium *T. cruzi* (Y strain)-infected mice, treated for 60 consecutive days, p.o. with vehicle **(A)**; 10 mg/kg/d BZ-treated and **(B)** treated with the of 10 mg/kg/d DETC combined to 10 mg/kg/d BZ **(C)**. Amastigote nests were observed in A and B (arrowheads). Skeletal muscle of mice infected with Colombiana strain, for 100 *d* and treated for 30 consecutive days orally with 20 mg/kg/d BZ **(D)**, 20 mg/kg/d DSF **(E)** or combination of 10 mg/kg/d each **(F)**. Picro Sirius red staining was employed to demonstrate fibrosis. The combination using lowered concentrations was associated with reduced fibrosis **(F)**. Magnification: 200X.

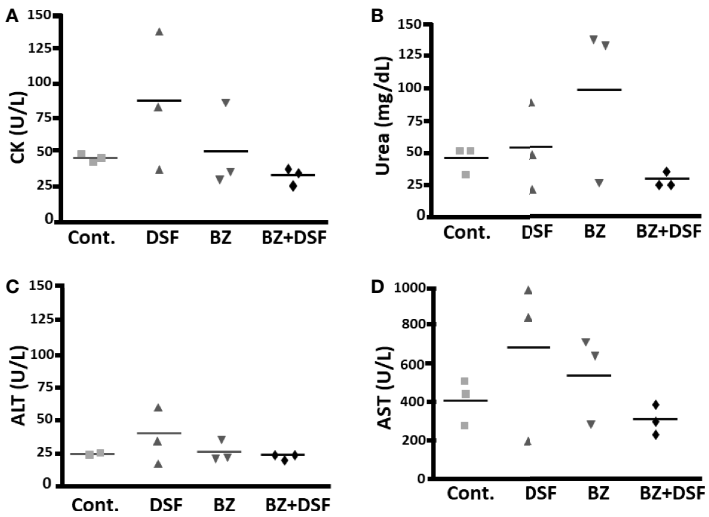

FIGURE 14
Systemic toxicity of mice treated with DSF and BZ, alone and in combination, by determining blood levels of creatine kinase **(A)**, urea **(B)**, alanine aminotransferase **(C)** and aspartate aminotransferase **(D)**; after 20 mg/kg BZ or DSF and the 10 mg/kg/d BZ + 10 mg/kg/d DSF. Contrary to isolated drugs, the combination, employing lowered dosages, did not increase plasma levels.

T.cruzi, by colorimetric and cytometric approaches, presumably by the formation of DS/DETC thiol-mediated conjugates with GSH (Jin et al., 1994). Similarly DSF reducing GSH levels, potentiate antiparasitic activity in malaria experimental models (De Jongh, 1953a; De Jongh, 1953b; Deharo et al., 2003). Therefore, the use DSF may overcome *T. cruzi* drug-resistance *via* different mechanisms.

The ultrastructural analysis performed here revealed surface membrane discontinuities, which may be explained by lipid peroxidation, corroborated by TBA determination, and the cell surface damage may lead to loss of cytoplasmic content culminating in necrosis and cell collapse observed by SEM. The analysis by TEM revealed remarkable damage on parasite ER and mitochondria, redox-active organelles. Oxidative stress induces ER stress (Liu et al., 2019; Esmaeili et al., 2022) and DSF triggers ROS-dependent ER stress (Shah O'Brien et al., 2019). The ER stress is related to the mitochondrial one (Wang et al., 2016; Kim et al., 2022; Yuan et al., 2022) and the latter can be promoted by the DETC-mediated SOD inhibition as well as by the reductions in GSH levels.

DSF causes ER stress associated with ROS production (Shah O'Brien et al., 2019). ER stress may cause the organelle cisternae dilation (Montalbano et al., 2013), which are not as conspicuous as the remarkable enlargement observed in *T. cruzi* here, *i.e.*, up to over 1000-fold, revealed by ultrastructural morphometry (not shown) and much higher than observed on mammalian cells. Such difference may be explained at least in part by a selective mechanism of action. It is noteworthy that ER stress was shown to be implicated in the CD cardiomyopathy in a murine model (Ayyappan et al., 2019). DETC can enhance ER stress in a kidney model (Kang et al., 2020), whereas its derivative DETC-MeSO (S-methyl-N, N-diethylthiocarbamate sulfoxide) can decrease ER stress markers in a stroke rat model (Mohammad-Gharibani et al., 2014).

The ubiquitin system comprises therapy target in diverse disorders (Wertz and Wang, 2019), and proteasome can be exploited as chemotherapy target for parasitic protozoa (Cromm and Crews, 2017; Xie et al., 2019). Parasite COP9 signalosomes comprise potential targets for chemotherapy (Ghosh et al., 2020). Interestingly DSF inhibits the ubiquitin-proteasome system (Cvek and Dvorak, 2008; Kona et al., 2011). The ER stress-associated cisternae dilation can be detected by EM (Riggs et al., 2005; Akiyama et al., 2009), so we employed the ultrastructural approach to help elucidating antiparasitic agents' mechanisms of action (Vannier-Santos and De Castro, 2009). The inhibition of proteasome function causes the accumulation of precursor proteins within ER cisternae (Hoefer and Groettrup, 2021) and accumulation of misfolded proteins may cause ER dilation (Sun et al., 2014) and trigger oxidation-reduction futile cycles producing H_2O_2 and depleting reduced GSH pools in the ER (Malhotra et al., 2008).

The *T. cruzi* intracellular Ca^{2+} homeostasis is an important therapeutic target (Benaim et al., 2020) and calcium can be transferred from the ER to mitochondria during stress *via* mitochondria associated membranes (MAM), also termed ER–mitochondria encounter structure (ERMES), and the Ca^{2+} overload may be implicated in mitochondrial damage (Mohsin et al., 2020). We have previously described the ER-mitochondria connection in *Leishmania braziliensis* treated with histone deacetylase (HDAC) inhibitors, including the nuclear envelope in the trypanosomatid parasite (Ângelo de Souza et al., 2020). HDAC inhibitors cause ER stress (Chen et al., 2017) and lead to the formation of mitochondria-ER tight binding, associated with ER cisternae enlargement, but it was much less pronounced than reported here. A similar mitochondria-ER association was detected here (Figure 5E), but since both compartments were remarkably enlarged, an eventual connection interpretation could be misleading.

Like the ER alterations, the DETC mitochondrial effects observed on the parasite cells were not detected on the mammalian cells, as previously reported in *Leishmania*-infected macrophage (Khouri et al., 2010). Remarkably enlarged mitochondria with washed out matrix were previously observed in both *T. cruzi* (Menezes et al., 2006) and *Leishmania amazonensis* (Vannier-Santos et al., 2008) exposed to 1,4-diamino-2-butanone a biocide that impairs the *T. cruzi* redox homeostasis (Soares et al., 2012) and induces lipoperoxidation (Menezes et al., 2006; Vannier-Santos et al., 2008). This putrescine analogue can inhibit polyamine transport and biosynthesis, affecting numerous parasite cell functions (Vannier-Santos and Suarez-Fontes, 2017), therefore involving different pharmaceutical targets (Roberts and Ullman, 2017). Polyamines play a pivotal role in trypanosomatid parasites, including the antioxidant protection from lipid peroxidation (Hernández et al., 2006). Also, this polycation metabolism is important for the antioxidant role of the spermidine-GSH adduct Trypanothione (N1, N8-Bis(glutathionyl)spermidine, TSH). TSH metabolism and SOD are drug targets for *T. cruzi* infection (Beltran-Hortelano et al., 2017; Piñeyro et al., 2021). Both NFX and BZ interfere with TSH metabolism (Maya et al., 1997; Maya et al., 2007), and TSH confers *T. cruzi* resistance to BZ and NFX (Maya et al., 2004; Faúndez et al., 2005; Mesías et al., 2019). TSH and tryparedoxin take part in BZ-resistance (González-Chávez et al., 2019) and the enzyme comprises a drug target (González-Chávez et al., 2015).

The fluorescent probe H_2DCFDA labeling indicates the ROS production and the oxidative stress triggering may be due both to SOD inhibition by DETC (Heikkila et al., 1976; Heikkila et al., 1978) as well as to lowering reduced glutathione levels (vide supra). The DSF-mediated glutathionylation enhances the $O_2^{\bullet-}$ and H_2O_2 production in mitochondria (Hirschenson and Mailloux, 2021) and SOD inhibition was previously shown to reduce *T. cruzi* parasitemia in murine infection (Olmo et al., 2015). The SOD inhibition observed here was significant on the parasite *in vitro*, but not *in vivo*, again possibly indicating a selective mechanism. Interestingly, the *T. brucei* SOD gene *sodb1*

deletion increases sensitivity to NFX and BZ (Prathalingham et al., 2007) and SOD inhibition enhances NFX antitumoral activity (Koto et al., 2011). In this regard, the DSF and DETC strongly inhibit *T. cruzi* SOD (Giulivi et al., 1988), and is trypanocidal (de Freitas Oliveira et al., 2021), also exerting leishmanicidal effects (Khouri et al., 2010). Interestingly, the *T. cruzi* Fe-SOD is found within parasite mitochondria, preventing programmed cell death (Piacenza et al., 2007). The immunofluorescence labeling of TcSOD in the parasite kinetoplast is relevant since it can preclude DNA fragmentation (Piacenza et al., 2007). In the TEM images shown here, we observed DETC-treated parasites with kDNA disorganization as well as mitochondrial damage. In this regard, arginase inhibition, causing redox imbalance, lead to kDNA disorganization in *Leishmania* (Cruz et al., 2013). SOD downmodulation may pose a dual advantage in CD therapy, since the enzymes are involved in intracellular survival, as scape mechanism from macrophage production of superoxide (Martínez et al., 2019), but also drug resistance (Nogueira et al., 2006; Campos et al., 2014; Campos et al., 2017). In this regard, the Sirtuin TcSir2rp3 induces the overexpressing TcFeSOD-A activities increasing *T. cruzi* resistance to BZ and NFX (dos Santos Moura et al., 2021).

Thiocarbamates chelate copper and trigger its accumulation and lipid peroxidation (Tonkin et al., 2004; Valentine et al., 2009; Viquez et al., 2009). Besides, copper-containing nanoparticles trigger oxidative stress and ER stress (Liu et al., 2021). Copper chelated by DSF induces cancer cells apoptosis in a ROS and mitochondria-dependent manner (Ren et al., 2021).

Ferroptosis is a programed cell death mechanism (Stockwell et al., 2017) characterized by mitochondria with enhanced matrix electron density and swollen cristae (Dixon et al., 2012). Such alterations were observed by TEM here, so this mechanism may be triggered by DSF. It should be kept in mind that different cell death mechanisms such as necrosis, apoptosis, and autophagy may be triggered simultaneously (dos Anjos et al., 2016). Interestingly, in a murine model of sepsis, the induction of pyroptosis and ferroptosis is associated with downregulation of the mitochondrial aldehyde dehydrogenase (Cao et al., 2022) and since DSF and DETC inhibit this enzyme (Deitrich and Erwin, 1971) may also trigger ferroptosis on parasite cells.

Inhibition of cystine uptake, employed in GSH (Badgley et al., 2020) synthesis, transport causes ER stress associated with ferroptosis in cancer cells (Dixon et al., 2014) and tryparedoxin peroxidase-deficient *Trypanosoma brucei* parasites undergo ferroptosis (Bogacz and Krauth-Siegel, 2018). Mitochondria are involved in cysteine-deprivation leading to ferroptosis (Gao et al., 2019).

The drug combination using DSF offers important advantages, which may be both economical (Cvek, 2012; Soave et al., 2016) and pharmacological, since this compound protects normal cells (Jia and Huang, 2021), can diminish the toxicity of different drugs such as cis-diamminedichloroplatinum (Wysor et al., 1982), including myocardial protection (Sonawane et al., 2018) and *circa* 30% of the CD patients develop heart disease, characterized by arrhythmias among other cardiac manifestations (Saraiva et al., 2021). It is worth mentioning that DSF can suppress cardiac arrhythmogenesis (Sander et al., 2021). Nevertheless, DETC and DSF were reported to cause neuropathies (Worner, 1982; Frisoni and Di Monda, 1989). In addition, BZ and NFX may cause neuropsychiatric reactions (Jackson et al., 2020). In this regard, it is noteworthy that DSF and its derivatives were also reported to act as neuroprotective agents (Zhao et al., 2000; Ningaraj et al., 2001; Libeu et al., 2012; Mohammad-Gharibani et al., 2014; Prentice et al., 2015). The eventual neurotoxic activity may be due at least in part to high dosages used in the past (Gessner and Gessner, 1992) and oxidative stress produced by copper accumulation leading to lipid peroxidation (Tonkin et al., 2004), although DSF may exert antioxidant effects (Kyle et al., 1989). This property is relevant since both BZ (Pedrosa et al., 2001; Rigalli et al., 2016) and CD (de Oliveira et al., 2007; Gupta et al., 2009) are associated with oxidative stress.

Histopathological samples revealed no amastigote nests detected in tissues of animals treated with low doses of the DSF-BZ combination, which showed mild inflammatory infiltrates and did not display significant fibrosis as assessed a by the picrosirius red staining. CD is an inflammatory infection (Talvani and Teixeira, 2011) associated with fibrosis and pyroptosis (Cerbán et al., 2020). The *T. cruzi* infection leads to ROS formation in the mitochondria, triggering PARP-1 and NF-kappaB activation, culminating in the production of pro-inflammatory cytokines such as Il-12 and IFN-γ (Ba et al., 2010), involved in cardiomyopathy pathophysiology (Cunha-Neto et al., 1998). In this regard, DSF is anti-inflammatory (Kanai et al., 2011), of potential use for inflammatory disorders (Guo et al., 2022), inhibiting oxidative stress and inflammasome activation, preventing cardiac damage (Wei et al., 2022), suppressing fibrosis (Zhang et al., 2021) and pyroptosis (Hu et al., 2020; Li et al., 2022; Zhou et al., 2022). The immune response to *T. cruzi* infection associated with myocardial fibrosis involves TGF-β (Chaves et al., 2019), and this cytokine comprises a therapeutic target in the CD cardiac damage (Waghabi et al., 2022). In this regard, DSF can inhibit TGF-β receptor signal transduction (Jiang et al., 2021).

Systemic toxicity assays based on the measurement of plasmatic CK, AST, ALT, and urea indicate decreased or insignificant toxicity. DSF was shown to reduce toxicity of several drugs such as cis-diamminedichloroplatinum, a property termed "disulfiram rescue" for saving the treated organism (Wysor et al., 1982; Roemeling et al., 1986). DETC is also considered a rescue agent (Gandara et al., 1990).

Because of promising *in vitro* and *in vivo* results, we are starting a clinical trial with the DSF-BZ combination (Saraiva et al., 2021), comprising a *bona fide* translational approach.

Taken together, the present data and the cytoprotective capacity of DSF/DETC as well as the resistance reversion potential, such a combination may be safe and effective, even in refractory CD cases.

Data availability statement

The raw data supporting the conclusions of this article will be made available by the authors, without undue reservation.

Ethics statement

The animal study was reviewed and approved by Comissão de Ética no Uso de Animais do Instituto Oswaldo Cruz/Fiocruz. lic. no. L012/2020.

Author contributions

JA-S, DM, JF, MA, and DV-d-S: experiment execution; RS, AV, SP, AS-F: Data interpretation, discussion and translational research planning; SA, Histopathological analysis; MV-S: Project conception, study planning, funding obtaining, student supervision, microscopy interpretation; discussion. All authors contributed to the article and approved the submitted version.

Funding

Conselho Nacional de Desenvolvimento Científico e Tecnológico (CNPq), grant number 314717/2020 and Fundação Carlos Chagas Filho de Amparo à Pesquisa do Estado do Rio de Janeiro (FAPERJ) grant number 260475/2021, 259286/2021, provide most of the scholarships of the team as well as consumables used in the experiments. Oswaldo Cruz Institute (IOC)/Oswaldo Cruz Fundation (Fiocruz) provides the general infrastructure and supports the open access publication fees.

Acknowledgments

The authors acknowledge the valuable partnership of Farmanguinhos and INI/Fiocruz as well as the contributions FIOCRUZ technological platforms. To Dr. Marcus Fernandes Oliveira for valuable discussions and critical reading of the manuscript.

Conflict of interest

The authors declare that the research was conducted in the absence of any commercial or financial relationships that could be construed as a potential conflict of interest.

Publisher's note

References

Aguilera, E., Alvarez, G., Cerecetto, H., and González, M. (2019). Polypharmacology in the treatment of Chagas disease. *Curr. Med. Chem.* 26 (23), 4476–4489. doi: 10.2174/0929867325666180410101728

Akiyama, M., Hatanaka, M., Ohta, Y., Ueda, K., Yanai, A., Uehara, Y., et al. (2009). Increased insulin demand promotes while pioglitazone prevents pancreatic beta cell apoptosis in Wfs1 knockout mice. *Diabetologia* 52 (4), 653–663. doi: 10.1007/s00125-009-1270-6

Andrade, S. G., Kloetzel, J. K., Borges, M. M., and Ferrans, V. J. (1994). Morphological aspects of the myocarditis and myositis in *Calomys callosus* experimentally infected with *Trypanosoma cruzi*: fibrogenesis and spontaneous regression of fibrosis. *Mem. Inst. Oswaldo Cruz.* 89 (3), 379–393. doi: 10.1590/S0074-02761994000300017

Andrade, S. G., Magalhães, J. B., and Pontes, A. L. (1985). Evaluation of chemotherapy with benznidazole and nifurtimox in mice infected with *Trypanosoma cruzi* strains of different types *Bull. World Health Organ.* 63 (4), 721–726.

Ângelo de Souza, L., Silva e Bastos, M., de Melo Agripino, J., Souza Onofre, T., Apaza Calla, L. F., Heimburg, T., et al. (2020). Histone deacetylases inhibitors as new potential drugs against *Leishmania braziliensis*, the main causative agent of new world tegumentary leishmaniasis. *Biochem. Pharmacol.* 180, 114191. doi: 10.1016/j.bcp.2020.114191

Askgaard, G., Friis, S., Hallas, J., Thygesen, L. C., and Pottegård, A. (2014). Use of disulfiram and risk of cancer. *Eur. J. Cancer Prev.* 23 (3), 225–232. doi: 10.1097/CEJ.0b013e3283647466

Ayyappan, J. P., Lizardo, K., Wang, S., Yurkow, E., and Nagajyothi, J. F. (2019). Inhibition of ER stress by 2-aminopurine treatment modulates cardiomyopathy in a murine chronic Chagas disease model. *Biomol Ther. (Seoul).* 27 (4), 386–394. doi: 10.4062/biomolther.2018.193

Badgley, M. A., Kremer, D. M., Maurer, H. C., DelGiorno, K. E., Lee, H. J., Purohit, V., et al. (2020). Cysteine depletion induces pancreatic tumor ferroptosis in mice. *Science* 368 (6486), 85–89. doi: 10.1126/science.aaw9872

Ba, X., Gupta, S., Davidson, M., and Garg, N. J. (2010). *Trypanosoma cruzi* induces the reactive oxygen species-PARP-1-RelA pathway for up-regulation of cytokine expression in cardiomyocytes. *J. Biol. Chem.* 285 (15), 11596–11606. doi: 10.1074/jbc.M109.076984

Beltran-Hortelano, I., Alcolea, V., Font, M., and Pérez-Silanes, S. (2022). Examination of multiple *Trypanosoma cruzi* targets in a new drug Discov approach for Chagas disease. *Bioorg. Med. Chem.* 58, 116577. doi: 10.1016/j.bmc.2021.116577

Beltran-Hortelano, I., Perez-Silanes, S., and Galiano, S. (2017). Trypanothione reductase and superoxide dismutase as current drug targets for *Trypanosoma cruzi*:

An overview of compounds with activity against Chagas disease. *Curr. Med. Chem.* 24 (11), 1066–1138. doi: 10.2174/0929867323666161227094049

Benaim, G., Paniz-Mondolfi, A. E., Sordillo, E. M., and Martinez-Sotillo, N. (2020). Disruption of intracellular calcium homeostasis as a therapeutic target against *Trypanosoma cruzi*. *Front. Cell. Infect. Microbiol.* 10, 46. doi: 10.3389/fcimb.2020.00046

Bodenner, D. L., Dedon, P. C., Keng, P. C., Katz, J. C., and Borch, R. F. (1986) Selective protection against cis-diamminedichloroplatinum(II)-induced toxicity in kidney, gut, and bone marrow by diethyldithiocarbamate *Cancer Res.* 46 (6), 2751–2755.

Bogacz, M., and Krauth-Siegel, R. L. (2018). Tryparedoxin peroxidase-deficiency commits trypanosomes to ferroptosis-type cell death. *ELife* 7, e37503. doi: 10.7554/eLife.37503

Bustamante, J. M., Craft, J. M., Crowe, B. D., Ketchie, S. A., and Tarleton, R. L. (2014). New, combined, and reduced dosing treatment protocols cure *Trypanosoma cruzi* infection in mice. *J. Infect. Dis.* 209 (1), 150–162. doi: 10.1093/infdis/jit420

Campos, M. C. O., Castro-Pinto, D. B., Ribeiro, G. A., Berredo-Pinho, M. M., Gomes, L. H. F., da Silva Bellieny, M. S., et al. (2013). P-glycoprotein efflux pump plays an important role in *Trypanosoma cruzi* drug resistance. *Parasitol. Res.* 112 (6), 2341–2351. doi: 10.1007/s00436-013-3398-z

Campos, M. C. O., Leon, L. L., Taylor, M. C., and Kelly, J. M. (2014). Benznidazole-resistance in *Trypanosoma cruzi*: Evidence that distinct mechanisms can act in concert. *Mol. Biochem. Parasitol.* 193 (1), 17–19. doi: 10.1016/j.molbiopara.2014.01.002

Campos, M. C. O., Phelan, J., Francisco, A. F., Taylor, M. C., Lewis, M. D., Pain, A., et al. (2017). Genome-wide mutagenesis and multi-drug resistance in American trypanosomes induced by the front-line drug benznidazole. *Sci. Rep.* 7 (1), 14407. doi: 10.1038/s41598-017-14986-6

Cao, Z., Qin, H., Huang, Y., Zhao, Y., Chen, Z., Hu, J., et al. (2022). Crosstalk of pyroptosis, ferroptosis, and mitochondrial aldehyde dehydrogenase 2-related mechanisms in sepsis-induced lung injury in a mouse model. *Bioengineered* 13 (3), 4810–4820. doi: 10.1080/21655979.2022.2033381

Carper, W. R., Dorey, R. C., and Beber, J. H. (1987) Inhibitory effect of disulfiram (Antabuse) on alcohol dehydrogenase activity. *Clin. Chem.* 33 (10), 1906–1908.

Castillo-Neyra, R., Chou Chu, L., Quispe-Machaca, V., Ancca-Juarez, J., Malaga Chavez, F. S., Bastos Mazuelos, M., et al. (2015). The potential of canine sentinels for reemerging *Trypanosoma cruzi* transmission. *Prev. Vet. Med.* 120 (3–4), 349–356. doi: 10.1016/j.prevetmed.2015.04.014

Castro, J. A., DeMecca, M. M., and Bartel, L. C. (2006). Toxic side effects of drugs used to treat Chagas' disease (American trypanosomiasis). *Hum. Exp. Toxicol.* 25 (8), 471–479. doi: 10.1191/0960327106het653oa

Castro, J. A., and Diaz de Toranzo, E. G. (1988). Toxic effects of nifurtimox and benznidazole, two drugs used against American trypanosomiasis (Chagas' disease). *Biomed. Environ. Sci.* 1 (1), 19–33.

Celes, F. S., Trovatti, E., Khouri, R., Van Weyenbergh, J., Ribeiro, S. J. L., Borges, V. M., et al. (2016). DETC-based bacterial cellulose bio-curatives for topical treatment of cutaneous leishmaniasis. *Sci. Rep.* 6 (1), 38330. doi: 10.1038/srep38330

Cerbán, F. M., Stempin, C. C., Volpini, X., Carrera Silva, E. A., Gea, S., and Motran, C. C. (2020). Signaling pathways that regulate *Trypanosoma cruzi* infection and immune response. *Biochim. Biophys. Acta Mol. Basis Dis.* 1866 (5), 165707. doi: 10.1016/j.bbadis.2020.165707

Chaves, A. T., Menezes, C. A. S., Costa, H. S., Nunes, M. C. P., and Rocha, M. O. C. (2019). Myocardial fibrosis in Chagas disease and molecules related to fibrosis. *Parasite Immunol.* 41 (10), e12663. doi: 10.1111/pim.12663

Chen, Y., Tsai, Y.-H., and Tseng, S.-H. (2017). HDAC inhibitors and RECK modulate endoplasmic reticulum stress in tumor cells. *Int. J. Mol. Sci.* 18 (2), 258. doi: 10.3390/ijms18020258

Coura, J. R., and Viñas, P. A. (2010). Chagas disease: a new worldwide challenge. *Nature* 465 (S7301), S6–S7. doi: 10.1038/nature09221

Crespillo-Andújar, C., Chamorro-Tojeiro, S., Norman, F., Monge-Maillo, B., López-Vélez, R., and Pérez-Molina, J. A. (2018). Toxicity of nifurtimox as second-line treatment after benznidazole intolerance in patients with chronic Chagas disease: when available options fail. *Clin. Microbiol. Infect.* 24 (12), 1344.e1–1344.e4. doi: 10.1016/j.cmi.2018.06.006

Cromm, P. M., and Crews, C. M. (2017). Targeted protein degradation: from chemical biology to drug Discov. *Cell Chem. Biol.* 24 (9), 1181–1190. doi: 10.1016/j.chembiol.2017.05.024

Cruz, E., de, M., da Silva, E. R., Maquiaveli, C.do C., Alves, E. S., Lucon, J. F.Jr., et al. (2013). Leishmanicidal activity of *Cecropia pachystachya* flavonoids: arginase inhibition and altered mitochondrial DNA arrangement. *Phytochemistry* 89, 71–77. doi: 10.1016/j.phytochem.2013.01.014

Cunha-Neto, E., Rizzo, L. V., Albuquerque, F., Abel, L., Guilherme, L., Bocchi, E., et al. (1998). Cytokine production profile of heart-infiltrating T cells in Chagas' disease cardiomyopathy. *Braz. J. Med. Biol. Res.* 31 (1), 133–137. doi: 10.1590/S0100-879X1998000100018

Cvek, B. (2012). Nonprofit drugs as the salvation of the world's healthcare systems: the case of antabuse (disulfiram). *Drug Discov Today* 17 (9–10), 409–412. doi: 10.1016/j.drudis.2011.12.010

Cvek, B., and Dvorak, Z. (2008). The value of proteasome inhibition in cancer. *Drug Discov Today* 13 (15–16), 716–722. doi: 10.1016/j.drudis.2008.05.003

da Costa, K. M., Valente, R. C., Salustiano, E. J., Gentile, L. B., Freire-de-Lima, L., Mendonça-Previato, L., et al. (2018). Functional characterization of ABCC proteins from *Trypanosoma cruzi* and their involvement with thiol transport. *Front. Microbiol.* 9. doi: 10.3389/fmicb.2018.00205

de Freitas Oliveira, J. W., da Silva, M. F. A., Damasceno, I. Z., Rocha, H. A. O., da Silva Júnior, A. A., and Silva, M. S. (2022). *In vitro* validation of antiparasitic activity of PLA-nanoparticles of sodium diethyldithiocarbamate against *Trypanosoma cruzi*. *Pharmaceutics* 14 (3), 497. doi: 10.3390/pharmaceutics14030497

de Freitas Oliveira, J. W., Torres, T. M., Moreno, C. J. G., Amorim-Carmo, B., Damasceno, I. Z., Soares, A. K. M. C., et al. (2021). Insights of antiparasitic activity of sodium diethyldithiocarbamate against different strains of *Trypanosoma cruzi*. *Sci. Rep.* 11 (1), 11200. doi: 10.1038/s41598-021-90719-0

Deharo, E., Barkan, D., Krugliak, M., Golenser, J., and Ginsburg, H. (2003). Potentiation of the antimalarial action of chloroquine in rodent malaria by drugs known to reduce cellular glutathione levels. *Biochem. Pharmacol.* 66 (5), 809–817. doi: 10.1016/S0006-2952(03)00396-4

Deitrich, R. A., and Erwin, V. G. (1971). Mechanism of the inhibition of aldehyde dehydrogenase *in vivo* by disulfiram and diethyldithiocarbamate. *Mol. Pharmacol.* 7 (3), 301–307.

De Jongh, D. K. (1953a). Effect of tetra-ethylthiuramdisulphide (T.T.S.) on the antimalarial activity of quinine in *Plasmodium berghei* infections in mice. *Acta Physiol. Pharmacol. Neerl.* 3 (1), 34–37.

De Jongh, D. K. (1953b). Effect of tetra-ethylthiuramdisulphide on the antimalarial activity of quinine in *Plasmodium gallinaceum* infections in chickens. *Acta Physiol. Pharmacol. Neerl.* 3 (1), 38–44.

de Oliveira, T. B., Pedrosa, R. C., and Filho, D. W. (2007). Oxidative stress in chronic cardiopathy associated with Chagas disease. *Int. J. Cardiol.* 116 (3), 357–363. doi: 10.1016/j.ijcard.2006.04.046

Dias, J. C. P., Novaes Ramos, A., Dias Gontijo, E., Luquetti, A., Shikanai-Yasuda, M. A., Rodrigues Coura, J., et al. (2016). II consenso brasileiro em doença de chaga. *Epid. Serv. Saúde* 25 (21), 1–10. doi: 10.5123/S1679-49742016000500002

Dixon, S. J., Lemberg, K. M., Lamprecht, M. R., Skouta, R., Zaitsev, E. M., Gleason, C. E., et al. (2012). Ferroptosis: an iron-dependent form of nonapoptotic cell death. *Cell* 149 (5), 1060–1072. doi: 10.1016/j.cell.2012.03.042

Dixon, S. J., Patel, D. N., Welsch, M., Skouta, R., Lee, E. D., Hayano, M., et al. (2014). Pharmacological inhibition of cystine–glutamate exchange induces endoplasmic reticulum stress and ferroptosis. *ELife* 3, e02523. doi: 10.7554/eLife.02523

dos Anjos, D. O., Sobral Alves, E. S., Gonçalves, V. T., Fontes, S. S., Nogueira, M. L., Suarez-Fontes, A. M., et al. (2016). Effects of a novel β–lapachone derivative on *Trypanosoma cruzi*: Parasite death involving apoptosis, autophagy and necrosis. *Int. J. Parasitol. Drugs Drug Resist.* 6 (3), 207–219. doi: 10.1016/j.ijpddr.2016.10.003

dos Santos Moura, L., Santana Nunes, V., Gomes, A. A. S., Sousa, A. C., de, C. N., Fontes, M. R. M., et al. (2021). Mitochondrial sirtuin TcSir2rp3 affects TcSODA activity and oxidative stress response in *Trypanosoma cruzi*. *Front. Cell. Infect. Microbiol.* 11, 773410. doi: 10.3389/fcimb.2021.773410

Duschak, V. G. (2011). A decade of targets and patented drugs for chemotherapy of cChagas disease. *Recent Pat. Anti-Infect. Drug Discov* 6 (3), 216–259. doi: 10.2174/157489111796887864

Duschak, V. G. (2016). Targets and patented drugs for chemotherapy of Chagas disease in the last 15 years-period. *Recent Pat. Anti-Infect. Drug Discov* 11 (2), 74–173. doi: 10.2174/1574891X11666161024165304

Duschak, V. G. (2019). Major kinds of drug targets in Chagas disease or American trypanosomiasis. *Curr. Drug Targets* 20 (11), 1203–1216. doi: 10.2174/1389450120666190423160804

Elliott, W. C., Newcom, S. R., Houghton, D. C., Baines-Hunter, J., and Bennett, W. M. (1983). Cis-diamminedichloroplatinum(II) nephrotoxicity: Tubular function after rescue with sodium diethyldithiocarbamate in rats. *Cancer Res.* 43 (8), 3759–3762.

Engel, J. C., Franke de Cazzulo, B. M., Stoppani, A. O., Cannata, J. J., and Cazzulo, J. J. (1987). Aerobic glucose fermentation by *Trypanosoma cruzi* axenic culture amastigote-like forms during growth and differentiation to epimastigotes. *Mol. Biochem. Parasitol.* 26 (1-2), 1–10. doi: 10.1016/0166-6851(87)90123-x

Enriquez, G. F., Bua, J., Orozco, M. M., Wirth, S., Schijman, A. G., Gürtler, R. E., et al. (2014). High levels of *Trypanosoma cruzi* DNA determined by qPCR and infectiousness to *Triatoma infestans* support dogs and cats are major sources of

parasites for domestic transmission. *Infect. Genet. Evol.* 25, 36–43. doi: 10.1016/j.meegid.2014.04.002

Esmaeili, Y., Yarjanli, Z., Pakniya, F., Bidram, E., Łos, M. J., Eshraghi, M., et al. (2022). Targeting autophagy, oxidative stress, and ER stress for neurodegenerative disease treatment. *J. Control Release* 345, 147–175. doi: 10.1016/j.jconrel.2022.03.001

Faúndez, M., López-Muñoz, R., Torres, G., Morello, A., Ferreira, J., Kemmerling, U., et al. (2008). Buthionine sulfoximine has anti-*Trypanosoma cruzi* activity in a murine model of acute Chagas' disease and enhances the efficacy of nifurtimox. *Antimicrob. Agents Chemother.* 52 (5), 1837–1839. doi: 10.1128/AAC.01454-07

Faúndez, M., Pino, L., Letelier, P., Ortiz, C., López, R., Seguel, C., et al. (2005). Buthionine sulfoximine increases the toxicity of nifurtimox and benznidazole to *Trypanosoma cruzi*. *Antimicrob. Agents Chemother.* 49 (1), 126–130. doi: 10.1128/AAC.49.1.126-130.2005

Fivelman, Q. L., Adagu, I. S., and Warhurst, D. C. (2004). Modified fixed-ratio isobologram method for studying *in vitro* interactions between atovaquone and proguanil or dihydroartemisinin against drug-resistant strains of *Plasmodium falciparum*. *Antimicrob. Agents Chemother.* 48 (11), 4097–4102. doi: 10.1128/AAC.48.11.4097-4102.2004

Franco-Paredes, C., Bottazzi, M. E., and Hotez, P. J. (2009). The unfinished public health agenda of Chagas disease in the era of globalization. *PloS Negl. Trop. Dis.* 3 (7), e470. doi: 10.1371/journal.pntd.0000470

Frisoni, G. B., and Di Monda, V. (1989). Disulfiram neuropathy: a review 1971-1988) and report of a case. *Alcohol Alcohol.* 24 (5), 429–437.

Gandara, D. R., Wiebe, V. J., Perez, E. A., Makuch, R. W., and DeGregorio, M. W. (1990). Cisplatin rescue therapy: Experience with sodium thiosulfate, WR2721, and diethyldithiocarbamate. *Crit. Rev. Oncol. Hematol.* 10 (4), 353–365. doi: 10.1016/1040-8428(90)90010-P

Gao, M., Yi, J., Zhu, J., Minikes, A. M., Monian, P., Thompson, C. B., et al. (2019). Role of mitochondria in ferroptosis. *Mol. Cell.* 73 (2), 354–363.e3. doi: 10.1016/j.molcel.2018.10.042

García-Hernández, R., Manzano, J. I., and Castanys S and Gamarro, F. (2012). *Leishmania donovani* develops resistance to drug combinations. *PloS Negl. Trop. Dis.* 6 (12), e1974. doi: 10.1371/journal.pntd.0001974

Gessner, P. K., and Gessner, T. (1992). Disulfiram and its metabolite, diethyldithiocarbamate. *Springer Netherlands* 452 pp. doi: 10.1007/978-94-011-2328-0

Ghosh, S., Farr, L., Singh, A., Leaton, L. A., Padalia, J., Shirley, D. A., et al. (2020). COP9 signalosome is an essential and druggable parasite target that regulates protein degradation. *PloS Pathog.* 16 (9), e1008952. doi: 10.1371/journal.ppat.1008952

Giulivi, C., Turrens, J. F., and Boveris, A. (1988). Chemiluminescence enhancement by trypanocidal drugs and by inhibitors of antioxidant enzymes in *Trypanosoma cruzi*. *Mol. Biochem. Parasitol.* 30 (3), 243–251. doi: 10.1016/0166-6851(88)90093-X

González-Chávez, Z., Olin-Sandoval, V., Rodíguez-Zavala, J. S., Moreno-Sánchez, R., and Saavedra, E. (2015). Metabolic control analysis of the *Trypanosoma cruzi* peroxide detoxification pathway identifies tryparedoxin as a suitable drug target. *Biochim. Biophys. Acta* 1850 (2), 263–273. doi: 10.1016/j.bbagen.2014.10.029

González-Chávez, Z., Vázquez, C., Mejia-Tlachi, M., Márquez-Dueñas, C., Manning-Cela, R., Encalada, R., et al. (2019). Gamma-glutamylcysteine synthetase and tryparedoxin 1 exert high control on the antioxidant system in *Trypanosoma cruzi* contributing to drug resistance and infectivity. *Redox Biol.* 26, 101231. doi: 10.1016/j.redox.2019.101231

González, L., García-Huertas, P., Triana-Chávez, O., García, G. A., Murta, S. M. F., and Mejía-Jaramillo, A. M. (2017). Aldo-keto reductase and alcohol dehydrogenase contribute to benznidazole natural resistance in *Trypanosoma cruzi*. *Mol. Microbiol.* 106 (5), 704–718. doi: 10.1111/mmi.13830

Guggenbühl Noller, J. M., Froeschl, G., Eisermann, P., Jochum, J., Theuring, S., Reiter-Owona, I., et al. (2020). Describing nearly two decades of Chagas disease in Germany and the lessons learned: A retrospective study on screening, detection, diagnosis, and treatment of *Trypanosoma cruzi* infection from 2000 – 2018. *BMC Infect. Dis.* 20 (1), 919. doi: 10.1186/s12879-020-05600-8

Guo, W., Chen, S., Li, C., Xu, J., and Wang, L. (2022). Application of disulfiram and its metabolites in treatment of inflammatory disorders. *Front. Pharmacol.* 12. doi: 10.3389/fphar.2021.795078

Gupta, S., Wen, J. J., and Garg, N. J. (2009). Oxidative stress in Chagas disease. *Interdiscip. Perspect. Infect. Dis.* 2009, 1–8. doi: 10.1155/2009/190354

Harrington, B. S., Ozaki, M. K., Caminear, M. W., Hernandez, L. F., Jordan, E., Kalinowski, N. J., et al. (2020). Drugs targeting tumor-initiating cells prolong survival in a post-surgery, post-chemotherapy ovarian cancer relapse model. *Cancers* 12 (6), 1645. doi: 10.3390/cancers12061645

Heikkila, R. E., Cabbat, F. S., and Cohen, G. (1976). *In vivo* inhibition of superoxide dismutase in mice by diethyldithiocarbamate. *J. Biol. Chem.* 251 (7), 2182–2185. doi: 10.1016/S0021-9258(17)33675-X

Heikkila, R. E., Cabbat, F. S., and Cohen, G. (1978). Inactivation of superoxide dismutase by several thiocarbamic acid derivatives. *Experientia* 34 (12), 1553–1554. doi: 10.1007/BF02034668

Hernández, S. M., Sánchez, M. S., and de Tarlovsky, M. N. S. (2006). Polyamines as a defense mechanism against lipoperoxidation in *Trypanosoma cruzi*. *Acta Trop.* 98 (1), 94–102. doi: 10.1016/j.actatropica.2006.02.005

Hersh, E. M., Brewton, G., Abrams, D., Bartlett, J., Galpin, J., Gill, P., et al. (1991). Ditiocarb sodium (diethyldithiocarbamate) therapy in patients with symptomatic HIV infection and AIDS. A randomized, double-blind, placebo-controlled, multicenter study. *JAMA* 265 (12), 1538–1544. doi: 10.1001/jama.1991.03460120052035

Hill, J. A., and Cowen, L. E. (2015). Using combination therapy to thwart drug resistance. *Future Microbiol.* 10 (11), 1719–1726. doi: 10.2217/fmb.15.68

Hirschenson, J., and Mailloux, R. J. (2021). The glutathionylation agent disulfiram augments superoxide/hydrogen peroxide production when liver mitochondria are oxidizing ubiquinone pool-linked and branched chain amino acid substrates. *Free Radic. Biol. Med.* 172, 1–8. doi: 10.1016/j.freeradbiomed.2021.05.030

Hoefer, F., and Groettrup, M. (2021). Silencing of the proteasome and oxidative stress impair endoplasmic reticulum targeting and signal cleavage of a prostate carcinoma antigen. *Biochem.Biophys. Res. Commun.* 554, 56–62. doi: 10.1016/j.bbrc.2021.03.023

Hu, J. J., Liu, X., Xia, S., Zhang, Z., Zhang, Y., Zhao, J., et al. (2020). FDA-Approved disulfiram inhibits pyroptosis by blocking gasdermin d pore formation. *Nat. Immunol.* 21 (7), 736–745. doi: 10.1038/s41590-020-0669-6

Jørgensen, C. H., Pedersen, B., and Tønnesen, H. (2011). The efficacy of disulfiram for the treatment of alcohol use disorder. *Alcoholism: Clin. Exp. Res.* 35 (10), 1749–1758. doi: 10.1111/j.1530-0277.2011.01523.x

Jackson, Y., Wyssa, B., and Chappuis, F. (2020). Tolerance to nifurtimox and benznidazole in adult patients with chronic Chagas' disease. *J. Antimicrob. Chemother.* 75 (3), 690–696. doi: 10.1093/jac/dkz473

Jedlitschky, G., Leier, I., Buchholz, U., Center, M., and Keppler, D. (1994). ATP-dependent transport of glutathione s-conjugates by the multidrug resistance-associated protein. *Cancer Res.* 54 (18), 4833–4836.

Jia, Y., and Huang, T. (2021). Overview of antabuse® (Disulfiram) in radiation and cancer biology. *Cancer Manage. Res.* 13, 4095–4101. doi: 10.2147/CMAR.S308168

Jiang, H., Zhao, Y., Tang, H., Duan, S., Li, M., Yang, X., et al. (2021). Tetraethylthiuram disulphide alleviates pulmonary fibrosis through modulating transforming growth factor-β signalling. *Pharmacol. Res.* 174, 105923. doi: 10.1016/j.phrs.2021.105923

Jin, L., Davis, M. R., Hu, P., and Baillie, T. A. (1994). Identification of novel glutathione conjugates of disulfiram and diethyldithiocarbamate in rat bile by liquid chromatography-tandem mass spectrometry. evidence for metabolic activation of disulfiram *in vivo*. *Chem. Res. Toxicol.* 7 (4), 526–533. doi: 10.1021/tx00040a008

Kanai, K., Itoh, N., Ito, Y., Nagai, N., Hori, Y., Chikazawa, S., et al. (2011). Anti-inflammatory potency of oral disulfiram compared with dexamethasone on endotoxin-induced uveitis in rats. *J. Vet. Med. Science.* 73 (4), 517–520. doi: 10.1292/jvms.10-0239

Kang, J., Sun, Y., Deng, Y., Liu, Q., Li, D., Liu, Y., et al. (2020). Autophagy-endoplasmic reticulum stress inhibition mechanism of superoxide dismutase in the formation of calcium oxalate kidney stones. *Biomed. Pharmacother.* 121, 109649. doi: 10.1016/j.biopha.2019.109649

Kannappan, V., Ali, M., Small, B., Rajendran, G., Elzhenni, S., Taj, H., et al. (2021). Recent advances in repurposing disulfiram and disulfiram derivatives as copper-dependent anticancer agents. *Front. Mol. Biosci.* 8, 741316. doi: 10.3389/fmolb.2021.741316

Khouri, R., Novais, F., Santana, G., de Oliveira, C. I., Vannier dos Santos, M. A., Barral, A., et al. (2010). DETC induces *Leishmania* parasite killing in human *in vitro* and murine *in vivo* models: A promising therapeutic alternative in leishmaniasis. *PloS One* 5 (12), e14394. doi: 10.1371/journal.pone.0014394

Kim, S. H., Seo, H., Kwon, D., Yuk, D. Y., and Jung, Y. S. (2022). Taurine ameliorates tunicamycin-induced liver injury by disrupting the vicious cycle between oxidative stress and endoplasmic reticulum stress. *Life* 12 (3), 354. doi: 10.3390/life12030354

Kona, F. R., Buac, D., and Burger, A. (2011). Disulfiram, and disulfiram derivatives as novel potential anticancer drugs targeting the ubiquitin proteasome system in both preclinical and clinical studies. *Curr. Cancer Drug Targets* 11 (3), 338–346. doi: 10.2174/156800911794519798. XXXM.

Koto, K. S., Lescault, P., Brard, L., Kim, K., Singh, R. K., Bond, J., et al. (2011). Antitumor activity of nifurtimox is enhanced with tetrathiomolybdate in medulloblastoma. *Int. J. Oncol.* 38 (5), 1329–1341. doi: 10.3892/ijo.2011.971

Kyle, M. E., Serroni, A., and Farber, J. L. (1989). The inhibition of lipid peroxidation by disulfiram prevents the killing of cultured hepatocytes by allyl

alcohol, tert-butyl hydroperoxide, hydrogen peroxide and diethyl maleate. *Chem. Biol. Interact.* 72 (3), 269–275. doi: 10.1016/0009-2797(89)90003-3

Lane, J. E., Ribeiro-Rodrigues, R., Suarez, C. C., Bogitsh, B. J., Jones, M. M., Singh, P. K., et al. (1996). *In vitro* trypanocidal activity of tetraethylthiuram disulfide and sodium diethylamine-n-carbodithioate on *Trypanosoma cruzi*. *Am. J. Trop. Med. Hyg.* 55 (3), 263–266. doi: 10.4269/ajtmh.1996.55.263

Lee, B. Y., Bacon, K. M., Bottazzi, M. E., and Hotez, P. J. (2013). Global economic burden of Chagas disease: a computational simulation model. *Lancet Infect. Dis.* 13 (4), 342–348. doi: 10.1016/S1473-3099(13)70002-1

Lehár, J., Krueger, A. S., Avery, W., Heilbut, A. M., Johansen, L. M., Price, E. R., et al. (2009a). Synergistic drug combinations tend to improve therapeutically relevant selectivity. *Nat. Biotechnol.* 27 (7), 659–666. doi: 10.1038/nbt.1549

Lehár, J., Krueger, A. S., Zimmermann, G. R., and Borisy, A. A. (2009b). Therapeutic selectivity and the multi-node drug target. *Discov Med.* 8 (43), 185–190.

Levi, G. C., Lobo, I. M. F., Kallás, E. G., and Amato Neto, V. (1996). Etiological drug treatment of human infection by *Trypanosoma cruzi*. *Rev. Inst. Med. Trop. São Paulo.* 38 (1), 35–38. doi: 10.1590/S0036-46651996000100007

Libeu, C. A. P., Descamps, O., Zhang, Q., John, V., and Bredesen, D. E. (2012). Altering APP proteolysis: Increasing sAPPalpha production by targeting dimerization of the APP ectodomain. *PloS One* 7 (6), e40027. doi: 10.1371/journal.pone.0040027

Liu, Y., Tong, Z., Shi, J., Li, R., Upton, M., and Wang, Z. (2021). Drug repurposing for next-generation combination therapies against multidrug-resistant bacteria. *Theranostics* 11 (10), 4910–4928. doi: 10.7150/thno.56205

Liu, X., Zhang, R., Huang, L., Zheng, Z., Vlassara, H., Striker, G., et al. (2019). Excessive oxidative stress contributes to increased acute ER stress kidney injury in aged mice. *Oxid. Med. Cell. Longev.* 2019, 1–15. doi: 10.1155/2019/2746521

Li, N., Wang, Y., Wang, X., Sun, N., and Gong, Y.-H. (2022). Pathway network of pyroptosis and its potential inhibitors in acute kidney injury. *Pharmacol. Res.* 175, 106033. doi: 10.1016/j.phrs.2021.106033

Loe, D. W., Deeley, R. G., and Cole, S. P. (1998). Characterization of vincristine transport by the *M*r 190,000 multidrug resistance protein (MRP): evidence for cotransport with reduced glutathione. *Cancer Res.* 58 (22), 5130–5136.

Loo, T. W., Bartlett, M. C., and Clarke, D. M. (2004). Disulfiram metabolites permanently inactivate the human multidrug resistance p-glycoprotein. *Mol. Pharm.* 1 (6), 426–433. doi: 10.1021/mp049917l

Loo, T. W., and Clarke, D. M. (2000). Blockage of drug resistance *in vitro* by disulfiram, a drug used to treat alcoholism. *J. Nat. Cancer Inst.* 92 (11), 898–902. doi: 10.1093/jnci/92.11.898

Lu, C., Li, X., Ren, Y., and Zhang, X. (2021). Disulfiram: a novel repurposed drug for cancer therapy. *Cancer Chemother. Pharmacol.* 87 (2), 159–172. doi: 10.1007/s00280-020-04216-8

Lu, Y., Pan, Q., Gao, W., Pu, Y., Luo, K., He, B., et al. (2022). Leveraging disulfiram to treat cancer: mechanisms of action, delivery strategies, and treatment regimens. *Biomaterials* 281, 121335. doi: 10.1016/j.biomaterials.2021.121335

Malhotra, J. D., Miao, H., Zhang, K., Wolfson, A., Pennathur, S., Pipe, S. W., et al. (2008). Antioxidants reduce endoplasmic reticulum stress and improve protein secretion. *Proc. Natl. Acad. Sci.* 105 (47), 18525–18530. doi: 10.1073/pnas.0809677105

Martínez, A., Prolo, C., Estrada, D., Rios, N., Alvarez, M. N., Piñeyro, M. D., et al. (2019). Cytosolic Fe-superoxide dismutase safeguards *Trypanosoma cruzi* from macrophage-derived superoxide radical. *Proc. Natl. Acad. Sci.* 116 (18), 8879–8888. doi: 10.1073/pnas.1821487116

Martiny, A., Vannier-Santos, M. A., Borges, V. M., Meyer-Fernandes, J. R., Assreuy, J., Cunha e Silva, N. L., et al. (1996). *Leishmania*-induced tyrosine phosphorylation in the host macrophage and its implication to infection. *Eur. J. Cell Biol.* 71 (2), 206–215.

Maya, J. D., Cassels, B. K., Iturriaga-Vásquez, P., Ferreira, J., Faúndez, M., Galanti, N., et al. (2007). Mode of action of natural and synthetic drugs against *Trypanosoma cruzi* and their interaction with the mammalian host. *Comp. Biochem. Physiol. A. Mol. Integr. Physiol.* 146 (4), 601–620. doi: 10.1016/j.cbpa.2006.03.004

Maya, J. D., Repetto, Y., Agosín, M., Ojeda, J. M., Tellez, R., Gaule, C., et al. (1997). Effects of nifurtimox and benznidazole upon glutathione and trypanothione content in epimastigote, trypomastigote and amastigote forms of *Trypanosoma cruzi*. *Mol. Biochem. Parasitol.* 86 (1), 101–106. doi: 10.1016/S0166-6851(96)02837-X

Maya, J. D., Rodríguez, A., Pino, L., Pabón, A., Ferreira, J., Pavani, M., et al. (2004). Effects of buthionine sulfoximine nifurtimox and benznidazole upon trypanothione and metallothionein proteins in *Trypanosoma cruzi*. *Biol. Res.* 37 (1), 61–69. doi: 10.4067/S0716-97602004000100007

Mazur, K. L., Feuser, P. E., Valério, A., Poester Cordeiro, A., de Oliveira, C. I., Assolini, J. P., et al. (2019). Diethyldithiocarbamate loaded in beeswax-copaiba oil nanoparticles obtained by solventless double emulsion technique promote promastigote death *in vitro*. *Colloids Surf. B. Biointerfaces.* 176, 507–512. doi: 10.1016/j.colsurfb.2018.12.048

Mejia, A. M., Hall, B. S., Taylor, M. C., Gómez-Palacio, A., Wilkinson, S. R., Triana-Chávez, O., et al. (2012). Benznidazole-resistance in *Trypanosoma cruzi* is a readily acquired trait that can arise independently in a single population. *J. Infect. Dis.* 206 (2), 220–228. doi: 10.1093/infdis/jis331

Mejía-Jaramillo, A. M., Fernández, G. J., Montilla, M., Nicholls, R. S., and Triana-Chávez, O. (2012). *Trypanosoma cruzi* strains resistant to benznidazole occurring in Colombia. *Biomedica* 32 (2), 196–205. doi: 10.1590/S0120-41572012000300007

Menezes, D., Valentim, C., Oliveira, M. F., and Vannier-Santos, M. A. (2006). Putrescine analogue cytotoxicity against *Trypanosoma cruzi*. *Parasitol. Res.* 98 (2), 99–105. doi: 10.1007/s00436-005-0010-1

Meraz-Torres, F., Plöger, S., Garbe, C., Niessner, H., and Sinnberg, T. (2020). Disulfiram as a therapeutic agent for metastatic malignant melanoma–old myth or new logos? *Cancers* 12 (12), 3538. doi: 10.3390/cancers12123538

Mesías, A. C., Sasoni, N., Arias, D. G., Pérez Brandán, C., Orban, O. C. F., Kunick, C., et al. (2019). Trypanothione synthetase confers growth, survival advantage and resistance to anti-protozoal drugs in *Trypanosoma cruzi*. *Free Rad. Biol. Med.* 130, 23–34. doi: 10.1016/j.freeradbiomed.2018.10.436

Miller, A. C., and Blakely, W. F. (1992). Inhibition of glutathione reductase activity by a carbomoylating nitrosourea: Effect on cellular radiosensitivity. *Free Rad. Biol. Med.* 12 (1), 53–62. doi: 10.1016/0891-5849(92)90058-O

Mittal, M., Khan, K., Pal, S., Porwal, K., China, S. P., Barbhuyan, T. K., et al. (2014). The thiocarbamate disulphide drug, disulfiram induces osteopenia in rats by inhibition of osteoblast function due to suppression of acetaldehyde dehydrogenase activity. *Toxicol. Sci.* 139 (1), 257–270. doi: 10.1093/toxsci/kfu020

Mohammad-Gharibani, P., Modi, J., Menzie, J., Genova, R., Ma, Z., Tao, R., et al. (2014). Mode of action of s-Methyl-N, n-diethylthiocarbamate sulfoxide (DETC-MeSO) as a novel therapy for stroke in a rat model. *Mol. Neurobiol.* 50 (2), 655–672. doi: 10.1007/s12035-014-8658-0

Mohsin, A. A., Thompson, J., Hu, Y., Hollander, J., Lesnefsky, E. J., and Chen, Q. (2020). Endoplasmic reticulum stress-induced complex I defect: Central role of calcium overload. *Arch. Biochem. Biophys.* 683, 108299. doi: 10.1016/j.abb.2020.108299

Montalbano, R., Waldegger, P., Quint, K., Jabari, S., Neureiter, D., Illig, R., et al. (2013). Endoplasmic reticulum stress plays a pivotal role in cell death mediated by the pan-deacetylase inhibitor panobinostat in human hepatocellular cancer cells. *Transl. Oncol.* 6 (2), 143–IN6. doi: 10.1593/tlo.12271

Monteiro, A. C., Abrahamson, M., Lima, A. P., Vannier-Santos, M. A., and Scharfstein, J. (2001). Identification, characterization and localization of Chagasin, a tight-binding cysteine protease inhibitor in *Trypanosoma cruzi*. *J. Cell Sci.* 114 (Pt 21), 3933–3942. doi: 10.1242/jcs.114.21.3933

Moukdar, F., Robidoux, J., Lyght, O., Pi, J., Daniel, K. W., and Collins, S. (2009). Reduced antioxidant capacity and diet-induced atherosclerosis in uncoupling protein-2-deficient mice. *J. Lipid. Res.* 50 (1), 59–70. doi: 10.1194/jlr.M800273-JLR200

Müller, J., and Hemphill, A. (2016). Drug target identification in protozoan parasites. *Expert. Opin. Drug Discov* 11 (8), 815–824. doi: 10.1080/17460441.2016.1195945

Nagendra, S. N., Shetty, K. T., Rao, K. M., and Rao, B. S. (1994). Effect of disulfiram administration on rat brain glutathione metabolism. *Alcohol* 11 (1), 7–10. doi: 10.1016/0741-8329(94)90004-3

Neal, R. A., and van Bueren, J. (1988). Comparative studies of drug susceptibility of five strains of *Trypanosoma cruzi in vivo* and *in vitro*. *Trans. R. Soc Trop. Med. Hyg.* 82 (5), 709–714. doi: 10.1016/0035-9203(88)90208-8

Nechushtan, H., Hamamreh, Y., Nidal, S., Gotfried, M., Baron, A., Shalev, Y. I., et al. (2015). A phase IIb trial assessing the addition of disulfiram to chemotherapy for the treatment of metastatic non-small cell lung cancer. *Oncologist* 20 (4), 366–367. doi: 10.1634/theoncologist.2014-0424

Ningaraj, N. S., Chen, W., Schloss, J. V., Faiman, M. D., and Wu, J. Y. (2001). S-methyl-N,N-diethylthiocarbamate sulfoxide elicits neuroprotective effect against n-methyl-D-aspartate receptor-mediated neurotoxicity. *J. Biomed. Sci.* 8 (1), 104–113. doi: 10.1007/BF02255978

Ningaraj, N. S., Schloss, J. V., Williams, T. D., and Faiman, M. D. (1998). Glutathione carbamoylation with s-methyl N,N-diethylthiolcarbamate sulfoxide and sulfone. *Biochem. Pharmacol.* 55 (6), 749–756. doi: 10.1016/S0006-2952(97)00513-3

Nogueira, F. B., Krieger, M. A., Nirdé, P., Goldenberg, S., Romanha, A. J., and Murta, S. M. F. (2006). Increased expression of iron-containing superoxide dismutase-a (TcFeSOD-a) enzyme in *Trypanosoma cruzi* population with *in vitro*-induced resistance to benznidazole. *Acta Trop.* 100 (1–2), 119–132. doi: 10.1016/j.actatropica.2006.10.004

O'Brien, A., Barber, J. E. B., Reid, S., Niknejad, N., and Dimitroulakos, J. (2012). Enhancement of cisplatin cytotoxicity by disulfiram involves activating transcription factor 3. *Anticancer Res.* 32 (7), 2679–2688.

Ohno, Y., Hirota, K., Kawanishi, T., and Takanaka, A. (1990). Loss of viability after disulfiram treatment without preceding depletion of intracellular GSH. *J. Toxicol. Sci.* 15 (2), 63–73. doi: 10.2131/jts.15.63

Olivera, M. J., Cucunubá, Z. M., Valencia-Hernández, C. A., Herazo, R., Agreda-Rudenko, D., Flórez, C., et al. (2017). Risk factors for treatment interruption and severe adverse effects to benznidazole in adult patients with Chagas disease. *PloS One* 12 (9), e0185033. doi: 10.1371/journal.pone.0185033

Olmo, F., Urbanová, K., Rosales, M. J., Martín-Escolano, R., Sánchez-Moreno, M., and Marín, C. (2015). An *in vitro* iron superoxide dismutase inhibitor decreases the parasitemia levels of *Trypanosoma cruzi* in BALB/c mouse model during acute phase. *Int. J. Parasitol. Drugs Drug Resist.* 5 (3), 110–116. doi: 10.1016/j.ijpddr.2015.05.002

Palos, I., Lara-Ramirez, E. E., Lopez-Cedillo, J. C., Garcia-Perez, C., Kashif, M., Bocanegra-Garcia, V., et al. (2017). Repositioning FDA drugs as potential cruzain inhibitors from *Trypanosoma cruzi*: Virtual screening, *in vitro* and *in vivo* studies. *Molecules* 22 (6), 1015. doi: 10.3390/molecules22061015

Parker, E. R., and Sethi, A. (2011). Chagas disease: Coming to a place near you. *Dermatol. Clin.* 29 (1), 53–62. doi: 10.1016/j.det.2010.08.011

Pedrosa, R. C., de Bem, A. F., Locatelli, C., Pedrosa, R. C., Geremias, R., and Filho, D. W. (2001). Time-dependent oxidative stress caused by benznidazole. *Redox Rep.* 6 (4), 265–270. doi: 10.1179/135100001101536328

Pérez-Molina, J. A., Crespillo-Andújar, C., Bosch-Nicolau, P., and Molina, I. (2021). Trypanocidal treatment of Chagas disease. *Enferm. Infecc. Microbiol. Clin. (Engl Ed)* 39 (9), 458–470. doi: 10.1016/j.eimce.2020.04.012

Pérez-Molina, J. A., and Molina, I. (2018). Chagas disease. *Lancet* 391 (10115), 82–94. doi: 10.1016/S0140-6736(17)31612-4

Piacenza, L., Irigoín, F., Alvarez, M. N., Peluffo, G., Taylor, M. C., Kelly, J. M., et al. (2007). Mitochondrial superoxide radicals mediate programmed cell death in *Trypanosoma cruzi*: cytoprotective action of mitochondrial iron superoxide dismutase overexpression. *Biochem. J.* 403 (2), 323–334. doi: 10.1042/BJ20061281

Piñeyro, M. D., Arias, D., Parodi-Talice, A., Guerrero, S., and Robello, C. (2021). Trypanothione metabolism as drug target for trypanosomatids. *Curr. Pharm. Des.* 27 (15), 1834–1846. doi: 10.2174/1381612826666201211115329

Prathalingham, S. R., Wilkinson, S. R., Horn, D., and Kelly, J. M. (2007). Deletion of the *Trypanosoma brucei* superoxide dismutase gene *sodb1* increases sensitivity to nifurtimox and benznidazole. *Antimicrob. Agents Chemother.* 51 (2), 755–758. doi: 10.1128/AAC.01360-06

Prentice, H., Modi, J. P., and Wu, J. Y. (2015). Mechanisms of neuronal protection against excitotoxicity, endoplasmic reticulum stress, and mitochondrial dysfunction in stroke and neurodegenerative diseases. *Oxid. Med. Cell. Long.* 2015, 1–7. doi: 10.1155/2015/964518

Ren, Y., Lin, Y., Chen, J., and Jin, Y. (2021). Disulfiram chelated with copper promotes apoptosis in osteosarcoma *via* ROS/mitochondria pathway. *Biol. Pharm. Bull.* 44 (10), b21–00466. doi: 10.1248/bpb.b21-00466

Repetto, Y., Opazo, E., Maya, J. D., Agosin, M., and Morello, A. (1996). Glutathione and trypanothione in several strains of *Trypanosoma cruzi*: Effect of drugs. *Comp. Biochem. Physiol. B Biochem. Mol. Biol.* 115 (2), 281–285. doi: 10.1016/0305-0491(96)00112-5

Rigalli, J. P., Perdomo, V. G., Ciriaci, N., Francés, D. E., Ronco, M. T., Bataille, A. M., et al. (2016). The antitripanocide benznidazole promotes adaptive response to oxidative injury: Involvement of the nuclear factor-erythroid 2-related factor-2 (Nrf2) and multidrug resistance associated protein 2 (MRP2). *Toxicol. Appl. Pharmacol.* 304, 90–98. doi: 10.1016/j.taap.2016.05.007

Riggs, A. C., Bernal-Mizrachi, E., Ohsugi, M., Wasson, J., Fatrai, S., Welling, C., et al. (2005). Mice conditionally lacking the wolfram gene in pancreatic islet beta cells exhibit diabetes as a result of enhanced endoplasmic reticulum stress and apoptosis. *Diabetologia* 48 (11), 2313–2321. doi: 10.1007/s00125-005-1947-4

Roberts, S., and Ullman, B. (2017). Parasite polyamines as pharmaceutical targets. *Curr. Pharm. Des.* 23 (23), 3325–3341. doi: 10.2174/1381612823666170601101644

Roemeling, R. V., Olshefski, R., Langevin, T., Berestka, J., Reusch, J. J., Reusch, J. E. B., et al. (1986). Cisplatin chronotherapy and disulfiram rescue reduce toxicity without interfering with anticancer activity: animal findings and preliminary clinical experiences. *Chronobiol. Int.* 3 (1), 55–64. doi: 10.3109/07420528609083160

Salomão, K., de Souza, E. M., Carvalho, S. A., da Silva, E. F., Fraga, C. A. M., Barbosa, H. S., et al. (2010). *In vitro* and *in vivo* activities of 1,3,4-thiadiazole-2-arylhydrazone derivatives of megazol against *Trypanosoma cruzi*. *Antimicrob. Agents Chemother.* 54 (5), 2023–2031. doi: 10.1128/AAC.01241-09

Sander, P., Feng, M., Schweitzer, M. K., Wilting, F., Gutenthaler, S. M., Arduino, D. M., et al. (2021). Approved drugs ezetimibe and disulfiram enhance mitochondrial Ca^{2+} uptake and suppress cardiac arrhythmogenesis. *Br. J. Pharmacol.* 178 (22), 4518–4532. doi: 10.1111/bph.15630

Saraiva, R. M., Portela, L. F., Silveira, G.P.Eda, Gomes, N. L. da S., Pinto, D. P., Silva, A. C. A., et al. (2021). Disulfiram repurposing in the combined chemotherapy of Chagas disease. *Med.: Case Rep. Study Protoc.* 2 (7), e0110. doi: 10.1097/MD9.0000000000000110

Sauna, Z. E., Peng, X.-H., Nandigama, K., Tekle, S., and Ambudkar, S. V. (2004). The molecular basis of the action of disulfiram as a modulator of the multidrug resistance-linked ATP binding cassette transporters MDR1 (ABCB1) and MRP1 (ABCC1). *Mol. Pharmacol.* 65 (3), 675–684. doi: 10.1124/mol.65.3.675

Schmidtova, S., Kalavska, K., Gercakova, K., Cierna, Z., Miklikova, S., Smolkova, B., et al. (2019). Disulfiram overcomes cisplatin resistance in human embryonal carcinoma cells. *Cancers* 11 (9), 1224. doi: 10.3390/cancers11091224

Sedlak, J., and Lindsay, R. H. (1968). Estimation of total, protein-bound, and nonprotein sulfhydryl groups in tissue with ellman's reagent. *Anal. Biochem.* 25, 192–205. doi: 10.1016/0003-2697(68)90092-4

Shah O'Brien, P., Xi, Y., Miller, J. R., Brownell, A. L., Zeng, Q., Yoo, G. H., et al. (2019). Disulfiram (Antabuse) activates ROS-dependent ER stress and apoptosis in oral cavity squamous cell carcinoma. *J. Clin. Med.* 8 (5), 611. doi: 10.3390/jcm8050611

Sinclair, J. M. A., Chambers, S. E., Shiles, C. J., and Baldwin, D. S. (2016). Safety and tolerability of pharmacological treatment of alcohol dependence: comprehensive review of evidence. *Drug Saf.* 39 (7), 627–645. doi: 10.1007/s40264-016-0416-y

Soares, C. O., Colli, W., Bechara, E. J. H., and Alves, M. J. M. (2012). 1,4-Diamino-2-butanone, a putrescine analogue, promotes redox imbalance in *Trypanosoma cruzi* and mammalian cells. *Arch. Biochem. Biophys.* 528 (2), 103–110. doi: 10.1016/j.abb.2012.09.005

Soave, C., Viola-Rhenals, M., Elghoul, Y. K., Peng, T., and Dou, Q. P. (2016). Repositioning an old anti-alcoholism drug: disulfiram as a selective, effective and economical anticancer agent. *J. Dev. Drugs* 05 (02), 1000e147. doi: 10.4172/2329-6631.1000e147

Sonawane, V. K., Mahajan, U. B., Shinde, S. D., Chatterjee, S., Chaudhari, S. S., Bhangale, H. A., et al. (2018). A chemosensitizer drug: disulfiram prevents doxorubicin-induced cardiac dysfunction and oxidative stress in rats. *Cardiovasc.Toxicol* 18 (5), 459–470. doi: 10.1007/s12012-018-9458-y

Stockwell, B. R., Friedmann Angeli, J. P., Bayir, H., Bush, A. I., Conrad, M., Dixon, S. J., et al. (2017). Ferroptosis: A regulated cell death nexus linking metabolism, redox biology, and disease. *Cell* 171 (2), 273–285. doi: 10.1016/j.cell.2017.09.021

Strömme, J. H. (1963). Effects of diethyldithiocarbamate and disulfiram on glucose metabolism and glutathione content of human erythrocytes. *Biochem. Pharmacol.* 12 (7), 705–715. doi: 10.1016/0006-2952(63)90046-7

Sueth-Santiago, V., Moraes, J. B., Sobral Alves, E. S., Vannier-Santos, M. A., Freire-de-Lima, C. G., Castro, R. N., et al. (2016). The effectiveness of natural diarylheptanoids against *Trypanosoma cruzi*: cytotoxicity, ultrastructural alterations and molecular modeling studies. *PloS One* 11 (9), e0162926. doi: 10.1371/journal.pone.0162926

Sun, W., Sanderson, P. E., and Zheng, W. (2016). Drug combination therapy increases successful drug repositioning. *Drug Discov Today* 21 (7), 1189–1195. doi: 10.1016/j.drudis.2016.05.015

Sun, S., Shi, G., Han, X., Francisco, A. B., Ji, Y., Mendonça, N., et al. (2014). Sel1L is indispensable for mammalian endoplasmic reticulum-associated degradation, endoplasmic reticulum homeostasis, and survival. *Proc. Natl. Acad. Sci. U.S.A.* 111 (5), E582–E591. doi: 10.1073/pnas.1318114111

Talvani, A., and Teixeira, M. M. (2011). Inflammation and Chagas disease. *Adv. Parasitol.* 76, 171–194. doi: 10.1016/B978-0-12-385895-5.00008-6

Teston, A. P. M., Monteiro, W. M., Reis, D., Bossolani, G. D. P., Gomes, M. L., de Araújo, S. M., et al. (2013). *In vivo* susceptibility to benznidazole of *Trypanosoma cruzi* strains from the Western Brazilian Amazon. *Trop. Med. Int. Health* 18 (1), 85–95. doi: 10.1111/tmi.12014

Tonkin, E. G., Valentine, H. L., Milatovic, D. M., and Valentine, W. M. (2004). N,N-diethyldithiocarbamate produces copper accumulation, lipid peroxidation, and myelin injury in rat peripheral nerve. *Toxicol. Sci.* 81 (1), 160–171. doi: 10.1093/toxsci/kfh190

Valentine, H. L., Viquez, O. M., Amarnath, K., Amarnath, V., Zyskowski, J., Kassa, E. N., et al. (2009). Nitrogen substituent polarity influences dithiocarbamate-mediated lipid oxidation, nerve copper accumulation, and myelin injury. *Chem. Res. Toxicol.* 22 (1), 218–226. doi: 10.1021/tx8003714

Vannier-Santos, M., and De Castro, S. (2009). Electron microscopy in antiparasitic chemotherapy: a (close) view to a kill. *Curr. Drug Targets* 10 (3), 246–260. doi: 10.2174/138945009787581168

Vannier-Santos, M. A., and Lins, U. (2001). Cytochemical techniques and energy-filtering transmission electron microscopy applied to the study of parasitic protozoa. *Biol. Proced. Online.* 3, 8–18. doi: 10.1251/bpo19

Vannier-Santos, M. A., Menezes, D., Oliveira, M. F., and de Mello, F. G. (2008). The putrescine analogue 1,4-diamino-2-butanone affects polyamine synthesis, transport, ultrastructure and intracellular survival in. *Leishmania amazonensis Microbiol.* 154 (10), 3104–3111. doi: 10.1099/mic.0.2007/013896-0

Vannier-Santos, M. A., and Suarez-Fontes, A. M. (2017). Role of polyamines in parasite cell architecture and function. *Curr. Pharm. Des.* 23 (23), 3342–3358. doi: 10.2174/1381612823666170703163458

Vázquez, C., Mejia-Tlachi, M., González-Chávez, Z., Silva, A., Rodríguez-Zavala, J. S., Moreno-Sánchez, R., et al. (2017). Buthionine sulfoximine is a multitarget inhibitor of trypanothione synthesis in *Trypanosoma cruzi*. *FEBS Lett.* 591 (23), 3881–3894. doi: 10.1002/1873-3468.12904

Viquez, O. M., Lai, B., Ahn, J. H., Does, M. D., Valentine, H. L., and Valentine, W. M. (2009). N,N-diethyldithiocarbamate promotes oxidative stress prior to myelin structural changes and increases myelin copper content. *Toxicol. Appl. Pharmacol.* 239 (1), 71–79. doi: 10.1016/j.taap.2009.05.017

Waghabi, M. C., Ferreira, R. R., Abreu, R., da, S., Degrave, W., de Souza, E. M., et al. (2022). Transforming growth factor-ß as a therapeutic target for the cardiac damage of Chagas disease. *Mem. Inst. Oswaldo Cruz.* 117, e210395. doi: 10.1590/0074-02760210395

Wang, J., Yang, X., and Zhang, J. (2016). Bridges between mitochondrial oxidative stress, ER stress and mTOR signaling in pancreatic β cells. *Cell. Signal.* 28 (8), 1099–1104. doi: 10.1016/j.cellsig.2016.05.007

Wei, S., Xiao, Z., Huang, J., Peng, Z., Zhang, B., and Li, W. (2022). Disulfiram inhibits oxidative stress and NLRP3 inflammasome activation to prevent LPS-induced cardiac injury. *Int. Immunopharmacol.* 105, 108545. doi: 10.1016/j.intimp.2022.108545

Wertz, I. E., and Wang, X. (2019). From Discov to bedside: targeting the ubiquitin system. *Cell Chem. Biol.* 26 (2), 156–177. doi: 10.1016/j.chembiol.2018.10.022

WHO - World Health Organization. (2021) *Chagas disease (American trypanosomiasis)*. Available at: https://www.who.int/health-topics/Chagas-disease#tab=tab_1 (Accessed March 13, 2022).

Wongsrichanalai, C., Pickard, A. L., Wernsdorfer, W. H., and Meshnick, S. R. (2002). Epidemiology of drug-resistant malaria. *Lancet Infect. Dis.* 2 (4), 209–218. doi: 10.1016/s1473-3099(02)00239-6

Worner, T. M. (1982). Peripheral neuropathy after disulfiram administration: Reversibility despite continued therapy. *Drug Alcohol Depend.* 10 (2–3), 199–201. doi: 10.1016/0376-8716(82)90013-8

Wysor, M. S., Zwelling, L. A., Sanders, J. E., and Grenan, M. M. (1982). Cure of mice infected with *Trypanosoma rhodesiense* by cis-diamminedichloroplatinum (ii) and disulfiram rescue. *Science* 217 (4558), 454–456. doi: 10.1126/science.7201165

Xie, S. C., Dick, L. R., Gould, A., Brand, S., and Tilley, L. (2019). The proteasome as a target for protozoan parasites. Expert Opin. *Ther. Targets* 23 (11), 903–914. doi: 10.1080/14728222.2019.1685981

Yang, Y., Deng, Q., Feng, X., and Sun, J. (2015). Use of the disulfiram/copper complex for breast cancer chemoprevention in MMTV-erbB2 transgenic mice. *Mol. Med. Rep.* 12 (1), 746–752. doi: 10.3892/mmr.2015.3426

Yang, Z., Guo, F., Albers, A. E., Sehouli, J., and Kaufmann, A. M. (2019). Disulfiram modulates ROS accumulation and overcomes synergistically cisplatin resistance in breast cancer cell lines. *Biomed. Pharmacother.* 113, 108727. doi: 10.1016/j.biopha.2019.108727

Yoshino, H., Yamada, Y., Enokida, H., Osako, Y., Tsuruda, M., Kuroshima, K., et al. (2020). Targeting NPL4 *via* drug repositioning using disulfiram for the treatment of clear cell renal cell carcinoma. *PloS One* 15 (7), e0236119. doi: 10.1371/journal.pone.0236119

Yuan, M., Gong, M., He, J., Xie, B., Zhang, Z., Meng, L., et al. (2022). IP3R1/GRP75/VDAC1 complex mediates endoplasmic reticulum stress-mitochondrial oxidative stress in diabetic atrial remodeling. *Redox Biol.* 52, 102289. doi: 10.1016/j.redox.2022.102289

Zhang, Y., Zhang, R., and Han, X. (2021). Disulfiram inhibits inflammation and fibrosis in a rat unilateral ureteral obstruction model by inhibiting gasdermin d cleavage and pyroptosis. *Inflamm. Res.* 70 (5), 543–552. doi: 10.1007/s00011-021-01457-y

Zhao, A., Wu, Z.-Q., Pollack, M., Rollwagen, F. M., Hirszel, P., and Zhou, X. (2000). Disulfiram inhibits TNF-alpha-induced cell death. *Cytokine* 12 (9), 1356–1367. doi: 10.1006/cyto.2000.0725

Zheng, W., Sun, W., and Simeonov, A. (2018). Drug repurposing screens and synergistic drug-combinations for infectious diseases. *Br. J. Pharmacol.* 175 (2), 181–191. doi: 10.1111/bph.13895

Zhou, Q., Wang, W., Yang, F., Wang, H., Zhao, X., Zhou, Y., et al. (2022). Disulfiram suppressed peritendinous fibrosis through inhibiting macrophage accumulation and its pro-inflammatory properties in tendon bone healing. *Front. Bioeng. Biotechnol.* 10, 823933. doi: 10.3389/fbioe.2022.823933

Zimmermann, G. R., Lehár, J., and Keith, C. T. (2007). Multi-target therapeutics: when the whole is greater than the sum of the parts. *Drug Discov Today* 12 (1–2), 34–42. doi: 10.1016/j.drudis.2006.11.008

Zingales, B. (2018). *Trypanosoma cruzi* genetic diversity: Something new for something known about Chagas disease manifestations, serodiagnosis and drug sensitivity. *Acta Trop.* 184, 38–52. doi: 10.1016/j.actatropica.2017.09.017

Zingales, B., Araujo, R. G. A., Moreno, M., Franco, J., Aguiar, P. H. N., Nunes, S. L., et al. (2015). A novel ABCG-like transporter of *Trypanosoma cruzi* is involved in natural resistance to benznidazole. *Mem. Inst. Oswaldo Cruz.* 110 (3), 433–444. doi: 10.1590/0074-02760140407

frontiers | Frontiers in Cellular and Infection Microbiology

TYPE Original Research
PUBLISHED 30 November 2022
DOI 10.3389/fcimb.2022.1017040

OPEN ACCESS

EDITED BY
Alberto Enrique Paniz Mondolfi,
Icahn School of Medicine at Mount Sinai, United States

REVIEWED BY
Kathryn Jones,
Baylor College of Medicine, United States
Claudia M. Calvet,
Laboratory of Cellular Ultrastructure, Oswaldo Cruz Foundation, Brazil

*CORRESPONDENCE
Roberto Rodrigues Ferreira
robertoferreira@ioc.fiocruz.br
Mariana Caldas Waghabi
mariana@ioc.fiocruz.br

SPECIALTY SECTION
This article was submitted to Parasite and Host, a section of the journal Frontiers in Cellular and Infection Microbiology

RECEIVED 11 August 2022
ACCEPTED 08 November 2022
PUBLISHED 30 November 2022

CITATION
Ferreira RR, de Souza EM, Vilar-Pereira G, Degrave WMS, Abreu RdS, Meuser-Batista M, Ferreira NVC, Ledbeter S, Barker RH, Bailly S, Feige J-J, Lannes-Vieira J, de Araújo-Jorge TC and Waghabi MC (2022) In Chagas disease, transforming growth factor beta neutralization reduces *Trypanosoma cruzi* infection and improves cardiac performance. *Front. Cell. Infect. Microbiol.* 12:1017040.
doi: 10.3389/fcimb.2022.1017040

In Chagas disease, transforming growth factor beta neutralization reduces *Trypanosoma cruzi* infection and improves cardiac performance

Roberto Rodrigues Ferreira[1,2]*, Elen Mello de Souza[3], Glaucia Vilar-Pereira[4], Wim M. S. Degrave[1], Rayane da Silva Abreu[1], Marcelo Meuser-Batista[5], Nilma Valéria Caldeira Ferreira[5], Steve Ledbeter[6], Robert H. Barker[6], Sabine Bailly[7], Jean-Jacques Feige[7], Joseli Lannes-Vieira[4], Tania C. de Araújo-Jorge[2] and Mariana Caldas Waghabi[1]*

[1]Laboratório de Genômica Funcional e Bioinformática, Instituto Oswaldo Cruz, Fundação Oswaldo Cruz (Fiocruz), Rio de Janeiro, Brazil, [2]Laboratório de Inovações em Terapias, Ensino e Bioprodutos, Instituto Oswaldo Cruz, Fundação Oswaldo Cruz (Fiocruz), Rio de Janeiro, Brazil, [3]Laboratório de Virologia Molecular, Instituto Oswaldo Cruz, Fundação Oswaldo Cruz (Fiocruz), Rio de Janeiro, Brazil, [4]Laboratório de Biologia das Interações, Instituto Oswaldo Cruz, Fundação Oswaldo Cruz (Fiocruz), Rio de Janeiro, Brazil, [5]Departamento de Anatomia Patológica e Citopatologia, Instituto Nacional de Saúde da Mulher, da Criança e do Adolescente Fernandes Figueira, Fundação Oswaldo Cruz (Fiocruz), Rio de Janeiro, Brazil, [6]Tissue Protection and Repair, Sanofi-Genzyme R&D Center, Framingham, MA, United States, [7]Laboratory BioSanté, Université Grenoble Alpes, INSERM, CEA, Grenoble, France

Chronic Chagasic cardiomyopathy (CCC), a progressive inflammatory and fibrosing disease, is the most prominent clinical form of Chagas disease, a neglected tropical disease caused by *Trypanosoma cruzi* infection. During CCC, the parasite remains inside the cardiac cells, leading to tissue damage, involving extensive inflammatory response and irregular fibrosis. Among the fibrogenic factors is transforming growth factor-β (TGF-β), a key cytokine controlling extracellular matrix synthesis and degradation. TGF-β is involved in CCC onset and progression, with increased serum levels and activation of its signaling pathways in the cardiac tissue, which crucially contributes to fibrosis. Inhibition of the TGF-β signaling pathway attenuates *T. cruzi* infection and prevents cardiac damage in an experimental model of acute Chagas disease. The aim of this study was to investigate the effect of TGF-β neutralization on *T. cruzi* infection in both *in vitro* and *in vivo* pre-clinical models, using the 1D11 monoclonal antibody. To this end, primary cultures of cardiac cells were infected with *T. cruzi* trypomastigote forms and treated with 1D11. For *in vivo* studies, 1D11 was administered in different schemes for acute and chronic phase models (Swiss mice infected with 10^4 parasites from the Y strain and C57BL/6 mice infected with 10^2 parasites from the Colombian strain, respectively). Here we show that the addition of 1D11 to cardiac cells greatly

reduces cardiomyocyte invasion by *T. cruzi* and the number of parasites per infected cell. In both acute and chronic experimental models, *T. cruzi* infection altered the electrical conduction, decreasing the heart rate, increasing the PR interval and the P wave duration. The treatment with 1D11 reduced cardiac fibrosis and reversed electrical abnormalities improving cardiac performance. Taken together, these data further support the major role of the TGF-β signaling pathways in *T. cruzi*-infection and their biological consequences on parasite/host interactions. The therapeutic effects of the 1D11 antibody are promising and suggest a new possibility to treat cardiac fibrosis in the chronic phase of Chagas' heart disease by TGF-β neutralization.

KEYWORDS

cardiac fibrosis, Chagas disease, TGF-β, 1D11, treatment

Introduction

Chagas disease, also known as American trypanosomiasis, is caused by the flagellate protozoan *Trypanosoma cruzi*, transmitted by a triatomine insect vector, commonly known as kissing bugs (World Helth Organization, 2021). Chagas disease presents distinct and successive acute and chronic phases. In humans, signals of the acute phase begin 6 to 10 days after infection and last for about 4 to 8 weeks (Steverding, 2014). In most cases, the acute phase is hardly identified with the absence of symptoms or by presenting nonspecific clinical symptoms, such as fever and malaise (Chagas, 1909; Dias, 1984; Rassi et al., 2008). If not treated or in case of treatment failure, the acute phase progresses into the chronic phase (Marin-neto et al., 2002; Coura, 2007). Chronic chagasic cardiomyopathy (CCC) is the main and most severe clinical manifestation of chronic Chagas disease, representing an important problem in terms of public health (Álvarez et al, 2014) and social impact (Amieva et al., 2021). In the affected individuals, alterations in heart function such as arrhythmias, apical aneurysms, thromboembolism and progressive heart failure may result in sudden death (Rassi et al., 2010). CCC is also the most common cause of non-ischemic cardiomyopathy in Latin America, representing approximately 10,000 deaths/year in patients between 30 and 50 years old, in endemic areas of Chagas disease (Rassi et al., 2010; Bocchi et al., 2017).

In the chronic phase of infection the parasite remains in myocardial cells contributing to the damage in cardiac tissue, which involves inflammatory response, cell death, and focal fibrosis (Sato et al., 1993; Andrade, 1999; Rassi et al., 2012). Mononuclear cells-enriched cardiac inflammation is directly related to the intensity of myocardial fibrosis, a biological process conducted by cytokines and growth factors that act on fibroblasts and stimulate collagen production (Rossi, 1998; Pereira et al., 2014; Pereira et al., 2015). This damage leads to structural modifications involving tissue repair and remodeling, and results in replacement of cardiac tissue with connective tissue, characteristic of the fibrotic process (Ihn, 2002; Zamilpa et al, 2014). In view of the importance of fibrosis in cardiac involvement during CCC, mechanisms involved in this process represent potential targets for therapeutic strategies to prevent or reverse fibrosis to improve the prognosis of patients with CCC, since there are still no specific treatments for this phase of the disease. The molecule that stands out as a key regulator in the production and remodeling of the extracellular matrix in fibrosis is TGF-β.

TGF-β is a multifunctional cytokine, which plays a role in regulating processes such as cell apoptosis, embryogenesis, epithelial cell migration and epithelial-mesenchymal transitions (Moustakas and Heldin, 2005). In mammals, there are three isoforms of TGF-β: TGF-β1, TGF-β2 and TGF-β3. These isoforms share homology of about 70% in the amino acid sequence and are encoded by distinct genes located in different chromosomes (Huang et al., 2014). However, TGF-β main biological activities are associated with the regulation of cell proliferation and differentiation, immunosuppressive activities, and regulation of the deposition of extracellular matrix components (Reisdorf et al., 2001; Moustakas and Heldin, 2005). Several studies have reported the involvement of TGF-β in cardiac fibrosis (Eghbali et al., 1991; Okada et al., 2005; Tan et al., 2010; Bhandary et al., 2018; Frangogiannis, 2020; Ko et al., 2022) and in other organs such as kidney, liver and lung (Daniels et al., 2004; Wang et al., 2005; Gellibert et al., 2006; Petersen et al., 2008; Dewidar et al., 2019; Gu et al., 2020; Inui et al., 2021).

In the last two decades, our group has been studying the role of TGF-β as an inducer of several pathological processes in Chagas disease (Ferreira et al., 2022; Waghabi et al., 2022). We already investigated TGF-β pathway inhibition in experimental

models of acute and chronic Chagas heart disease using SB431542 and GW788388, which are two selective inhibitors of the kinase activity of the TGF-β type 1 receptor TβR1/ALK5 (Waghabi et al., 2007; de Oliveira et al., 2012; Ferreira et al., 2019). The treatment with TGF-β pathway inhibitors improved cardiac parameters as it (i) reduced the prolonged PR and QTc intervals, increased heart rate, and reversed sinus arrhythmia, and atrial and atrioventricular conduction disorders; (ii) reversed the loss of connexin-43 enriched intercellular plaques and fibrosis of the cardiac tissue; (iii) reduced activation and expression of TGF-β intracellular proteins (Smad2/3); (iv) modulated protein expression of fibrosis regulators (MMP-9, reduced TIMP-1/TIMP-2/TIMP-4); and (v) partially restored GATA-6 and Tbox-5 transcription, supporting cardiac recovery (Ferreira et al., 2019). Understanding the mechanisms triggered by the strategies inhibiting TGF-β activity and the interference of these factors in the development of Chagas' cardiopathy are of great importance. It makes TGF-β a relevant target for the development of therapies for chronic heart disease patients. However, the clinical use of inhibitors of TGF-β receptor kinase activity could induce some deleterious secondary effects, such as heart-valve lesions, physeal dysplasia and an increase in femur and tibia thickness (Anderton et al., 2011). Thus, investigating new compounds that inhibit the TGF-β pathways by other mechanisms is of utmost importance. In the present study, we used *in vitro* and pre-clinical models to investigate the effect of a neutralizing antibody (1D11), directed against the three TGF-β isoforms, on *T. cruzi* infection.

Methods

Ethics statement

All mice procedures were carried out in strict accordance with the recommendations in the Guide for the Care and Use of Laboratory Animals of the Brazilian National Council of Animal Experimentation (http://www.cobea.org.br/) and the federal law 11.794 (8 October 2008). Protocols used in this study were approved by the Institutional Committee for Animal Ethics of Fiocruz (CEUA/Fiocruz, Licenses LW10/14 and LW42-11). All efforts were made to minimize animal suffering.

Parasites

Trypomastigotes of the Y strain of *T. cruzi* were obtained from the blood of infected mice at the peak of parasitemia (Meirelles et al., 1986) and were maintained in serum-free medium with 2% bovine serum albumin.

The Colombian *T. cruzi* DTU I strain (Zingales et al., 2012) was maintained by serial passages in specific pathogen-free C57BL/6 mice by IP injection of 5,000 blood trypomastigotes in 0.2 mL of pyrogen-free saline (BioManguinhos-Fiocruz, Brazil) every 35 days post-infection (dpi), the parasitemia peak using this inoculum.

Primary cultures of cardiomyocytes

Cardiac cells from mouse embryos were obtained, and as previously described these cells were contaminated with few fibroblasts and endothelial cells (Meirelles et al., 1986). Cells were maintained in Eagle's medium (Sigma) supplemented with 7% fetal calf serum (FCS) (Sigma), 100 μg/ml gentamicin (Sigma), 1 mM L-glutamine (Sigma), and 2.5 mM $CaCl_2$.

Drug

1D11 is a murine IgG1 monoclonal antibody that neutralizes all three TGF-β isoforms. The 1D11 antibody and its isotype matched murine IgG1 control (13C4) were produced by Genzyme Corporation (Sanofi-Genzyme, USA). The vehicle used for these antibodies was composed of 20 mM histidine, 135 mM NaCl, 10 mM methionine, 0.01% tween 80.

Infection and treatment in *in vitro* assays

Cardiac cells were seeded over gelatin-coated glass coverslips in 24-well plates (1 x 10^5 cells/well) for 24 h at 37°C under an atmosphere of 5% CO_2. Cultures were incubated with fresh medium containing 25, 100 and 200 μg/mL 1D11 and 100 μg/mL 13C4 or vehicle for 2 h before infection or during the addition of trypomastigotes of the Y strain in a parasite-to-host cell proportion of 10:1. Parasites were also pre-treated with 100 μg/mL 1D11 for 2 h before infection. At the time indicated, cells were washed with phosphate-buffered saline (PBS), fixed in Bouin's solution, and stained with Giemsa solution. The percentage of cardiac cells containing parasites and the number of parasites per infected cell were determined by counting 400 cells/slide on two distinct coverslips at 24, 48, 72, and 96 h post infection. Analysis was performed with a Zeiss microscope at a magnification of x400. Data are means ± standard deviations from three independent experiments.

Infection and treatment in *in vivo* assays

Acute phase model

Male Swiss mice (age 6 to 8 weeks, weight 18 to 20 g) were obtained from the animal facilities of ICTB (Instituto de Ciência e Tecnologia em Biomodelos (ICTB/FIOCRUZ, Rio de Janeiro, Brazil). Mice were housed for at least 1 week before parasite infection under environmental factors and sanitation according to the "Guide for the Care and Use of Laboratory Animals". Infection

was performed by intraperitoneal (IP) injection of 10^4 bloodstream trypomastigotes from the Y strain of *T. cruzi*. Sex and age-matched noninfected mice were maintained under identical conditions.

Chronic phase model

Female C57BL/6 mice (H-2^b, aged 4 to 6 weeks) were obtained from the animal facilities of ICTB (FIOCRUZ, Rio de Janeiro, Brazil). Animals were housed for at least one week before parasite infection at Animal Facility/IOC under environmental factors and sanitation according to "Guide for the Care and Use of Laboratory Animals". For all experimental procedures, C57BL/6 mice were infected by IP injection of 100 blood trypomastigotes of the Colombian strain of *T. cruzi* (Ferreira et al., 2019). Parasitemia was employed as a parameter to establish acute and chronic phases using 5 µL of blood obtained from the tail vein and it was also individually checked by direct microscopic counting of parasites, as previously described (Brener, 1962; Waghabi et al., 2009).

1D11 treatment

Treatment was performed by intraperitoneal (IP) administration (0.2 mL) of the 1D11 antibody, and its isotype matched murine IgG1 control (13C4). For determination of the best dose, 1D11 was IP administered to Y-infected mice at 5 dpi with 1.25, 2.5, 5 and 10 mg/Kg. Further, as the best-chosen dose, mice received 5mg/Kg 1D11 in different schemes of treatment for acute and for chronic phase assays. The control group received vehicle buffer using the same scheme.

Experimental groups

Mice were divided into the following groups respecting the limit of 5 animals per cage: untreated and non-infected (NI), untreated and *T. cruzi* infected (*T. cruzi*) and 1D11 treated and *T. cruzi* infected, using 5 treatment schemes for the acute phase studies: single dose at 3 dpi (SD d3), single dose at 5 dpi (SD d5), day 0+ three times a week (d0+ 3xw), day 3+ once a week (d3+ 1xw), and day 3+ three times a week (d3+ 3xw). For chronic phase studies, mice were divided into the following groups: untreated and non-infected (NI), untreated and *T. cruzi* infected (*T. cruzi*) and 1D11 treated and *T. cruzi* infected, using 2 treatment schemes: single dose at 120 dpi (SD d120) and day 120+ once a week (d120+ 1xw). Eight to 10 mice from each group were used for analysis at each different dpi, and three independent experiments were performed to assure reproducibility.

Mortality and parasitemia

The mortality of the mice was checked daily until 30 dpi (for acute phase model) and until 150 dpi (for chronic phase model) and expressed as a percentage of cumulative mortality. To check the effects of treatments on parasite circulation, parasitemia was individually checked by direct microscopic counting of parasites in 5 µl of blood, as described above.

Electrocardiography analysis

ECG recording and analysis were performed in all groups of infected and non-infected animals. Mice were IP tranquilized with diazepam (20 mg/Kg), fixed in the supine position and the transducers were carefully placed subcutaneously according to chosen preferential derivation (DII). Traces were recorded using a digital system (Power Lab 2/20) connected to a bio-amplifier at 2 mV for 1 s (PanLab Instruments, Spain). Filters were standardized between 0.1 and 100 Hz and traces were analyzed using the Scope software for Windows V3.6.10 (PanLab Instruments, Barcelona, Spain). ECG parameters were recorded for at least 2 min and evaluated in the acute (at 15 dpi) and chronic phases (at 120, 150 and 180 dpi), using the following standard criteria: the heart rate, monitored by beats/minute (bpm), and the variation at P wave and PR, QRS and correct QT intervals (QTc), all measured in milliseconds (ms). The ECG parameters were analyzed as previously described (Ferreira et al., 2019).

Histological assessment of cardiac fibrosis

Formalin-fixed tissues were dehydrated and embedded in paraffin. Sections (3 µm) were stained by Masson's trichrome as previously described (Ferreira et al., 2019). Sections were observed using a Nikon microscope coupled with image acquisition systems (Nikon) and the images were assessed for percentage area of collagen using CellProfiler image analysis software (http://www.cellprofiler.org). In addition, percent of Masson's Trichrome stained area (light blue areas) was quantified for each heart section in a 10x microscopic magnification. Two heart sections were made for each mouse, and 4-6 fields were quantified per section to obtain whole tissue information.

Statistical analysis

Differences between infected and non-infected groups and between infected mice, 1D11 treated or not, were considered statistically significant when *p< 0.05, **p< 0.01, and ***p< 0.001, as determined by GraphPad Prism 8.0 software (GraphPad Software Inc., San Diego, CA, USA). All the analyses were performed using the non-parametric Mann–Whitney test.

Results

1D11 treatment decreases *T. cruzi* invasion of cardiac cells *in vitro*

Given that it was previously demonstrated that TGF-β and its receptors are required for *T. cruzi* entry into cardiomyocytes (Ming et al., 1995; Waghabi et al, 2005; Waghabi et al., 2007), we first tested the use of 1D11 during the process of invasion of these cells by *T. cruzi*. To this end, cardiac cells were treated with 25, 100 and 200 µg/ml 1D11 for 24 h during *T. cruzi* Y strain infection. Figure 1A demonstrates that the addition of 100 and 200 µg/ml

10.3389/fcimb.2022.1017040

1D11 reduced *T. cruzi* host cell infection. We also tested the pre-treatment of both parasites (TC PT) and cardiac cells (CM PT) with 100 μg/ml 1D11 (Figure 1B) and observed similar effect as compared to 1D11 addition during infection (DI). Thus, we chose to use 100 μg/ml 1D11 in the next steps to continue the investigation of TGF-β neutralization during *in vitro T. cruzi* infection on cardiac cells. We performed a kinetic study from 24 h until 96 h of *T. cruzi* infection, and observed a sustained lower percentage of *T. cruzi* infected cardiac cells after the inhibition of TGF-β even after 96 h post infection (Figure 1C). Quantification of the percentage of infected cells is shown in Figures 1A–C

1D11 treatment inhibits the intracellular *T. cruzi* cell cycle

We have previously demonstrated that TGF-β is implicated in *T. cruzi* infection and controls its intracellular life cycle (Waghabi et al., 2005, 2007), thus we examined whether the TGF-β neutralization with 1D11 during the process of *T. cruzi* infection could affect the intracellular parasite cycle. For this purpose, cells were treated with 100 μg/ml 1D11, and compared with controls. Our results showed that the addition of 1D11 reduced the number of intracellular forms of the parasite (Figure 1D). Quantification of the number of intracellular parasites during the cycle showed that there was already a significant difference in the mean number of intracellular parasite forms, at 48 h post infection. This difference increased throughout the infection, reaching the highest differences, at 96 h (Figure 1D).

Comparison of the different schemes of treatment with 1D11 *in vivo*

In the second set of experiments, 5mg/Kg antibody was administered *in vivo* by IP injection in male Swiss mice infected with 10^4 bloodstream trypomastigotes of the Y strain in the acute model. Evaluating parasitemia and survival rates, we observed that treatment starting at 3 dpi (SD d3) was not beneficial to infected mice, resulting in similar parasitemia peak and mortality as compared to untreated group (*T. cruzi*). On the

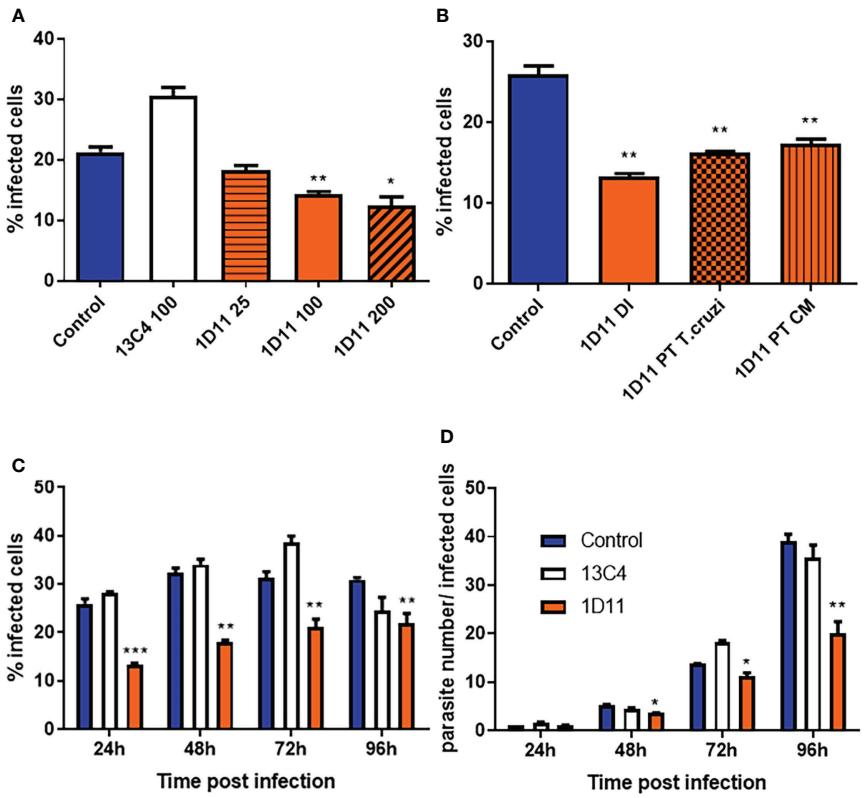

FIGURE 1
1D11 treatment decreases *T. cruzi* invasion of cardiomyocytes and the parasite number per infected cells. The percentage of cardiac cells containing parasites **(A–C)** and the number of parasites per infected cell **(D)** were determined by counting 400 cells/slide on two distinct coverslips at 24, 48, 72, and 96 h post infection. Data are means ± standard deviations from three independent experiments. Significant differences between infected cells treated or not with 1D11 are indicated by *p < 0.05 **p< 0.01, ***p< 0.001.

10.3389/fcimb.2022.1017040

other hand, a single dose of 1D11 treatment at 5dpi (SD d5) showed best results in decreasing the parasitemia peak and protecting mice from death (Supplemental Figures 1A–C). Thus, for the subsequent studies, the treatment scheme of 1D11 d5 was chosen. The next step was to test the best dose of 1D11 to be IP administered, and to this end we performed a dose-response assay with 1.25, 2.5, 5 and 10 mg/Kg of 1D11. The results showed a dose-dependent inhibition of parasitemia at 8 dpi from 1.25 up to 10 mg/Kg of 1D11 (Supplemental Figures 1D–F) and 5mg/Kg 1D11 d5 was considered as the best dose as it presented similar results as compared to the 10mg/Kg dose (Supplemental Figures 1D–F).

1D11 treatment reduced parasitemia and increased mice survival rates in acutely *T. cruzi*-infected mice

All assays were thus performed with the 5 mg/Kg dose of 1D11 in a single dose scheme at 5 dpi. Under these conditions, 1D11 led to a significant reduction at the peak of parasitemia, reaching 60% of reduction on circulating parasites and 65% of reduction on mortality rates of the mice after 30 dpi (Figures 2A, B).

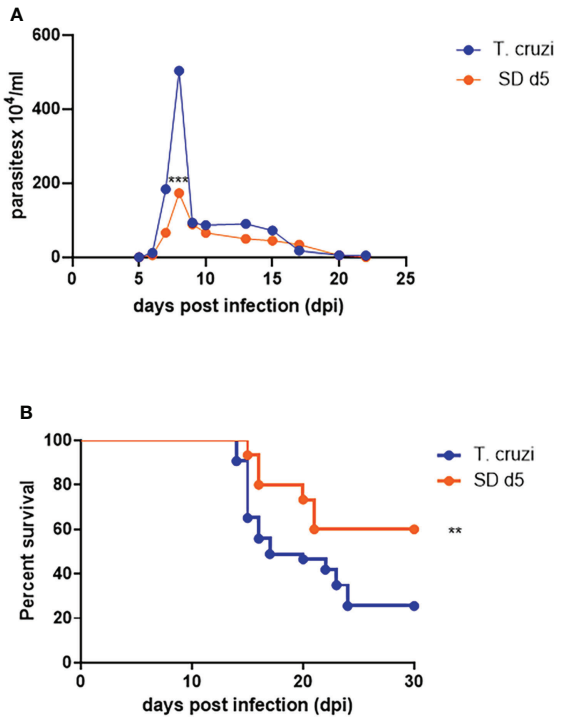

FIGURE 2
1D11 best dose administration in a single dose scheme at 5 dpi reduced the peak of parasitemia and improved the survival rates. The treatment reduced **(A)** the peak of parasitemia and **(B)** mortality rates after 30 dpi. Data are means ± standard deviations from three independent experiments. Significant differences between infected mice treated or not with 1D11 are indicated by **p< 0.01, ***p< 0.001.

1D11 treatment prevented heart damage during acute phase of *T. cruzi* infection

At 15 dpi, ECG parameters were evaluated, and the analysis of the ECG traces demonstrated atrial ventricular block with PR interval higher than 40 ms, leading to sinus bradycardia in sham-treated *T. cruzi*- infected mice as compared to the non-infected control group (472.8 and 774.2 bpm, respectively, Figure 3A). ECG analysis demonstrated that at 15 dpi, all mice presented a significant decrease in heart rate, as measured by beats per minute (bpm) (Figure 3B), associated with a significant increase of QRS complex (Figure 3C), PR (Figure 3D) and QTc (Figure 3E) intervals, when compared with sex- and age-matched non-infected (NI) controls. 1D11 IP administration significantly limited the bpm decrease at 15 dpi, with a mean heart rate of 549.2 bpm (Figure 3B). Further, improved QRS complex, PR and QTc intervals were observed in presence of 1D11 (Figures 3C–E).

1D11 treatment increased mice survival rates in chronically *T. cruzi*-infected mice

After characterizing the successful effect of a single IP dose of 1D11 during the experimental acute phase of Chagas disease, we aimed to test the possible benefits of such administration in chronic *T. cruzi* infected mice, in which the fibrotic feature is already installed in mice hearts. In the chronic model assay, *T. cruzi*-infected animals presented a circulating parasite peak at 42 dpi. This evaluation was an important step for the confirmation that the animals were infected and would develop Chagas disease (data not shown), and thus, only mice presenting parasites at the parasitemia peak were considered for chronic infection evaluations. Given that best results of 1D11 treatment during the acute phase were obtained with the single dose scheme, we decided to sustain this scheme during the chronic phase and also included a group of mice treated once a week for 30 days starting at 120 dpi, when cardiac damage has already been installed. About 90% of the infected animals survived the acute phase and progressed to the chronic phase of Chagas disease (120 dpi). When treated with 1D11 in both schemes (SD d120 and d120+ 1xw), we observed an increase of approximately 15% in survival of these animals at 150 dpi (Figure 4). We did not detect significant variation in body weight between studied groups. Weighing of the heart, liver, kidney, and spleen was also performed, and a significant increase was observed in liver and spleen weight of infected animals compared to the control group,

10.3389/fcimb.2022.1017040

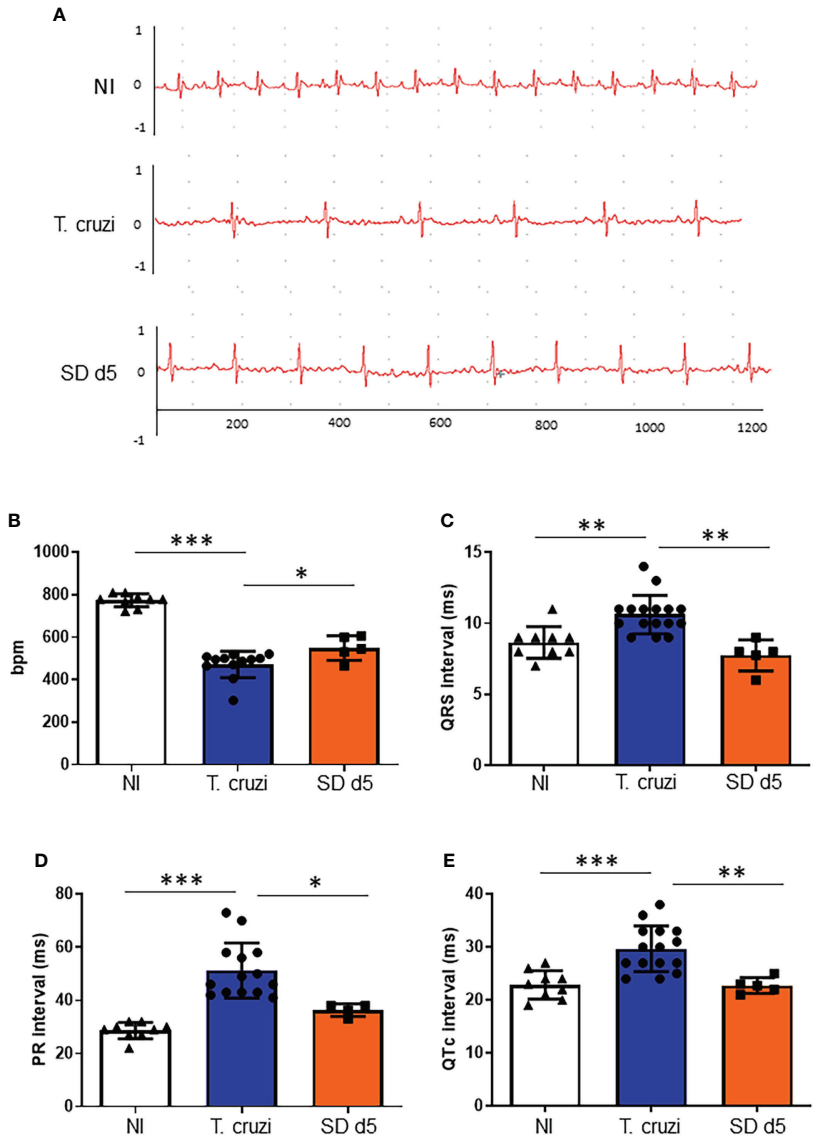

FIGURE 3
1D11 IP administration restored electrocardiographic parameters. 1D11 was administered at 5 dpi by intraperitoneal injection in male Swiss mice infected with 10^4 bloodstream trypomastigotes of the Y strain. Representative electrocardiographic tracings of each group at 15 dpi are shown **(A)**. 1D11 treatment resulted in best heart rate, in beats per minute (bpm) **(B)**; PR interval in milliseconds **(C)**; QRS interval **(D)** and QTc interval in milliseconds **(E)**. Significant differences between non infected and infected mice treated or not with 1D11 are indicated by *p< 0.05 **p< 0.01, ***p< 0.001.

but the 1D11 treatments was not able to act on these alterations (data not shown).

1D11 treatment reversed cardiac altered electrical conduction in *T. cruzi*-infected mice models

We further tested the effects of 1D11 administration in animals chronically infected with *T. cruzi* focusing on the heart parameters. To this end, we performed electrocardiogram analysis at the end of the experiment at 150 dpi. Electropherograms were selected to demonstrate the evolution of cardiac electrical alterations observed in the same mouse; thus, an electropherogram of a mouse in 120 dpi (m1 120 dpi) indicates the presence of atrium-ventricular blockage grade 1 (AVB1), which clearly evolved into an atrium-ventricular blockage grade 2 (AVB2) in 150 dpi (m1 150 dpi). After 1D11 administration in single dose, mice improved the heart electrical disorders; in Figure 5, we showed a mouse ECG tracing

10.3389/fcimb.2022.1017040

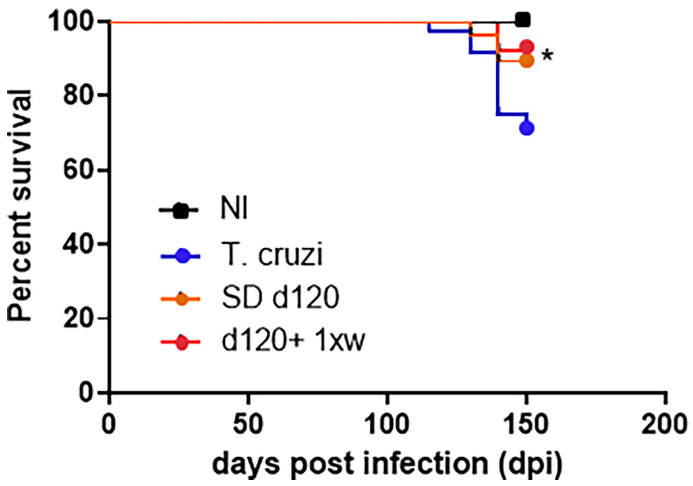

FIGURE 4
1D11 treatment increased mice survival rates in chronically *T. cruzi*-infected mice. After 120 dpi 1D11 was administered in two schemes: single dose at 120 dpi (SD d120) and starting at 120 dpi + once a week (d120+ 1xw). Significant differences between non infected and infected mice treated or not with 1D11 are indicated by *p< 0.05.

before starting 1D11 treatment at 120 dpi (m2 120 dpi) with AVB2, and after 1D11 SD d120 treatment an AVB1 profile was observed (m2 SD d120 150 dpi) indicating an improved cardiac electrical function. Moreover, we observed that best results were obtained by treatment with 1D11 in a single dose (SD d120) as compared to the group which received treatment once a week for 30 days after 120 dpi (d120+ 1xw) (Figures 5, D). The 1D11 single dose scheme increased heart rate parameters (*T. cruzi* = 405.4 ± 64.3/SD d120 = 507.2 ± 43.8; Figure 5B); decreased PR interval (*T. cruzi* = 45.7 ± 2.8/SD d120 = 42.2 ± 2.5; Figure 5C) and P wave duration (*T. cruzi* = 14.1± 1.5/SD d120 = 13.0 ± 1.1; Figure 5D). Mice treated with 1D11 d120+ 1xw just improved PR interval (*T. cruzi* = 45.7 ± 2.8/d120+ 1xw = 43.7 ± 2; Figure 5C) with no effect on other parameters. TGF-β neutralization by 1D11 administration had no effect on the prolonged QTc observed in mice chronically infected by *T. cruzi* (Figure 5D).

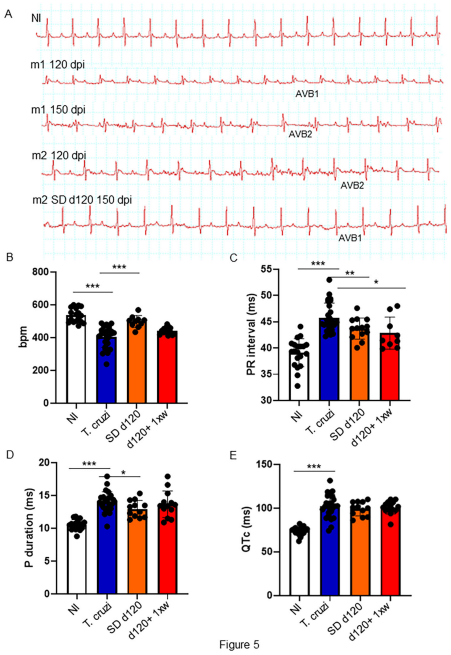

FIGURE 5
1D11 reverses ECG abnormalities in a mouse model of chronic Chagas' heart disease. Representative electrocardiographic tracings of each group at 150 dpi are shown **(A)**. 1D11 SD d120 treatment resulted in best heart rate, in beats per minute (bpm) **(B)**; PR interval in milliseconds **(C)**; P duration in milliseconds **(D)** and QTc interval in milliseconds **(E)**. Significant differences between non infected and infected mice treated or not with 1D11 are indicated by *p< 0.05, **p< 0.01, ***p< 0.001.

1D11 treatment restored collagen deposition in chronically *T. cruzi*-infected mice model

The most important histopathological finding in CCC is cardiac fibrosis, both in humans and in experimental models (Rossi, 1998). Thus, we assessed whether treatment with 1D11 could reverse heart fibrosis. As already demonstrated in this model, we identified a significant increase in collagen deposition in the heart of animals with 120 and 150 dpi (Figures 6A, B, respectively). Both 1D11 treatment schemes decreased heart

10.3389/fcimb.2022.1017040

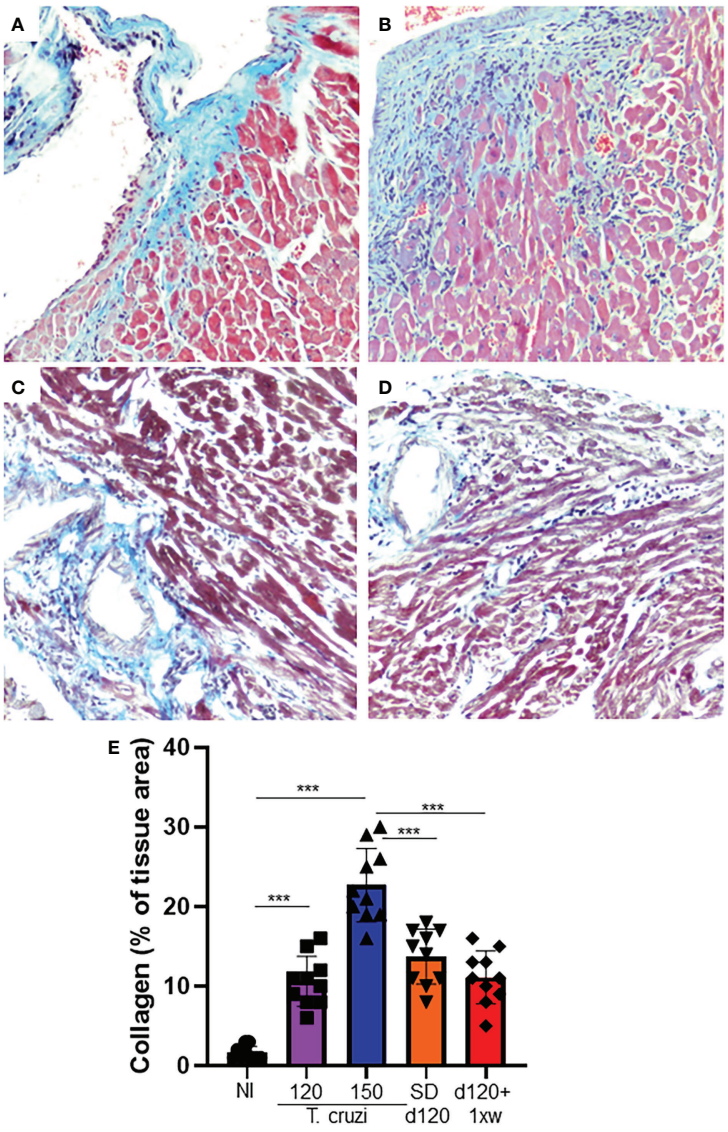

Figure 6

FIGURE 6
1D11 treatment reverses heart fibrosis in mice chronically infected with T. cruzi. After 120 dpi 1D11 was administered in two schemes: **(C)** a single dose at 120 dpi (SD d120) and **(D)** starting at 120 dpi + once a week (d120+ 1xw). **(A)** Non-infected (NI) and **(B)** infected mice were sacrificed at 150 dpi for fibrosis assessment. Heart sections were stained for collagen deposition by Masson's trichrome (light blue staining). **(E)** Percent of Masson's Trichrome stained area (light blue areas) was quantified on microscopic images of heart sections using CellProfiler image analysis software. Data is a representative image of 10 independent mice per group. Significant differences between non infected and infected mice treated or not with 1D11 are indicated by ***p < 0.001.

fibrosis, but we still observed a higher percent of area of collagen deposition in the heart of infected animals as compared to non-infected ones (Figure 6C–E). Although 1D11 d120+ 1xw treated mice presented a slight reduction in the collagen area as compared to the group of mice treated in a single dose scheme, SD d120, it was not statistically significant (Figure 6C–E).

Discussion

Even more than a century after its discovery, many challenges remain unresolved when the subject is Chagas disease. Therapeutic and prognostic methods must still be improved (Vilar-Pereira et al., 2016; Pérez-Molina and Molina, 2018). Here, we aimed to investigate the role of TGF-β on *T. cruzi*

infection using the 1D11 monoclonal antibody, which neutralizes the three isoforms of TGF-β in *in vitro* and pre-clinical models. We showed that addition of 1D11 to cardiac cells reduces cardiomyocyte invasion by *T. cruzi* and the number of parasites per infected cell. In both acute and chronic experimental models, *T. cruzi* infection altered the electrical conduction: decreasing the heart rate, increasing the PR interval and the P wave duration. The treatment with 1D11 reversed electrical abnormalities, improved cardiac performance, and reduced cardiac fibrosis.

In 2007, we demonstrated that SB-431542, an inhibitor of ALK5, inhibited *T. cruzi*-induced activation of the TGF-β pathway in epithelial cells and in cardiomyocytes. We also described that addition of SB-431542 reduced cardiomyocyte invasion by *T. cruzi*. Furthermore, we concluded that SB-431542 treatment significantly reduced the number of parasites per infected cell and of trypomastigote differentiation and release. To confirm these data we first tested a neutralizing antibody that recognizes human TGF-β 1, 2 and 3 (1D11, Genzyme) on infected cardiac cells from mouse embryos treated with different concentrations of the antibody. The addition of 1D11 reproduced our previous findings: (1) it inhibited cardiac cells invasion by *T. cruzi*, (2) it reduced the percentage of cells infected with *T. cruzi*; and (3) it reduced the number of parasites per infected cell. These results are important, since they demonstrate that neutralizing TGF-β activity before its binding to cell receptors not only inhibits *T. cruzi* invasion but also acts through inhibiting parasite proliferation probably impairing the infection of neighbor's cells.

Fibrosis is one of the most significant histopathologic findings of CCC, being associated with the presence of inflammatory infiltrates and degeneration of cardiac cells (Rossi and Bestetti, 1995; Rossi, 2001). The mechanisms driving the progression of fibrosis in different organs and tissues are similar and have common features. The progressive accumulation of connective tissue and excessive deposition of extracellular matrix components result in the replacement of normal tissue architecture and loss of functional activity. This process is mediated by soluble cytokines and growth factors, which regulate cell migration, proliferation, and differentiation, as well as the synthesis and degradation of extracellular matrix components, amongst which TGF-β (Gharee-Kermani and Pham, 2001; Hata and Chen, 2016).

In the present study, 1D11 modulated parasitemia and survival rates. Moreover, TGF-β neutralization also improved the cardiac function, when compared with the control group, corroborating other data in the literature. A previous study performed by our group showed that GW788388, a potent selective inhibitor of ALK5, administrated in an acute model of Chagas disease significantly decreased parasitemia, and improved cardiac electrical conduction as measured by PR interval in electrocardiography, restored connexin43 expression, increased survival and decreased cardiac fibrosis. Here, we also showed that TGF-β neutralization starting at 5 dpi exerts beneficial actions through inhibiting the progression of heart commitment by electrical disorders, such as arrythmias.

Recently we investigated TGF-β pathway inhibition by GW788388, using an experimental model of chronic Chagas' heart disease (Ferreira et al., 2019). Treatment with the TGF-β receptor inhibitor improved several cardiac parameters, with reversion of heart fibrosis followed by a better heart function. However, the clinical use of inhibitors of TGF-β receptor kinase activity could induce some deleterious secondary effects (reviewed in Araújo-Jorge et al., 2012). Thus, here we also investigated the monoclonal antibody 1D11 during the experimental chronic phase of Chagas disease. 1D11 antibody has already been studied in other preclinical models; it was applied in a model of kidney fibrotic disease in which it was observed that mice receiving 1D11 from day 3 presented prevention of glomerular fibrosis even when started after the onset of proteinuria (Liang et al., 2016). A more recent work used 1D11 to demonstrate that aberrant activation of transforming growth factor-β (TGF-β) mobilizes mesenchymal/stromal stem cells in blood, which are recruited for the prostatic stromal hyperplasia (Wang et al., 2017). Hypertensive induced myocardial fibrosis was also studied under the effect of 1D11 *in vivo* and *in vitro* treatment (Wong et al., 2018), where it was shown that connective tissue growth factor (CTGF) expression is dependent on TGF-β signaling in a model of myocardial fibrosis. Another study also demonstrated the beneficial IP administration of 1D11 in a model of hepatic fibrosis (Ling et al., 2013). 1D11 administration was also effective to prevent radiation-induced lung injury (Anscher et al., 2006). These important findings corroborate the application of TGF-β neutralization in the complex cardiac fibrotic disorder observed by *T. cruzi* infection.

1D11 therapy ameliorates critical aspects of the disease. Therefore, TGF-β emerges as a candidate to treat the fibrosis deregulation associated with chronic Chagas' heart disease and to improve patient prognosis. These data strongly reinforce that the treatment with antibodies could represent a new therapeutic strategy to address acute and chronic phases of Chagas disease that warrants further clinical exploration. We have conducted a series of studies investigating the role of TGF-β and its pathway inhibition. Here, we have again reinforced the importance of using TGF-β pathway inhibitors in Chagas chronic disease development. Thus, as a strategic step, pharmaceuticals worldwide should reinforce the development of humanized antibodies against TGF-β to become suitable for human tests. Finally, on-target anti-TGF-β therapies should be addressed in clinical trials in order to test its efficacy in patients presenting the cardiac disorder due to chronic Chagas disease.

Data availability statement

The raw data supporting the conclusions of this article will be made available by the authors, without undue reservation.

Ethics statement

The animal study was reviewed and approved by Institutional Committee for Animal Ethics of Fiocruz (CEUA/Fiocruz, Licenses LW10/14 and LW42-11).

Author contributions

Conceptualization: SL, ES, MW. Formal analysis: RF, RA, GV-P, MM-B, NF, ES, JL-V, TA-J, MW. Funding acquisition: SL, JL-V, MW. Investigation: RF, RA, GV-P, MM-B, RB, ES, MW. Methodology: RF, RA, GV-P, MM-B, NF, ES, MW. Project administration: MW Resources: WD, JL-V. Supervision: ES, MW. Writing – original draft: RF, MW. Writing – review and editing: WD, ES, SL, JL-V, TA-J, SB. All authors contributed to the article and approved the submitted version.

Funding

This work was supported by grants from MCW-Fundação Oswaldo Cruz (FIOCRUZ), JLV Fundação de Amparo à Pesquisa do Estado do Rio de Janeiro (FAPERJ), Temáticos/process E-26/110.153/2013, and JLV-Conselho Nacional de Desenvolvimento Cientifico e Tecnologico (CNPq), DECIT negligenciadas process 403979/2012-9.

Acknowledgments

The authors would like to thank the Laboratory Animals Breeding Center from Institute Oswaldo Cruz for technical support on animal care. The collaboration between the Brazilian and French teams was supported by an INSERM-FIOCRUZ collaborative program and the collaboration between the Brazilian and Genzyme teams was supported by the Genzyme-FIOCRUZ partnership developed under the leadership of Carlos Morel from the Health Technological Development Center (Centro de Desenvolvimento Tecnológico em Saúde -CDTS), Fundação Oswaldo Cruz, Rio de Janeiro, RJ, Brazil.

Conflict of interest

The authors declare that the research was conducted in the absence of any commercial or financial relationships that could be construed as a potential conflict of interest.

The reviewer CC declared a shared affiliation with the authors RF, ES, WD, RA, and MW to the handling editor at the time of review.

Publisher's note

All claims expressed in this article are solely those of the authors and do not necessarily represent those of their affiliated organizations, or those of the publisher, the editors and the reviewers. Any product that may be evaluated in this article, or claim that may be made by its manufacturer, is not guaranteed or endorsed by the publisher.

Supplementary material

The Supplementary Material for this article can be found online at: https://www.frontiersin.org/articles/10.3389/fcimb.2022.1017040/full#supplementary-material

SUPPLEMENTARY FIGURE 1
D11 administration affected parasitemia and mortality. Treatment was administered in different schemes: single dose at 3 dpi (1D11 d3), single dose at 5 dpi (1D11 d5), treatment starting at day 0+ three times a week (1D11 d0+ 3xw), starting at day 3+ once a week (1D11 d3+ 1xw) and starting at day 3+ three times a week (1D11 d3+ 3xw). Parasitemia was measured by direct counting of parasites in blood all along the acute phase **(A–E)**. Percent survival was monitored during the experiment until 30 dpi **(B–F)**. 1D11 treatment showed inhibition of parasitemia peak at 8 dpi in different schemes: 1D11 d5, 1D11 d0+ 1xw, 1D11 d3+ 1xw and 1D11 d0+ 3xw **(C)**. 1D11 treatment also showed a dose-dependent inhibition of parasitemia peak from 0.1 up to 10 mg/kg of 1D11 **(D)**. Data are means ± standard deviations from three independent experiments. Significant differences between infected mice treated or not with 1D11 are indicated by *p< 0.05 **p< 0.01, ***p< 0.001.

References

Álvarez, J. M., Fonseca, R., Borges da Silva, H., Marinho, C. R., Bortoluci, K. R., Sardinha, L. R., et al. (2014). Chagasdiseasestill many unsolved issues. *Inflammation* 912965, 1–9. doi: 10.1155/2014/912965

Amieva, C., Carrillo, C., Mordeglia, C., Gortari, M. C., Scazzola, M. S., and Sanmartino, M. (2021). ""A kaleidoscope of words and senses to (Re)Think the chagas problem: Experiences in Argentina and brazil,"," in *Arts and health promotion* (Cham: Springer International Publishing), 197–215. doi: 10.1007/978-3-030-56417-9_12

Anderton, M. J., Mellor, H. R., Bell, A., Sadler, C., Pass, M., Powell, S., et al. (2011). Induction of heart valve lesions by small-molecule ALK5 inhibitors. *Toxicol. Pathol.* 39 (6), 916–924. doi: 10.1177/0192623311416259

Andrade, Z. A. (1999). Immunopathology of chagas disease. *Mem. Inst. Oswaldo Cruz* 94, 71–80. doi: 10.1590/S0074-02761999000700007

Anscher, M. S., Thrasher, B., Rabbani, Z., Teicher, B., and Vujaskovic, Z. (2006). Antitransforming growth factor-β antibody 1D11 ameliorates normal tissue damage caused by high-dose radiation. *Int. J. Radiat. Oncol. Biol. Phys.* 65, 876–881. doi: 10.1016/j.ijrobp.2006.02.051

Araújo-Jorge, T. C., Waghabi, M. C., Bailly, S., and Feige, J. J. (2012). The TGF-β pathway as an emerging target for chagas disease therapy. *Clin. Pharmacol. Ther.* 92, 613–621. doi: 10.1038/clpt.2012.102

Bhandary, B., Meng, Q., James, J., Osinska, H., Gulick, J., Valiente-Alandi, I., et al. (2018). Cardiac fibrosis in proteotoxic cardiac disease is dependent upon myofibroblast TGF-β signaling. *J. Am. Heart Assoc.* 7, e010013. doi: 10.1161/JAHA.118.010013

Bocchi, E. A., Bestetti, R. B., Scanavacca, M. I., and Cunha Neto, E. (2017). And issa, V Chronic chagas heart disease management. *S.J. Am. Coll. Cardiol.* 70, 1510–1524. doi: 10.1016/j.jacc.2017.08.004

Brener, Z. (1962). Therapeutic activity and criterion of cure on mice experimentally infected with trypanosoma cruzi. *Rev. Inst Med. Trop. Sao Paulo.* 4, 389–396.

Chagas, C. (1909). Nova Tripanozomiaze humana: estudos sobre a morfolojia e o ciclo evolutivo do schizotrypanum cruzi n. gen., n. sp., ajente etiolojico de nova entidade morbida do homem. *Mem. Inst. Oswaldo Cruz* 1, 159–218. doi: 10.1590/S0074-02761909000200008

Coura, J. R. (2007). Chagas disease: what is known and what is needed–a background article. *Mem. Inst. Oswaldo Cruz* 102 Suppl, 113–122. doi: 10.1590/S0074-02762007000900018

Daniels, C. E., Wilkes, M. C., Edens, M., Kottom, T. J., Murphy, S. J., Limper, A. H., et al. (2004). Imatinib mesylate inhibits the profibrogenic activity of TGF-β and prevents bleomycin-mediated lung fibrosis. *J. Clin. Invest.* 114, 1308–1316. doi: 10.1172/JCI200419603

de Oliveira, F. L., Araújo-Jorge, T. C., de Souza, E. M., de Oliveira, G. M., Degrave, W. M., Feige, J. J., et al. (2012). Oral administration of GW788388, an inhibitor of transforming growth factor beta signaling, prevents heart fibrosis in chagas disease. *PloS Negl. Trop. Dis.* 6, e1696. doi: 10.1371/journal.pntd.0001696

Dewidar, B., Meyer, C., Dooley, S., and Meindl-Beinker, A. (2019). TGF-β in hepatic stellate cell activation and liver fibrogenesis–updated 2019. *Cells* 8, 1419. doi: 10.3390/cells8111419

Dias, J. C. P. (1984). Acute chagas disease. *Mem. Inst. Oswaldo Cruz* 79, 85–91.

Eghbali, M., Tomek, R., Sukhatme, V. P., Woods, C., and Bhambi, B. (1991). Differential effects of transforming growth factor-β1 and phorbol myristate acetate on cardiac fibroblasts: Regulation of fibrillar collagen mRNAs and expression of early transcription factors. *Circ. Res.* 69, 483–490. doi: 10.1161/01.RES.69.2.483

Ferreira, R. R., Abreu, R., da, S., Vilar-Pereira, G., Degrave, W., Meuser-Batista, M., et al. (2019). TGF-β inhibitor therapy decreases fibrosis and stimulates cardiac improvement in a pre-clinical study of chronic chagas' heart disease. *PloS Negl. Trop. Dis.* 13, 1–27. doi: 10.1371/journal.pntd.0007602

Ferreira, R. R., Waghabi, M. C., Bailly, S., Feige, J. J., Hasslocher-Moreno, A. M., Saraiva, R. M., et al. (2022). The search for biomarkers and treatments in chagas disease: Insights from TGF-beta studies and immunogenetics. *Front. Cell. Infect. Microbiol.* 11. doi: 10.3389/fcimb.2021.767576

Frangogiannis, N. G. (2020). Transforming growth factor–ß in tissue fibrosis. *J. Exp. Med.* 217, 1–16. doi: 10.1084/jem.20190103

Gellibert, F., de Gouville, A.-C., Woolven, J., Mathews, N., Nguyen, V.-L., Bertho-Ruault, C., et al. (2006). Discovery of 4-{4-[3-(Pyridin-2-yl)-1 h -pyrazol-4-yl]pyridin-2-yl}- n -(tetrahydro-2 h - pyran-4-yl)benzamide (GW788388): A potent, selective, and orally active transforming growth factor-β type I receptor inhibitor. *J. Med. Chem.* 49, 2210–2221. doi: 10.1021/jm0509905

Gharee-Kermani, M., and Pham, S. (2001). Role of cytokines and cytokine therapy in wound healing and fibrotic diseases. *Curr. Pharm. Des.* 7, 1083–1103. doi: 10.2174/1381612013397573

Gu, Y. Y., Liu, X. S., Huang, X. R., and Yu, X. Q. (2020). And lan, h Diverse role of TGF-β in kidney disease. *Y. Front. Cell Dev. Biol.* 8. doi: 10.3389/fcell.2020.00123

Hata, A., and Chen, Y.-G. (2016). TGF-β signaling from receptors to smads. *Cold Spring Harb. Perspect. Biol.* 8, a022061. doi: 10.1101/cshperspect.a022061

Huang, T., Schor, S. L., and Hinck, A. P. (2014). Biological activity differences between TGF-β1 and TGF-β3 correlate with differences in the rigidity and arrangement of their component monomers. *Biochemistry* 53, 5737–5749. doi: 10.1021/bi500647d

Ihn, H. (2002). Pathogenesis of fibrosis: role of TGF-β and CTGF. *Curr. Opin. Rheumatol.* 14, 681–685. doi: 10.1097/00002281-200211000-00009

Inui, N., Sakai, S., and Kitagawa, M. (2021). Molecular pathogenesis of pulmonary fibrosis, with focus on pathways related to TGF-β and the ubiquitin-proteasome pathway. *Int. J. Mol. Sci.* 22, 6107. doi: 10.3390/ijms22116107

Ko, T., Nomura, S., Yamada, S., Fujita, K., Fujita, T., Satoh, M., et al. (2022). Cardiac fibroblasts regulate the development of heart failure *via* Htra3-TGF-β-IGFBP7 axis. *Nat. Commun.* 13, 1–17. doi: 10.1038/s41467-022-30630-y

Liang, X., Schnaper, H. W., Matsusaka, T., Pastan, I., Ledbetter, S., and Hayashida, T. (2016). Anti-TGF-β antibody, 1D11, ameliorates glomerular fibrosis in mouse models after the onset of proteinuria. *PloS One* 11, e0155534. doi: 10.1371/journal.pone.0155534

Ling, H., Roux, E., Hempel, D., Tao, J., Smith, M., Lonning, S., et al. (2013). Transforming growth factor β neutralization ameliorates pre-existing hepatic fibrosis and reduces cholangiocarcinoma in thioacetamide-treated rats. *PloS One* 8, e54499. doi: 10.1371/journal.pone.0054499

Marin-neto, J. A., César, O., Filho, D. A., Pazin-filho, A., and Preto, R. (2002). Forma indeterminada da moléstia de chagas . proposta de novos critérios de caracterização e perspectivas de tratamento precoce da cardiomiopatia. *Arq. Bras. Cardiol.* 79, 623–627.

Meirelles, M. N., de Araujo-Jorge, T. C., Miranda, C. F., de Souza, W., and Barbosa, H. S. (2002). Interaction of *Trypanosoma cruzi* with heart muscle cells: Ultrastructural and cytochemical analysis of endocytic vacuole formation and effect upon myogenesis in vitro. *Eur. J. Cell Biol.* 41 (2), 198–206.

Ming, M., Ewen, M. E., and Pereira, M. E. A. (1995). Trypanosome invasion of mammalian cells requires activation of the TGFβ signaling pathway. *Cell* 82, 287–296. doi: 10.1016/0092-8674(95)90316-X

Moustakas, A., and Heldin, C.-H. (2005). Non-smad TGF-β signals. *J. Cell Sci.* 118, 3573–3584. doi: 10.1242/jcs.02554

Okada, H., Takemura, G., Kosai, K., Li, Y., Takahashi, T., Esaki, M., et al. (2005). Postinfarction gene therapy against transforming growth factor-β signal modulates infarct tissue dynamics and attenuates left ventricular remodeling and heart failure. *Circulation* 111, 2430–2437. doi: 10.1161/01.CIR.0000165066.71481.8E

Pereira, I. R., Vilar-Pereira, G., Moreira, O. C., Ramos, I. P., Gibaldi, D., Britto, C., et al. (2015). Pentoxifylline reverses chronic experimental chagasic cardiomyopathy in association with repositioning of abnormal CD8+ T-cell response. *PloS Negl. Trop. Dis.* 9, e0003659. doi: 10.1371/journal.pntd.0003659

Pereira, I. R., Vilar-Pereira, G., Silva, A. A., Moreira, O. C., Britto, C., Sarmento, E. D. M., et al. (2014). Tumor necrosis factor is a therapeutic target for immunological unbalance and cardiac abnormalities in chronic experimental chagas' heart disease. *Mediators Inflammation* 22 (2014), 798078. doi: 10.1155/2014/798078

Pérez-Molina, J. A., and Molina, I. (2018). Chagas disease. *Lancet* 391, 82–94. doi: 10.1016/S0140-6736(17)31612-4

Petersen, M., Thorikay, M., Deckers, M., Van Dinther, M., Grygielko, E. T., Gellibert, F., et al. (2008). Oral administration of GW788388, an inhibitor of TGF-β type I and II receptor kinases, decreases renal fibrosis. *Kidney Int.* 73, 705–715. doi: 10.1038/sj.ki.5002717

Rassi, A., Dias, J. C. P., Marin-Neto, J. A., and Rassi, A. (2008). Challenges and opportunities for primary, secondary, and tertiary prevention of chagas' disease. *Heart* 95, 524–534. doi: 10.1136/hrt.2008.159624

Rassi, A.Jr., Rassi, A., and Marcondes de Rezende, J. (2012). American Trypanosomiasis (Chagas disease). *Infect. Dis. Clin. North Am.* 26, 275–291. doi: 10.1016/j.idc.2012.03.002

Rassi, A.Jr., Rassi, A., and Marin-Neto, J. A. (2010). Chagas disease. *Lancet* 375, 1388–1402. doi: 10.1016/S0140-6736(10)60061-X

Reisdorf, P., Lawrence, D. A., Sivan, V., Klising, E., and Martin, M. T. (2001). Alteration of transforming growth factor-β1 response involves down-regulation of Smad3 signaling in myofibroblasts from skin fibrosis. *Am. J. Pathol.* 159, 263–272. doi: 10.1016/S0002-9440(10)61692-6

Rossi, M. A. (1998). Fibrosis and inflammatory cells in human chronic chagasic myocarditis: scanning electron microscopy and immunohistochemical observations. *Int. J. Cardiol.* 66, 183–194. doi: 10.1016/S0167-5273(98)00208-3

Rossi, M. A. (2001). Connective tissue skeleton in the normal left ventricle and in hypertensive left ventricular hypertrophy and chronic chagasic myocarditis. *Med. Sci. Monit.* 7, 820–832.

Rossi, M. A., and Bestetti, R. B. (1995). The challenge of chagasic cardiomyopathy. *Cardiology* 86, 1–7. doi: 10.1159/000176822

Sato, S., Burke, A. P., Benson, W., Mergner, W., Tracy, S., Gauntt, C., et al. (1993). The pathology of murine coxsackievirus B3 myocarditis: An *in situ* hybridization study. *Cardiovasc. Pathol.* 2, 107–115. doi: 10.1016/1054-8807(93)90022-T

Steverding, D. (2014). The history of chagas disease. *Parasit Vectors* 317, 1–8.

Tan, S. M., Zhang, Y., Connelly, K. A., Gilbert, R. E., and Kelly, D. (2010). Targeted inhibition of activin receptor-like kinase 5 signaling attenuates cardiac dysfunction following myocardial infarction. *J. Am. J. Physiol. Circ. Physiol.* 298, H1415–H1425. doi: 10.1152/ajpheart.01048.2009

Vilar-Pereira, G., Resende Pereira, I., de Souza Ruivo, L. A., Cruz Moreira, O., da Silva, A. A., Britto, C., et al. (2016). Combination chemotherapy with suboptimal doses of benznidazole and pentoxifylline sustains partial reversion of experimental chagas' heart disease. *Antimicrobial Agents Chemotherapy* 60, 4297-4309. doi: 10.1128/AAC.02123-15

Waghabi, M. C., Ferreira, R. R., Abreu, R., da, S., Degrave, W., de Souza, E. M., et al. (2022). Transforming growth factor-ß as a therapeutic target for the cardiac damage of chagas disease. *Mem. Inst. Oswaldo Cruz* 117, e210395. doi: 10.1590/0074-02760210395

Waghabi, M. C., Keramidas, M., Bailly, S., Degrave, W., Mendonça-Lima, L., Maria de Nazaré, C. S., et al. (2005). Uptake of host cell transforming growth

factor-β by trypanosoma cruzi amastigotes in cardiomyocytes: potential role in parasite cycle completion. *Am. J. Pathol.* 167, 993–1003. doi: 10.1016/S0002-9440(10)61189-3

Waghabi, M. C., Keramidas, M., Calvet, C. M., Meuser, M., Nazare, M., Soeiro, C., et al. (2007). SB-431542, a transforming growth factor beta inhibitor, impairs Trypanosoma cruzi infection in cardiomyocytes and parasite cycle completion. *Antimicrobial Agents Chemotherapy* 51, 2905–2910. doi: 10.1128/AAC.00022-07

Waghabi, M. C., de Souza, E. M., de Oliveira, G. M., Keramidas, M., Feige, J. J., Araújo-Jorge, T. C., et al. (2009). Pharmacological inhibition of transforming growth factor beta signaling decreases infection and prevents heart damage in acute Chagas' disease. *Antimicrob. Agents Chemother.*, 53 (11), 4694–4701. doi: 10.1128/AAC.00580-09

Wang, S., Wilkes, M. C., Leof, E. B., and Hirschberg, R. (2005). Imatinib mesylate blocks a non-smad TGF-β pathway and reduces renal fibrogenesis *in vivo*. *FASEB J.* 19, 1–11. doi: 10.1096/fj.04-2370com

Wang, L., Xie, L., Tintani, F., Xie, H., Li, C., Cui, Z., et al. (2017). Aberrant transforming growth factor- β activation recruits mesenchymal stem cells during prostatic hyperplasia. *Stem Cells Transl. Med.* 6, 394–404. doi: 10.5966/sctm.2015-0411

Wong, C. K. S., Falkenham, A., Myers, T., and Légaré, J.-F. (2018). Connective tissue growth factor expression after angiotensin II exposure is dependent on transforming growth factor-β signaling *via* the canonical smad-dependent pathway in hypertensive induced myocardial fibrosis. *J. Renin-Angiotensin-Aldosterone Syst.* 19, 147032031875935. doi: 10.1177/1470320318759358

World Helth Organization (2021) *Chagas disease (American trypanosomiasis)*. Available at: https://www.who.int/health-topics/chagas-diseasehttps://www.who.int/health-topics/chagas-disease#.

Zamilpa, R., Navarro, M. M., Flores, I., and Griffey, S. (2014). Stem cell mechanisms during left ventricular remodeling post-myocardial infarction: Repair and regeneration. *World J. Cardiol.* 6, 610. doi: 10.4330/wjc.v6.i7.610

Zingale, B., Miles, M. A., Campbell, D. A., Tibayrenc, M., Macedo, A. M., Teixeira, M. M., et al (2012). The revised Trypanosoma cruzi subspecific nomenclature: rationale, epidemiological relevance and research applications. *Infect Genet Evol* 12 (2), 240–53. doi: 10.1016/j.meegid.2011.12.009

Frontiers in
Cellular and Infection Microbiology

Investigates how microorganisms interact with their hosts

Explores bacteria, fungi, parasites, viruses, endosymbionts, prions and all microbial pathogens as well as the microbiota and its effect on health and disease in various hosts.

Discover the latest Research Topics

See more →

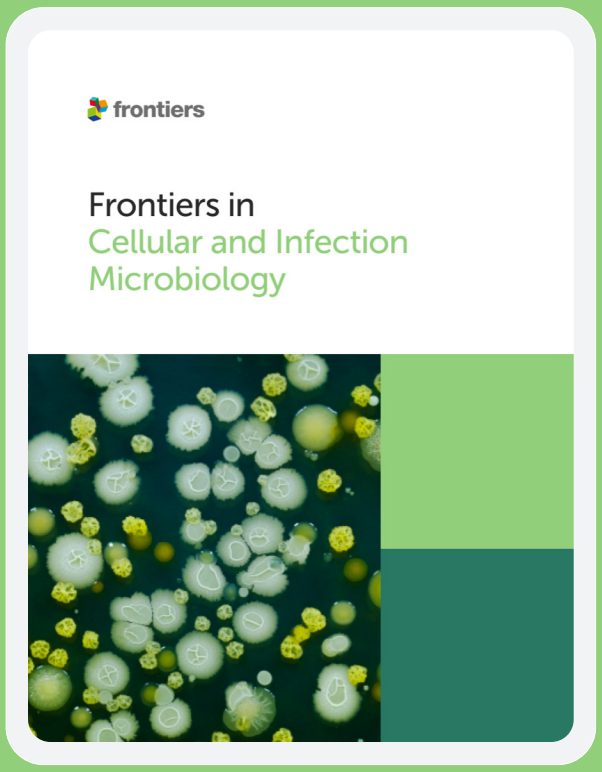

Frontiers

Avenue du Tribunal-Fédéral 34
1005 Lausanne, Switzerland
frontiersin.org

Contact us

+41 (0)21 510 17 00
frontiersin.org/about/contact